The University Of Sheffield.

A study of ADPKD pathogenesis and treatment in zebrafish models

By:

Aylin Rebecca Metzner

A thesis submitted in partial fulfilment of the requirements for the degree of Doctor of Philosophy

The University of Sheffield
Faculty of Medicine, Dentistry and Health
Department of Infection, Immunity & Cardiovascular Disease

September 2016

Abstract

Autosomal-dominant polycystic kidney disease (ADPKD) is one of the most common monogenic diseases with a worldwide incidence of 1/1000. It is caused by mutations in *PKD1* or *PKD2*. Around 10% of all end-stage renal disease results from ADPKD, translating into an annual cost of €1.5 billion across Europe. Although tolvaptan has recently been licensed for use in patients with evidence of rapid disease progression, it is only moderately effective and associated with significant side effects, resulting in the urgent need to identify new treatments.

In this project, a *pkd2* zebrafish mutant (*pkd2*^{hu2173}) was used for compound library screens with commercial drug libraries. The dorsal tail curvature phenotype, the most penetrant ADPKD-related trait in this mutant, was chosen as the assay read-out. After thorough testing, the most promising compounds were studied in three-dimensional mammalian cyst assays using both canine (MDCK) and human (Ox161c1; *PKD1*$^{-/-}$) cell lines. Experiments in cyst assays largely confirmed the hit compounds as relevant to cyst formation and expansion. Several hits linked to pathways previously implicated in other ADPKD models including androgens, prostaglandins and TGFβ but the precise role of others remains to be identified.

Using a novel kidney calcium-reporter zebrafish line *enpep:Gal4;UAS:GCaMP7a*, *in vivo* Ca^{2+} levels were found to be reduced in *pkd2* mutant fish compared to sibling controls. Genetic interactions between *pkd2* and *elipsa*, a ciliary protein, were observed for tail curvature and glomerular dilatation, providing the first evidence of a non-redundant function for *pkd2* in the zebrafish pronephros.

In conclusion, this study has identified several new compounds and pathways relevant to cystogenesis using a zebrafish *pkd2* model and provided the first evidence of a non-redundant function for *pkd2* in the zebrafish kidney. The zebrafish *pkd2* mutant will continue to be a useful model to study ADPKD pathogenesis and potential treatments.

Acknowledgements

First and foremost, I would like to thank my two supervisors for their continuous support during this project. I am especially grateful to Albert Ong who has given me the opportunity to work with him, one of the leaders in the field of ADPKD, on a project of this scale. He provided the intellectual background and helped steer the project into the right direction. Freek van Eeden, my secondary supervisor, always had an open door for me and tirelessly provided methodological and moral support. Thank you both for helping my project and me in the past three years. Needless to say, without your support I could not have done it.

Eleanor Markham, Freek's technician who tirelessly maintained my fish lines and helped out whenever asked, deserves a special "thank you". Without her I would not have managed. Sarah Baxendale helped with setting up the compound screen, Morgane Lannoy imparted her knowledge on the cell culture assays and the aquarium staff did a great job with fish maintenance and providing knowledgeable help. Thank you also to all the others in the van Eeden, Ong, Wilkinson, Bandmann and Chico labs for lending a hand or an ear during different phases in my project.

Special thanks also goes to the Bateson Centre in general, which connects so many people with its interdisciplinary approach and to the TranCYST ITN for providing opportunities to present my work on meetings across Europe and giving feedback from a variety of specialties.

Thank you also to all my friends here in Sheffield, who shared my experience as PhD student. Most of us are far away from home and I am grateful that we have formed our own little family here in the UK.

I would also like to thank our funding bodies, without whom this project would not have been possible: EU-FP7/2007-2013, grant agreement no. 317246 (TranCYST) funded my research as Marie Curie Early Stage Researcher. The small molecule screening was carried out in the Sheffield Zebrafish Screening Unit supported by the MRC Pump Priming grant G0802527 and the lightsheet microscopy for zebrafish imaging was funded by the British Heart Foundation, grant BHF IG 142370.

Last but not least, I would like to direct a few words to my family and friends back home in Germany in our native tongue:

Danke liebe Familie und liebe Freunde für den Rückhalt, den ihr mir während dieses Projekts gegeben habt - ohne euch wäre das hier nicht möglich gewesen. Danke Mama und Papa; ihr habt immer an mich geglaubt und mir gelegentlich auch mal einen Schubs in die richtige Richtung gegeben. Und ein ganz besonderer Dank geht an Chris, meinen Wegbegleiter seit nunmehr 10 Jahren - du bist mein Fels in der Brandung.

Table of Contents

Abbreviations

11-KT	11-ketotestosterone
2-APB	2-aminoethoxydiphenyl borate
aa	amino acids
AC	adenylate cyclase
ADPKD	autosomal-dominant polycystic kidney disease
ALK	activin receptor-like kinase
AR	androgen receptor
ARPKD	autosomal-recessive polycystic kidney disease
avpr	Arginine vasopressin receptor
BFA	Brefeldin A
bp	base pairs
CaMK-II	Ca^{2+}/calmodulin-dependent protein kinase type II
cAMP	cyclic adenosine monophosphate
cmlc2	*cardiac myosin light chain 2*
col2a1	collagen type II alpha 1
Cox-II	cyclooxygenase-II
CRISPR	clustered regularly interspaced short palindromic repeats
CT	computer tomography
DAPT	N-[N-(3,5-Difluorophenacetyl)-L-alanyl]-S-phenylglycine t-butyl ester
DHT	dihydrotestosterone
DMEM	Dulbecco's Modified Eagle Medium
DMSO	Dimethyl sulfoxide
dpf	days post fertilisation
ECM	extracellular matrix
EDTA	ethylenediaminetetraacetic acid
EGFR	epidermal growth factor receptor
ENU	*N*-ethyl-*N*-nitrosourea
ER	endoplasmic reticulum
ERK	extra-cellular-signal-regulated kinase
ESRD	end-stage renal disease
EtOH	ethanol
FC	flashing cell
FDA	Food and Drug Administration
FFC	frequently flashing cell
G3PDH	glycerol-3-phosphatase dehydrogenase
GABA	gamma-aminobutyric acid
GFP	green fluorescent protein
GFR	glomerular filtration rate
GSK	GlaxoSmithKline
HDAC	histone deacetylase
hEGF	human epidermal growth factor
hpf	hours post fertilisation
IFT	intraflagellar transport
IP3R	inositol trisphosphate receptor
JAK	Janus kinase
KDR	kinase insert domain receptor
kif3a	Kinesin family member 3A
KV	Kupffer's vesicle
L/R	left/right axis

LB	lysogeny broth
LCC	L-type calcium channel
LDWT	London wildtype
MAP4K4	mitogen-activated protein kinase kinase kinase kinase 4
MAPK	mitogen-activated protein kinase
MDCK	Madin-Darby canine kidney
MEK	mitogen-activated protein kinase kinase
MeOH	methanol
MO	morpholino or morphant
MRI	magnetic resonance imaging
mTOR	mammalian target of rapamycin
PBS	phosphate buffered saline
PBTw	phosphate buffered saline with Tween20
PC1	polycystin 1
PC2	polycystin 2
PCR	polymerase chain reaction
PDE	phosphodiesterase
PFA	paraformaldehyde
PGE2	prostaglandin E2
PGH2	prostaglandin H2
pH3	phospho-histone H3
PI3K	phosphoinositide 3-kinase
PKD	polycystic kidney disease
Pkd1	polycystin 1
Pkd1l	polycystin 1-like
Pkd2	polycystin 2
Pkd2l	polycystin 2-like
PKIS	published kinase inhibitor set
PTU	phenylthiourea
RCF	recurrently flashing cell
RYR	ryanodine receptor
SAP	shrimp alkaline phosphatase
SDS	sodium dodecyl sulfate
SEM	standard error of the mean
SSC	saline-sodium citrate buffer
STAT	Signal Transducer and Activator of Transcription
STIM	stromal interaction molecule
TGFBR1	transforming growth factor-beta receptor type-1
traf3ip1	Tumor necrosis factor receptor associated factor 3 interacting protein 1
TRP	transient-receptor potential
TRPP2	transient-receptor potential polycystic 2
TRPV4	transient-receptor potential cation channel subfamily V member 4
TSA	trichostatin A
TSC	tuberous sclerosis
UNC	University of North Carolina
vegf	vascular endothelial growth factor
VP2R	vasopressin V2 receptor
VPA	valproic acid
WT	wildtype
wt1b	Wilms tumour 1 b

Introduction

1. PKD – polycystic kidney disease

ADPKD, autosomal-dominant polycystic kidney disease, is one of the most common monogenic diseases worldwide with estimated incidences of 1/400 to 1/1000 (Sutters *et al.*, 2003). Although the prevalence of diagnosed ADPKD cases varies between populations, potentially due to differences in screening policy and health care delivery, autopsy studies suggest that more than 1/500 people could be affected (Chan, 1993; Dalgaard, 1957).

In ADPKD, the diseased kidneys contain numerous fluid-filled epithelial cysts (see Figure 1 A) which may develop from any part of the nephron and cause bilateral renal enlargement. Cysts arise as spherical dilatations or small out-pouchings, enlarge progressively and eventually separate from the rest of the renal tubule. Cyst development is generally accompanied by the destruction of renal parenchyma, interstitial fibrosis, cellular infiltration and loss of functional nephrons (reviewed in (Chang *et al.*, 2008)). However, cysts are not limited to the kidneys and extrarenal manifestations most commonly include cysts in the liver, but also in the spleen, pancreas, arachnoid membrane and seminal vesicles. Other non-cystic vascular manifestations such as intracranial arterial aneurysms, artery dissections and coronary artery aneurysms are present in a minority of patients (reviewed in (Torres & Harris, 2009)).

Typically, ADPKD patients present between 20 - 40 years of age but cases in childhood (under 15 years) and even *in utero* have been reported. Common symptoms include abdominal pain, polyuria, urinary tract infections, haematuria and hypertension (reviewed in (Loftus *et al.*, 2013) and (Wilson, 2004b)). Abdominal pain is the most reported symptom in adults and can be caused by cyst haemorrhage, infection or renal stones. Around half of all ADPKD patients will have reached end-stage renal disease (ESRD) by the fifth decade of life (Hateboer *et al.*, 1999). Glomerular filtration remains normal in most patients until the fourth to sixth decade of life, despite the constant growth of cysts, due to compensatory hyperfiltration. By the time filtration rates decline, the kidneys are markedly enlarged and distorted.

Diagnosis typically relies on imaging techniques. For cost and safety reasons, renal ultrasound is the most widely used method. However, MRI (magnetic resonance imaging) or CT (computer tomography) provide increased sensitivity to detect smaller cysts. CT or MRI render pictures at much higher resolutions and cysts of 3 mm rather than 10 mm are easily detected (Bae *et al.*, 2010).

ADPKD accounts for ca. 10 % of patients with ESRD which translates into ca. 35,000 patients across Europe – making ADPKD the fourth most common cause of ESRD (Torres *et al.*, 2007). The clinical and economic burden caused by this disease is enormous with an estimated annual cost of € 1.5 billion for ESRD within the 27 EU-member states alone (currently including the UK) (Spithoven *et al.*, 2014). Risk factors for ADPKD include genotype, age, sex, kidney function and total kidney volume (reviewed in (Ong *et al.*, 2015)). Of note, males with ADPKD typically have a faster progression and larger cystic kidneys than female patients (Cornec-Le Gall *et al.*, 2013; Harris *et al.*, 2006).

To date, only one drug has been approved to slow the progression of ADPKD (tolvaptan). However, this treatment is associated with high rates of adverse effects related to increased aquaresis (thirst, polyuria and nocturia, (Torres *et al.*, 2012)) and a low incidence of liver toxicity. A preventative treatment for this devastating disease has not yet been found.

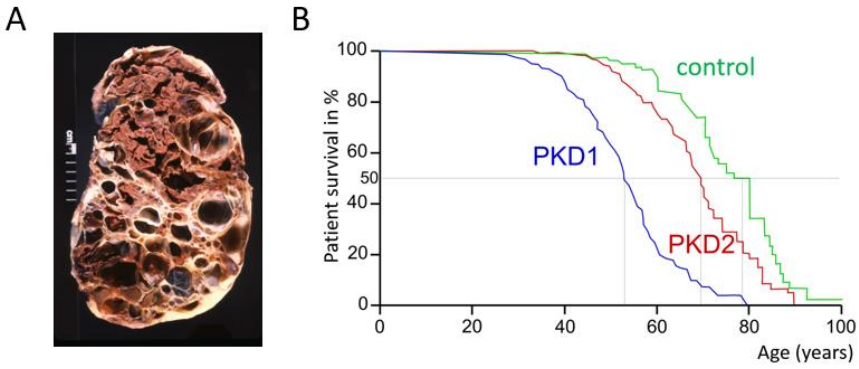

Figure 1 (A) Image of a polycystic kidney with a plethora of cysts by Ed Uthman from Houston, TX, USA - Adult Polycystic Kidney, CC BY 2.0, https://commons.wikimedia.org/w/index.php?curid=3062826. (B) Survival rates of heathly controls (green), patients with a *PKD2* mutation (red) and patients with a *PKD1* mutation (blue) by age based on data in (Hateboer *et al.*, 1999).

2. The genetic basis of ADPKD

Two genes have been linked to ADPKD: *PKD1*, which harbours mutations in ca. 85 % of patients, and *PKD2,* accounting for the remaining 15 %. Mutations in *PKD2* are characterised by a later onset and slower rate of progression to ESRD (*PKD1* 53.0 years and *PKD2* 69.1, see Figure 1 B, (Hateboer *et al.*, 1999)) but phenotypically, patients with mutations in *PKD1* and *PKD2* are clinically indistinguishable. The existence of a third gene causing ADPKD, *PKD3*, was debated in the past but has now largely been excluded (Paul *et al.*, 2014).

Patients with a truncating mutation in *PKD1* generally have the worst renal prognosis. Non-truncating mutations of *PKD1* result in intermediate progression rates and *PKD2* mutations show the best prognosis (reviewed in (Ong *et al.*, 2015)). Slower disease progression with *PKD2* mutations has been attributed to the formation of fewer cysts in the early stages of

disease rather than slower cyst growth (Harris *et al.*, 2006). Intriguingly, mutations in the 5' half of *PKD1* also correlate with earlier onset of renal failure and more frequent aneurism ruptures compared to mutations in the 3' half (Rossetti *et al.*, 2003) – however, this has not been confirmed in later studies (Cornec-Le Gall *et al.*, 2013). No such associations have been reported for *PKD2* (Magistroni *et al.*, 2003). Deleterious mutations in either one or both *PKD* genes have been shown to always result in the clinical ADPKD phenotype (Giamarchi *et al.*, 2010; Newby *et al.*, 2002). Transheterozygous patients ($PKD1^{+/-}$;$PKD2^{+/-}$) have also been reported and exhibit a more severe clinical progression than simple heterozygotes (Pei *et al.*, 2001). A strong intrafamilial phenotypic variability, even with identical mutations, suggests additional modifiers, which could be either genetic or environmental (Persu *et al.*, 2004).

The two protein products of *PKD1* and *PKD2*, PC1 (polycystin-1) and PC2 (polycystin-2) respectively, form a heterodimeric complex via their C-terminal tails (see Figure 2 A) which is thought to function as a receptor-ion channel. The PC1/PC2 complex is interacts with a variety of other proteins regulating multiple signalling pathways that maintain tubular structure and function in the kidney (reviewed in (Ong & Harris, 2005b)).

There has been a consensus that the PC1/PC2 complex acts as mechanosensor in primary cilia mediating flow-dependent Ca^{2+} influx which in turn activates Ca^{2+} release from intracellular stores like the ER, e.g. via PC2, see Figure 2 B (Koulen *et al.*, 2002; Nauli *et al.*, 2003) – although this has been recently disputed (Delling *et al.*, 2013). Cystic cells isolated from ADPKD patients lack flow-sensitive calcium signalling, show reduced ER calcium stores and lower intracellular calcium concentrations (Xu *et al.*, 2007). Manipulation of a single primary cilium in cultured canine kidney cells caused an increase in intracellular calcium levels in the stimulated cell as well as the surrounding ones (Praetorius, Frokiaer*, et al.*, 2003; Praetorius *et al.*, 2001; Praetorius & Spring, 2003). Cells treated with antibodies for *PKD1* and *PKD2* did not show these calcium transients, which are dependent on intracellular and extracellular calcium pools (Koulen *et al.*, 2002; Nauli *et al.*, 2003). This suggests the PC1/PC2 complex initiates flow-induced intracellular calcium signalling. Overexpression, haploinsufficiency or absence of PC2 gradually decreases Ca^{2+} release form intracellular stores (Torres & Harris, 2009).

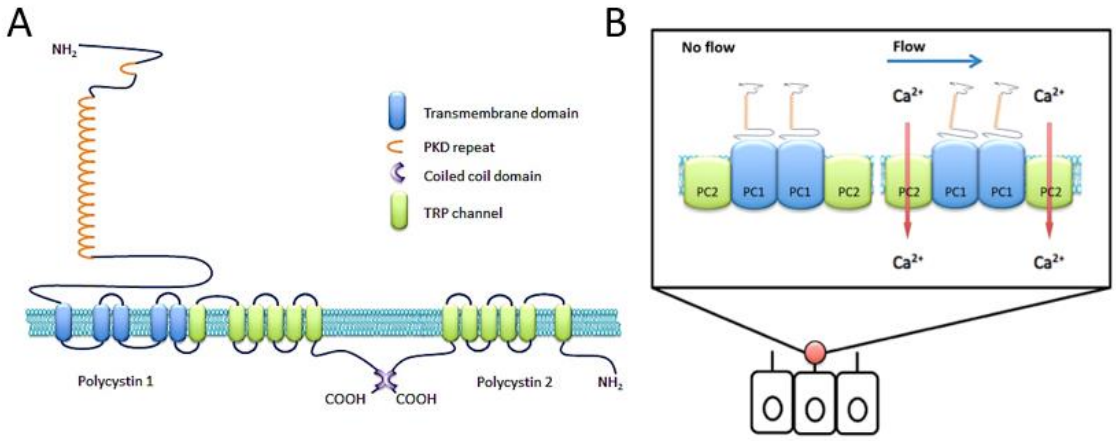

Figure 2 (A) Diagram of the PC1 (left) and the PC2 (right) and their interaction through coiled-coil domains in the C-termini. Homology domains are shown in the key. (B) Polycystin complex as mechanosensory calcium channel in primary cilia without and with flow (left and right respectively).

3. The polycystin family across various species

In the next paragraphs, protein structure, expression, interaction partners and putative functions of PC1 and PC2 will be described in detail with a focus especially on human, rodent and zebrafish data. Zebrafish were the main model organism studied during this project and are therefore focussed on particularly. Similarly, there will be a greater focus on *PKD2* and PC2, as a knockout model of this gene was used. A more detailed account of zebrafish and their value as model will be given in the following chapters: "Zebrafish as a model organism" and "Zebrafish models of ADPKD: *pkd*-deficient embryos".

Figure 3 depicts the evolutionary relationships of *PKD1* and *PKD2* (A and B respectively) in humans, mice and zebrafish with orthologue sequence identity given in percent. The zebrafish *pkd1b* gene is missing in Figure 3 A, as current database annotations suggest it is not a direct orthologue of human *PKD1*.

To clarify, human polycystin genes are referred to as *PKD* genes, rodent orthologues are *Pkd* genes and the zebrafish varieties are denoted as *pkd* genes. These traditional denominations will be upheld throughout the text and will help identify the referenced species.

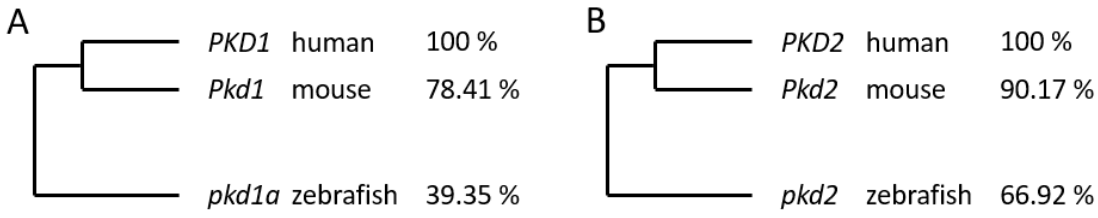

Figure 3 Schematic evolutionary trees of (A) *PKD1* and (B) *PKD2* genes of *Homo sapiens*, *Mus musculus* and *Danio rerio* with sequence identiy in percent. Data derived from the Ensembl database (http://www.ensembl.org), August 19th 2016.

3.1. Human *PKD1*

PKD1 was identified in 1995 by the International Polycystic Kidney Disease Consortium (The International Polycystic Kidney Disease Consortium, 1995) and is located on chromosome 16p13.3 and translates into the 460 kDa polycystin-1 protein. It is a 4,302-amino acid type I membrane glycoprotein with a long N-terminal extracellular domain (3,074 amino acids), 11 transmembrane domains (1132 aa) and a short intracellular C-terminus (197 aa) (Hughes *et al.*, 1995). PC1 interacts with PC2 via a coiled-coil domain in the C-terminus to form a heterodimer (Figure 2 A); this interaction has been shown to be critical for functional regulation of both proteins (Newby *et al.*, 2002).

The entire PC1 N-terminus has been proposed to have the biomechanical properties of a mechanosensor (Qian *et al.*, 2005). It might sense laminar flow in the nephric tubules and trigger a PC2-dependent Ca^{2+} signal, hence acting as a sensor for the glomerular filtration rate (Figure 2 B) (Qian *et al.*, 2005). In addition to its mechanosensory function, the PC1/PC2 complex has been implicated in mediating or regulating cell-cell and cell-matrix adhesion (reviewed in (Wilson, 2011)). Homotypic PC1 interactions via the PKD domains and heterophilic interactions of PC1 with the E-cadherin/catenin complex (and other proteins), as well as increased integrin-mediated adhesiveness to collagen in PKD cyst cells have been described (Huan *et al.*, 1999; Ibraghimov-Beskrovnaya *et al.*, 2000; Roitbak *et al.*, 2004; Streets *et al.*, 2003; Streets *et al.*, 2009; Wilson *et al.*, 1999).

PC1 has been localised to multiple subcellular locations in renal epithelial cells including primary cilia, cytoplasmic apical vesicles, focal adhesions and a variety of lateral membrane junctions (tight junctions, adherens junctions and desmosomes) (Boletta *et al.*, 2001; Griffin *et al.*, 1996; Huan *et al.*, 1999; Kim *et al.*, 2000; Newby *et al.*, 2002; Scheffers *et al.*, 2000; Wilson *et al.*, 1999; Yoder *et al.*, 2002), reviewed in (Ong, 2000)).

In humans, 40 splice variants of *PKD1* and three paralogues have been reported (listed in Table 1) (Martin *et al.*, 2004). To date (accession 18.08.2016), 2323 different *PKD1* mutations have been identified in patients, of which 1895 are definitely pathogenic, most of them unique to a single family (Autosomal Dominant Polycystic Kidney Disease Mutation Database: PKDB, http://pkdb.mayo.edu/).

Gene name & Ensembl identifier	Length in aa	Length in bp (cDNA)	Chromosome	ID %
PKD1 ENSG00000008710	4302	14138	16	
PKD1L1 ENSG00000158683	2849	9092	7	14.74
PKD1L2 ENSG00000166473	2459	7379	16	25
PKD1L3 ENSG00000277481	1732	5199	16	16.40

Table 1 The *PKD1* family in *Homo sapiens*. Data derived from the Ensembl database (http://www.ensembl.org), August 18th 2016.

3.2. *Pkd1* in model organisms

Pkd1 was first fully sequenced in mice in 1995 (The International Polycystic Kidney Disease Consortium, 1995) and many knockout and overexpression mouse strains have been created since. Homozygous knockout models are almost all embryonic lethal (Kim *et al.*, 2000; Lantinga-van Leeuwen *et al.*, 2007; Lu *et al.*, 2001). In mice, *Pkd1* is expressed at high levels in embryos but down-regulated shortly after birth (reviewed in (Ong & Harris, 2005b)). Levels of *Pkd1* expression have been increased and decreased in mice, both of which resulted in cystic kidney phenotypes - stressing the importance of PC1 dosage for normal tissue architecture (Lantinga-van Leeuwen *et al.*, 2004; Pritchard *et al.*, 2000). Conditional *Pkd1* knockouts show varying progressions of PKD but the developmental stage at which gene inactivation occurs, determines disease severity (Piontek *et al.*, 2007; Takakura *et al.*, 2009). In one model, inactivation of *Pkd1* before postnatal day 13 results in severe cystic kidneys within 3 weeks, whereas inactivation at day 14 or later results in cysts only after 5 months (Piontek *et al.*, 2007). Of note, heterozygous *Pkd1* knockout mice without symptoms also exhibit decreased intracellular Ca^{2+} levels at approximately half of WT concentrations, although these animals did not develop cysts (Ahrabi *et al.*, 2007). Cartilage defects like an undulating spinal chord and jaw phenotypes have been observed in addition to cystic kidneys in *Pkd1* knockout animals (Boulter *et al.*, 2001; Kolpakova-Hart *et al.*, 2008).

In zebrafish, *pkd1* is present as two paralogous genes, *pkd1a* and *pkd1b,* that are more closely related to human *PKD1* than the *PKD1L* orthologues (Mangos *et al.*, 2010). *pkd1a* is broadly expressed in chondrogenic tissues and *pkd1b* is primarily expressed in the nervous system (Mangos *et al.*, 2010). *pkd1a* knockdown results in hydrocephalus, jaw defects and kidney cysts (but only in 10 - 20 % of morphant embryos) and *pkd1b* knockdown does not cause a visible phenotype. Disruption of both *pkd1* paralogues however, results in a multi-organ phenotype similar to *pkd2* loss-of-function but without L/R asymmetry defects (see below, (Mangos *et al.*, 2010)). This suggests that *pkd1b* may have overlapping or redundant functions with *pkd1a*, and its knockout is necessary for a fully penetrant phenotype (Mangos *et al.*, 2010). In *pkd1* double knockdown zebrafish, renal dilations were observed in ca. 20 % of the embryos.

Tissue expression of murine *Pkd1* is similar to zebrafish - occurring in the notochord, floor plate as well as other chondrogenic tissues (Boulter *et al.*, 2001), but has also been detected in the perichondrial mesenchyme in the head (Lu *et al.*, 2001). Delayed ossification of the skull and spinal chord in *Pkd1*-deficient animals are similar in both species (Lu *et al.*, 2001; Mangos *et al.*, 2010). The low penetrance of cyst formation seen in *pkd1* knockdown zebrafish

experiments mimics that of gene knockout after post-natal day 14 in juvenile mice and may suggest the necessity of additional factors than *Pkd1* mutation for cysts formation (Piontek *et al.*, 2007; Takakura *et al.*, 2008). The mouse orthologues of human *PKD1* and *PKD1L1* genes are listed in Table 2.

Ensembl identifier & gene name	Length in aa	Length in bp (cDNA)	Chromosome	ID %
Pkd1 ENSMUSG00000032855	4293	14170	17	100
Pkd1l1 ENSMUSG00000046634	2521	7631	11	15.59
Pkd1l2 ENSMUSG00000034416	2461	7386	8	17.64
Pkd1l3 ENSMUSG00000048827	2201	6606	8	14.40

Table 2 The *Pkd1* family in *Mus musculus*. Data derived from the Ensembl database (http://www.ensembl.org), August 18th 2016.

Zebrafish gene annotations are less sophisticated for the *pkd1*-family compared to mammals. Furthermore, there are five paralogues, one of which has not yet been annotated. Currently, no *pkd1l1* and *pkd1l3* genes are annotated, although there were at the beginning of this project, suggesting a recent change in annotations.

Ensembl identifier & gene name	Length in aa	Length in bp (cDNA)	Chromosome	ID %
pkd1a ENSDARG00000030417	3629	15472	1	100
pkd1b ENSDARG00000033029	3827	12367	12	25.27
pkd1l2a ENSDARG00000105344	1124	4430	7	19.75
pkd1l2b ENSDARG00000101214	1442	6338	7	19.69
ENSDARG00000099162	2153	6459	24	17.47

Table 3 The *pkd1* family in *Danio rerio*. Data derived from the Ensembl database (http://www.ensembl.org), August 18th 2016.

3.3. Human *PKD2*

PKD2 was identified in 1996 (Mochizuki *et al.*, 1996), is located on chromosome 4p21 and gives rise to the 110 kDa polycystin-2 protein. It is a 968-amino acid type II membrane glycoprotein with six-transmembrane domains and intracellular N- and C-termini. The N-terminus contains a ciliary-targeting RVxP motif (Arginine, Valine, X, Proline) (Geng *et al.*, 2006). *PKD2* has significant homology to the transient receptor potential (TRP) family of store-operated calcium channels and is likely to function similarly as a non-selective calcium channel, hence its further denomination as *TRPP2* (Giamarchi *et al.*, 2006). It can function both alone or in the presence of PC1 (Gonzalez-Perrett *et al.*, 2001; Hanaoka, Qian, *et al.*, 2000; Qian *et al.*, 1997).

PC2 has been localised to primary cilia, apical monocilia, endoplasmic reticulum (ER)/Golgi membranes, lamellipodia, mitotic spindles and the basolateral cell surface. Unlike *PKD1*, its expression appears to be maintained at a constant level into adult life (Cai *et al.*, 1999; Foggensteiner *et al.*, 2000; Gallagher *et al.*, 2000; Luo *et al.*, 2003b; Newby *et al.*, 2002; Ong & Harris, 2005b; Rundle *et al.*, 2004). Apical monocilia can function as mechanosensory flow sensors with intracellular calcium release in response to cilia bending and PC2 antibodies have been shown to block this flow-induced calcium release (Nauli *et al.*, 2003; Praetorius *et al.*, 2001).

To date (accession 17.08.2016), 463 different *PKD2* mutations have been identified of which 438 are definitely pathogenic, most of them unique to a single family (Autosomal Dominant Polycystic Kidney Disease Mutation Database: PKDB, http://pkdb.mayo.edu/). In humans, seven splice variants and two paralogues have been reported for *PKD2*, the latter are listed in Table 4.

Gene name & Ensembl identifier	Length in aa	Length in bp (cDNA)	Chromosome	ID %
PKD2 ENSG00000118762	968	5056	4	100
PKD2L1 ENSG00000107593	805	3043	10	48.45
PKD2L2 ENSG00000078795	523	2333	5	46.47

Table 4 The *PKD2* family in *Homo sapiens*. Data derived from the Ensembl database (http://www.ensembl.org), August 18th 2016.

3.4. *Pkd2* in model organisms

Pkd2 is a Ca^{2+}-permeable cation channel associated with primary cilia and proposed to be involved in a ciliary mechanosensory complex. In the zebrafish pronephros, *pkd2* has been localised to the basolateral membrane as well as luminal cilia, suggesting it may function both as a ciliary mechanosensory channel as well as a Ca^{2+} release channel in ER membranes (Obara *et al.*, 2006). Mammalian studies have localised PC2 to intracellular ER and Golgi membranes and to apical, non-motile cilia of renal epithelia and mouse node cells (Foggensteiner *et al.*, 2000; Pazour *et al.*, 2002). *Pkd2* loss-of-function has been shown to cause L/R patterning defects in mice and in zebrafish (Bisgrove *et al.*, 2005; Pennekamp *et al.*, 2002).

Mouse knockouts of *Pkd2* develop embryonic kidney cysts, vascular and heart septal defects and randomized organ laterality (Pennekamp *et al.*, 2002; Wu *et al.*, 2000). In mouse models with targeted disruption of *Pkd1* or *Pkd2,* renal development progresses normally until embryonic day 14.5 when cysts begin to form (Boulter *et al.*, 2001; Kim *et al.*, 2000; Lu *et al.*, 1997; S. Muto *et al.*, 2002; Wu *et al.*, 1998). This suggests that polycystins are not essential for nephron induction but for maturation and maintenance of the tubular architecture (Ong &

Harris, 2005b). Homozygous *Pkd2* knockout mice usually die in the embryonic period; in heterozygous animals, a mild renal cyst phenotype can be detected in older mice but is highly variable (Boulter *et al.*, 2001; Lu *et al.*, 1997). Mouse orthologues of *PKD2* and *PKD2L* genes are listed in Table 5.

Ensembl identifier & gene name	Length in aa	Length in bp (cDNA)	Chromosome	ID %
Pkd2 ENSMUSG00000034462	966	5219	5	100
Pkd2l1 ENSMUSG00000037578	760	3321	19	49.74
Pkd2l2 ENSMUSG00000014503	621	2421	18	44.44

Table 5 The *Pkd2* family in *Mus musculus*. Data derived from the Ensembl database (http://www.ensembl.org), August 18th 2016.

Pkd2, unlike *Pkd1,* mutations cause asymmetry defects in murine and zebrafish models. PC2 in the monocilia of the mouse embryonic node or the zebrafish equivalent, the Kupffer's vesicle (Essner *et al.*, 2002), could mediate asymmetric Ca^{2+} signalling prior to L/R (left/right) establishment (McGrath *et al.*, 2003). *Pkd1* has not been linked to this phenotype; however, recent studies have revealed *Pkd1l1* to be expressed in the node and mutations in this paralogue lead to L/R asymmetry defects in mice (Field *et al.*, 2011; Kamura *et al.*, 2011). Interestingly, no significant differences have been detected regarding cilia number or length in the zebrafish Kupffer's vesicle in *pkd2* morphants or in the mouse embryonic node of *Pkd2* mutants (Bisgrove *et al.*, 2005; McGrath *et al.*, 2003; Obara *et al.*, 2006). This indicates that in *Pkd2* mutants, ciliary structure is normal, but signal transduction is disrupted.

In zebrafish, *pkd2* is located on chromosome 1, consists of 3336 bp (14 exon mRNA, 904 aa protein) and shares 67 % conservation compared to human *PKD2*. Zebrafish *pkd2* knockdown animals (morphants) exhibit a 51 % rate of reverse heart looping and a similar rate for gut looping (Bisgrove *et al.*, 2005). At 40 hpf, *pkd2* morphants have a rather unique phenotype: an upward curled tail, hence the further denomination of the *pkd2* mutant - *curly up* or *cup* (from when it was isolated in a phenotype-based screen in the mid-1990's (Brand *et al.*, 1996)). In addition to L/R asymmetry and body axis defects, *pkd2* morphants exhibit cystic kidneys, cardiac oedema and hydrocephalus; phenotypes also found in *Pkd2* mouse mutants (Wu *et al.*, 1998; Wu *et al.*, 2000). One previous study suggests that the mechanisms leading to the formation of pronephric cysts in *pkd2*-deficient zebrafish are different from other cystic mutants (Sullivan-Brown *et al.*, 2008). Notably, cyst development seems to be restricted to the glomerulus in *pkd2* morphants, contrary to general dilations in other cystic mutants. Obara et al. reported evidence that supports the theory of a partial occlusion of the pronephric tubules, which could lead to a build-up of fluid causing glomerular dilatation (Obara *et al.*, 2006). However, "cystic kidneys" of *pkd2* knockdown and ciliary knockout

models as described in the zebrafish literature are rather dilated glomeruli and not truly renal cysts.

In early development, *pkd2* mRNA is widely expressed in the zebrafish embryo; the domains of highest expression later becoming ciliated tissues, including the pronephric duct primordia and the Kupffer's vesicle (KV). Maternal *pkd2* was not observable by *in situ* hybridisation (Bisgrove *et al.*, 2005) although it has been detected using RT-PCR (Schottenfeld *et al.*, 2007; Sun *et al.*, 2004). Zygotic expression is initiated at the onset of gastrulation in the blastoderm margin. At this point, *pkd2* is found in the hypoblast of the dorsal midline and to the dorsal forerunner cells. In the early somite stages, *pkd2* is ubiquitously expressed but with higher expression in the KV which persists to the 6-somite stage. Subsequently, expression is detected in the pronephric duct primordia and the neural floorplate and at 24 hpf, in the brain. Later, at 3 dpf, *pkd2* expression is reduced to the pharyngeal arches and the pectoral fin buds (Bisgrove *et al.*, 2005).

The expression patterns of *pkd2* and *pkd1a* overlap partially, particularly around the Kupffer's vesicle at the tailbud stage, the head regions at 24 hpf, the pharyngeal arches and pectoral fins at 72 hpf. There are no discernible regions of co-expression of *pkd2* and *pkd1b*. Table 6 lists the annotated *pkd2* and *pkd2l* genes in zebrafish, however at this stage no *pkd2l2* paralogue has been identified.

Ensembl identifier & gene name	Length in aa	Length in bp (cDNA)	Chromosome	ID %
pkd2 ENSDARG00000014098	904	3336	1	100
pkd2l1 ENSDARG00000022503	790	2718	13	45.19

Table 6 The *pkd2* family in *D. rerio*. Data derived from the Ensembl database (http://www.ensembl.org), August 18th 2016.

In zebrafish, both *pkd1* orthologues (a and b) and *pkd2* have been reported to regulate extracellular matrix (ECM) formation and a malfunction of this regulation leads to the development of a dorsal axis curvature (Mangos *et al.*, 2010). Knockdown of *col2a1* mRNA (*collagen II type alpha 1*) or the use of collagen-crosslinking inhibitors rescued the curly tail phenotype. It has been suggested that PC1 and/or PC2 regulate a negative feedback loop that normally inhibits deposition of multiple collagens (Mangos *et al.*, 2010). An altered ECM status has been associated with the ADPKD phenotype in human and animal tissues as well as cell culture models (Candiano *et al.*, 1992; Igarashi *et al.*, 2002; Malhas *et al.*, 2002; Schafer *et al.*, 1994; Somlo *et al.*, 1993; Subramanian *et al.*, 2012). In mRNA profiling studies on kidneys of a PKD rat model (Han:SPRD), matrix genes are prominently upregulated in cystic tissues (Riera *et al.*, 2006). It appears polycystins are required for the transition from persistently collagen-expressing embryonic cells to a mature differentiated phenotype and a

disruption leads to an overproduction of ECM and a distortion of the embryonic axis (Mangos *et al.*, 2010).

Apart from PC1, PC2 has been reported to interact with a number of key proteins including fibrocystin, inositol trisphosphate receptor (IP3R), ryanodine receptor (RYR) and several other TRP channels (reviewed in (Mangolini *et al.*, 2016)). The association of PC2 with a variety of other calcium channels especially in the ER (IP3R, RYR, (Anyatonwu *et al.*, 2007; Li *et al.*, 2005)) and in primary cilia (TRPV4, (Kottgen *et al.*, 2008)) suggest a pleiotropic role of PC2 in cellular calcium signalling – some of these interaction partners are depicted in Figure 4 and will be elaborated upon in greater detail in the next two chapters. Protein phosphorylation can regulate PC2 trafficking and localisation: retrograde trafficking between the ER, Golgi and plasma membrane is dependent on Ser812 (Kottgen *et al.*, 2005) and the N-terminal Ser76 is critical for localization to the lateral plasma membrane but not to primary cilia (Streets *et al.*, 2006).

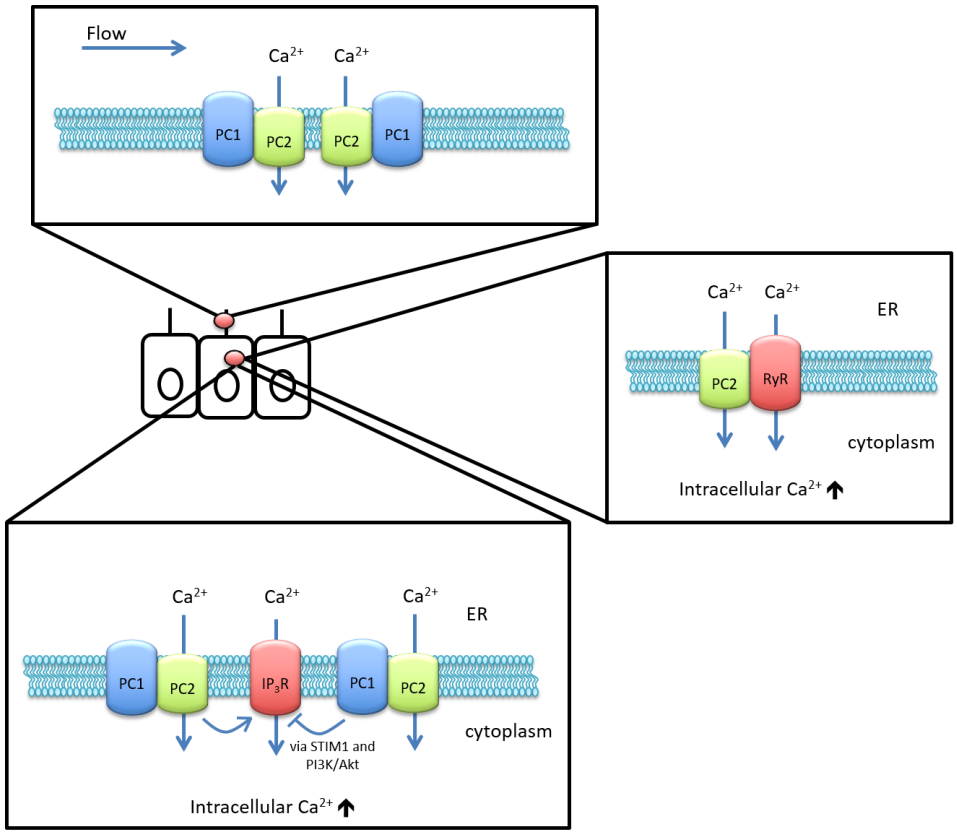

Figure 4 PC1 and PC2 in various cellular compartmens and their putative interaction partners. ER: endoplasmic reticulum, IP3R: inositol triphosphate receptor, RYR: ryanodine receptor, STIM: stromal interaction molecule, PI3K: phosphoinositide 3-kinase.

4. Why do cysts form?

Two main hypotheses have been proposed as to why and how renal cysts form in ADPKD: a two-hit model and a threshold model. Both hypotheses have merits in their own rights, but neither fully explains the situation and it is possible that a combination of the two represents the truth. Additionally, a third hypothesis has been proposed recently, the "third-hit" hypothesis, which might involve stress factors such as renal injury (Weimbs, 2011).

To explain the focal nature of the cysts, since only ~ 1 % of nephrons develop cysts in ADPKD, a two-hit mechanism with loss-of-heterozygosity has been proposed (Germino, 1997; Grantham *et al.*, 1987; Pei *et al.*, 1999; Qian *et al.*, 1996; Wu *et al.*, 1998). In this model, a germline mutation in one allele and a somatic mutation/reduced expression of a second allele of either *PKD* gene is required for cystogenesis (Pei *et al.*, 1999; Watnick *et al.*, 1998; Wu *et al.*, 2002).

The second theory on how cysts form is called haploinsufficiency, or threshold model. Here, the loss of one allele leads to a 50% reduction in gene dosage and despite the presence of a normal allele, a phenotype arises due to stochastic changes in protein concentration (Lantinga-van Leeuwen *et al.*, 2004). This hypothesis is supported by the observation that hypomorphic alleles can cause cyst formation (Hopp *et al.*, 2012; Jiang *et al.*, 2006; Pei *et al.*, 2012) and the severity of cyst formation has been linked to quantitative changes in gene dosage of *Pkd1* in mouse models: ~40 % PC1 cause a slowly progressive form and ~20 % PC1 a rapidly progressing form of ADPKD (Hopp *et al.*, 2012). The precise thresholds could vary between animals, developmental stages, tissues, cell types and nephron segments (Fedeles *et al.*, 2011; Piontek *et al.*, 2007; Raphael *et al.*, 2009). Interestingly, in all ADPDK model organisms, even in hypomorphs, cyst development is focal (Hopp *et al.*, 2012).

To this date it remains unclear how the loss of polycystin-function leads to the clinical phenotype, but five key cellular abnormalities associated with cyst formation have been identified: Increased cell proliferation and apoptosis, enhanced fluid secretion, abnormal cell-matrix interactions, alterations in cell polarity and abnormal ciliary structure or function (reviewed in (Chang *et al.*, 2008) and (Wilson, 2011)). How these are linked to mutations in *PKD1* or *PKD2* remains largely unclear. Two of the most consistent signalling abnormalities reported in ADPKD models are changes in intracellular calcium and cAMP concentrations, the former is reduced and the latter elevated in patient tissues and models (reviewed in (Mangolini *et al.*, 2016; Torres *et al.*, 2006)). Most of the key abnormalities mentioned above could be directly or indirectly linked to this deregulation of Ca^{2+} and cAMP and will be elaborated upon in the next paragraphs (illustration of interactions in Figure 5).

Upon activation, the PC1/PC2 complex is thought to initiate extracellular Ca^{2+} entry, which in turn triggers Ca^{2+} release from internal stores. High intracellular Ca^{2+} levels inhibit the production of cAMP by inhibiting Ca^{2+}-sensitive cAMP-synthesising adenylate cyclases (AC5 and AC6) or stimulating Ca^{2+}-sensitive phosphodiesterases (PDE1) which hydrolyse cAMP (Choi *et al.*, 2011; Sussman *et al.*, 2014; Torres *et al.*, 2014; Ye *et al.*, 2016). In ADPKD however, Ca^{2+} levels are decreased and consequently cAMP concentrations increase (Yamaguchi *et al.*, 2006). The exact causes of this decrease in intracellular Ca^{2+} remain debated but it has been hypothesised that loss of the polycystin genes in the cilia results in loss of ciliary Ca^{2+} signal transduction. Alternatively, loss of PC2 could lead to impairments of ER calcium release; PC2 itself is proposed to be an ER Ca^{2+} release channel (Giamarchi *et al.*, 2010; Koulen *et al.*, 2002; Mekahli *et al.*, 2012) and its loss might impair Ca^{2+} fluxes. Additionally, PC2 has many interaction partners in the ER, most of which are other Ca^{2+} channels, i.e. RyR and IP3R (Anyatonwu *et al.*, 2007; Li *et al.*, 2005), and the absence of this interaction might inhibit ER Ca^{2+} release.

Increased cell proliferation and apoptosis have been consistently associated with ADPKD in several models and an increase of tubular proliferative activity (e.g. transgenic expression of oncogenes or growth factors) leads to cyst formation (Calvet, 1998). Of note, lowering intracellular Ca^{2+} levels in WT cells can result in increased proliferation and Ca^{2+} channel activators reportedly rescue the proliferative response in cyst-derived cells (Yamaguchi *et al.*, 2006). Elevated cAMP concentrations caused by decreased intracellular Ca^{2+} concentrations could lead to cyst formation via two pathways: enhancing fluid secretion via the activation of apically located Cl^- channels (Wallace, 2011) and by stimulating cell proliferation via several mechanisms including the B-Raf/MEK/ERK pathway (MEK: mitogen-activated protein kinase kinase, ERK: extra-cellular-signal-regulated kinase, reviewed in (Mangolini *et al.*, 2016)). In cell culture models of ADPKD, forskolin, an activator of adenylate cyclase stimulates cyst formation by increasing cAMP synthesis (Hanaoka & Guggino, 2000; Yamaguchi *et al.*, 1995). Similarly, renal deletion of a Ca^{2+}-inhibitable adenylate cyclase (AC6, *adenylate cyclase 6*) in *Pkd1*$^{-/-}$ mice improved renal outcomes (Rees *et al.*, 2014). A reduction of intracellular Ca^{2+} inhibits a negative regulator of B-Raf but normal growth can be restored in cystic cells by restoring Ca^{2+} levels, inhibiting the cAMP-dependent B-Raf activation (Yamaguchi *et al.*, 2006). The activation of the B-Raf/MEK/ERK pathway in ADPKD also causes an increase in mTOR (mammalian target of rapamycin) signalling and therefore protein synthesis by inhibiting the negative regulator of mTOR, the TSC1/TSC2 (tuberous sclerosis) complex (Aguiari *et al.*, 2003; Mekahli *et al.*, 2013).

Other pathways linking defects of the polycystin complex to cell cycle regulation include the JAK/STAT pathway and the transcriptional regulator ID2 (reviewed in (Ong & Harris, 2005a)). PC1 and PC2 affect JAK2/STAT3 (Janus kinase/Signal Transducer and Activator of Transcription), which, in turn, appear to regulate the transcription of the cyclin-dependent kinase inhibitor p21; therefore increasing proliferation even in non-cystic tubules (Bhunia *et al.*, 2002; Chang *et al.*, 2006). PC2 also has been implicated in retaining p21 in the cytoplasm by binding to the ID2 protein (Li *et al.*, 2005). Generally, regulation of proliferation underlies complex signalling cascades (well beyond the ones mentioned here), all of which may be deregulated in ADPKD.

Enhanced fluid secretion is essential for cyst formation and it appears that tubular epithelia may switch from an absorptive to a predominantly secretory phenotype in ADPKD. Fluid secretion appears to be mainly driven by Cl^- efflux causing passive movement of Na^+ and water (Grantham *et al.*, 1995). A study proposed that loss of functional PC1 in ADPKD results in the upregulation of store-operated Ca^{2+} entry after a Ca^{2+}-release stimulus and that the subsequent activation of transepithelial Cl^- secretion plays an important role in cyst development and expansion (Wildman *et al.*, 2003).

The constant destruction of healthy parenchyma due to cyst expansion could also enhance the formation of abnormal cell-matrix interactions. In ADPKD patients, cyst epithelia sit on an expanded basement membrane of altered composition and a defect in *laminin alpha 5* has been shown to cause PKD in mice (Goldberg *et al.*, 2010). Furthermore, PC1 has directly been implicated in cell-cell adhesion in renal epithelial cells, a disruption of which could be an early initiating event for ADPKD cyst formation (Streets *et al.*, 2003), as well as cell-matrix adhesion (Wilson, 2004a).

Several papers have reported abnormalities in cell polarity in cystic tissues, however these finding have not always been consistent in all models (reviewed in (Chang *et al.*, 2008; Wilson, 2004a)). Altered basolateral trafficking, abnormalities in planar cell polarity or oriented cell division could all play a role in ADPKD pathogenesis.

Genes that lead to structural abnormalities of primary cilia have been commonly associated with a cystic phenotype and many cystoproteins, including PC1 and PC2, have been immunolocalised to primary cilia or centrosomes. In *PKD1*-null cells, flow-induced ciliary Ca^{2+} signals are severely impaired (Nauli *et al.*, 2003; Nauli *et al.*, 2006; Xu *et al.*, 2007) and implicate a ciliary connection. However, zebrafish and mouse models do not exhibit deformed cilia or reduced cilia numbers (McGrath *et al.*, 2003; Obara *et al.*, 2006).

Nevertheless, cilia could be implicated in ADPKD, if not due to structural cilia defects then via impaired signal transduction.

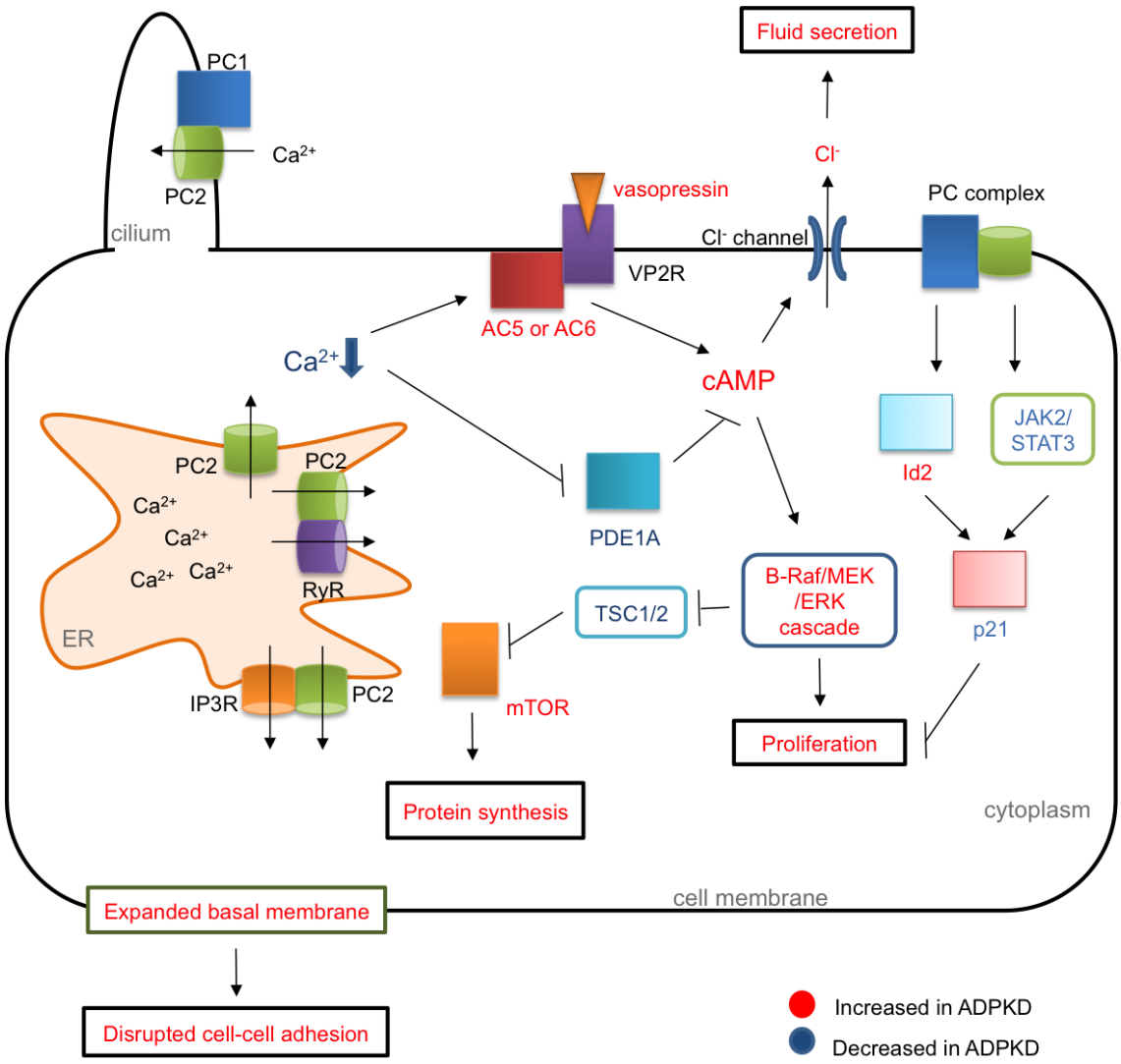

Figure 5 Diagram of deregulated pathways in ADPKD with focus on two main components, calcium and cAMP as well as their putative effects. Proteins or pathways upregulated in ADPKD are indicated with red and downregulation in blue letters. AC: adenylate cyclase, cAMP: cyclic adenosine monophosphate, ER: Endoplasmic reticulum, ERK: extra-cellular-signal-regulated kinase, IP3R: inositol triphosphate receptor, JAK2: Janus kinase 2, MEK: mitogen-activated protein kinase kinase, mTOR: mammalian target of rapamycin, PC1: polycystin-1, PC2: polycystin-2, PDE1A: phosphodiesterase 1 A, PI3K: phosphoinositide 3-kinase, RYR: ryanodine receptor, STAT3: Signal Transducer and Activator of Transcription 3, TSC: tuberous sclerosis, VP2R: vasopressin 2 receptor. Information mainly based on the reviews of (Mangolini *et al.*, 2016; Torres *et al.*, 2006).

In summary, polycystins are essential for the maintenance of a differentiated tubular epithelium phenotype, see Figure 6. Reduction in one of these proteins below a critical threshold results in a phenotypic switch characterised by inability to maintain planar polarity, increased rates of proliferation and apoptosis, expression of a secretory phenotype and remodelling of extracellular matrix. The molecular mechanisms responsible for these phenotypic switches are unknown but given the proposed participation of the polycystins in numerous signalling pathways at multiple subcellular locations, they are likely to be complex (reviewed in (Torres & Harris, 2009)).

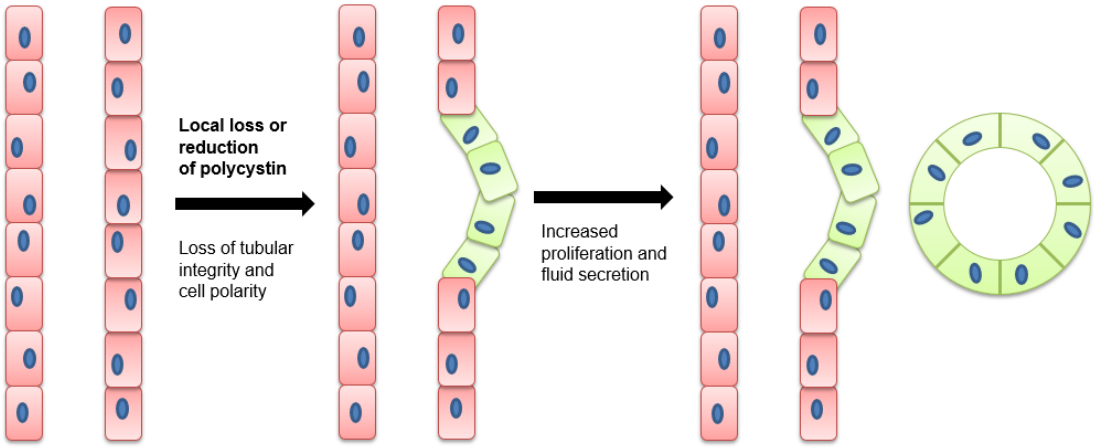

Figure 6 Progression from classical tubular renal structures with subsequent *PKD* gene loss (green cells) to cystic epithelia.

5. Current treatment targets and clinical trials

Presently, only one drug has been approved for treatment of ADPKD, tolvaptan (marketed by Otsuka as JINARC in the UK). Current therapies mostly target the symptoms of the disease but tolvaptan delays the onset of ESRD by about 6.5 years (Erickson *et al.*, 2013). There is no preventative treatment for ADPKD at the moment. The most important therapeutic measure is blood pressure control as heart disease is the main factor concerning morbidity and mortality; infection and neurological events (like aneurysm rupture) are the next common causes (Fick *et al.*, 1995; Perrone *et al.*, 2001). Interestingly, L-type calcium channel inhibitors like nifedipine, often used to treat hypertension, have been reported to have adverse effects on renal outcomes and it has been proposed that other drugs might be more beneficial for ADPKD patients (Astor *et al.*, 2008; Saruta *et al.*, 2009).

Until recently, GFR (glomerular filtration rate) was the main indicator for clinical trial success but since it only starts declining in the later stages of the disease, it may not be a good predictor for treatment outcome in the early stages. Renal growth occurs early in disease, has been shown to be exponential in patients and is likely to be a good early surrogate marker for disease progression (Grantham *et al.*, 2008).

Three main strategies have emerged from recent findings in an attempt to delay the onset of ESRD: Reducing cell proliferation, lowering cAMP levels and inhibiting fluid secretion. A number of preclinical and clinical trials are currently underway or have been completed and some promising compounds are in the development pipeline. Primarily, the aberrant signalling pathways Ca^{2+}, cAMP and mammalian target of rapamycin (mTOR) (Leuenroth *et al.*, 2007; Tao *et al.*, 2005; Torres *et al.*, 2009), have been implicated in ADPKD and clinical trials targeting these pathways have been conducted. Other treatment options such as

somatostatin analogues, HDAC inhibitors and curcumin, mostly aiming to modulate the same three signalling cascades - Ca^{2+}, cAMP and mTOR - are also currently being explored but will not be elaborated upon here.

As described previously, low intracellular Ca^{2+} levels in ADPKD allow an increase of cAMP concentration, which enhances fluid secretion and proliferation. mTOR is a kinase which regulates cell proliferation and cell size. In patients with ADPKD, the mTOR pathway has been shown to be upregulated in cystic kidney tissue. mTOR can be inhibited by tuberin (TSC2 protein) and it has been suggested that loss of the tuberin-binding site in PC1 could enhance ADPKD phenotypes (Wildman *et al.*, 2003). Rodent preclinical trials with the mTOR inhibitor rapamycin were very promising (Serra *et al.*, 2010), however, initial clinical trials with rapamycin and sirolimus have been disappointing (Grantham *et al.*, 2011; Levey *et al.*, 2011; Tao *et al.*, 2005). A recent clinical trial suggested that a low-dose treatment with an mTOR inhibitor improves renal function (Braun *et al.*, 2014) and the natural compound resveratrol, which has been linked to mTOR inhibition, represses renal growth in a PKD rat model (Han:SPRD, (Wu *et al.*, 2016)).

Vasopressin V2 receptor antagonists and somatostatin have shown positive effects in inhibiting disease development and progression in rodent models and in clinical trials (Gattone *et al.*, 2003; Higashihara *et al.*, 2011; Torres *et al.*, 2012; Torres *et al.*, 2007; Torres *et al.*, 2004). These drugs inhibit fluid secretion and cell proliferation via a decrease of cAMP levels through the inhibition of adenylate cyclases (reviewed in (Torres & Harris, 2009)).

Triptolide, an active diterpene of the Chinese medicine *Lei Gong Teng*, is currently undergoing phase III clinical trials. It successfully reduced renal expansion in murine models and in a small, uncontrolled clinical trial (Chen *et al.*, 2014; Leuenroth *et al.*, 2010; Leuenroth *et al.*, 2008; Leuenroth *et al.*, 2007). Although the proposed mechanism of action for triptolide is to activate PC2 channel, other modes of action are also possible.

Once disease progression has reached ESRD, the only remaining treatment options besides symptom reduction are dialysis or kidney transplantation. Transplantation, being the treatment of choice, has no greater risk of complications in ADPKD patients compared to the general population. In cases where a nephrectomy is indicated, hand-assisted laparoscopic nephrectomy is favourable to open nephrectomy regarding blood loss, postoperative pain and recovery time (Desai *et al.*, 2008; Kramer *et al.*, 2009).

6. Zebrafish as a model organism

The zebrafish, *Danio rerio*, has become a very popular model organism during the past decades. Owing to the relatively low cost, short generation time (2-3 months) and easy access, it provides a comparatively inexpensive alternative *in vivo* model to mammalian systems. A single female can lay up to 200 eggs per week, which develop rapidly into transparent embryos. Most major structures and organs are formed by 48 hpf when the larvae hatch and begin swimming freely. The embryo's transparency allows for *in vivo* imaging of internal organs by using fluorescent markers. Zinc-finger nucleases and TALEN methodologies have in the past provided tools for targeted gene editing whereas the recently developed CRISPR/Cas9 system has advanced gene manipulation to a more efficient level. The CRISPR (Clustered Regularly Interspaced Short Palindromic Repeats)/*Cas9* system was discovered as part of the immune system in bacteria and archaea (Horvath *et al.*, 2010). Recent studies, however, have utilized it to create target-specific mutagenesis in a variety of models, zebrafish being amongst them (Chang *et al.*, 2013; Hwang *et al.*, 2013).

6.1. Zebrafish development

The development of zebrafish is very rapid and some of the stages and their timing after fertilisation depicted in Figure 7. By 24 hpf anlagen of all organs and other vital structures, such as the blood vessels and spinal column have formed and subsequently mature to full function (stages of development extensively described in (Kimmel *et al.*, 1995)). Kidney formation, for instance, is completed by 48 hpf and glomerular filtration matures until about 4 dpf. Classically, this rapid development in a transparent embryo have made zebrafish a useful tool for geneticists and developmental studies. Their small size, easy handling and rapidly growing bioinformatics databases also make them an interesting model to address a variety of basic research questions.

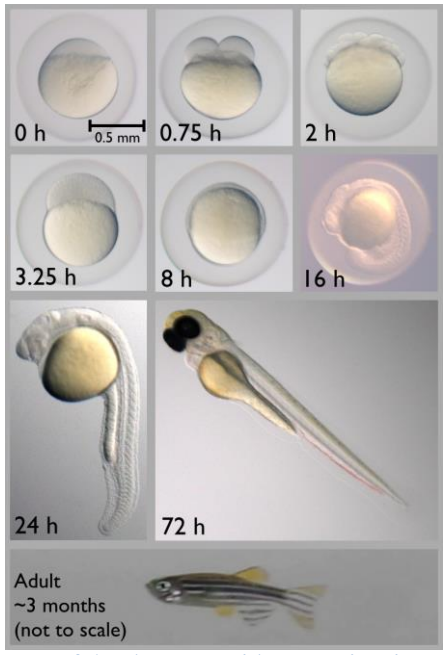

Figure 7 Examples of zebrafish stages of development with respective times post fertilisation. 0 h: fertilisation and one-cell stage; 0.75 h 2-cell stage; 2 h: 64-cell stage; 3.25 h: high stage; 8 h: 75 % epiboly; 16 h: 14-somite stage; 24 h: Prim-5 stage; 72 h: protruding mouth stage. By Ed Hendel - CC BY-SA 4.0, https://commons.wikimedia.org/w/index.php?curid=37054608.

6.2. Zebrafish chemical screens

High-throughput chemical screens are typically conducted in cell culture models, however zebrafish have emerged in recent years as an *in vivo* alternative. Three zebrafish embryos in 250 µl medium containing drugs of interest can comfortably develop in a single well of a 96-well plate for 2-3 days. In the past 15 years, a multitude of small molecule screens have been performed on zebrafish. There are different approaches to finding active compounds in small molecule screens (Peterson *et al.*, 2011; Rennekamp *et al.*, 2015) and during this project a phenotype-driven approach was taken – an ADPKD-related phenotype was chosen as readout in the absence of a validated target. Screens can use a validated target as readout i.e. modulation of a particular gene or pathway related to the desired outcome, but since no such target has been described for ADPKD zebrafish models, a phenotypic screen was conducted. Some examples of previous screens aiming to discover novel drug candidates for specific disease phenotypes include: an aortic coarctation phenotype (Hong *et al.*, 2006), protection from aminoglycoside-induced utricular hair cell loss (Owens *et al.*, 2008) and long QT syndrome (Peal *et al.*, 2011). HDAC inhibition, identified as a potential APDKD-modifier during a small-scale compound screen on zebrafish *pkd2* mutants, has subsequently proven effective in rodent models, underlining the general validity of this approach (Fan *et al.*, 2012; Xia *et al.*, 2010).

7. Mammalian and zebrafish renal development

The main functions of the kidneys in any species are removal of nitrogenous waste and homeostasis of ion, metabolite and fluid concentrations (osmolality), as well as pH levels within vital levels. Basically, blood is first filtered by the glomeruli and ions or small molecules are recovered from or excreted into the filtrate by active epithelial transport (Jacobson, 1981). The functional units of the kidney are called nephrons and each nephron has three major sub-units: glomerulus, tubule and collecting duct. The glomerulus acts as a blood filter with specialised basket-like cells, the podocytes. Small molecules, ions and blood fluid pass through the podocytes' slit-diaphragm, a sort of "mesh", into the urinary space. This glomerular filtrate is then drained into tubules where salt and water are reabsorbed and the remaining waste is transported via the collecting duct to the excretion site.

Three distinct kidney types with increasing complexity arose during vertebrate evolution: pronephros, mesonephros and metanephros. In the course of embryonic development, the pronephros is the first to form and in teleost fish and amphibians, this is the functional kidney of early larval life (Vize *et al.*, 1997). In juvenile stages during fish and frog development, a mesonephros forms around and along the pronephros by adding more nephrons from surrounding tissues and this mesonephros then functions as the final adult kidney. The most complex kidney form, the metanephros is found exclusively in amniotes (mammals, birds and reptiles) and is especially adapted to produce concentrated urine by water retention. In mammals, the pronephros is only a vestigial organ and the mesonephros is the functional kidney during foetal life. Both structures are transient and will degenerate (see Figure 8) or in case of males, become part of the reproductive system (Dressler, 2006).

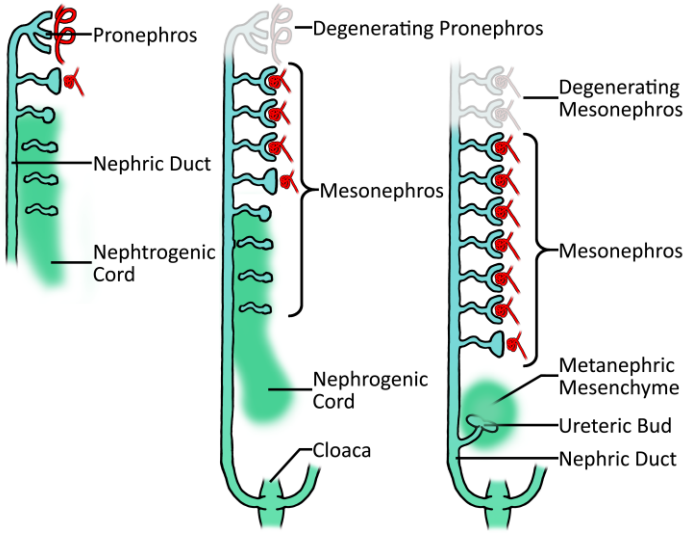

Figure 8 Schematic depiction of the sequential development and degeneration of the pronephros and mesonephros, as well as the induction of the ureteric bud and metanephric mesenchyme during kidney development in mammals. By Ashley Sawle - CC BY-SA 3.0, https://commons.wikimedia.org/w/index.php?curid=7047612.

During the embryonic and early larval stages, the zebrafish kidney consists of a pronephros; two glomeruli which are fused at the midline, just ventral to the dorsal aorta, and two laterally extending tubules connecting into ducts (Drummond, 2000). The development of the zebrafish kidney is depicted in Figure 9 and basically completed by 2 dpf; maturation of filtration commences from thereon. In zebrafish, cells destined to form the pronephros arise from the ventral mesoderm. There, a particular band of tissue, the intermediate mesoderm, gives rise to kidney and blood cells (Kimmel *et al.*, 1990). Tubule formation takes place by mesenchyme to epithelial transition, which is completed with polarisation of the epithelia at 24 hpf (Drummond *et al.*, 1998). Vascularisation of the glomerulus does not take place until 36-40 hpf (tubule development has long been completed) when the glomerular primordia come in contact with the overlying dorsal aorta. Subsequently, by 40-48 hpf, endothelial cells invade the glomerular epithelium (via *vegf - vascular endothelial growth factor* signalling, (Majumdar *et al.*, 1999) and become surrounded by podocytes. Filtration commences after shear stress-induced capillary formation and is leaky at 48 hpf but matures to size-selectivity by 4 dpf (Kramer-Zucker, Wiessner*, et al.*, 2005). Later in larval life, the mesonephros develops by the addition of nephrons from the surrounding mesenchyme - this will remain the functional kidney throughout adult life.

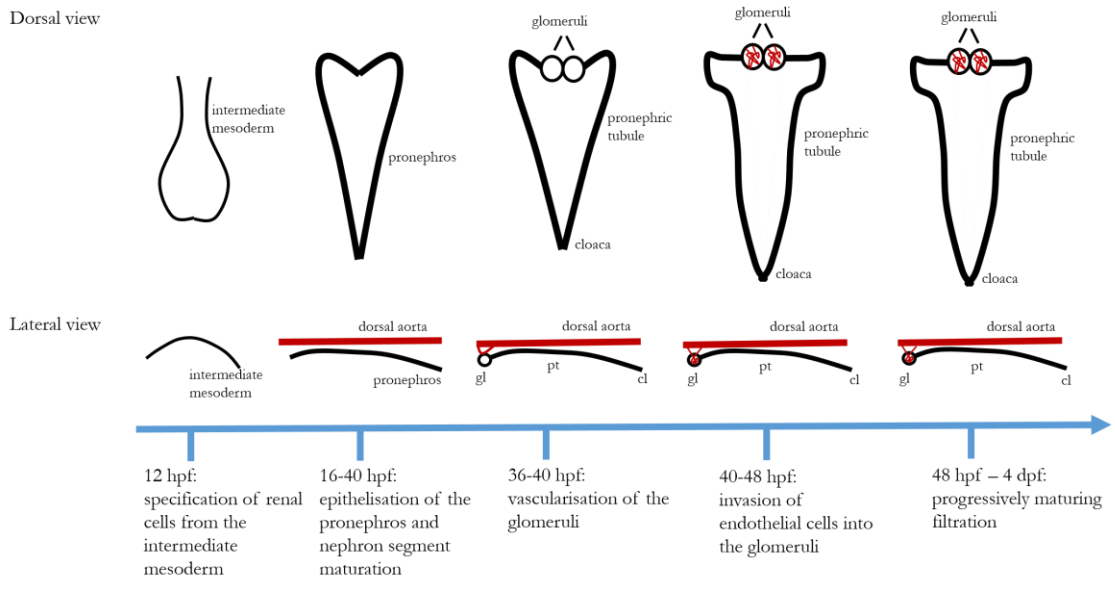

Figure 9 Stages of early zebrafish renal development with timescale as well as dorsal and lateral views of the developing organ. Based on descriptions in (Drummond *et al.*, 2010). gl: glomerulus; pt: pronephric tubule, cl: cloaca.

The zebrafish pronephric kidney is composed of the same cell types as all vertebrate kidneys and the transcription factors regulating organogenesis have highly conserved functions in mammalian and teleost kidney developments (Drummond *et al.*, 2010). Tubule segmentation, responsible for the highly specialised secretion and absorption functions of individual segments, is controlled by conserved genes. Furthermore, seven of the ten metanephric

mammalian segments have been found in zebrafish and the absence of the remaining segments can be attributed to the lack of need of a freshwater species to conserve water as rigorously as terrestrial species (Wingert *et al.*, 2011; Wingert *et al.*, 2007). Defects in genes associated with human polycystic kidney disease also cause pronephric "cyst" formation in zebrafish, underlining the relevance of fish to study this type of disorder (Hostetter *et al.*, 2003; Liu *et al.*, 2002; Low *et al.*, 2006; Otto *et al.*, 2003; Sun *et al.*, 2004; Sun *et al.*, 2001).

There are, however, also notable differences comparing the zebrafish pronephros to the mammalian metanephros. As described before, the absence of the thin limb segment (the loop of Henle) can likely be attributed to the low requirement of freshwater teleosts for water retention and urine concentration. The complex collecting duct system in mammals with its thousands of nephrons is not required in a two-nephron pronephros and hence only a single short segment connects to the cloaca for drainage. Most intriguing is the entirely unique cell type present in a particular segment of the teleost pronephros: cell clusters that are known as the Corpuscles of Stannius and responsible for calcium and phosphate homeostasis (Kaneko *et al.*, 1992).

8. The ciliary hypothesis of ADPKD

Cilia are hair-like organelles that protrude apically from non-dividing polarized cells in almost every cell or tissue in the body. There are two classes of cilia: motile and non-motile (or primary) cilia. The structural components between those ciliary types are the same but ultrastructurally, motile cilia have a "9+2" and primary cilia a "9+0" design; the motile "+2" refers to the presence of a central pair of microtubules (Figure 10 A). The assembly of cilia is facilitated by a specialised process, microtubule-dependent intraflagellar transport (IFT), which is highly conserved throughout evolution – see Figure 10 B (Pazour, 2004).

ADPKD is generally considered a ciliopathy, although no structural or motility defects in renal cilia have been described in murine and zebrafish *pkd1* or *pkd2* knockout models (Obara *et al.*, 2006; Sullivan-Brown *et al.*, 2008). Cystic kidneys are often associated with defects in ciliary function and it could be hypothesised that loss of *Pkd2* results in loss of ciliary signalling (Kramer-Zucker *et al.*, 2005; Pazour, 2004). Interestingly, no significant differences have been detected regarding cilia number or length in the zebrafish Kupffer's vesicle in *pkd2* morphants or in the mouse embryonic node of *Pkd2* mutants (Bisgrove *et al.*, 2005; McGrath *et al.*, 2003; Obara *et al.*, 2006). This indicates that in *Pkd2* mutants, ciliary structure is normal, but signal transduction is disrupted.

One of the main differences comparing the fish pronephros and the mammalian metanephros are the different types of cilia found in these tissues. Mammalian metanephric

cells have mainly primary cilia (non-motile) with occasional motile cilia in humans (Kramer-Zucker *et al.*, 2005; Ong & Wagner, 2005) whereas the zebrafish pronephros is completely lined with motile cilia, which contribute to fluid movement (Kramer-Zucker *et al.*, 2005). A loss of motility in motile cilia, also called ciliary dyskinesia (or Kartagener syndrome) leads to poor mucociliary clearance in the respiratory tract, loss of fertility and *situs inversus* in humans. In zebrafish it causes a classical ciliary mutant phenotype, including renal dilations in zebrafish (van Rooijen *et al.*, 2008). Renal cysts are not a symptom in the human syndrome, possibly owing to the fact that the zebrafish pronephros is lined with motile cilia whereas the mammalian kidney exhibits non-motile cilia. These ciliary differences therefore raise an important limitation of zebrafish embryos as models for ADPKD.

Renal epithelial cells are sensitive to flow (Praetorius *et al.*, 2001) and both zebrafish pronephric motile cilia and mammalian metanephric non-motile cilia are PC2-positive. It has been shown that non-motile cilia can function as mechanosensors for flow (Nauli *et al.*, 2003; Praetorius *et al.*, 2001) and even motile cilia, previously thought to be non-sensory, have been shown to possess sensory functions (Bloodgood, 2010). PC2 has been localised to motile cilia in other tissues such as the female reproductive tract and the mouse embryonic node; they may relay mechanosensory information via beat frequency or changes in membrane potential (Andrade *et al.*, 2005; McGrath *et al.*, 2003; Stommel *et al.*, 1980; Woolf *et al.*, 2004).

However, there are obvious differences when comparing zebrafish classical ciliary mutants (some of which are listed in Table 7), where e.g. the intraflagellar transport is disrupted and functional cilia are lacking, with *pkd* mutants. First, the axis curvature phenotype is opposite i.e. ventral in cilia mutants and dorsal in *pkd2* mutants. Furthermore, in another zebrafish model of ADPKD (*polaris* mutant) restoration of ciliary length rescued the L/R axis defects but cyst development was not prevented (Brown *et al.*, 2003). These studies suggest that *pkd2* loss-of-function may not be a classical ciliopathy. Although no structural or motility cilia defects were observed in PKD knockout models, a recent zebrafish study suggests that ciliary stability is influenced by *pkd2* and *CaMK-II* (Ca^{2+}/*calmodulin-dependent protein kinase type II*) as embryos deficient in these genes (morphants) fail to from pronephric ducts properly. Additionally, these embryos exhibited anterior renal cysts and destabilised cloacal cilia with ciliary disassembly starting at 48 hpf and no motile cilia remaining by 72 hpf (Rothschild *et al.*, 2011). Constitutively active *CaMK-II* was able to restore duct formation in *pkd2* morphants suggesting *pkd2*-mediated Ca^{2+} signalling plays a role in cilia stability.

name	phenotype	gene affected	publications
lrcc50^{hu255H}	Curly down tail, renal dilations, ciliary dyskinesia	dnaaf1 (formerly lrcc50)	originally described in 1
elipsa^{tp49d}	Curly down tail, renal dilations, loss of cilia	traf1ip3	2, 3, originally described in: 4
locke	Curly down tail, renal dilations, shortened cilia	ccdc40	5, 6, 7, originally described in: 8
swt (switch hitter^{tm317})	Curly down tail, renal dilations	dnaaf1 (formerly lrcc50)	5, originally described in: 4
kurly	Curly down tail, renal dilations	c10h21orf59	5, originally described in: 4
ift mutants	Curly down tail, renal dilations	ift genes (currently 23 genes described in zebrafish)	many described from the screens 4 and 9

Table 7 List of some classical ciliary mutants described in recent publications. This list is by no means complete and merely serves to illustrate common phenotypes. References: 1 (van Rooijen *et al.*, 2008), 2 (Omori *et al.*, 2008), 3 (Malicki *et al.*, 1996), 4 (Brand *et al.*, 1996), 5 (Sullivan-Brown *et al.*, 2008), 6 (Zhao *et al.*, 2011), 7 (Zhao *et al.*, 2007), 8 (Chen *et al.*, 1997), 9 (Sun *et al.*, 2004).

However, the fact that *pkd2* morphants display *situs inversus* (Bisgrove *et al.*, 2005), which is classically linked to defects in motile cilia left/right patterning, suggests ADPKD is a ciliopathy. In the mouse node as well as the zebrafish Kupffer's vesicle, beating cilia create a unidirectional flow, which is necessary for asymmetric left-right pattering and correct axis formation (Kramer-Zucker *et al.*, 2005; Nonaka *et al.*, 1998). If this flow is disrupted either by defects in ciliary structure or function, L/R patterning becomes randomised. Interestingly, nodal cilia are structurally primary cilia (9+0) but are motile. As *pkd2* mutants develop cilia normally and *pkd1* mutants to this date have not been described to exhibit L/R defects (but *PKD1*-deficient cells are unable to respond to fluid flow with a Ca^{2+} influx (Nauli *et al.*, 2003)), it may be surmised that *PKD1* and *PKD2* have additional functions than mere mechanosensing in the cilium and that the modes for cyst formation may not be the same as in "classical" ciliopathies.

Interestingly, *Pkd1* is not expressed in the mouse node and it used to be unclear how *Pkd2* could act as mechanosensory channel without its presumed sensor *Pkd1*. However, recent studies have revealed that *Pkd1l1* is expressed in the node and mutations in *Pkd1l1* lead to L/R patterning defects (Field *et al.*, 2011; Kamura *et al.*, 2011). Calcium transients in the cytoplasm are abolished by loss of PC1 or PC2 function (Nauli *et al.*, 2003), but in cilia, PKD1L1 and PKD2L1 are responsible for calcium entry (DeCaen *et al.*, 2013; Delling *et al.*, 2013). Interaction of PC2 with TRPV4 or TRPC1 in the cilia may also be responsible for flow detection (Bai *et al.*, 2008; Kottgen *et al.*, 2008). However, neither *PKD1L1, TRPC1* or *TRPV4* mutations have been linked to cystogenesis (reviewed in (Mangolini *et al.*, 2016)). It is therefore difficult to attribute the phenotypes solely to either loss of cilia structure, motility and flow or to loss of mechanosensors and/or signal transduction.

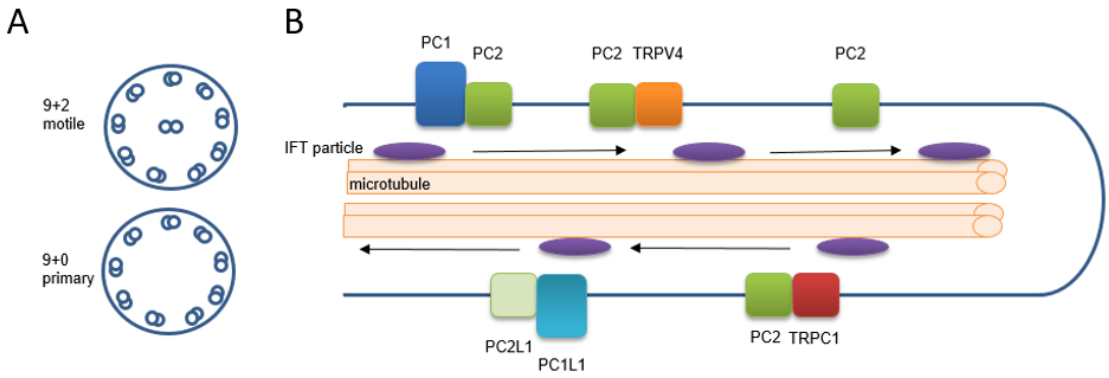

Figure 10 Schematic depictions of ciliary structure. (A) Motile 9+2 and primary cilia 9+0 microtubular structures inside the cilium. (B) Graph of intraflagellar transport (IFT) along the ciliary microtubules with IFT particles (purple) and *PKD1* and *PKD2* protein products with various interaction partners attributed to cilia and ciliary functions.

9. ADPKD models

9.1. Rodent models

There are many different rodent models mimicking the effects of ADPKD, which are reviewed in detail in (Happe *et al.*, 2014; Nagao *et al.*, 2012) and will be summarised here briefly.

Many murine models with mutations in *Pkd1* and/or *Pkd2* have been generated some of which are tissue-specific, hypomorphic, conditional or tissue-specific and conditional. Most of the knockouts and inducible knockouts show a very rapid progression. Interestingly, the time point of inactivation seems to play crucial role in severity. Hypomorphic alleles typically display a slower progression rate. Of note, murine overexpression models with human proteins also recapitulate the development of cystic kidney, indicating that gene dosage is important.

Furthermore, there are some non-*Pkd1*/*Pkd2* rodent models that also develop polycystic kidneys. Some of these comprise models that mimic ARPKD (autosomal-recessive PKD) more closely, such as the *Pck* rat or the *Pkhd1* mouse, and others nephronophthisis, like *Jck* mice and *Cy* rats.

9.2. Zebrafish models of ADPKD: *pkd*-deficient embryos

The *pkd2*$^{hu2173/hu2173}$ mutant used during this project was identified from a library of mutagenized fish in the early 2000s during an ENU-mutagenesis screen. The *pkd2* ^{hu2173} mutant allele carries a point mutation in exon 5 leading to a truncated protein (Freek van Eeden, unpublished). In this mutant, a guanine base is replaced with an adenine resulting in a stop codon in amino acid 302 of 904. Reduced to one-third of its original length, the

resulting protein is presumed to have lost its function, creating a null mutation in homozygous animals. The typical axis deformation with its upward curled tail as described from morpholino injections (Bisgrove *et al.*, 2005) has been observed and can be seen in Figure 11. Table 8 summarises all *pkd2* mutant alleles described to date (accession 02.09.2016) with their associated phenotypes and publications. Additionally to *pkd2* mutant alleles, a number of *pkd2* knockdown strategies with different morpholinos have also been published. A summary of the morpholinos and the respective phenotypes can be found in Table 9.

Figure 11 Zebrafish *pkd2*$^{hu2173/hu2173-/-}$ mutant with dorsal axis curvature at 2 dpf and age-matched WT sibling.

pkd2 zebrafish allele	phenotype	additional information	publications
hu2173	curly up tail, L/R patterning defect, cardiac, ocular and trunk oedema	used during this project, point mutation	1
hi4166	curly up tail, L/R patterning defects	used in compound screen in 16, transgenic insertion	2, 3, 4, 5, 6, 16
sa18074	not described	point mutation	1
sa18283	not described	point mutation	1
tc321	curly up tail, L/R patterning defect	unknown	7, 8, 9, 10, 11, 12, 13, 14
tg226d	curly up tail, L/R patterning defect	unknown	8, 13
tp85a	curly up tail, L/R patterning defect	unknown	8, 11, 13
ty30	curly up tail, L/R patterning defect	unknown	8, 10, 11, 13

Table 8 List of *pkd2* mutant alleles described to date (accession 02.09.2016). Based on information from zfin.org. References: 1 (Busch-Nentwich, 2013), 2 (Sun *et al.*, 2004), 3 (Mangos *et al.*, 2010), 4 (Paavola *et al.*, 2013), 5 (Amsterdam *et al.*, 2004), 6 (Yuan *et al.*, 2015), 7 (Bisgrove *et al.*, 2005), 8 (Brand *et al.*, 1996), 9 (Le Corre *et al.*, 2014), 10 (Schottenfeld *et al.*, 2007), 11 (Chen *et al.*, 1997), 12 (Goetz *et al.*, 2014), 13 (Haffter *et al.*, 1996), 14 (Heckel *et al.*, 2015), 15 (Roxo-Rosa *et al.*, 2015), 16 (Cao *et al.*, 2009).

pkd2 morpholino	phenotype	sequence	publications
pkd2ATGMO or hi4166 oligo 1	curly up tail, L/R patterning defects, oedema, hydrocephalus, renal dilations	5' - AGGACGAACGCGACTGGAGCTCATC - 3'	1, 2, 3, 4, 5, 6, 7, 8, 9, 10, 11
pkd2 AUG MO	curly up tail, L/R patterning defects, oedema, hydrocephalus, renal dilations	5' - ACTGGAGtTCATCGTGTATTTCTAC - 3'	12
pkd2 SP MO	curly up tail, L/R patterning defects, oedema, hydrocephalus, renal dilations	5' - TAGTTTTCAACCTACTTATGCAGAG - 3'	12
pkd2 MO ATG	curly up tail, L/R patterning defects, hydrocephalus, renal dilations	5' - GCTCATCGTGTATTTCTACAGTAAC - 3'	13, 14, 15
pkd2 MOex3	curly up tail, L/R patterning defects, hydrocephalus, renal dilations	5' - AATTACTTTCCAGAAGTCCTCCATG - 3'	13, 15, 16, 17, 18, 19
pkd2 MOex5	curly up tail, L/R patterning defects, hydrocephalus, renal dilations	5' - GATCAACCCGTTACCTGACAATACA - 3'	13, 17
pkd2 MOex12	curly up tail, L/R patterning defects, hydrocephalus, oedema, renal dilations	5' - CAGGTGATGTTTACACTTGGAACTC - 3'	13, 16, 20, 21
pkd2 MOex13	curly up tail, L/R patterning defects, hydrocephalus, renal dilations	5' - CATCATCATCACCTCCATGACTCCA - 3'	13
cup augMO	curly up tail, L/R patterning defects, hydrocephalus, renal dilations	5' - AGCTCATCGTGTATTTCTACAGTAA - 3'	6, 22
9697-S1	curly up tail, L/R patterning defects, hydrocephalus, renal dilations	5' - GAAACGGGCCTTCTGTGAACTACAG - 3'	6
9697-S2	curly up tail, L/R patterning defects, hydrocephalus, renal dilations	5' - TTAACATACGCAGTGCCATTCTTGG - 3'	6

Table 9 *pkd2* morpholinos and respective morphant animals described to date (accession 02.09.2016) according to zfin.org. References: 1 (Sun *et al.*, 2004), 2 (Cao *et al.*, 2009), 3 (Fogelgren *et al.*, 2011), 4 (Giamarchi *et al.*, 2010), 5 (Paavola *et al.*, 2013), 6 (Schottenfeld *et al.*, 2007), 7 (Sullivan-Brown *et al.*, 2008), 8 (Francescatto *et al.*, 2010), 9 (Sussman *et al.*, 2014), 10 (Zhao *et al.*, 2011), 11 (Pavel *et al.*, 2016), 12 (Bisgrove *et al.*, 2005), 13 (Obara *et al.*, 2006), 14 (Coxam *et al.*, 2014), 15 (Goetz *et al.*, 2014), 16 (Mangos *et al.*, 2010), 17 (Fu *et al.*, 2008), 18 (Gao *et al.*, 2010), 19 (Kottgen *et al.*, 2008), 20 (Le Corre *et al.*, 2014), 21 (Vasilyev *et al.*, 2009), 22 (Roxo-Rosa *et al.*, 2015).

Renal cyst formation has so far only been observed in *pkd2* morphants but not in mutants, see Table 8 and Table 9 (also described by (Cao *et al.*, 2009; Schottenfeld *et al.*, 2007; Sun *et al.*, 2004)). Generally, *pkd2* morphants have been shown to develop cystic kidneys, left-right asymmetry defects and dorsal-axis curvature - except for renal cysts, these phenotypes have been confirmed in mutants. Even though a variety of mutants with renal dilations have been associated with body axis curvatures, almost all descriptions encompass ventrally curved body axes (Drummond *et al.*, 1998). This makes the *curly up* or *cup* phenotype unique. An altered ECM has long been associated with ADPKD in human and animal tissues, as well as cell culture models and mRNA expression in these tissues shows an upregulation in matrix genes (Candiano *et al.*, 1992; Riera *et al.*, 2006; Schafer *et al.*, 1994; Somlo *et al.*, 1993). In chemical *pkd2* knockdown with a morpholino, it has been shown that the curvature phenotype is linked to alterations in ECM secretion or assembly (Mangos *et al.*, 2010). An analysis of somite and actin fibre morphology revealed no significant difference (Freek van Eeden, unpublished), supporting the theory of ECM overproduction as the primary cause for dorsal axis curvature rather than other structural defects (Mangos *et al.*, 2010).

A number of pathways that seem to influence the curly tail phenotype have been proposed and are summarised in Table 10. Published work suggests that increased collagen production (Mangos *et al.*, 2010) and/or deposition (Le Corre *et al.*, 2014) play major roles in causing the

curly tail phenotype. Generally, *pkd* knockdown or knockout is characterised by an upregulation of collagen-synthesising enzymes (confirmed by *in situ* hybridisation) and knockdown of one of these enzymes, *col2a1 (collagen type II alpha 1)*, reduced the dorsal axis curvature (Mangos *et al.*, 2010). Furthermore, knockdown of *sec10*, an exocyst protein linked to ciliogenesis, as well as *sec24d* knockdown, involved in Golgi to ER transport, caused a decrease in curvature severity (Fogelgren *et al.*, 2011; Le Corre *et al.*, 2014). Interestingly, chemical knockdown of Golgi/ER transport with Brefeldin A (BFA) also reduced the *cup* phenotype. In combination, these experiments suggest that ECM overproduction and/or overdeposition cause the curly tail in *pkd*-deficient animals. HDAC inhibition also seems to decrease curvature severity in *pkd2* mutants via an unknown mechanism (Cao *et al.*, 2009). cAMP has been implicated in the curvature phenotype with the observation that knockdown of *pde1a (phosphodiesterase a 1)*, a calcium-inducible cAMP-degrading enzyme, aggravates the *pkd2* curly tail (Sussman *et al.*, 2009). Of note, cell culture experiments have revealed a complicated relationship of cAMP levels and collagen expression via TGFβ (Perez-Aso *et al.*, 2014). Moderate stimulation with cAMP (~ 150% control concentration) stimulated collagen 1 and 3 syntheses whereas maximal increases of cAMP (~ 16,000% of control) inhibited collagen 1 but increased collagen 3 production via the TGFβ pathway (Perez-Aso *et al.*, 2014).

cup-contributing pathways	supporting evidence	publications
Increased collagen production	Knockdown of *col2a1* or chemical inhibition of collagen cross-linking reduced *cup* phenotype	1
Increased collagen deposition or secretion	Golgi/ER transport (*sec10* and *sec24d*) knockdown and chemical inhibition with Brefeldin A reduced *cup* phenotype	2, 3
Unknown	HDAC inhibition reduced *cup* phenotype	4
cAMP	Chemical inhibition of PKA and h*PDE1A* RNA reduced and knockdown of *pde1a* aggravated *cup* phenotype	5

Table 10 List of pathways influencing zebrafish the *pkd2* curvature phenotype. References: 1 (Mangos *et al.*, 2010), 2 (Fogelgren *et al.*, 2011), 3 (Le Corre *et al.*, 2014), 4 (Cao *et al.*, 2009), 5 (Sussman *et al.*, 2014).

No significant differences were observed at early developmental stages when blood velocity, heart rate and cardiac output in *pkd2* mutant with WT animals were compared (Freek van Eeden, unpublished). However, a recent study reported lower heart rates and increased arrhythmia in *pkd2* mutants (Paavola *et al.*, 2013). As systole and peak velocities were similar in WT and *pkd2* mutants a diastolic dysfunction has been suggested. Using isolated hearts in pacing chambers revealed impaired intracellular calcium cycling with the lack of a plateau phase (Paavola *et al.*, 2013). Additionally, heart looping is randomised in *pkd2* knockdown and knockout animals (Sun *et al.*, 2004).

10. Project aims

This project has three main aims: the phenotypic study of zebrafish ADPKD models, utilisation of one of these models in a large-scale compound screen and evaluation of renal calcium levels *in vivo* in wild-type animals and ADPKD zebrafish models.

During the characterisation of ADPKD zebrafish models, *pkd2* morphants, the *pkd2*$^{hu2173/hu2173}$ mutant and a cystic disease zebrafish model, the ciliary *elipsa* mutant, were phenotypically examined. Based on a study in mouse models (Ma *et al.*, 2013), complex interactions of cilia and *pkd2* were hypothesised which were re-evaluated in zebrafish. To this purpose, a cilia/*pkd2* double knockout line were be created in this project to compare zebrafish phenotypes to findings in murine studies.

Subsequent to the initial characterisation, an *in vivo* compound screen was be conducted on one of the models with an ADPKD-related phenotype as readout. Cao *et al.* have shown that the curvature phenotype is a suitable read-out in a small-scale chemical screen (Cao *et al.*, 2009). In this project a large-scale compound screen with two chemical libraries, spanning ~2400 small molecules, was conducted and findings were validated in two independent three-dimensional cyst culture models. The cell lines used for this purpose comprise canine MDCKII cells, a well-established renal cyst model, and human *PKD1*$^{-/-}$ Ox161c1 cells.

Lastly, a zebrafish renal calcium-reporter line was be established to study pronephric calcium levels *in vivo*. This was be the first description of pronephric calcium in zebrafish and the first in an intact organism (murine studies depend on the exteriorisation of the organ due to their opaque skin (Burford *et al.*, 2014; Szebenyi *et al.*, 2015)). Cell culture experiments suggest lower intracellular calcium in *PKD*-deficient cells, therefore lower pronephric calcium levels were be expected in *pkd2*$^{-/-}$ zebrafish embryos. After the initial characterisation of renal calcium in wild-type animals and ADPKD models, the compounds identified during the chemical screens were tested on their ability to modify pronephric calcium.

In conclusion, novel insights into the interplay between ADPKD and its modifying factors were be gained during this project and, hopefully, new avenues for potential therapeutic targets of this devastating disease were be presented.

Materials and Methods

1.1. Zebrafish maintenance

Zebrafish were kept under standard conditions (14 h light/10 dark cycle, temperature 26 – 28 °C (Brand *et al.*, 2002)). Rearing occurred in E3 medium (5 mM NaCl, 0.17 mM KCl, 0.33 mM $MgSO_4$, 0.33 mM $CaCl_2$ and methylene blue) and staging according to (Kimmel *et al.*, 1995). To prevent pigmentation, larvae were treated with PTU (phenylthiourea) beginning 24 hpf (28 °C) when necessary (Karlsson *et al.*, 2001). Zebrafish lines in this project included, amongst others, LDWT (London wild type), AB, *wt1b:GFP, UAS:GCaMP7a* and *pkd2*^{hu2173}. The *wt1b:GFP* line was originally generated by (Perner *et al.*, 2007) and exhibits GFP fluorescence from 17 hpf in all parts of the developing pronephros. GFP expression in this line has also been described in the exocrine pancreas, gut, heart sac, eyes and gill arches. The *elipsd*^{tp49d} mutant strain, is a ciliary mutant (point mutation, leading to a truncation of the protein) with loss of cilia from 30 hpf and was kindly provided by Jarema Malicki (Omori *et al.*, 2008). *GCaMP7a* allows real-time visualisation of intracellular calcium concentrations as it is a modified *GFP* that increases fluorescence in Ca^{2+} presence (Muto *et al.*, 2013). Animals were sacrificed using an overdose of Tricaine and fixed in 4 % PFA/PBS (paraformaldehyde/phosphate buffered saline). All procedures adhered to Home Office legislation.

1.2. Morpholino injections

Morpholinos are nucleic acid analogues complementary to an RNA target region and capable of knocking down the expression of a specified gene. In this project a previously published *pkd2* morpholino (Sun *et al.*, 2004) complementary to the ATG region of the zebrafish *pkd2* gene (5'-AGGACGAACGCGACTGGAGCTCATC-3') and a *p53* morpholino (5'-GCGCCATTGCTTTGCAAGAATTG-3') were injected into the 1- or 2-cell stage of zebrafish embryos. The morpholinos were synthesised by Gene Tools, LLC/USA. The final amounts injected of the *pkd2* morpholino were 2 ng/embryo and 1 pmol/embryo for the *p53* MO in a volume of 1 nl.

1.3. Creating transgenic zebrafish lines

Plasmids were created using the MultiSite Gateway Three-Fragment Vector Construction Kit (Invitrogen/USA) according to manufacturer's instructions. The fluorescent marker *cmlc2:eGFP* was used to visualise the transgenes (*cmcl2, cardiac myosin light chain 2*, drives expression in the heart, (Huang *et al.*, 2003)). Transgenic lines created during this project comprise of *enpep:Gal4* and *podocin:Gal4*. The *podocin* promoter (He *et al.*, 2011) was derived from a plasmid kindly provided by Lwaki Ebarasi from the Karolinska Institute,

Stockholm/Sweden, the *enpep* promoter was cloned by Eleni Leventa and cloned into a middle entry vector during this project (promoter described in (Seiler *et al.*, 2011)) and the *Gal4* plasmid was obtained from Nikolay Ogryzko. Final constructs contained a *cmlc2:GFP* marker and Tol2 sites and were coinjected at 25 ng/nl with 25 ng/nl *Tol2* mRNA (transcribed with mMessage mMachine kit (Life Technologies/USA) according to manufacturer's instructions) into one-cell stage embryos. Subsequently founders were identified by screening the offspring for GFP fluorescence and stabile transgenic lines established.

1.4. DNA extraction

1.4.1. DNA extraction from multiple embryos

Up to 20 embryos were placed in 310 µl extraction buffer (10 mM Tris HCl pH 8, 10 mM EDTA, 100 mM NaCl), 2% SDS (sodium dodecyl sulphate) and 4 µl 25 mg/ml proteinase K and incubated 75 minutes at 42 °C. After the tissue was dissolved, the solution was centrifuged for 5 min at 13000 rpm and the supernatant transferred into a sterile Eppendorf tube. 225 µl 4 M NaCl were added, the solution was mixed and centrifuged for 5 min at 13000 rpm. The supernatant was transferred into a sterile Eppendorf tube and 420 µl isopropanol were added. The components were mixed and centrifuged for 5 min at 13000 rpm. The supernatant was discarded and the DNA pellet washed with 250 µl 70 % EtOH, centrifuged briefly and the supernatant was discarded. This last wash step was repeated a second time. The pellet was then air-dried after which the DNA was diluted in 50 µl TE buffer (10 mM Tris pH 8 and 1 mM EDTA).

1.4.2. DNA extraction from single embryos

DNA extraction from single embryos was necessary for various applications, such as sequencing fish imaged on the lightsheet.

Single embryos were dechorionated, placed individually in sterile tubes and 50 µl of embryo digestion buffer (10 mM Tris HCl pH 8, 1 mM EDTA, 0.3 % Tween20 and 0.3 % NP40) were added. The embryos were subsequently heated for 10 min to 98 °C after which 2 µl proteinase K stock solution (25 mg/ml stock) were added. The embryos were then kept at 55 °C for 3 h, which was followed by an inactivation step for 10 min at 98 °C. 2 µl supernatant was subsequently used for PCR reactions.

1.4.3 DNA extraction from fin clips

DNA extraction from fin clipped tissue is typically used to identify carriers of recessive phenotypes such as *pkd2*^{hu2173} or *elipsa*.

Fin clips were conducted according to Home Office recommendations and clipped materials were transferred directly into 50 µl fresh base solution (1.25 M KOH and 10 mM EDTA in MilliQ H_2O) in a 96-well plate. The removed tissue was then incubated for 30 minutes at 95 C and the plate vortexed for 5 seconds. Subsequently 50 µl neutralisation buffer (2 M TrisHCl in MilliQ H_2O) were added to each sample and the plate vortexed again for 10 seconds. Lastly, the extract was centrifuged for 2 min at maximum speed and 1.5 µl supernatant used per PCR reaction.

1.5. Bacterial cultures, plasmid isolation and restriction digests

Plasmid or circular DNA can easily be propagated and multiplied in bacteria such as New England Biolabs' 10-beta *E. coli* strain. The transformation of plasmids into 10-beta cells occurred according to manufacturer's specifications. Bacterial colonies were selected with 50 µg/ml kanamycin, 100 µg/ml carbenicillin or 12.5 µg/ml chloramphenicol depending on plasmidic antibiotic-resistance genes. Glycerol stocks were prepared with a 1:1 ratio of culture and 80 % filter sterilized glycerol and stored at – 80 °C. For most subsequent applications the plasmid DNA was re-extracted from the bacteria. For small bacterial cultures (up to 10 ml) this was done using the QIAprep Spin Miniprep Kit (Qiagen/the Netherlands) according to the manufacturer's manual. For larger cultures up to 100 ml the NucleoBond Xtra Midi Kit (Macherey-Nagel/Germany) was employed according to manufacturer's instruction for high-copy plasmid purification protocol.

Restriction enzymes digests, e.g. to test whether a plasmid contains expected sequences, were performed with New England BioLabs (USA) enzymes according to manufacturer's instructions.

1.6. PCR

PCRs were conducted according to manufacturer's specifications with 2x ReddyMix by Thermo Scientific/USA, 5x Firepol Master Mix by SolisBioDyne/Estonia or Phusion High-Fidelity DNA Polymerase by New England BioLabs/USA. High-fidelity polymerases are less likely to produce mistakes while amplifying and were used in sensitive applications such as cloning. The subsequent table lists (Table 11) the oligonucleotides (designed with Primer3) used in various PCR applications. Generally, an annealing temperature of 50 °C was used.

Primer name	Primer sequence
Aa changes 1_for	CGCATTTTCGCATTAAGACAGA

Aa changes 1_rev	TCTCCAGTATCCTCTTCCCAC
Aa changes 2_for	AGCAGATGGACAGGTTGGTT
Aa changes 2_rev	GTTGATTTGTGCAAGCTGTGT
attB1R-podocin	GGGGACTGCTTTTTTGTACAAACTTGCCGTGATCAGAGATCTGTTG
attB4F-podocin	GGGGACAACTTTGTATAGAAAAGTTGTCTTGAAGACAATCGCGGGTTA
elipsa for new	TGTCTGTTTTCCAGGAGAGGA
elipsa ID for	TGTCTGTTTTCCAGGAGAGGA
elipsa ID rev	CTTCTCTCGTTCCCGCTCTT
elipsa rev new	TCTCTTTCTCGGCCTTTGTC
Gal4 probe For primer	TCTATCGAACAAGCATGCGA
Gal4 probe Rev primer	TAATACGACTCACTATAGGGACCTTTGTTACTACTCTCTTCCG
pkd2 seq for	TTTGTGTGGGTCTGGAATGA
pkd2 seq for new	ATGAGGATCTGCGAGACGAG
pkd2 seq new new for	CAATGAGGACAAGGCACCAT
pkd2 seq rev	CTGGGATCGACAACAAGACA
pkd2 seq rev new	GAAGTCCAAGAACACCGCTC
Seq enpep clones For	TGAGGAGAGTGTGTGGGTTC
Seq enpep clones Rev	CGACGGCCAGTGAATTATCA
Seq podocin clones For	GCACTGGCCTCCTGATATACT
Seq podocin clones Rev	CGACGGCCAGTGAATTATCA

Table 11 List of oligonucleotides ordered from IDT (Integrated DNA Technologies, USA) used in various PCR applications.

1.6.1. PCR purification

PCR products have to be purified and cleaned of salts and residual nucleotides for certain applications such as DNA sequencing. This was done for cloning purposes by either using the MinElute PCR Purification Kit (Qiagen/the Netherlands) or, if unspecific amplification had occurred, the MinElute Gel Extraction Kit (Qiagen/the Netherlands) according to the manufacturer's manuals. For sequencing, if no unspecific amplification occurred, PCR product was purified by adding 5 µl product to 3.95 µl MilliQ H_2O, 0.05 µl Exonuclease I and 1 µl SAP (shrimp alkaline phosphatase) before incubation for 45 min at 37 °C and inactivation for 15 min at 80 °C.

1.7. Measurement of glomerular and tubular dilation

To measure the pronephros *pkd2*$^{hu2173/hu2173-/-}$*;wt1b:GFP* embryos and *wt1b:GFP*-positive siblings were anaesthetised and immobilised in methylcellulose. Imaging occurred dorsally and glomerular area or tubular diameter was measured using ImageJ. Statistical analysis was conducted with GraphPad Prism.

1.8. Antibody staining

To assess cellular proliferation in the pronephric kidney a phospho-Histone H3 (pH3) antibody was chosen to stain cells in M-phase.

Embryos were fixed overnight in 4 % PFA and transferred into methanol (MeOH) via a series of increasing concentration. Embryos were stored at – 20 °C in 100 % MeOH. Staining commenced by rehydrating the embryos with a series of increasing concentrations of PBTw

(PBS with 0.1 % Tween-20) in MeOH followed by 4 washes of 5 min in PBTw. To improve permeabilisation embryos were incubated for 1 h in 10 µg/ml proteinase K, refixed in 4 % PFA for 20 min, washed 5 times for 5 min in PBTw and subsequently incubated in acetone form 7 min at – 20 °C. This was followed by 5 washes of 5 min in PBTw and a 2 h incubation step at room temperature in blocking solution (2 % blocking reagent, 0.1 % v/v Triton X-100, 1 % DMSO). The primary antibody then was applied at a concentration of 1:200 (ab5176) in blocking solution overnight at 4 °C. The following day the solution was removed, followed by five 20-minute washes in PBTw, a second 2 h block in blocking solution and incubation with the secondary antibody at a concentration of 1:1000 (Alexa Fluor 488). This was followed by five 20-minute washes, refixation in 4 % PFA for 30 min and transfer to 80 % glycerol via a series of increasing glycerol concentration. Stained embryos were stored at – 20 °C until imaging.

1.9. *In situ* hybridisation

To image gene-expression patterns *in situ* hybridisation was performed which allows visualisation of mRNA expression.

In situ probe synthesis was achieved by mixing the following reagents at room temperature (in order) before incubation for 2 h at 37 °C 1 µg linearised template DNA, MilliQ H_2O (to 13 µl total), 2 µl 10x DIG-UTP NTP labelling mix, 4 µl 5x transcription buffer, 0.5 µl RNAse inhibitor and 1 µl T7 RNA polymerase. Afterwards 1 µl of RNAse-free DNAseI was added before continuing incubation at 37 °C for another 20 min and stopping the reaction by adding 1 µl 0.5 M EDTA. Removal of DNA was checked on an agarose gel before continuing as follows: add 80 µl MilliQ H_2O and vortex, precipitate RNA with 33 µl 10 M NH4Ac and 350 µl ice cold EtOH by incubating at -20 °C for 2 h, spin at 13,300 rpm and 4 °C for 30 min and wash pellet with 0.5ml 70% ETOH before a final spin at 13,300 rpm at 4 °C for 10 minutes. The supernatant was then removed, the pellet air-dried for ca. 5 min, resuspended in 100 µl MilliQ H_2O and stored at -80 °C. Typically 1 µl probe was used for 200 µl hybridisation mix.

Embryos were fixed overnight in 4 % PFA and transferred via a series of increasing concentration into methanol. Embryos were stored at – 20 °C in 100 % MeOH at least over night. Staining commenced by rehydrating the embryos with a series of increasing concentrations of PBTw in MeOH followed by 4 washes of 5 min in PBTw. To improve permeabilisation embryos were incubated for 30 min in 10 µg/ml proteinase K (in 48 hpf embryos, 24 hpf embryos require no proteinase K treatment), refixed in 4 % PFA for 20 min and washed 3 times for 5 min in PBTw. Embryos where then incubated in pre-hybridisation

mix (50 % formamide, 5x SSC (saline-sodium citrate buffer), 0.1 % Tween20, 9.2 mM citric acid, 50 mg/ml heparin, 500 µg/ml tRNA – all diluted in MilliQ H_2O) for 1 h at 70 °C. The hybridisation mix was subsequently replaced with pre-hybridisation mix containing 500 ng probe and incubated over night at 70 °C. Next day the following washes occurred at 70 °C: 100% hybridisation buffer (50 % formamide, 5x SSC, 0.1 % Tween20, 9.2 mM citric acid – all diluted in MilliQ H_2O) for 5 min, 75% hybridisation buffer/25 % 2x SSC for 15 min, 50% hybridisation buffer/50 % 2x SSC for 15 min, 25% hybridisation buffer/75 % 2x SSC for 15 min and 2x SSC for 15 min. Subsequently the following washes occurred at room temperature: 75% 0.2 x SSC/25 % PBTw for 10 min, 50% 0.2 x SSC/50 % PBTw for 10 min, 25% 0.2 x SSC/75 % PBTw for 10 min and PBTw for 10 min. The samples were then incubated in blocking buffer (2 % blocking reagent in PBTw) at room temperature for several hours before a 1:5000 solution of anti-DIG antibody in blocking reagent was applied and samples transferred onto a shaker at 4 °C in the dark. On the third day of staining all steps were conducted at room temperature in the dark: First, a quick rinse with PBTw and four half-hour washes with PBTw were done, followed by applying an alkaline phosphate (AP) buffer (100 mM Tris pH 9.5, 100 mM NaCl, 0.1% Tween20 in MilliQ H_2O) for 15 min which was subsequently exchanged for AP buffer with 50 mM $MgCl_2$ (remainder as before) in two washes of 10 min. For the final staining 3.4 µl NBT and 3.5 µl BCIP were added per ml of AP buffer and the staining developed in the dark and checked regularly. Once the staining had reach sufficient colouring, the reaction was stopped by washing embryos three times for 5 min at 4 °C in the dark.

1.10. *In vivo* compound screen on *pkd2*$^{-/-}$ zebrafish

1.10.1. High-throughput compound screen

To conduct a high-throughput chemical screen exposing *pkd2*$^{-/-}$ zebrafish to two chemical libraries, Microsource Discovery's Spectrum library and the Published Kinase Inhibitor Set (PKIS, formerly GlaxoSmithKline and subsequently transferred to the University of North Carolina), zebrafish embryos were exposed in the following manner:

At ca. 24 hpf chorions were removed with pronase (2 mg/ml for 13 minutes), embryos were washed briefly and transferred back to 28 °C. As the curly tail phenotype does not appear at the same stage in all embryos (onset approx. 27 – 30 hpf), *pkd2* mutants were sorted into a separate dish containing screening medium (E3 medium, 0.75 x PTU and 1 % DMSO) as the curvature became apparent. Three embryos were subsequently transferred in 150 µl screening medium to each well of a 96-well plate and 100 µl prepared compound solution (compound diluted in screening medium, prepared the day prior and kept at – 20 °C) were

added to a final compound concentration of 10 μM. Exposed plates were incubated at 28 °C for 24 hpf before imaging each well with the Ash Phenosight system (automated 96-well plate microscope taking a single brightfield and GFP fluorescent image of each well allowing image acquisition of one plate in 10 minutes). Curvature analysis commenced using ImageJ software with the method described in (Mangos *et al.*, 2010). DMSO exposed controls were eventually combined as no significant differences between experimental days were observed and a large control group was established

Initial hits were chosen via a student's t-test and re-tested in a second round. Additionally, all compounds were re-tested where more than one embryo had died in the previous exposure round. Compounds were either re-tested at 10 μM (if it was apparent that one decaying embryo had deprived the others of oxygen needed for development) or 0.3 μM if the compound was toxic, after careful assessment of the images. Final hit compounds were determined using one-way anova analysis combining all data collected.

Subsequently hit compounds were re-ordered and re-testing commenced using the same conditions as before, also testing a variety of concentrations, or by starting exposures at late epiboly stages, in the latter embryos were not dechorionated. Imaging always commenced between 49-52 hpf (curvature is fully developed by 48 hpf and remains stable). Hit compound sources are listed below in Table 12 and further compounds of interest, which were ordered for mechanistic studies, are catalogued in Table 13.

Chemical	Supplier	Cat no.
2,5-di-tert-butyl-4-hydroxyanisole	Sigma-Aldrich	447323
diclofenac	Sigma-Aldrich	93484
zinc pyrithione	Sigma-Aldrich	H6377
5alpha-androstan-3,17-dione	Microsource Discovery Systems, Inc.	00107108
5,7,4'-trimethoxyflavone	Microsource Discovery Systems, Inc.	00300384
hexamethoxyquercetagetin	Microsource Discovery Systems, Inc.	01505383
prenyletin	Microsource Discovery Systems, Inc.	00100101
pimpinellin	Microsource Discovery Systems, Inc.	00300013
sphondin	Microsource Discovery Systems, Inc.	00300005

Table 12 Hit compounds re-ordered due to screen.

Chemical	Supplier	Cat no.
flutamide	Sigma-Aldrich	F9397
naringenin	Sigma-Aldrich	W530098
nifedipine	Sigma-Aldrich	N7634
sodium pyrithione	Sigma-Aldrich	H3261
testosterone	Sigma-Aldrich	R1881
11-ketotestosterone	Sigma-Aldrich	K8250
Bay K8644	Sigma-Aldrich	B112
Tolvaptan	Sigma-Aldrich	T7455
Zinc chloride	BDH	103794P

Table 13 Further compounds to study mechanistic functions.

All chemical structures shown in this thesis were obtained from PubChem (https://pubchem.ncbi.nlm.nih.gov/) and can still be accessed there.

1.10.1. Compound exposure with more than three larvae

After initial screening was completed and exposure of more than three embryos per treatment group became desirable, in particular for exposure of renal GCaMP7a embryos, exposures were conducted with up to 20 embryos per well in 6-well plates with 3 ml medium while keeping all other conditions the same unless otherwise stated. For earlier exposures, for example from epiboly, dechorionating was not an option as the embryos are too fragile at these states and exposures were conducted without removing the chorion. Thapsigargin treatments occurred by exposing the fish to 5 µM thapsigargin for 25 min and 2-APB (2-aminoethoxydiphenyl borate) was exposed for 2 h.

1.11. Cell culture

Cells were thawed after removal from the liquid nitrogen tank by heating them gently until semi-liquid, adding medium and transferring them to a prepared T75 flask with medium. To freeze cells confluent flasks were trypsinized, cells centrifuged for 5 min at 1000 rpm and resuspended in 90 % growth medium/10 % DMSO before rapidly transferring them to -80 °C in an appropriate box.

Cell lines were maintained in T75 flasks with the appropriate medium at the appropriate temperature. Canine MDCKII cells (first described in (Barker *et al.*, 1981)) were grown at 37 °C in Gibco DMEM/F-12 medium with 10 % FBS, 1 % Penicillin/Streptomycin and 1% L-glutamine. Immortalised, patient-derived Ox161c1 cells (first described in (Parker *et al.*, 2007)) were grown at 33 °C in Gibco DMEM/F-12 medium with 5 % Nu-Serum, 1 % Penicillin/Streptomycin and 1% L-glutamine.

1.12. Three-dimensional cyst culture

Three-dimensional cyst assays have been a long-standing method of studying cyst formation processes (McAteer *et al.*, 1986; Yamaguchi *et al.*, 1995). In 3D assays, cells are seeded into a matrix (i.e. collagen or matrigel) where they grow into spherical cysts over time (ca. 20 days) and are supplied with nutrients and/or drugs from the medium above (see Figure 12). After the growth/exposure period, the cysts are imaged and cyst size can be analysed as a marker for expansion or reduction processes. Two cell lines, which have been used during this project, will be described in more detail in the next two paragraphs.

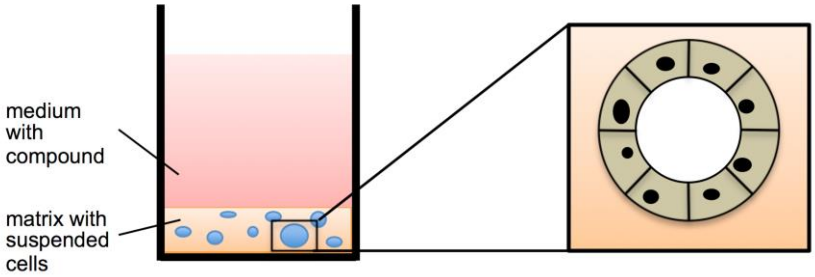

Figure 12 Schematic depiction of a three-dimensional cyst assay.

1.12.1. MDCKII cells

MDCKII cells were isolated in 1958 from normal renal epithelial cells of a female Cocker Spaniel (Barker *et al.*, 1981). This cell line is able to form cysts in a collagen matrix and has been shown to exhibit a well-established cell polarity with distinct basolateral and apical polarization (McAteer *et al.*, 1986; O'Brien *et al.*, 2002). Forskolin, an activator of adenylate cyclase, has been shown to have very strong cystogenic effects (Yamaguchi *et al.*, 2000), (Hanaoka & Guggino, 2000; Yamaguchi *et al.*, 1995)). Although MDCKII cells have not been derived from an ADPKD model, the common underlying processes of cystogenesis have been studied in depth using this line. Figure 13 depicts an example of typical DMSO and forskolin treated MDCKII cyst cells after 19 days of exposure.

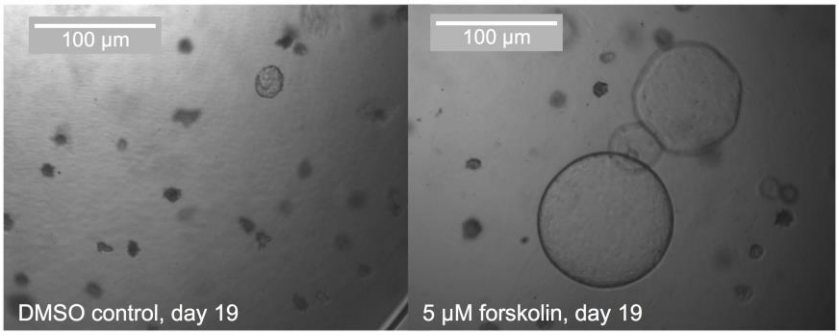

Figure 13 Example images at the endpoint of 3D cyst culture with MDCKII cells. (Left) DMSO control at day 19. (Right) 5 µM forskolin positive control at 19 days of exposure.

Cells were grown to confluence, washed in PBS, trypsinized before centrifuging for 5 min at 1000 rpm and resuspended in small amount of medium (ca. 400 µl). 70 % rat tail collagen, 20 % 11.76 mg/ml $NaHCO_3$ and 10 % 10 x MEM (minimum essential medium) were mixed gently on ice and 20,000 cells/ml matrix were added. 70 µl of collagen/cell mix was subsequently added to each well in a 96-well plate which polymerised in the incubator for ca. 10 min. Afterwards medium was added (Gibco DMEM/F-12 medium with 10 % FBS, 1 % Penicillin/Streptomycin and 1% L-glutamine) containing DMSO as control or the compounds of interest. 5 µM forskolin served as positive control. The medium (with compound) was prepared at the day of seeding the cells in a quantity sufficing the entirety of

the assay. Medium on the cells was exchanged every 2-3 days for 19 days. Cysts were imaged on days 10, 14 and 19 and analysed with ImageJ.

The rat tail collagen (enriched with collagen-I) had been extracted previously by one of my colleagues using the following protocol: Rat tail tendons were removed with forceps and kept in PBS on ice before discarding the PBS and adding 100 ml of 0.1 % acetic acid per rat tail. This mixture was stirred at 4 °C for a minimum of 72 h before centrifugation at 27,000 g for 20 min at 4 °C. The supernatant was used in subsequent experiments and stored at 4 °C.

1.12.2. Ox161c1 cells

Ox161c1 cells were derived from cystic renal tubules of a female ADPKD patient with a *PKD1* null-mutation in the N-terminal extracellular domain. The cells were subsequently immortalized and found to form cysts when grown in a matrigel matrix (Parker et al., 2007). The Ox161c1 cell line was obtained by transducing a primary culture with a replication-defective retroviralnvector (containing the temperature-sensitive LT antigen and the catalytic subunit of human telomerase). The LT antigen destabilizes at higher temperatures whereas a shift to 33 °C allows normal proliferative growth (Streets et al., 2003). The *PKD1* mutation in this cell line is predicted to cause a truncating mutation and the cells can therefore be described as $PKD1^{-/-}$ Human Ox161c1 cells form markedly smaller cysts and forskolin has a less pronounced effect in comparison to canine MDCKII cells. Although this cell line is less robust, it carries a *PKD1* mutation and thus can more closely the disease state. Figure 14 displays Ox161c1 cells exposed to DMSO or forskolin for 20 days.

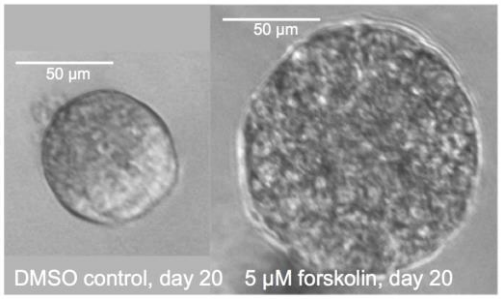

Figure 14 Example images at the endpoint of 3D cyst culture with Ox161c1 cells. (Left) DMSO control at day 20. (Right) 5 µM forskolin positive control at 20 days of exposure.

Cells were grown to confluence, washed in PBS, trypsinized before centrifuging for 5 min at 1000 rpm and resuspended in small amount of medium (ca. 400 µl). Matrigel and 20,000 cells/ml matrix were mixed gently on ice. 100 µl of matrix/cell mix was subsequently added to each well in a 96-well plate which polymerised in the incubator for ca. 10 min. Afterwards supplement medium was added (Gibco DMEM/F-12 medium with 10 % FBS, 1 % Penicillin/Streptomycin, 1% L-glutamine, 10 ng/ml hEGF, 5 µg/ml Hydrocortisone and 1x

ITS) containing DMSO as control or the compounds of interest. 5 μM forskolin served as positive control. The supplement medium (with compound) was prepared at the day of seeding the cells in a quantity sufficing the entirety of the assay. Medium on the cells was exchanged every 2-3 days for 20 days. Cysts were imaged on days 10, 14 and 20 and subsequently analysed with ImageJ.

1.13. Lightsheet microscopy

Alternatively to confocal microscopy, which illuminates the entire sample at once, usually with a high laser power, lightsheet microscopy has been established in recent years and commercial microscopes have become available such as the Zeiss Lightsheet Z.1 system. In lightsheet microscopy, only a very thin plane of the embryo is illuminated at a very low light intensity, causing less damage to the animals and a lower amount of GFP-bleaching.

For lightsheet microscopy, anaesthetised embryos were immobilised using 0.8 – 1 % low-melt agarose, which was drawn up with the embryo into a thin glass capillary where it polymerised. During the imaging process, the embryos were suspended from the capillary in an agarose cylinder into the imaging chamber containing embryo medium with tricaine. Images were processed with the ZEN black software from Zeiss.

1.14. Statistical analysis

All statistical analyses were performed using the GraphPad Prism software. The relevant analyses, as required for the individual datasets, were conducted and detailed information about the tests used is stated in the legend of each figure where appropriate. Data that did not reach statistical significance but exhibited a recognisable behaviour, judged by eye, are referred to throughout this thesis as "trends". No particular threshold of p-values was applied for such a statement.

Results and Discussion Chapter 1: Characterisation of zebrafish PKD models

Introduction

Zebrafish *pkd2* mutants and morphants share some phenotypes, like L/R patterning defects and a *curly up* tail, other traits, however, such as renal dilations, have been described exclusively in knockdown animals (see Introduction Chapter 9.2.). In order to select a trait for chemical library screens, the main aim of this project, a detailed characterisation of the *pkd2*^{hu2173} allele animals and *pkd2* morphants was carried out.

Furthermore, ADPKD is described to be a ciliopathy although a variety of arguments can be made against such a classification (see Introduction Chapter 8.). However, as PC2 and the PC-complex are localised to a large extent in primary cilia, the effect of cilia-abolition is of interest in *pkd2*$^{-/-}$. Particularly so, as a previous publication in a mouse model described that loss of cilia in *Pkd* mutants improved the renal cystic phenotype (Ma *et al.*, 2013). This publication reports that crossing *Pkd* mutant lines, which develops very large renal cysts, to a ciliary mutant line (*Kif3a*), which develops small kidney cysts, led to a less severe cystic phenotype in the double mutant animals compared to the *Pkd* single mutants (but cysts were still more severe than in the *Kif3a* mutant line). This research suggests that loss of malfunctioning ciliary polycystins is beneficial in an ADPKD model.

The *elipsa*^{tp49d}, referred to as *elipsa,* mutant strain was first described in (Drummond *et al.*, 1998) and further characterised in (Omori *et al.*, 2008) as a ciliary mutant. It probably has early ciliogenesis (since there are no observed L/R polarity defects, see Figure 27 A), but lacks cilia from at least 30 hpf (personal communication Niedharsan Pooranachandran). *elipsa* (or *traf3ip1*) encodes a ciliary trafficking protein that mediates interactions between *ift20* and *rab8* and this complex in turn facilitates IFT (intraflagellar transport) particle movement along the ciliary axoneme. Loss of *elipsa* therefore leads to loss of ciliogenesis. The *elipsa* transcript was reported as enriched in ciliated tissues such as the olfactory pits, lateral line organs and pronephric ducts (Omori *et al.*, 2008). *elipsa* mutants developed dilated pronephric glomeruli and tubules as well as a ventral axis curvature, which is characteristic for many ciliary mutants ((Kramer-Zucker *et al.*, 2005; Sullivan-Brown *et al.*, 2008), example in Figure 24 B). A curly down tail is not always accompanied by pronephric dilations (Brand *et al.*, 1996; Sullivan-Brown *et al.*, 2008) but it is commonly associated with disruptions of the intraflagellar transport, like in *elipsa* mutants.

In the following chapter *pkd2* mutants, *pkd2* morphants and the ciliary *elipsa* mutant, as well as a cross of the two mutant lines, will be described in detail.

Results

11. Characterisation of *pkd2* models

11.1. *pkd2*^{hu2173} mutation

The *pkd2*$^{hu2173/hu2173-/-}$ zebrafish mutant, henceforth referred to as *pkd2*$^{-/-}$, was created during an ENU-mutagenesis screen and carries a point mutation in exon 5, leading to a truncated protein (Freek van Eeden, unpublished). In this mutant allele a guanine base is replaced with an adenine base in position 1327 of the mRNA (see Figure 15 A), resulting in a stop codon at amino acid 302 of 904. The truncation occurs in the first extracellular loop (Figure 15 B). The channel pore of the PC2 protein is formed by the two transmembrane domains closest to the C-terminus (Pavel *et al.*, 2016) and as the *pkd2*^{hu2173} allele is predicted to result in a truncation in the first extra-cellular loop, well before the channel pore, presumably causing a null mutation. Phenotypically, the *pkd2*$^{-/-}$ zebrafish mutant shows the typical body axis deformation with its upward curled tail described for *pkd2* morpholino-injected embryos (chemical gene knockdown, originally described in (Sun *et al.*, 2004)), see Figure 17.

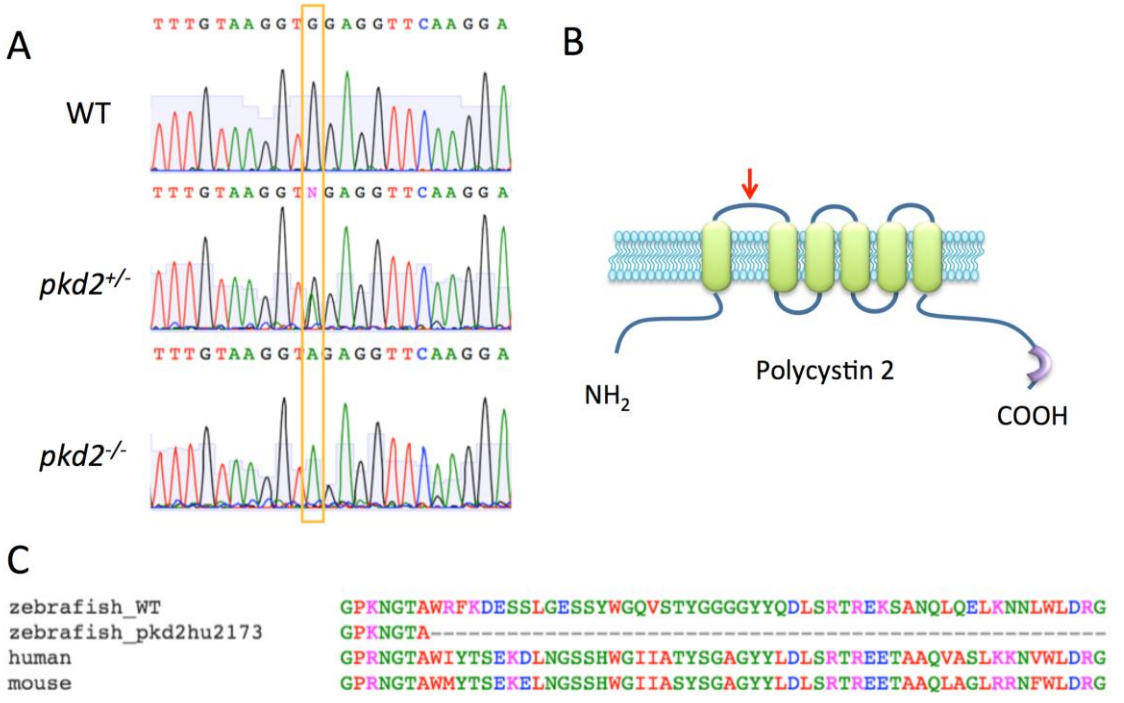

Figure 15 (A) Aligned DNA sequences of WT, *pkd2*$^{+/-}$ and *pkd2*$^{-/-}$; mutation of *pkd2*^{hu2173} framed by orange box. (B) Schematic depiction of polycystin 2 with the approximate site of truncation in *pkd2*^{hu2173} marked with red arrow. (C) PC2 amino acid alignments for zebrafish WT and *pkd2*^{hu2173}, human and mouse.

11.1.1. Mutant development

pkd2$^{-/-}$ zebrafish embryos develop the characteristic dorsal axis tail curvature previously described in *pkd2* morphants (Cao *et al.*, 2009; Schottenfeld *et al.*, 2007; Sun *et al.*, 2004) which has been attributed to excessive extracellular matrix deposition (Mangos *et al.*, 2010) or production (Le Corre *et al.*, 2014). This unique tail phenotype led to the original dubbing of the mutant strain as "*curly up*", or "*cup*" (Brand *et al.*, 1996). The first indications of the tail curvature can be observed by 24 - 25 hpf in some embryos (Figure 17 A), although the phenotype does not appear simultaneously in all individuals and onset can be delayed until about 29 hpf. Following initial onset, the curly tail becomes increasingly pronounced; by 48 hpf (Figure 17 C) the curvature has fully matured. There is some level of correlation between a delayed curvature onset and a less pronounced curvature phenotype, but this was not significant (Figure 16 A).

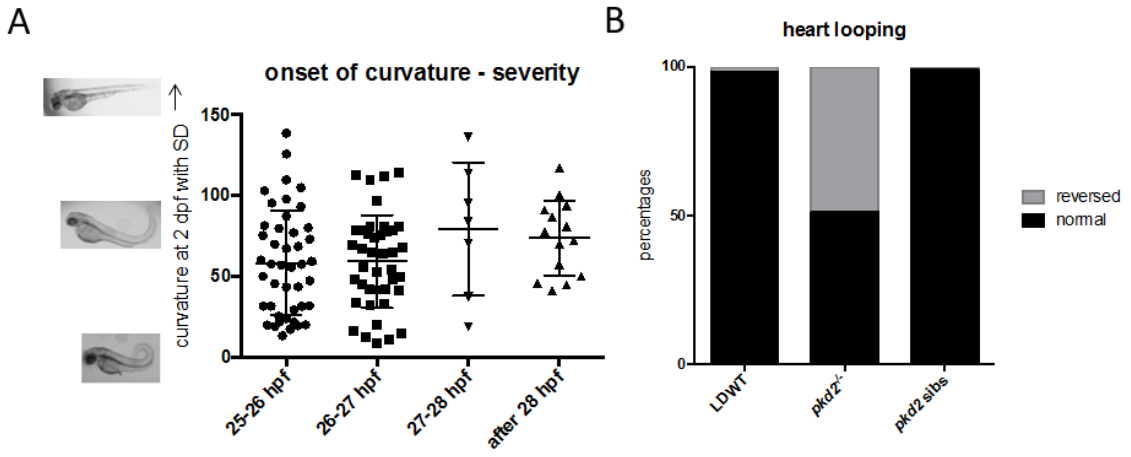

Figure 16 (A) Correlation of *pkd2*$^{-/-}$ curvature onset and severity. 180° - straight tail, 0° - tail crosses body axis; example images of curvature next to y-axis. No significances via one-way anova with Tukey's multiple comparison test. Error bars indicate SD. (B) Heart looping ratios in WT, *pkd2*$^{-/-}$ and *pkd2* siblings. n = 100 for each group.

Left/right polarity randomisation, another phenotype previously described in morphants, was confirmed for *pkd2*$^{-/-}$ with a rate of 49.3 % heart looping reversal (Figure 16 B). This indicates a full gene knockout, or null mutant, as there was complete randomisation.

Cardiac, trunk and head oedema became apparent at 4 dpf (Figure 17 F and I) and continued to develop during the next 24 h. By 5 dpf (Figure 17 G and K) oedema severity increased to the point where cardiac function was strongly impaired upon which the embryos were sacrificed.

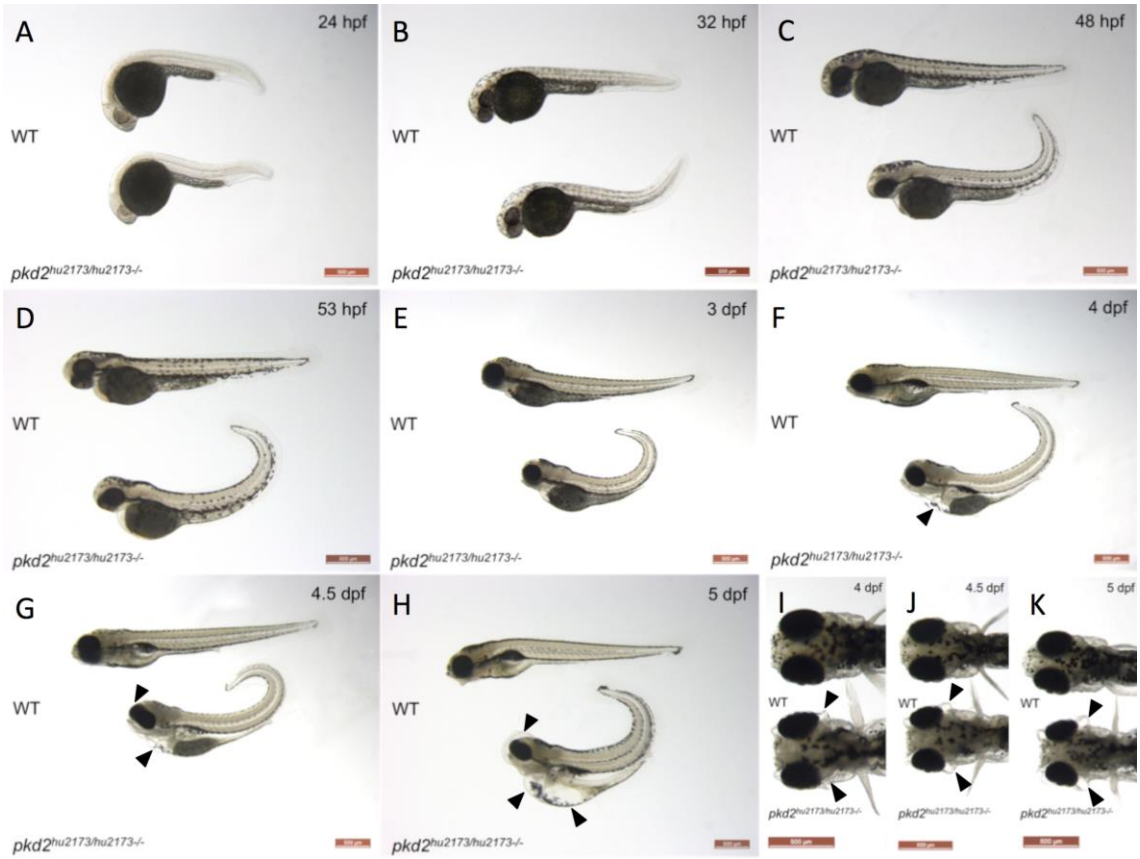

Figure 17 Morphology of *pkd2*$^{-/-}$ and WT embryos during development (A) 24 hpf, (B) 32 hpf, (C) 48 hpf, (D) 53 hpf, (E) 3 dpf, (F) 4 dpf, (G) 4.5 dpf, (H) 5 dpf. (I, J, K) Dorsal view of head region at 4, 4.5 and 5 dpf respectively. Arrowheads indicate oedema.

As cystic expansions in the kidneys were not initially observed in *pkd2*$^{-/-}$ mutants, although it had been described in morphants (Cao *et al.*, 2009; Schottenfeld *et al.*, 2007; Sun *et al.*, 2004), a more detailed analysis was performed. Glomerular sizes were measured in *pkd2*$^{-/-}$ and siblings utilizing the renal *GFP* expression of the *wt1b:GFP* line for imaging. The results are depicted in Figure 18. At 2 dpf, just after renal filtration onset, and 3 dpf glomerular size was similar between *pkd2*$^{-/-}$ and siblings. At 4 dpf and 5 dpf *pkd2*$^{-/-}$ glomeruli were significantly smaller compared to their siblings'. Interestingly, the mean kidney size still increases in *pkd2*$^{-/-}$ over time, but not at the rate of sibling controls.

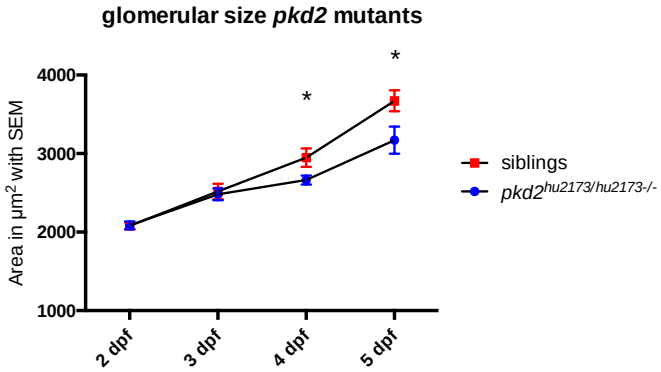

Figure 18 Glomerular sizes in 2 to 5 dpf *pkd2*$^{-/-}$ and siblings. Mean glomerular areas with SEM: 2 dpf, 2856 ± 436 *pkd2*$^{-/-}$ and 2847 ± 404 sibs; 3 dpf, 3396 ± 678 *pkd2*$^{-/-}$ and 3447 ± 856 sibs; 4 dpf, 3647 ± 504 *pkd2*$^{-/-}$ and 4035 ± 1040 sibs; 5 dpf, 4341 ± 1380 *pkd2*$^{-/-}$ and 5026 ± 1128 sibs. Significances via unpaired t-test; *: $p \leq 0.05$. n = 20 for each group and day with both glomeruli measured, i.e. 40 measurements per time and genotype.

11.2. *pkd2* morphant

Morpholino (MO) knock-down experiments were performed using a previously published morpholino sequence (first description in (Sun *et al.*, 2004)). Several publications since reported a dorsal axis curvature, L/R polarity defects and cystic kidneys in morphant animals (Francescatto *et al.*, 2010; Schottenfeld *et al.*, 2007). Injections with an initial morpholino batch ordered from GeneTools, LCC, USA resulted in none of the above described phenotypes and high rates mortality. Correspondence with the manufacturer revealed improper synthesis and a second batch was obtained. Subsequent injections at 2 ng *pkd2* MO per embryo (as in (Cao *et al.*, 2009)) produced the described phenotypes at high penetrance, with the exception of renal cysts. Cystic kidneys, or rather dilated glomeruli, were observed infrequently, at approximately 10 - 20% of injected embryos (example, see Figure 19 A). Concentrations lower than 2 ng caused great phenotype variability (Figure 19 B) and injections with 4 ng morpholino per embryo as previously reported in (Schottenfeld *et al.*, 2007; Sun *et al.*, 2004) resulted in high lethality and severe off-target effects (not shown).

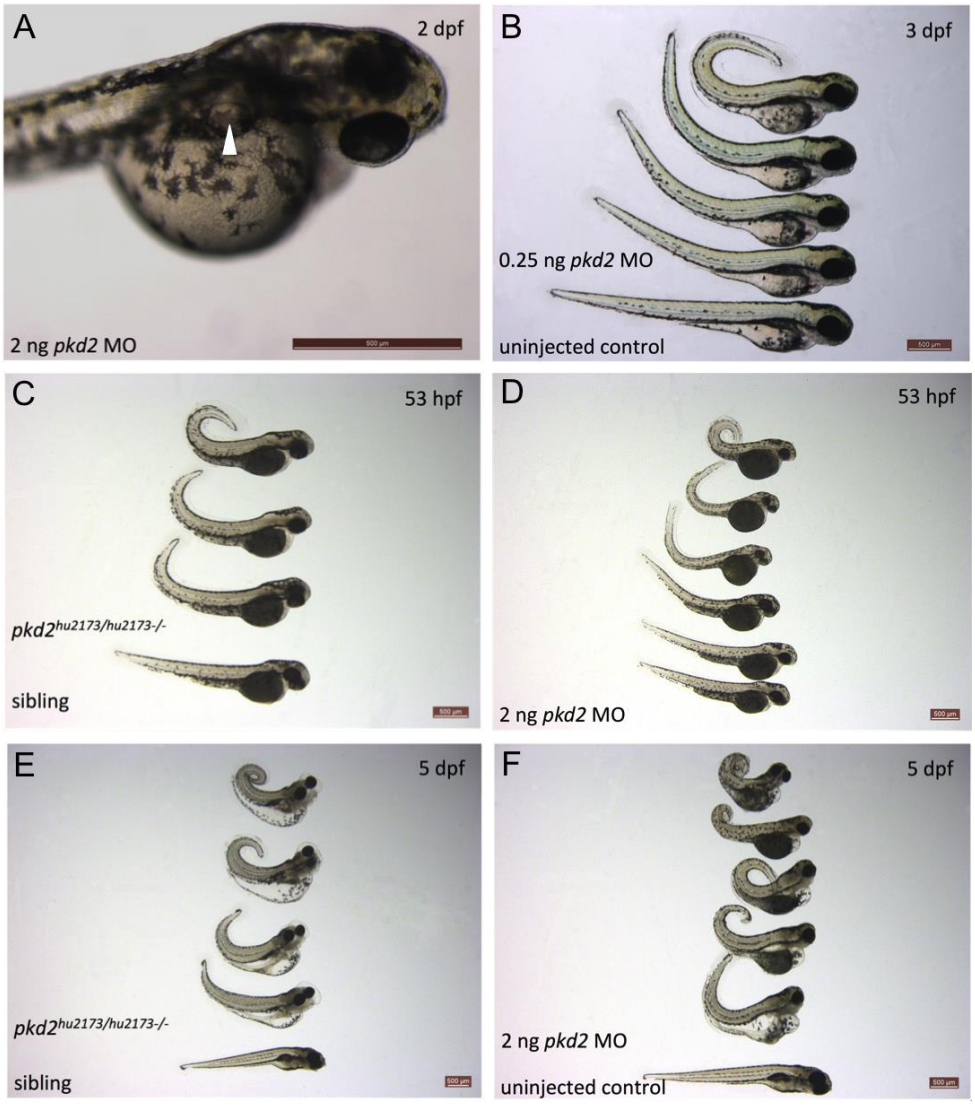

Figure 19 *pkd2* MO injections into WT strains compared to *pkd2*$^{-/-}$. (A) Cystic kidney (white arrowhead) at 2 dpf in *pkd2* MO. (B) Phenotype variability of 0.25 ng MO injected LDWT fish. Variability in *pkd2*$^{-/-}$ (C, E) and 2 ng *pkd2* MO injected AB fish (D, F) at 53 hpf and 5 dpf, respectively.

Body axis curvature, hydrocephalus and L/R randomisation were faithfully recapitulated in *pkd2* MO as previously described (Francescatto *et al.*, 2010; Schottenfeld *et al.*, 2007). The high prevalence of cystic kidneys in previous publications, however, was not observed. Most publications have reported between 60 % and 90 % glomerular dilations in *pkd2* morphant embryos, but only 10 – 20 % of embryos were observed with the phenotype during this project. As hydrocephalus and cystic kidneys were not present in *pkd2* mutants (also noted by (Cao *et al.*, 2009)) this might indicate they were the result of off-target morpholino effects. Both features have been observed as off-target effects in a variety of other morpholinos (Freek van Eeden oral communication).

Cardiac, trunk and ocular oedema were less pronounced in morphants compared to mutants, especially with regard to ocular oedema, a phenotype which was completely lacking in the morphants. Known off-target effects such as smaller eyes and necrosis in the brain were observed in MO-injected embryos (Figure 19 F) and subsequently the *pkd2* morpholino was

coinjected with a *p53* MO to negate this (Robu *et al.*, 2007). Co-injections with the *p53* morpholino are commonly done to minimize off-target effects. In this case, however, it did not result in visible improvements (Figure 20). This indicated the off-target effects observed in *pkd2* morphants were not mediated via *p53*-induced apoptosis.

Interestingly, phenotypes also varied between injections into two different wild-type strains LDWT and AB (see Figure 20 A and B). AB fish exhibited a more pronounced curvature and fewer deaths as well as reduced off-target effects (small eyes and necrosis in the brain). Subsequent sequencing of the morpholino target region revealed a single base mutation in LDWT (see Figure 20 C). The less severe *cup* induction in LDWT could be the result of this mismatch between morpholino and DNA sequence. Further experiments were hence conducted utilising the AB wildtype strain for *pkd2* MO injections.

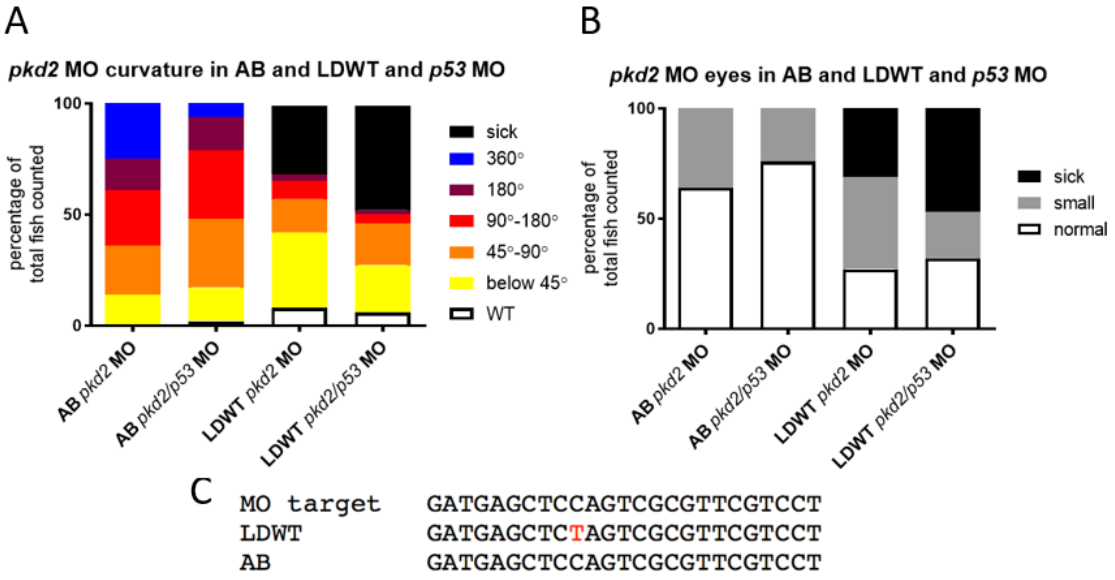

Figure 20 Phenotype analysis in *pkd2* morphants (2 ng per embryo) at 4 dpf in LDWT and AB background with and without coinjection of *p53* MO (1 pmol/embryo) to negate off-target effects. (A) Curvature in respective embryos classified according to severity in degrees with 0° being WT. N ≥ 44 embryos per group (44-71 embryos). (B) Eye phenotypes in respective embryos. (A) and (B) No significant differences via two-way anova with Tukey's multiple comparison test. N ≥ 36 embryos per group (36-71 embryos). (C) Sequences of the morpholino and LDWT and AB target sequences with the mutation in LDWT in red.

Quantification of the cystic kidney phenotype in *pkd2* morphants revealed an early expansion at 2 dpf and 3 dpf, which then plateaued while the sibling glomeruli caught up in size by 4 and 5 dpf (Figure 21).

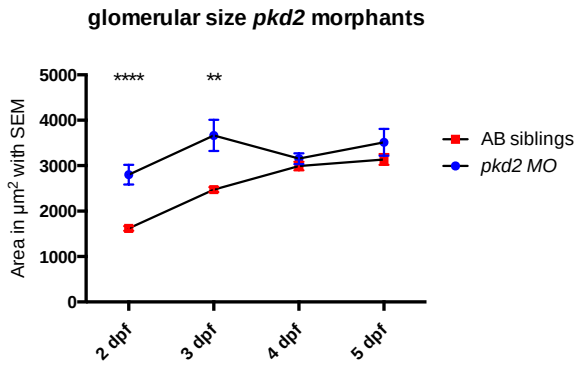

Figure 21 Glomerular sizes in 2 to 5 dpf *pkd2* morphants and siblings injected with 2 ng/embryo. Mean glomerular areas with SEM: 2 dpf, 2801 ± 217 *pkd2*$^{-/-}$ MO and 1618 ± 50 sibs; 3 dpf, 3665 ± 343 *pkd2*$^{-/-}$ MO and 2474 ± 55 sibs; 4 dpf, 3155 ± 119 *pkd2*$^{-/-}$ MO and 2992 ± 93 sibs; 5 dpf, 3515 ± 296 *pkd2*$^{-/-}$ MO and 3136 ± 119 sibs. Significances via unpaired t-test; ****: $p \leq 0.0001$, ***: $p \leq 0.001$, **: $p \leq 0.01$. n = 20 for each group and day with both glomeruli measured, i.e. 40 measurements per time and genotype.

11.3. Model disparities – kidney phenotype

As described above, zebrafish *pkd2* mutants and morphants exhibited several differences, particularly with regard to the cystic kidney and oedema phenotypes – with mutants never developing the former but more severe oedema (oedema depicted at 5 dpf in Figure 22 A). To evaluate whether the renal mutant phenotype could be rescued through the presence of maternal mRNA deposited in the egg, injections with a sub-phenotypic dosage of *pkd2* morpholino into the mutant embryos were performed. A sub-phenotypic dose was chosen to distinguish maternal effects from potential off-target MO effects. This low dose should be sufficient to reduce maternal *pkd2* RNA levels, which has previously been described as non-detectable via *in situ* hybridisation (Bisgrove *et al.*, 2005). The *pkd2* morpholino used during this project was an ATG MO and targeting the transcription start site of a protein ensures knockdown of both embryonic and maternal RNA message. The sub-phenotypic working dose of 0.05 ng/embryo was established by injecting a range of concentrations into WT embryos, assessing for lack of curvature and heart looping defects. 0.05 ng/embryo was the highest concentration not showing above phenotypes and injections into a *pkd2*$^{+/-}$ in-cross commenced. These sub-phenotypic injections significantly enhanced the curvature phenotype in MO injected mutants but had no effect on glomerular size (Figure 20). These results demonstrate likely effects of maternal *pkd2* mRNA on the tail curvature but not on glomerular dilatation. Generally, this indicated the possibility that the *pkd2* morpholino caused off-target effects in the glomerulus.

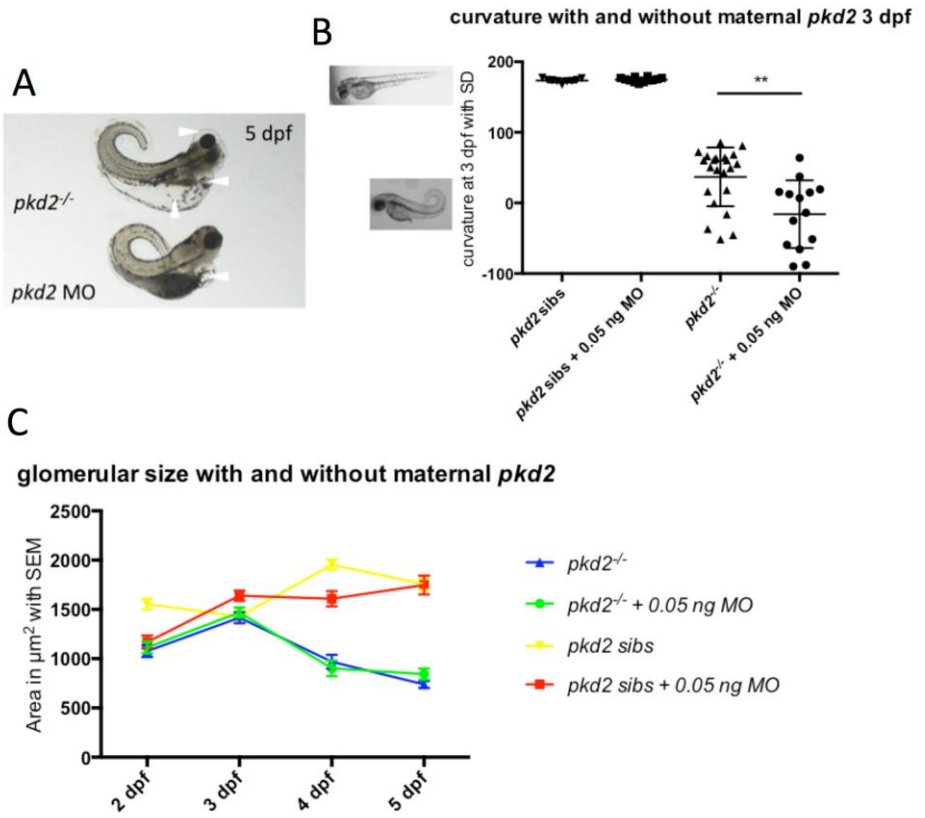

Figure 22 (A) *pkd2* mutant and morphant embryos at 5 dpf, arrowheads indicating oedema. (B) Curvature severity comparing siblings, MO injected siblings, *pkd2*$^{-/-}$ and MO injected *pkd2*$^{-/-}$ at 3 dpf. 180° - straight tail, 0° - tail crosses body axis; example images of curvature next to y-axis. Significance via unpaired t-test; **: $p \leq 0.01$. Error bars indicate SD. (C) Glomerular dilation of siblings, MO injected siblings, *pkd2*$^{-/-}$ and MO injected *pkd2*$^{-/-}$ at days 2, 3, 4 and 5. n = 20 for each group. No significant differences via two-way anova with Tukey's multiple comparison test. Error bars indicate SEM.

In the absence of observable pronephric dilations in the *pkd2* mutants, the possibility of an earlier cellular phenotype was considered i.e. upregulated proliferation. In murine models of cystic renal disease, an early increase in proliferation is often seen before the onset of cyst formation (Bello-Reuss, 2007; Ramasubbu *et al.*, 1998; Saadi-Kheddouci *et al.*, 2001). To assess whether increased cell proliferation was present in zebrafish models, a phosphohistoneH3 (pH3; M-phase marker) antibody staining was conducted on *pkd2* mutant and morphant embryos and respective controls. Figure 23 shows an increase in proliferation in the glomeruli at 2 dpf (not significant) and 3 dpf (significant) in the morphant embryos compared to their siblings. Renal filtration only commences at around 40 - 48 hpf and glomerular dilation occurs afterwards in morphant glomeruli, hence earlier time points were not evaluated. The renal tubules were not dilated in *pkd2* morphants (similar to reports in (Sullivan-Brown *et al.*, 2008)) and showed no change in proliferation rates. *pkd2* mutants showed no significant difference in proliferation anywhere along the pronephros compared to the controls at 2 dpf and 3 dpf, suggesting there is no *pkd2* regulation of proliferation in the pronephros at these stages.

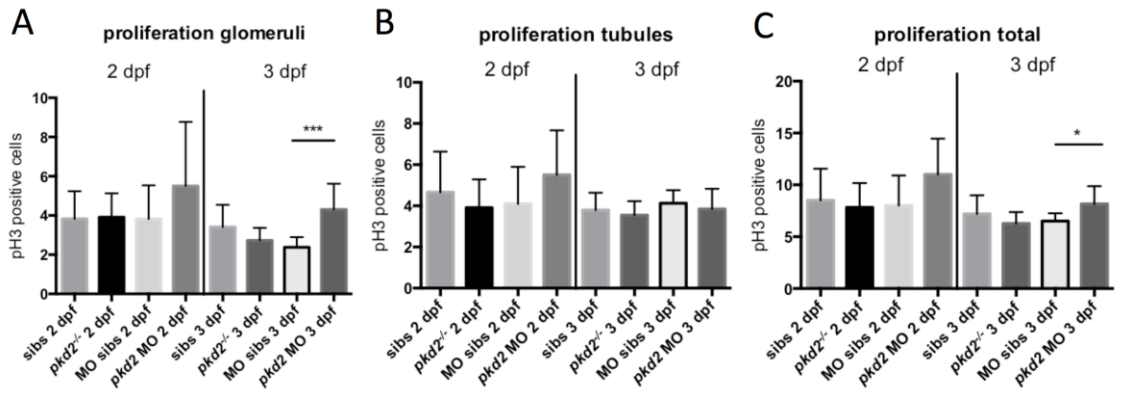

Figure 23 Proliferative cells in *pkd2* mutant and morphant embryos with respective controls at 2 and 3 dpf in the glomeruli (A), the tubules (as far as *wt1b:GFP* is expressed) (B) or the entire proximal pronephros (C) identified by pH3 antibody staining. n = 6-13 per group. Significances via unpaired t-test; ***: $p \leq 0.001$, *: $p \leq 0.05$. Error bars indicate SD. An example of a successful pH3 antibody stain can be seen in Figure 39.

As the main aim of this project was to conduct a compound screen on an ADPKD-related phenotype in zebrafish, *pkd2* mutants and morphants were exposed to 10 different chemicals at different concentrations. Further to the differences in glomerular dilation and proliferation in mutant and morphant embryos, an initial compound test found that the morphants collectively fared worse during drug exposures. Specifically, exposed morphants exhibited higher rates of necrosis, in particular in the brain, and a generally delayed development compared to unexposed controls (data not shown).

Due to these marked differences between *pkd2* mutant and morphant phenotypes, it was decided to abandon the original plan of conducting a large-scale compound screen on the cystic kidney phenotype of morphants in favour of using the dorsal axis curvature in mutants as a readout. This *curly up* phenotype is unique and all knockout or knockdown models described so far in the literature causing the *cup* phenotype in zebrafish are *pkd1*- or *pkd2*-related (Bisgrove *et al.*, 2005; Mangos *et al.*, 2010; Sun *et al.*, 2004).

12. Characterisation of *elipsa* and *elipsa/pkd2* double mutants

The lack of a cystic phenotype in *pkd2* mutants contrasts with that reported for other ciliary mutants in zebrafish where pronephric cysts are a constant feature (Kramer-Zucker, Olale, *et al.*, 2005; Sullivan-Brown *et al.*, 2008). Since *pkd2* and the PC complex are localised to primary cilia (although not exclusively), the lack of a cystic phenotype was surprising.

To test the hypothesis that *pkd2* could modify the phenotype of a cystic zebrafish mutant, *elipsa* mutants, which develop a cystic phenotype, were crossed with the *pkd2* mutant line to obtain double mutants.

12.1. A classical "cystic kidney" zebrafish line, the *elipsa* mutant

The curvature in *elipsa* mutants phenotype first became apparent at 26 - 28 hpf (Figure 24 A), when interestingly, it looked like the emerging *pkd2 curly up* phenotype. Until about 32 hpf the curvature continued to curl upwards, but by 48 hpf, the phenotype had transformed to a downward curl. The exact timing of this transition was not observed. The tail curvature subsequently matured until ca. 72 hpf.

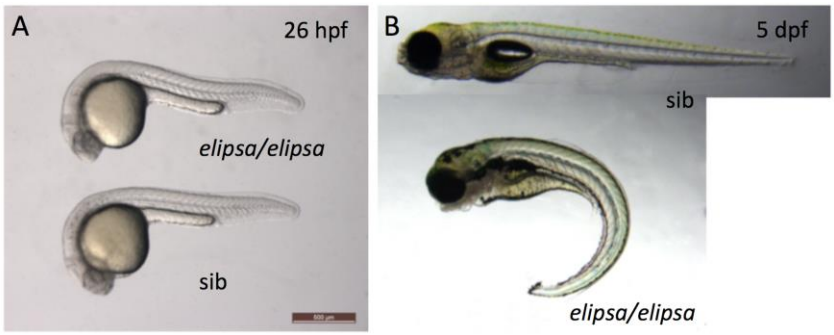

Figure 24 Morphology of *elipsa/elipsa*. (A) Curvature onset at 26 hpf compared to sibling. (B) Matured curvature at 5 dpf in contrast to sibling.

Most ciliary mutants reported in the literature exhibit dilated glomeruli and tubules (Kramer-Zucker, Olale*, et al.*, 2005; Sullivan-Brown *et al.*, 2008); in comparison, *pkd2* morphants have dilated glomeruli but normal tubules. The arrowheads in Figure 25 A depict dilated *elipsa* glomeruli at 52 hpf, not long after the onset of renal filtration, and Figure 25 C indicates a dilated pronephric tubule – quantifications of these phenotypes will be provided in the next chapter.

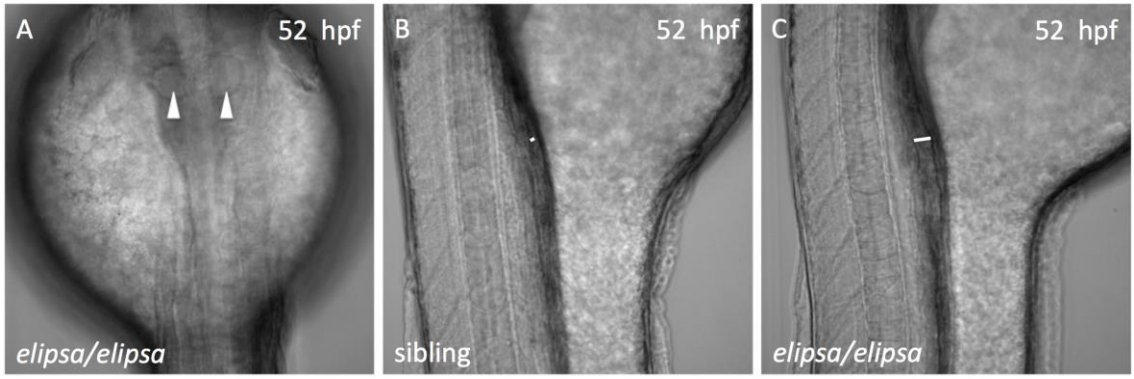

Figure 25 Detailed pronephric images at 52 hpf of (A) dilated glomeruli (indicated with white arrowheads) in *elipsa* mutant, (B) and (C) renal tubules in sibling and *elipsa* mutant, respectively. White bars in (B and C) indicate the width of dilated renal tubules.

12.2. *elipsa/pkd2* double mutant – enhanced renal and curly up phenotypes

pkd2 mutants, as described above, exhibited a pronounced *curly up* phenotype, whereas the ciliary *elipsa* mutants were characterized by a curly down phenotype, which has been observed in various ciliary trafficking mutants with similar severities (Kramer-Zucker *et al.*, 2005; Sullivan-Brown *et al.*, 2008). Interestingly, *pkd2/elipsa* double mutants displayed an enhanced dorsal axis curvature compared to *pkd2* siblings from as early as 32 hpf (Figure 26 A, quantified in Figure 27 C). This phenotype continued to become more pronounced until 50 hpf (Figure 26 B, quantified in Figure 27 F) at which point the *pkd2* curvature was fully developed. In the double mutants, however, the tail curvature continued to develop until about 72 hpf (Figure 26 C) which is similar in duration to the *elipsa* curvature maturation. Since analysis of *elipsa* and *pkd2* mutants necessitated a distinction of *curly up* from curly down, a straight tail was defined with a 0° angle and dorsal curvatures resulted in positive angles and ventral curvatures showed negative values (more details in Figure 27 B).

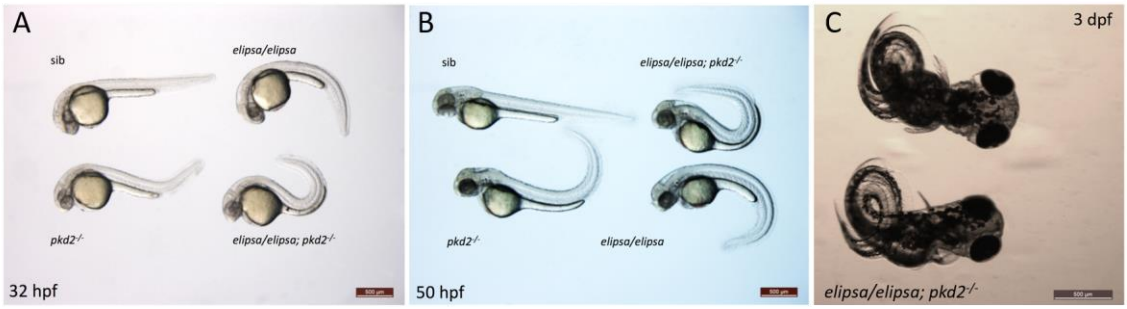

Figure 26 *elipsa*, *pkd2* and double mutants with siblings at 32 hpf (A) and 50 hpf (B). (C) Severe dorsal axis curvature in 3 dpf double mutants.

The renal dilation phenotype in *pkd2/elipsa* mutants was enhanced beyond that of *elipsa* levels (significant at 2 and 3 dpf (Figure 27 C and D)), indicating that loss of *pkd2* in the *elipsa* mutants enhanced the cystic kidney phenotype. There also was a larger spread of glomerular size in the double mutants compared to *elipsa* single mutants and average cystic size was significantly enhanced.

elipsa mutants have been confirmed to lack cilia from the age of 30 hpf (Niedharsan Pooranachandran, personal communication) but the fact that heart looping was not randomized (Figure 27 A), suggests early stage cilia were present as they are required in the Kupffer's vesicle to control body axis formation (Kramer-Zucker *et al.*, 2005). *pkd2* mutants, on the other hand, lack the left-determining signal during early body axis formation in the Kupffer's vesicle and PC2 in its role as a calcium channel is crucial for further signalling cascades during this developmental process (Bisgrove *et al.*, 2005; Schottenfeld *et al.*, 2007). Considering the functions of *elipsa* and *pkd2*, it was not surprising that double mutants exhibited body axis randomization as determined by heart looping randomisation (Figure 27 A).

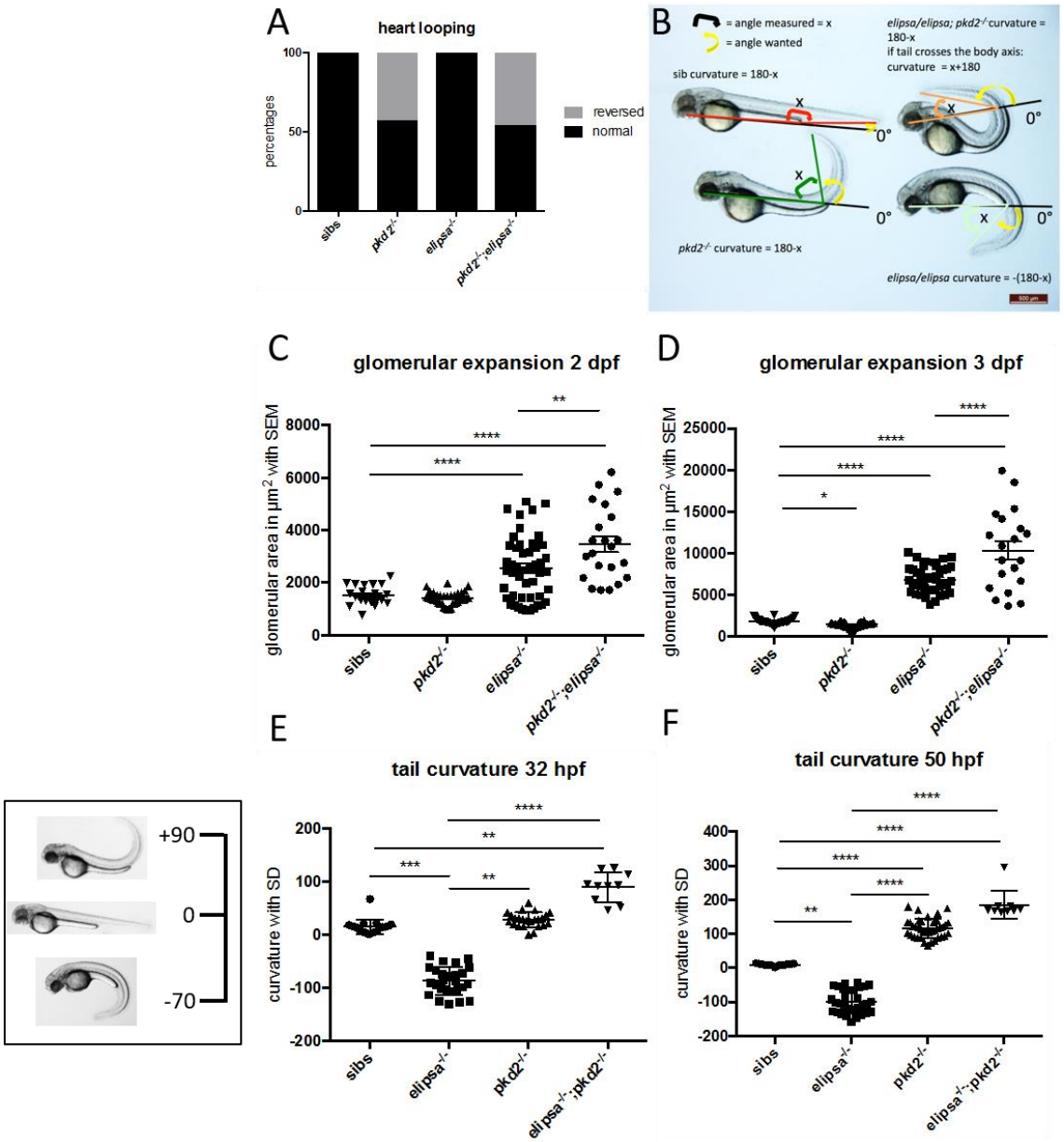

Figure 27 Various comparisons of siblings, *pkd2*$^{-/-}$, *elipsa/elipsa* and *elipsa/pkd2*. (A) Heart looping ratios. n ≥ 13 for each group. (B) Schematic indication of tail curvature measurements. (C) and (D) Glomerular size at 2 and 3 dpf respectively. Significances with one-way anova with Tukey's multiple comparison test; ****: p ≤ 0.0001, **: p ≤ 0.01, *: p ≤ 0.05. (E) and (F) Severity of tail curvature at 32 hpf and 50 hpf respectively. Box on left: Examples of curvature severity with corresponding scale in degrees. Significances with Kruskal-Wallis test with Dunn's multiple comparison test; ****: p ≤ 0.0001, ***: p ≤ 0.001, **: p ≤ 0.01. Error bars indicate SD.

Since the glomerular dilation phenotype in *pkd2* morphants was accompanied by an increase in proliferation, proliferation rates were subsequently quantified in *elipsa* single mutants and *elipsa/pkd2* double mutants at 2 dpf. Interestingly, both showed an increase in proliferation in the glomeruli (Figure 28 A) with the double mutants having a slightly lower proliferation rate compared to the *elipsa* single mutants (not significant). This diverged from the level of glomerular expansion, where double mutants surpass the *elipsa* dilation phenotype. Tubular proliferation levels showed the same trend (not significant, Figure 28 B). Overall proliferation in the pronephros (as identifiable via the *wt1b:GFP* transgene) was only significantly increased in *elipsa* mutants; the double mutants showed a trend towards an

increase in proliferation. This suggests the increase in dilation was not solely driven by proliferation.

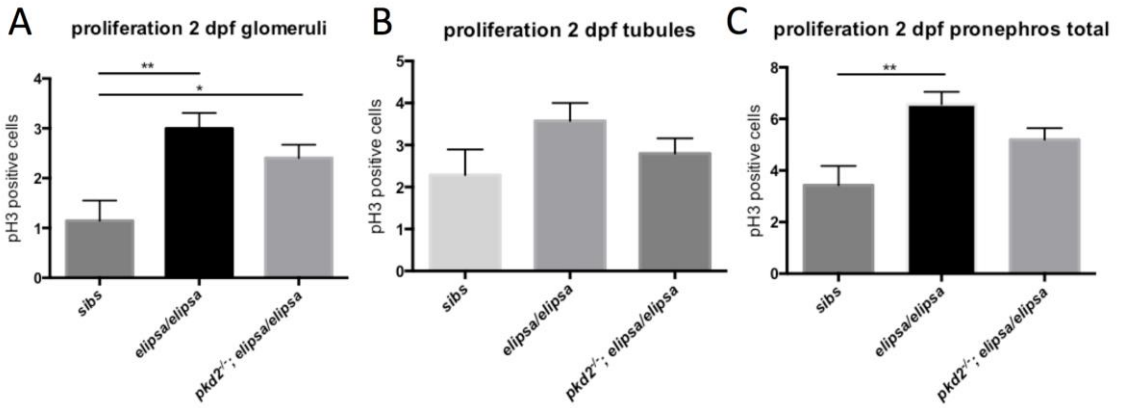

Figure 28 Average proliferation levels assessed via pH3 antibody staining in *elipsa/elipsa*, *pkd2/elipsa* and siblings at 2 dpf. (A) Average proliferation in the glomeruli, (B) in the pronephric tubules and (C) in the entire pronephros as determined by *wt1b:GFP* expression. Siblings: n = 7, *pkd2/elipsa*: n = 14, *elipsa/elipsa*: n = 7. Significances with one-way anova with Tukey's multiple comparison test; **: $p \leq 0.01$, *: $p \leq 0.05$. Error bars indicate SEM. An example of a successful pH3 antibody stain can be seen in Figure 39.

Interestingly, pronephric tubular dilation was also more severe in *elipsa* mutants compared to the double mutants at 5 dpf (not significant, Figure 29). Glomerular area beyond day 4 could unfortunately not be measured, as the distorted tissues above the kidney made it impossible to get clear images of the *GFP* expression below. It was difficult at these stages to capture measurable images in *pkd2* embryos as the *curly up* phenotype refracted the light, but became completely unfeasible in the double mutants due to the severe tail curvature. It is therefore possible that double mutants showed an aggravated early phenotype which was subsequently surpassed by the ciliary mutant.

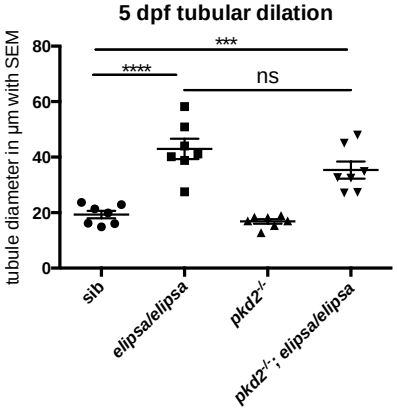

Figure 29 Renal tubular dilation at 5 dpf in *pkd2*$^{-/-}$, *elipsa/elipsa*, *pkd2/elipsa* and siblings. Significances via one-way anova with Tukey's multiple comparison test; ****: $p \leq 0.0001$, ***: $p \leq 0.001$ and non-significant (ns): $p > 0.05$. Error bars indicate SEM.

Discussion

1. Disparities between *pkd2* zebrafish models

pkd2$^{-/-}$ zebrafish embryos have been used to study *pkd2* function by several groups although they have consistently been reported not to develop pronephric cysts. Describing cystic kidneys in the zebrafish embryo pronephros is generally burdened with inaccuracy. What has been described in the literature as "cystic kidneys" in zebrafish embryos, in particular with regard to *pkd2* morpholino knockdown, is not, in truth, a cystic kidney. In general, cysts are defined as fluid-filled sacs surrounded by a membrane. Zebrafish "cystic kidneys", however, are merely dilated glomeruli, which remain part of the embryonic pronephros. Dilated glomeruli could be caused by a variety of factors, such as an increase in proliferation, an occlusion of renal tubules as suggested by (Obara *et al.*, 2006) in *pkd2* morphants, or the lack of cilia (abolishing filtrate movement). The latter two could both cause a build-up of fluid into the glomeruli, potentially inflating these structures due to hydrostatic pressure. With respect to zebrafish *pkd2* models, this raises the possibility of maternal mRNA contribution in mutants or off-target effects in morphants.

There are several possibilities why *pkd2* mutants and morphants differ with regard to their phenotype. All publications to date, described glomerular dilations in *pkd2* morphants to varying degrees of penetrance (Cao *et al.*, 2009; Francescatto *et al.*, 2010; Obara *et al.*, 2006; Sun *et al.*, 2004) whereas *pkd2* mutant alleles did not exhibit this trait (Cao *et al.*, 2009; Schottenfeld *et al.*, 2007; Sun *et al.*, 2004). In recent years, zebrafish morphant data has come under scrutiny for failing to adequately predict mutant phenotypes. More precisely, many morphants exhibited novel traits which were not recapitulated in respective mutant strains (reviewed in (Schulte-Merker *et al.*, 2014)). This could be due to the fact that chemical knockdowns can cause unpredictable off-target effects other than the classical necrosis in the brain and eye, both of which are widely observed (Robu *et al.*, 2007). Furthermore, morpholinos targeting the translation start site of a protein also remove maternal mRNA contributions deposited in the eggs upon laying. Blocking the maternal contribution in the case of *pkd2* caused an enhancement of the curvature phenotype but did not induce glomerular dilations – ruling out the effect of maternal effects on the latter.

A recent study by (Rossi *et al.*, 2015) proposed a different explanation for mutant/morphant disparities: Genetic knockout of a gene could lead to compensatory changes in other members of the same protein family therefore alleviating knockout phenotypes. They supported their hypothesis by injecting morpholinos into respective mutant strains and

showing that the homozygous mutants had a higher resistance towards the knockdown by exhibiting milder phenotypes than their heterozygous or WT siblings. This suggests other genes were compensating for gene loss to some degree. Experiments carried out in this project only targeted maternal mRNA contributions and no inference to compensatory effects in *pkd2* mutants can be made. Therefore, injections of the *pkd2* morpholino (2 ng/embryo rather than a sub-phenotypic dose) into the *pkd2* mutant strain would need to be carried out to shed light on whether there are genetic, compensatory effects preventing glomerular dilation.

Interestingly, *pkd2* mutants not only had no dilated renal phenotype but their glomeruli actually decreased in size compared to siblings from day 4. This development of smaller glomerular size in *pkd2* mutants could potentially be explained by the onset of oedema, which corresponds in timing (see above). Trunk oedema especially could increase hydrostatic pressures compressing the nearby kidney and prevent proper inflation of the glomeruli. Another explanation could be reduced blood pressure: Blood flow might be restricted in the tail area due to the curvature and severe cardiac oedema could prevent normal cardiac output. Both of these factors combined would result in decreased renal blood flow, hindering normal inflation of the glomeruli.

Of note, the pronephric phenotype in *pkd2* morphants did not show a persistent increase in glomerular size over all time points measured. Quantification of the cystic kidney phenotype in *pkd2* morphants revealed an early expansion at 2 dpf and 3 dpf, which then plateaued while sibling glomeruli caught up in size by 4 and 5 dpf. Morpholino effects, both targeted and off-target, wear off over time (the capacity for binding new RNA transcripts diminishes) and morphant phenotypes are therefore often transient. In this case, the glomerular data also suggests that no tubular occlusion occurred, contrary to previously published data (Obara *et al.*, 2006), since the same individuals were imaged over the entire course of the experiment. If the tubules were obstructed, glomerular dilation should continue to persist and increase in severity beyond 3 dpf, which was not the case.

2. Classic "cystic kidney" mutant and *pkd2/elipsa* double knockout

As *pkd2* mutants did not exhibit an obvious renal phenotype, a classical zebrafish "cystic kidney" mutant, the ciliary *elipsa* mutant, was also evaluated. *elipsa* (*traf3ip1)* mutations cause abolition of renal cilia from 30 hpf by disrupting IFT from this time point (in earlier development cilia are unaffected but fail to be maintained from 30 hpf (Omori *et al.*, 2008)). Like all other IFT mutants, this line exhibited a downward curly tail and renal dilations. Pronephric glomeruli and renal tubules along the entire length of the embryo were dilated.

Since *elipsa* mutants did not have laterality defects, it can be assumed that cilia form at early stages of development and become abolished subsequently. Interestingly, the axis curvature in its early stages looked exactly like the dorsal curly tail of *pkd2* mutants. How this then transformed into a down curl was not evaluated.

A genetic study in mice (Ma *et al.*, 2013) suggested that abolition of cilia in PKD mutants improved renal outcomes, indicating that improper polycystin function in the cilia contributes to cyst severity. In that study several *Pkd* mutant lines were crossed to a *Kif3a* knockout line (IFT disrupted) – both mouse strains form renal cysts but loss of *Pkd1* or *Pkd2* causes the more severe phenotype. In double knockout mice, however, renal outcomes were alleviated compared to $Pkd^{/-}$ (but enhanced compared to $Kif3a^{-/-}$). Of note, kidney-specific *Pkd1* knockout mice (Shibazaki *et al.*, 2008) exhibited a more severe and earlier phenotype than the kidney-specific *Kif3a* ciliogenesis knockout (Lin *et al.*, 2003). The zebrafish *pkd2/elipsa* double mutants exhibited an aggravated *curly up* phenotype compared to $pkd2^{-/-}$ and an increase in glomerular dilation compared to *elipsa/elipsa*. This suggested a likely genetic interaction between these two proteins, which will be discussed below.

A graphic scheme of the interactions described in the two paragraphs above, is depicted in Figure 30. In order to explain the phenotypes, it might be useful to think of the various players in basic genetic functions: Wild-type *pkd2* generally serves to counteract the *cup* phenotype and its loss results in an upward curl, it therefore can be described as having a down-curling function. It could be speculated that the downward curl in the cilia-less *elipsa* mutants is driven by a loss of inhibition of *pkd2* function and the over-activated *pkd2* causes as the curly down phenotype. This would suggest there is an inhibitory factor of *pkd2* located in the cilia. If this, however, were the only factor influencing tail curvature, double mutants should exhibit the same severity as *pkd2* mutants in this trait. The fact that the double mutant phenotype is aggravated is somewhat difficult to explain and it would need to invoke a second partially redundant signal specifically from the cilia or a non-ciliary function of *pkd2* after ciliary abolition. This ciliary factor also promotes downward curling but to a lesser extent than *pkd2* itself. Thus in a double mutant, the *pkd2* and the ciliary function, both originally promoting a downward curl, are lost and the dorsal curvature phenotype becomes aggravated.

With regard to the renal dilation phenotypes, loss of cilia causes an expansion of glomerular area; hence some sort of ciliary signal inhibits "cystic kidneys". In *pkd2/elipsa* double mutants this phenotype became exaggerated and it could be hypothesised that *pkd2* itself also has a weak cyst-suppressing function, which is not strong enough to drive renal dilation on its own if lost, but can enhance an already cystic phenotype.

To comply with the rule of maximum parsimony, implying the solution with the fewest factors required is the most likely, the ciliary signal inhibiting renal dilations and repressing the *curly up* phenotype have been summarised as "cilia" in Figure 30, although that function could stem from one or more multiple proteins in the cilia. It could be speculated at this protein with a paralogous function to *pkd2* be a *pkd2l (pkd2 like)* protein, i.e. *pkd2l1a* (*pkd2 like 1 a*) or *pkd2l1b* (*pkd2 like 1 b*) or another calcium channel, although we have no proof of either.

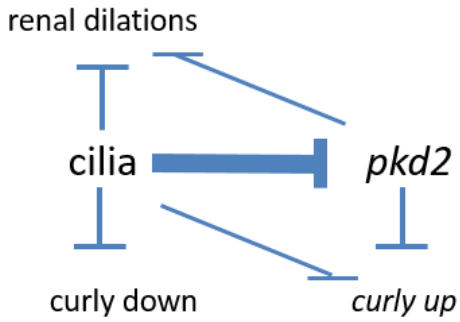

Figure 30 Schematic network of *pkd2* and cilia, depicting the complex interactions used to explain *pkd2*, *elipsa* and *pkd2/elipsa* mutant phenotypes.

Additionally to this complex network, there seem to be tissue-specific differences regarding the levels of *pkd2* and *elipsa* gene interaction. The exaggerated renal dilation phenotype in the zebrafish double mutants suggests that *pkd2* and *elipsa* converge on the same pathway and therefore enhance each other. Considering the slightly different premise of the experiments, this also does not entirely contradict the mouse publication (Ma *et al.*, 2013) as the *Pkd/Kif3a* double mutant mice were also reported to exhibit a more severe phenotype than the ciliary mutation on its own. The increase in severity of the *curly up* phenotype in the double mutants suggests *pkd2* to be downstream of the ciliary pathway, as *pkd2* produces the dominant trait. Conversely, the duration of curvature formation in the double mutants correlates with that of *elipsa* single mutants (lasting until 3 dpf), rather than *pkd2*-deficient animals.

It is possible that depending on the tissue and/or phenotype *elipsa* and *pkd2* act in different manners. The curvature phenotype suggests *pkd2* to be downstream of a ciliary signal, whereas the cystic phenotype indicates *pkd2* and cilia act in parallel the same pathway with the loss of both enhancing a cystic phenotype. These differences strongly suggest a context-specific function.

Results and Discussion Chapter 2: Screens for chemical modulators of the *pkd2* curly phenotype in zebrafish and validation in cell culture 3D cyst assays

Introduction

The main aim of this project was to find novel therapeutic targets for treatment ADPKD by conducting high-throughput chemical library screens on an ADPKD-related phenotype in a zebrafish model. It was shown that the cystic kidney phenotype of *pkd2* morphants was not recapitulated in *pkd2* mutants in addition to a range of other discrepancies (see Results and Discussion Chapter 1). As a consequence, and in order to avoid potential morpholino-artefacts, the curly tail phenotype of *pkd2* mutants was chosen as ADPKD-related readout in subsequent chemical screens. Unfortunately, this trait shows high phenotypic variability (Figure 32 C). In addition, the curvature phenotype did not appear in all embryos at the same time but its onset was spread across ca. 4 hours (25 – 29 hpf). Also, the later the onset, the less pronounced the curvature (Results and Discussion Chapter 1). Therefore, rigorous re-testing was necessary to reduce the risk of obtaining false positive hits. Two small-molecule libraries were screened for their effects on the curly tail phenotype, the Spectrum collection and the PKIS (Published Kinase Inhibitor Set) set.

The Spectrum compound collection provided by Microsource Discovery Systems, Inc. contains 2000 compounds – 50 % of which are clinical trial-stage drugs, 12 % are internationally marketed chemicals and the remaining 38 % are natural products (Rennekamp *et al.*, 2015). In recent years this set of chemicals has been used in multiple zebrafish screens with a variety of phenotypic readouts (Baxendale *et al.*, 2012; Kitambi *et al.*, 2012; Ridges *et al.*, 2012; Saydmohammed *et al.*, 2011).

The PKIS library was utilised in a second screen on the *pkd2* curvature during this project. This compound collection was originally developed by GlaxoSmithKline (GSK) and subsequently transferred to the University of North Carolina (UNC) within the timeframe of the project. The particular version of the PKIS collection used here was PKIS 1, consisting of 367 kinase-inhibiting compounds, covering a wide range of the 518 known kinases (Manning *et al.*, 2002).

Since only small amounts of compound were available from the drug libraries, testing commenced at a fixed concentration of 10 µM. Screening at 10 µM ensured a validation run could be performed where necessary. Screening the effects of compounds on *pkd2* mutants

commenced in 96-well plates, with three embryos per compound, exposed to 10 µM concentrations for 24 h (more detailed information is given in the Materials and Methods section). A schematic depiction of the screen workflow can be found in Figure 31.

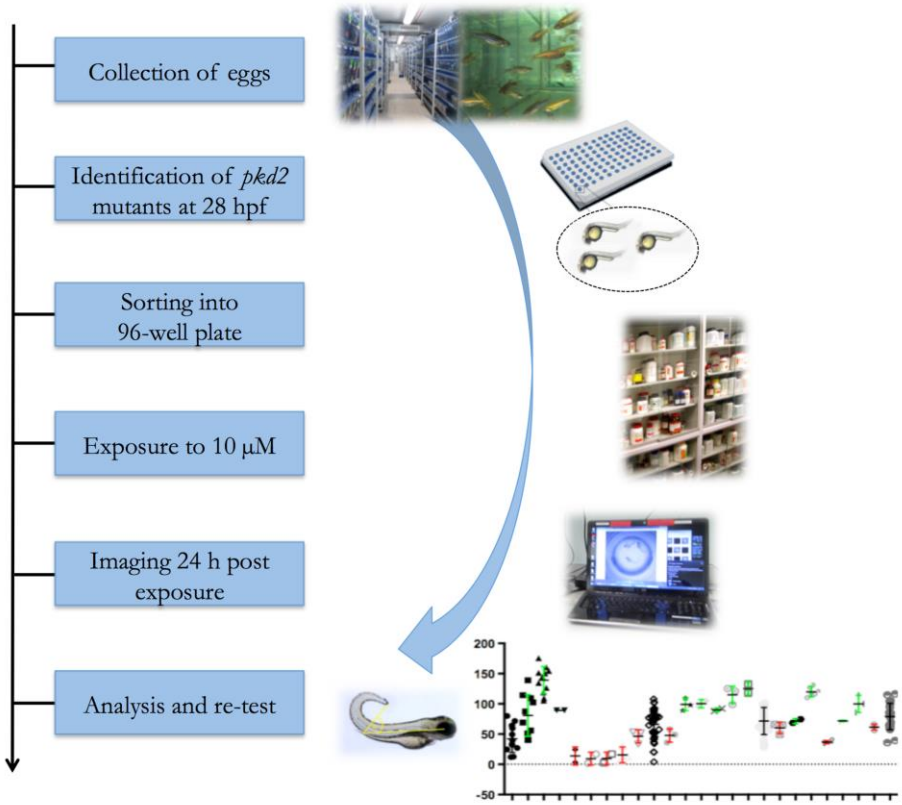

Figure 31 Workflow of compound screen on *pkd2* tail curvature phenotype.

Results

1. Utilising *pkd2*$^{-/-}$ zebrafish as ADPKD-related screening tool

TSA (trichostatin A) had been described previously as repressor of the curvature phenotype in a small-scale compound screen on *pkd2* mutants and served as positive control (Cao *et al.*, 2009). The analysis method of curvature severity was also derived from this publication and will be described in detail below. TSA, a HDAC inhibitor, proved to have a very narrow therapeutic index with a rapid onset of toxicity (400 nM - retardation of growth) and loss of curvature-repressing properties at slightly lower dosages (100 nM). Additionally, TSA caused an accumulation of blood in the area of the duct of Cuvier (Figure 32 B). Nevertheless, it was possible to utilise TSA as positive control, but the narrow therapeutic range and severe adverse effects discounted it as a promising candidate for further study. A quantification of TSA's effect on the tail curvature is depicted in Figure 32 D.

The analysis of *pkd2* tail curliness commenced by drawing a line from the lens in the eye to the end of the yolk extension and a second line from the yolk extension to the tip of the tail – the angle between those two lines served a measure of severity (example, see Figure 32 A). WT embryos therefore have an angle of 170 – 180 degrees, and in *pkd2* larvae, the smaller the angle, the more severe the *cup* phenotype. Negative values indicate the tail had crossed the body axis.

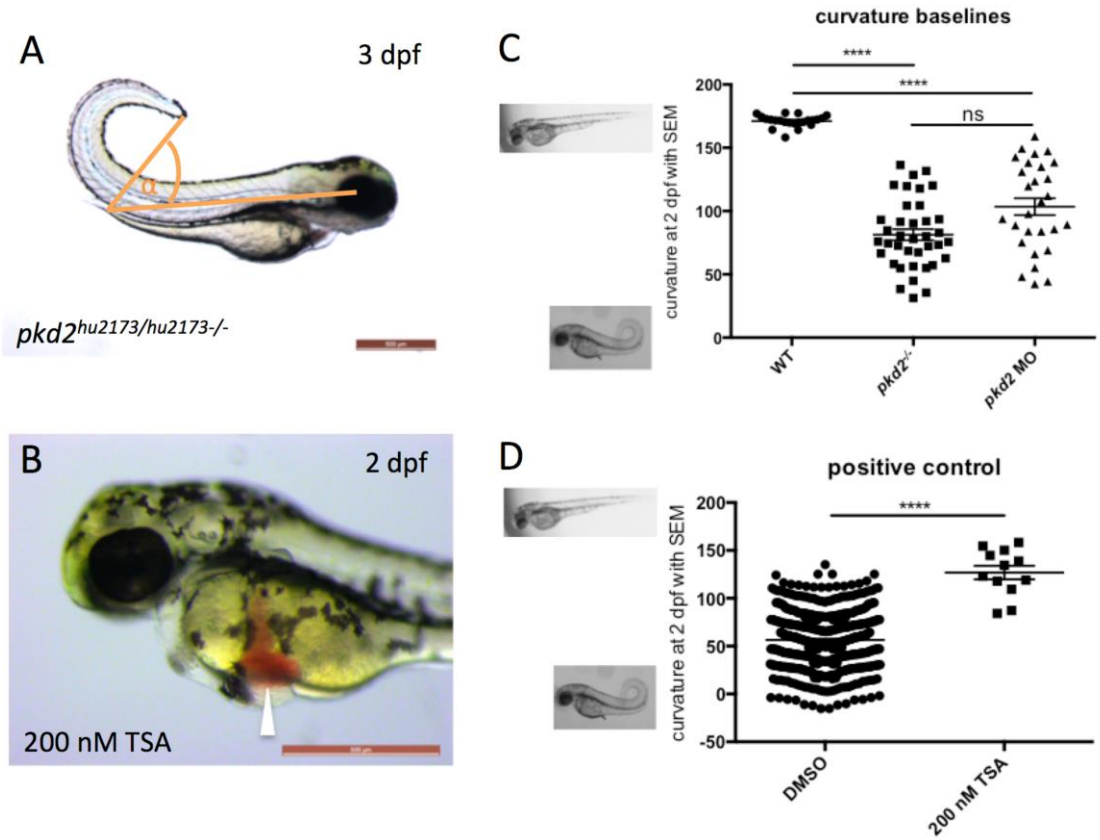

Figure 32 (A) *pkd2*$^{-/-}$ embryo at 3 dpf with schematic indication of curvature measurement. (B) Accumulation of blood in 2 dpf embryo exposed to 200 nM TSA from 27 hpf. Arrowhead indicates pooled blood in the duct of Cuvier (C) Curvature analysis at 2 dpf in *pkd2* mutants, morphants and siblings. Significances via Kruskal-Wallis test with Dunn's multiple comparison test; ****: $p \leq 0.0001$ and non-significant (ns): $p > 0.05$. (D) Analysis of curvature of *pkd2* mutants exposed from 27 hpf to DMSO or 200 nM TSA. Significance via Mann-Whitney test; **** $p \leq 0.0001$. (C) and (D) 180° - straight tail, 0° - tail crosses body axis; example images of curvature next to y-axis. Error bars indicate SEM.

2. Screen of the Spectrum collection

2.1. Zebrafish screen of Spectrum compounds

After the initial testing round was concluded, 200 compounds of interest were identified via t-test (see Materials and Methods) and re-testing commenced. The second test round and more rigorous statistical analysis (see Materials and Methods) reduced that number to 20 drugs and further testing with a cherry-picked batch of additional compound material (provided with the screening plates) eliminated another 7 chemicals. In the end, 13 compounds were identified to significantly and reproducibly alter the curvature phenotype (Figure 33). Of these 13 chemicals, 10 aggravated the curvature and three repressed the phenotype. Interestingly, most of the enhancing compounds clustered into three distinct chemical classes: three compounds were steroids, another three chemicals were coumarins and two compounds were flavonoids. Another flavonoid, naringenin, was subsequently included in further studies as it had been previously observed to induce dorsal curvature (Robert Wilkinson, personal communication).

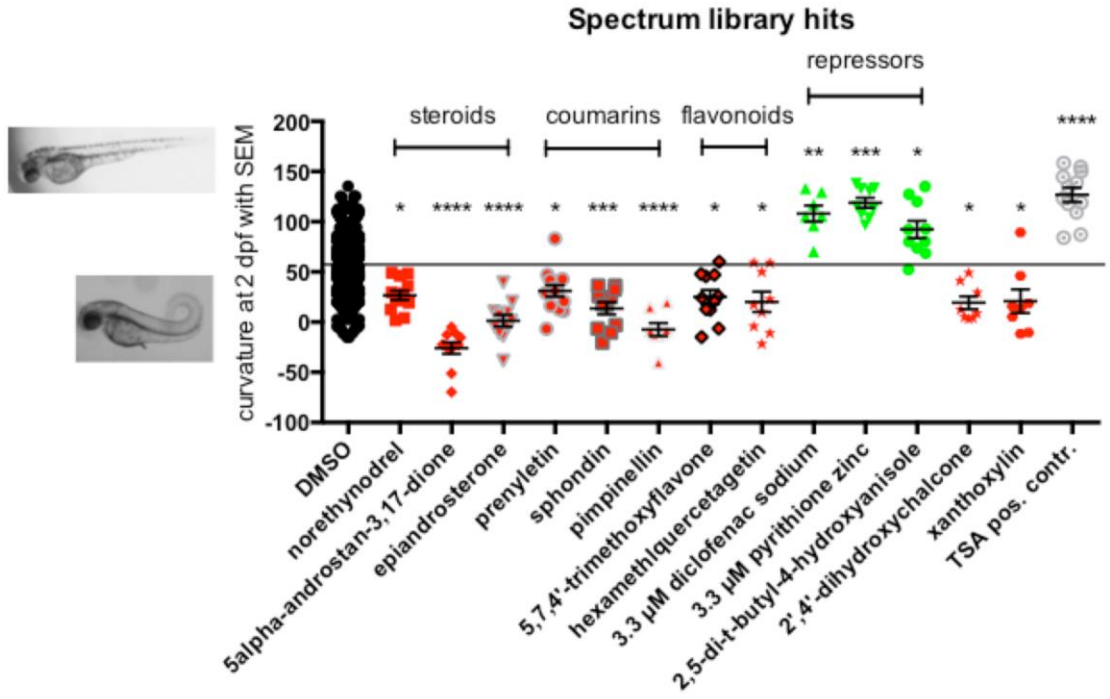

Figure 33 Combined data on hit compounds of the Spectrum library after initial compound screen, validation and cherry-picked compound exposures. Enhancers of *pkd2* curvature in red, repressors in green. Chemical classes as indicated. Mean of DMSO baseline indicated with black line. Significances via Kruskal-Wallis test with Dunn's multiple comparison test; ****: $p \leq 0.0001$, ***: $p \leq 0.001$, **: $p \leq 0.01$, *: $p \leq 0.05$. Error bars indicate SEM.

Hit compounds and more detailed descriptions, including relevant literature, can be found in Table 14.

Effect on *pkd2*$^{-/-}$	Chemical class	Compound name	Additional information	CAS number
enhancer	steroid	norethynodrel	progestin, formerly used as component in oral contraception[1]	68-23-5
enhancer		5alpha-androstan-3,17-dione	androgen, precursor of testosterone and estrogen, can function as bypass to anti-testosterone cancer treatment[2]	846-46-8
enhancer		epiandrosterone	androgen, precursor of testosterone and estrogen, non-competitive $GABA_A$ antagonist[3]	481-29-8
enhancer	coumarin	prenyletin	isolated from *Ptaeroxylon obliquum*, antifungal[4]	15870-91-4
enhancer		sphondin	isolated from *Heracleum maximum* root (mp 191-192 °C), Cox2 expression inhibition and PGE2 release inhibitor[5], antimycobacterial[6]	483-66-9
enhancer		pimpinellin	isolated from *Heracleum maximum* root (mp 118-119 °C), $GABA_A$ modulator[7], antimycobacterial[6]	131-12-4
enhancer	flavonoid	5,7,4'-trimethoxyflavone	isolated from *Cassia siamia* and *Citrus reticulata*, antioxidant[8], antihyperglycemic[9], adipocyte hypertrophy suppressor[10]	5631-70-9
enhancer		hexamethylquercetagetin	isolated from *Citrus spp*, antifungal, quercetin (very similar) inhibits EGFR pathway and prevents prostate cancer progression[25]	1251-84-9
enhancer		naringenin	highly prevalent in grapefruit[11], cardioprotective effects in cardiorenal syndrome[12], suppression of cytokine 3 expression[13], downregulation of AKT pathway[14], antihypertensive[15], interaction with PC2 in *Dictyostelium* and MDCK cells[26]	67604-48-2
enhancer	carboxylic ester	xanthoxylin	antifungal[16]	90-24-4
enhancer	chalcone	2',4'-dihydroxychalcone	isolated from *Flemingia chappar, Ceratiola ericoides, Acacia neovernicosa* and *Flourensia spp*, Cox2 inhibition[17], cell division inhibitor[18], induction of apoptosis[19], antileishmanial[20]	1776-30-3
repressor	phenylacetate	diclofenac sodium	NSAID, preferential Cox2/PGE2 inhibitor, L-type calcium channel inhibitor[21]	15307-79-6
repressor	pyridine	pyrithione zinc	antifungal, antibacterial, active ingredient in anti-dandruff shampoo, treatment for hidredenitis suppurativa[22] and seborrhoeic dermatitis[23]	13463-41-7
repressor	anisole	2,5-di-t-butyl-4-hydroxyanisole	3,5-di-t-butyl-4-hydroxyanisole (very similar) described to have Calcium antagonistic properties[24]	1991-52-2

Table 14 List of Spectrum library hit compounds, their effect on *pkd2*$^{-/-}$ curvature phenotype, the chemical class, CAS number and further information. [1] https://pubchem.ncbi.nlm.nih.gov/compound/norethynodrel, [2] (Chang *et al.*, 2011; Li *et al.*, 2015; Sharifi, 2012), [3] (Imamura *et al.*, 1998; Maninger *et al.*, 2009), [4] (Stein *et al.*, 2006), [5] (Yang *et al.*, 2002), [6] (O'Neill *et al.*, 2013), [7] (Singhuber *et al.*, 2011), [8] (Bala *et al.*, 2014), [9] (Takahashi *et al.*, 2006), [10] (Okabe *et al.*, 2014), [11] (Erlund *et al.*, 2001), [12] (Liu *et al.*, 2016), [13] (Wu *et al.*, 2016), [14] (Bao *et al.*, 2016), [15] (Alam *et al.*, 2013; Ikemura *et al.*, 2012), [16] (Vaz *et al.*, 1996), [17] (Salas *et al.*, 2016), [18] (Xie *et al.*, 2014), [19] (Sheng *et al.*, 2015), [20] (Passalacqua *et al.*, 2015), [21] (Yarishkin *et al.*, 2009), [22] (Danesh *et al.*, 2015), [23] (Naldi *et al.*, 2015), [24] (Fusi *et al.*, 2001; Fusi, *et al.*, 2001; Sgaragli *et al.*, 1993), [25] (Firdous *et al.*, 2014), [26] (Waheed *et al.*, 2014).

2.2. Effects of Spectrum library and related compounds in zebrafish

2.3. Further testing in *pkd2* mutants

Following the initial screen, chemicals were re-ordered from different suppliers where possible (to eliminate the possibility that curvature-modulating effects were due to batch impurities). Manufacturers of new batches can be found in the Materials and Methods section and in the Materials List. Furthermore, new compound material was obtained to ensure that the effects observed were not due to breakdown products.

To conduct functionality studies, some chemical classes were augmented with additional compounds. In the steroid class, apart from androstandione, the most potent human androgen, DHT (dihydrotestosterone, (Vollmer, 1963)), and the most potent fish androgen, 11-KT (11-ketotestosterone, (Hossain *et al.*, 2008)), were tested. Additionally, flutamide, an anti-androgen, which was described previously to counter androgen-effects in zebrafish (Schiller *et al.*, 2013; Schiller *et al.*, 2014), was obtained.

2.3.1.1. Curvature enhancers

In the steroid class, see Figure 34 A, androstandione proved to be more potent than any of the other steroids, enhancing the dorsal curvature from 2 μM (lowest concentration tested) whereas DHT and 11-KT only significantly altered the curvature at 50 μM and 30 μM respectively. Of note, androstandione was even more potent than observed initially at 10 μM screening concentration - the effect plateaued at 30 μM when all embryos exhibited tails that curled well beyond the body axis.

11-KT has been described as more potent in zebrafish than DHT (Hossain *et al.*, 2008), which was confirmed in this assay. As androstandione was even more potent than 11-KT, this suggested the possibility that this compound could be acting not only via the classical androgen receptor (AR) pathway but also by an additional unknown mechanism. Flutamide had no effects on the curly phenotype, indicating that intrinsic androgen levels play no role in body axis curvature.

All three coumarins (Figure 34 B) reproducibly enhanced the curvature as seen in the screen. Pimpinellin continued to be the strongest enhancer in this group but did not show any dose-response effects at the concentrations tested and neither did sphondin, the weakest coumarin enhancer. The effects of prenyletin reached a maximum at 50 μM.

Amongst the flavonoids (Figure 34 C), trimethoxyflavone remained the most potent curvature modulator but showed no dose-response curve at the concentrations tested. Naringenin caused an enhanced curvature at 55 μM but was difficult to dissolve at higher

concentrations; the compound precipitated from 70 µM. Furthermore, hexamethylquercetagetin proved very toxic at originally screened concentrations and was unable to recapitulate curvature-enhancing effects at non-toxic levels.

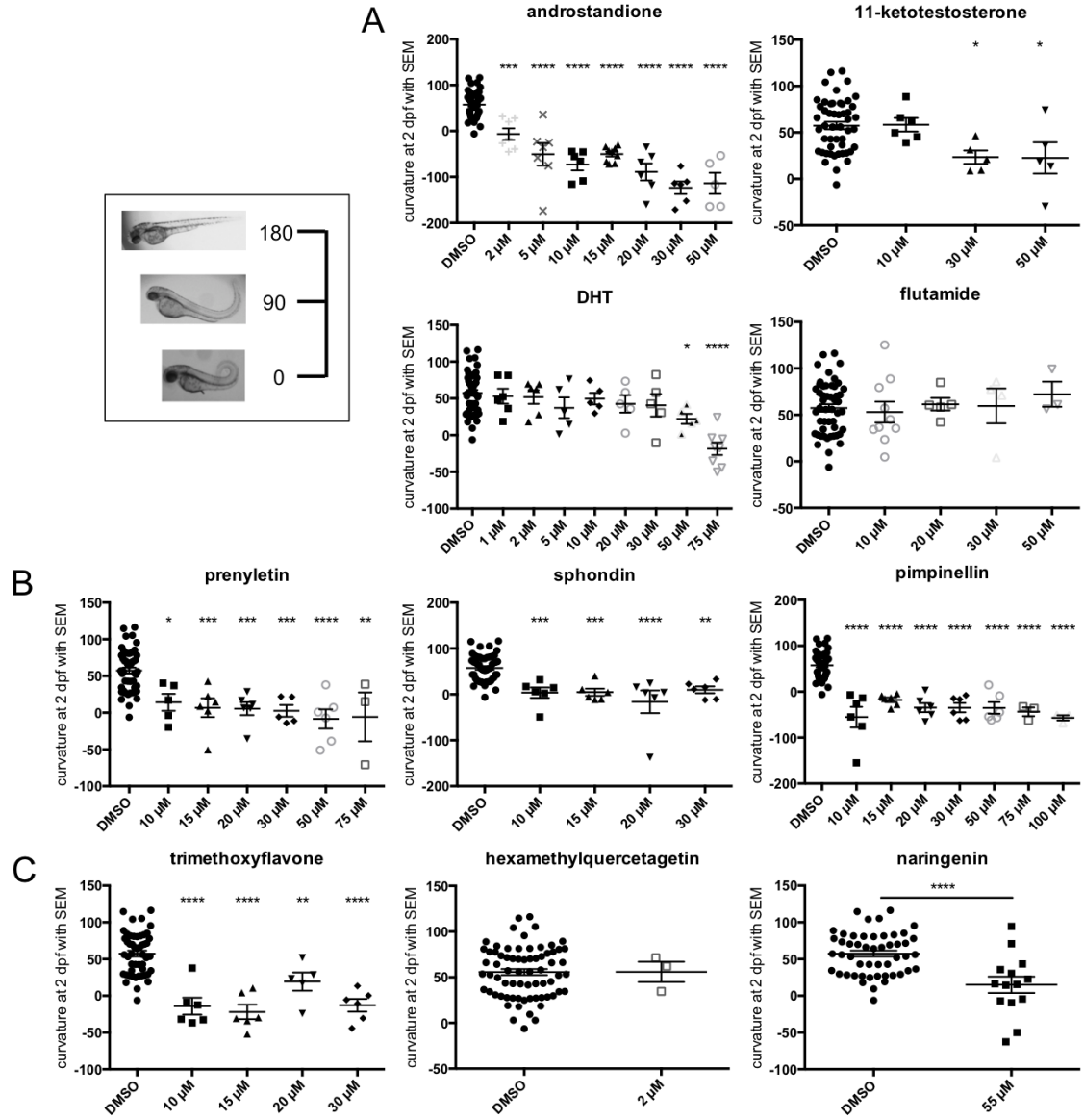

Figure 34 Results of tests with Spectrum library curvature-enhancing compounds. Box in top left corner: Examples of curvature severity with corresponding scale in degrees. (A) Androgens and flutamide (anti-androgen). (B) Coumarins. (C) Flavonoids. In most compounds more concentrations were tested but proved toxic; depicted are only concentrations causing no adverse effects. Significances via t-test (if two groups in graph) or one-way anova with Dunnett's multiple comparison test (if more than 2 groups); ****: $p \leq 0.0001$, ***: $p \leq 0.001$, **: $p \leq 0.01$, *: $p \leq 0.05$. Error bars indicate SEM.

2.3.1.2. Curvature repressors

Within the repressor group (Figure 35), one compound was a composite of two chemicals: zinc pyrithione contains both zinc and pyrithione ions. Subsequently sodium pyrithione and zinc chloride were obtained to determine which part of the compound was actively modulating the curvature phenotype (Figure 35 A). Zinc pyrithione was more toxic in re-tests than in the original compound batch and showed efficacy from as little as 0.25 μM and toxicity above 0.75 μM. Sodium pyrithione was also a potent repressor at 0.75 μM, in a similar manner to zinc pyrithione, indicating that the pyrithione ion was the active ingredient, especially as zinc chloride had no effect on the curly tail.

Diclofenac, the only repressor identified in the Spectrum screen with a well-known mechanism of action, also proved to be more toxic freshly obtained and had a narrow therapeutic range, repressing the curvature only at 0.3 and 0.4 μM and losing potency at lower concentrations (Figure 35 B). The effects of dihydroxyanisole were not reproducible with the re-ordered compound (Figure 35 B), suggesting that perhaps it had degraded in the library aliquot and a product of this process reduced the curvature. Alternatively, there is the possibility of impurities or cross-contamination being the cause of the original effect.

Brefeldin A (BFA), another described curvature repressor (Le Corre *et al.*, 2014) and ER to Golgi transport inhibitor (Donaldson *et al.*, 1992; Klausner *et al.*, 1992), was also tested to serve as secondary control. Although BFA was mildly toxic at the previously described concentrations of 1.5 to 2 μg/ml (Le Corre *et al.*, 2014), there were no adverse effects at 1 μg/ml and the curvature reducing effect was replicated (Figure 35 B).

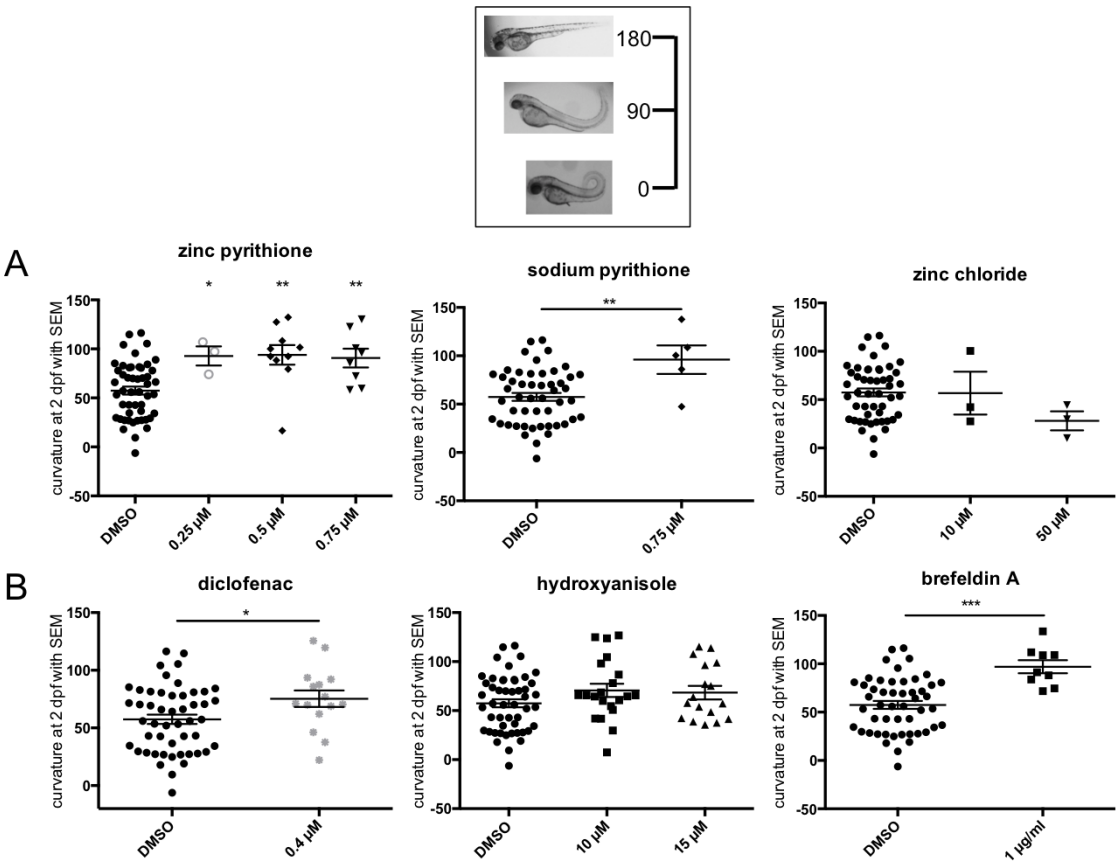

Figure 35 Further tests of Spectrum library with curvature-repressing compounds. Box at top: Examples of curvature severity with corresponding scale in degrees. In most compounds more concentrations were tested but proved toxic; depicted are only concentrations causing no adverse effects. Significances via t-test (if two groups in graph) or one-way anova with Dunnett's multiple comparison test (if more than 2 groups); ****: $p \leq 0.0001$, ***: $p \leq 0.001$, **: $p \leq 0.01$, *: $p \leq 0.05$ and non-significant (ns): $p > 0.05$. Error bars indicate SEM.

As the curvature phenotype had already begun to develop at the time point of the original compound screen (*pkd2*$^{-/-}$ could only be distinguished from siblings using the curvature phenotype for sorting), it could be argued that the developmental programme of the curly tail was already established, explaining why the repressors were unable to completely abolish the phenotype. To test this theory, embryos were exposed to the repressors from earlier time points, such as late epiboly and 24 hpf (before curvature onset) up to 2 or 3 dpf. There were, however, no marked effects on the curvature phenotype at any of the time points tested (Figure 36), suggesting that the curvature-reducing compounds have no effect on the actual developmental programme but rather inhibit the phenotype once it arises.

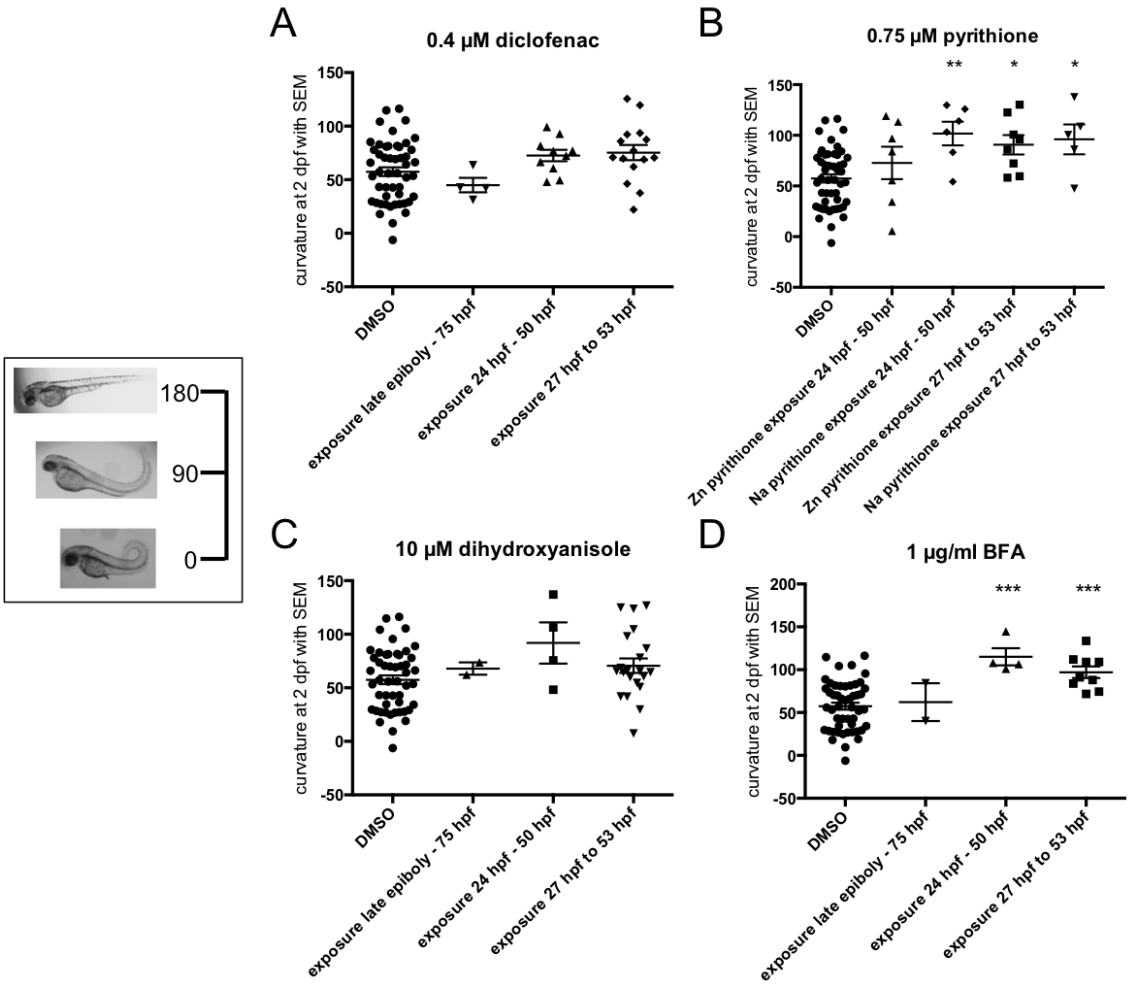

Figure 36 Repressor compound exposures from late epiboly or 24 hpf with comparison to the original screen setup (exposure from 27 hpf). Box on left: Examples of curvature severity with corresponding scale in degrees. (A) Diclofenac, (B) pyrithione, (C) dihydroxyanisole and (D) BFA. Significances via one-way anova with Dunnett's multiple comparison test; ***: $p \leq 0.001$, **: $p \leq 0.01$, *: $p \leq 0.05$. Error bars indicate SEM.

2.3.1.3. Compound co-exposures

Further experiments to study individual compound classes' mechanisms of action commenced by studying combination co-exposures (Figure 37). Here, the most potent representatives of the chemical classes were chosen: Pimpinellin for the coumarins, trimethoxyflavone amongst the flavonoids and androstandione as an androgen.

First, the enhancing chemicals were tested in co-exposures and the results are depicted in Figure 37 A. Combination of either flavonoid or coumarin with the steroid produced additive effects with regard to the curvature, although only the flavonoid/androgen exposure was significantly different. The coumarin and flavonoid co-exposure had no additive effects. This might indicate that coumarins and flavonoids share the mechanism of action whereas the steroids are enhancing the curvature via a different pathway.

Figure 37 B illustrates that flutamide, an anti-androgen, had no effect on the curvature individually and was also unable to overcome the effects of androstandione at any of the

concentrations tested. Higher amounts of flutamide in combination with the steroid proved toxic.

Unlike flutamide, diclofenac was able to reduce the effects of androstandione significantly, as well as the effects of pimpinellin (Figure 37 C). There was no observable influence of diclofenac on the potency of the flavonoid. This shows that diclofenac was able to reduce the effect of even the most potent enhancer; however, it was not able to negate it.

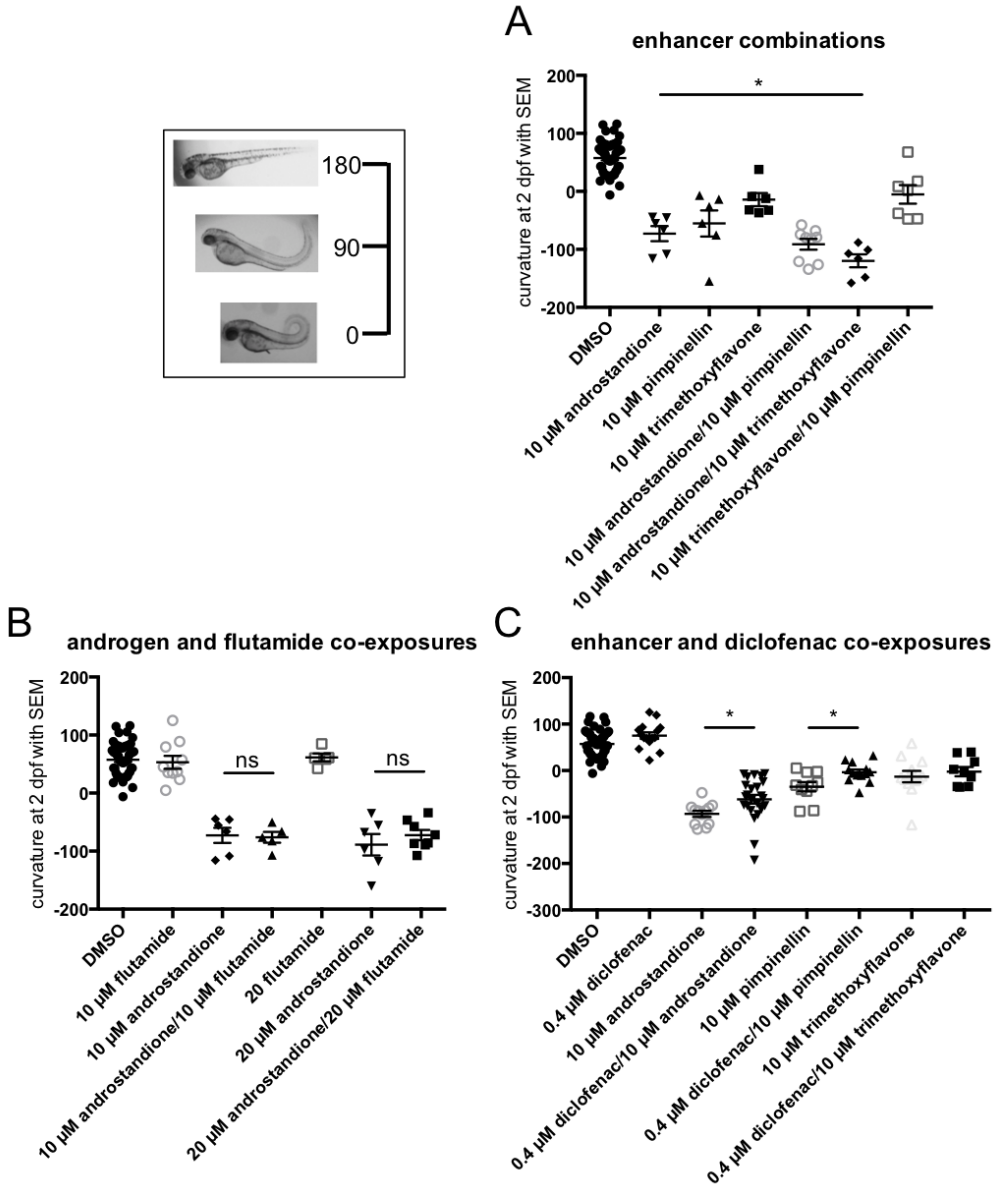

Figure 37 Co-exposures of various Spectrum compounds. Box in top left corner: Examples of curvature severity with corresponding scale in degrees. (A) Steroid, coumarin and flavonoid combinations. (B) Anti-androgen and androgen combinations. (C) Enhancer and diclofenac co-exposures. All significances via t-tests; *: $p \leq 0.05$ and non-significant (ns): $p > 0.05$. Error bars indicate SEM.

2.3.1.4. Androstandione and the connection to L-type calcium channel inhibition

As the AR (androgen receptor) is not markedly expressed in zebrafish embryonic tissues at the stages when the screen was conducted (Bertrand *et al.*, 2007), and androstandione was more potent than 11-KT, supposedly the most powerful fish androgen (Hossain *et al.*, 2008), other mechanisms of action for this steroid were considered. Interestingly, several L-type calcium channel inhibitors such as nifedipine also enhanced the curvature in the screen, but were initially rejected as a result of stringent cut-offs. Furthermore, there is evidence that DHT is a potent L-type calcium channel inhibitor (Scragg *et al.*, 2004). This, combined with the consideration that *pkd2* is a calcium channel and its knockout causes the curly tail phenotype, led to a re-evaluation of the L-type calcium channel inhibitors and subsequently nifedipine and BayK8644 (L-type channel activator) were ordered. Nifedipine, as in the initial screen results, was a weak curvature enhancer, whereas BayK8644 had no effect on the curly tail (Figure 38 A). Interestingly, although BayK8644 individually did not affect the curvature, it was able to abolish the enhancing effects of nifedipine, even exhibiting a trend towards repressing curliness, in co-exposures (not significant).

Surprisingly, co-exposure of nifedipine and androstandione resulted in a reduced efficacy compared to androstandione and there was a greater variability in phenotype severity (Figure 38 B). This could suggest that androstandione is the more potent L-type inhibitor of the two and co-exposure led to competitive inhibition, therefore causing a wider spread. BayK8644 was able to reduce androstandione's effects in co-exposures, but this was not significant.

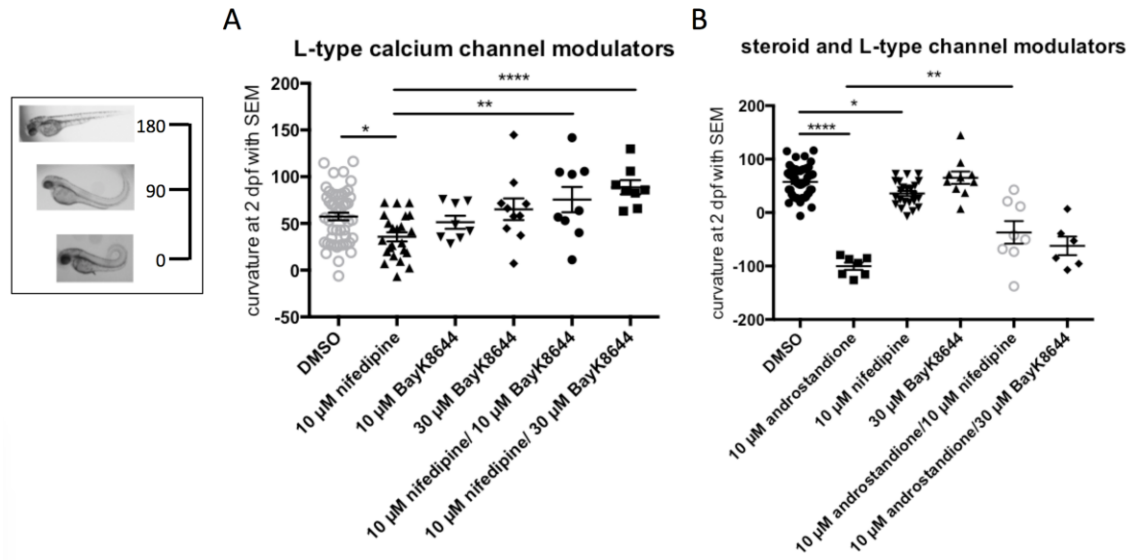

Figure 38 Effects of L-type calcium channel modulators on: (A) *pkd2* curvature and (B) steroid-induced enhancement of *pkd2* curvature in co-exposure with androstandione. Box on left: Examples of curvature severity with corresponding scale in degrees. All significances via one-way anova with Dunnett's multiple comparison test.; ****: $p \leq 0.0001$, **: $p \leq 0.01$, *: $p \leq 0.05$. Error bars indicate SEM.

Some evidence in human studies suggest that receiving L-type calcium channel inhibitors worsens renal outcomes of ADPKD patients (Abe *et al.*, 1983; Astor *et al.*, 2008; Fujiwara *et al.*, 1998; Homma *et al.*, 2013; Saruta *et al.*, 2009). To test the effects of nifedipine on glomerular expansion in zebrafish, *pkd2* mutants and siblings were exposed to nifedipine or DMSO. Figure 39 A demonstrates that nifedipine slightly reduced glomerular size in siblings compared to DMSO controls but more importantly - there was a significant difference in glomerular area between siblings and *pkd2* mutants in the nifedipine-exposed group, showing that nifedipine enlarged renal size in *pkd* knock-out fish. This seems to confirm PKD knockout-specific effects of L-type calcium channel inhibitors.

Androstandione has been linked in a few recent publications to increases in proliferation, especially with regard to prostate cancer patients receiving anti-testosterone treatments (Chang *et al.*, 2011; Li *et al.*, 2015; Sharifi, 2012). Mechanistically it has been proposed that cancers convert androstandione to DHT thereby undermining therapy. As *pkd2* mutants have a slightly higher proliferation in the ventral parts of the body axis, which might affect the tail curliness (see DMSO controls in Figure 39 B), the effect of androstandione on proliferation levels were analysed. Contrary to expectations, androstandione downregulated proliferation significantly in *pkd2* mutants and proliferation in siblings also showed a downward trend (Figure 39 B).

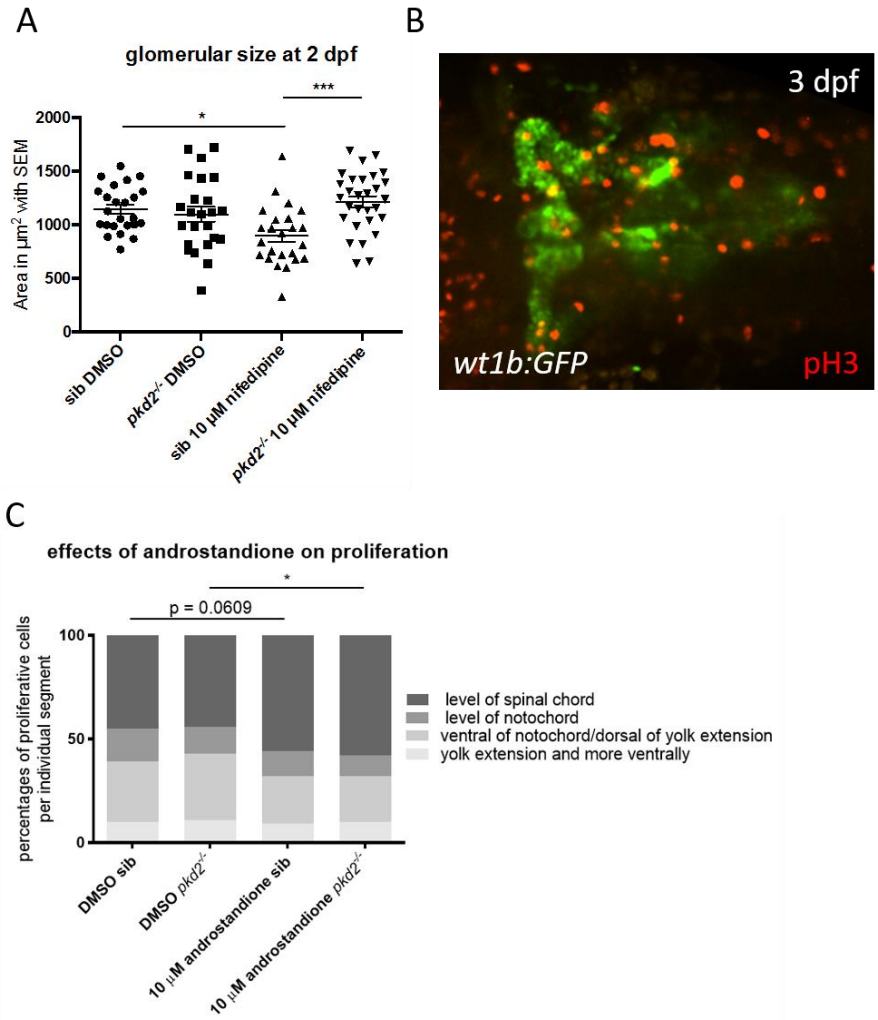

Figure 39 Effects of nifedipine and androstandione on glomerular expansion and overall proliferation respectively. (A) Glomerular area at 2 dpf in *pkd2* mutants and siblings exposed to DMSO or 10 µM nifedipine. Significances via one-way anova with Tukey's multiple comparison test; ***: $p \leq 0.001$, *: $p \leq 0.05$. Error bars indicate SEM. (B) Example image of pH3 stain used for quantification with *wt1b:GFP* transgene to localise the cells to renal epithelia. (C) Effects on proliferation on *pkd2* mutants and siblings of androstandione and DMSO controls. Significances via Chi-squared tests. *: $p \leq 0.05$. DMSO treated siblings: n = 25, DMSO treated *pkd2* mutants: n = 19, androstandione treated siblings: n = 30, androstandione treated *pkd2* mutants: n = 15.

2.3.1.5. Known ADPKD modulators tolvaptan and triptolide

Lastly, the effects of known PKD modulators tolvaptan and triptolide on the tail curvature were tested. Tolvaptan is currently the only drug approved for slowing the progression of ADPKD and triptolide is currently in a phase III clinical trial (https://clinicaltrials.gov/ct2/show/NCT02115659). Tolvaptan is a vasopressin 2 receptor antagonist and lowers cAMP levels in patients but may cause severe adverse effects, leading to high dropout rates in clinical trials (Torres *et al.*, 2012). Although zebrafish have several vasopressin type 2 receptors (*avpr2a*, *avpr2b* and *avpr2l* - *arginine vasopressin receptor*), which are expressed at these developmental stages (at least in the central nervous system (Iwasaki *et al.*, 2013), no other data was published at the time this thesis was written), tolvaptan did not affect the curly tail (Figure 40 A). This could be explained due to tolvaptan not binding to the zebrafish receptor

variety, or it binding only to one of the paralogues, which might be insufficient to reduce the phenotype. Alternatively, the zebrafish ADPKD-related phenotype of a curly tail might not be regulated via the vasopressin/cAMP pathway.

The latter theory is furthered by the observation that exposures with other known ADPKD modulators, such as 8-bromo-cAMP, PGE2 and forskolin, did not affect the *pkd2* curvature at any of the concentrations tested (8-bromo-cAMP: 10 µM to 1 mM, forskolin: 0.1 to 0.5 µM – overall very toxic, PGE2: 0.05 µM to 5 µM – toxic at higher concentrations, data not shown). Forskolin and 8-bromo-cAMP have both been used previously in zebrafish (10 µM forskolin and 1 µM 8-bromo-cAMP; in 4 dpf larvae (Kumai *et al.*, 2014)), but they had no effect on the curvature phenotype.

Triptolide is a traditional Chinese medicine derived from the Thunder God Vine, *Tripterygium wilfordii* and reportedly represses ADPKD by activating PC2 (Leuenroth *et al.*, 2008), although other mechanisms are also discussed. Since zebrafish *pkd2* mutants have no functional PC2 but triptolide was still able to reduce the curvature phenotype, this suggests that it is not acting via PC2 in zebrafish (Figure 40 B). It was however, also very toxic to embryos and only the lowest concentration tested (0.5 µM) did not result in noticeable toxicity.

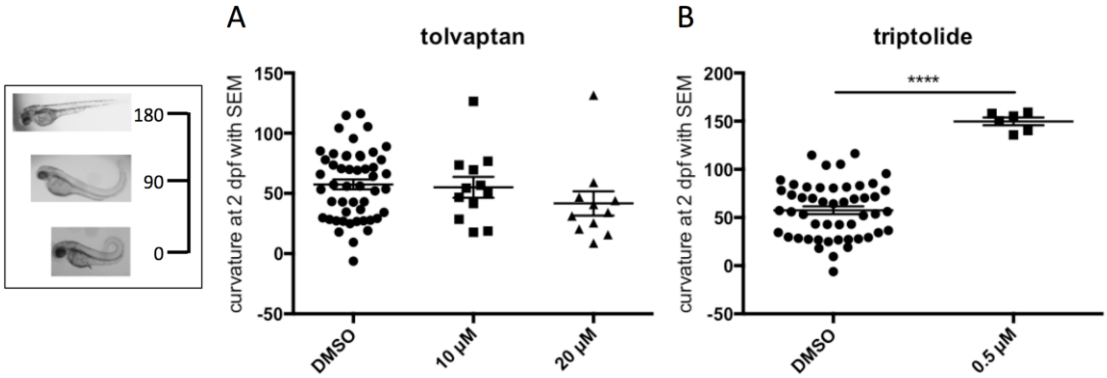

Figure 40 Effects of ADPKD drugs on *pkd2* curvature. Box on left: Examples of curvature severity with corresponding scale in degrees. (A) Tolvaptan, a vasopressin 2 receptor antagonist. Higher concentrations were tested, but resulted in precipitation. (B) Triptolide, currently in clinical trials. Significances via one-way anova with Dunnett's multiple comparison test (A) and unpaired t-test (B); ****: $p \leq 0.0001$. Error bars indicate SEM.

2.4. Spectrum and related compounds in WT, *elipsa* and *pkd2*$^{-/-}$

pkd2 mutant zebrafish did not exhibit a discernible renal phenotype but ciliary mutants, such as *elipsa*, characteristically have glomerular dilations (see Results Chapter 1). These renal dilations in zebrafish are commonly referred to as "cystic kidneys" in the literature, although expanded glomeruli are very different compared to cysts (fluid-filled capsules distinct from the surrounding tissues via a membrane) in an organ. The phenotype most closely resembling renal cysts in zebrafish embryos described to date are dilated glomeruli. WT controls, *elipsa*

mutants and *pkd2* mutants were exposed to chemicals of interest and glomerular size evaluated.

Figure 41 shows the results of these compound exposures with regard to the glomerular area of WT, *pkd2* and *elipsa* embryos. In WT embryos (Figure 41 A) 11-KT, flutamide and nifedipine decreased glomerular area significantly, whereas sphondin and trimethoxyflavone increased it. Interestingly, androstandione did not significantly affect the glomeruli, but co-exposure with nifedipine caused an additive effect beyond the potency of nifedipine alone. This decrease of glomerular size in the co-exposure could be attributed to the arising cardiac oedema phenotype - decreasing cardiac output and subsequently hindering glomerular inflation.

In compound-exposed *pkd2* mutants, (Figure 41 B) flutamide caused smaller glomeruli, as it did in WT embryos, suggesting that, although it had no effect on the curvature phenotype, there is some effect on glomerular morphology. Nifedipine and androstandione co-exposure in

pkd2$^{-/-}$ did not cause any oedema but also reduced glomerular area, indicating that perhaps oedema were not the driving force behind the shrinkage observed in WT embryos. None of the tested compounds exhibited the ability to increase glomerular size in *pkd2* mutants.

In *elipsa* mutants (Figure 41 C), which have a glomerular dilation phenotype, none of the compounds reduced glomerular area significantly. Interestingly, four compounds aggravated the already dilated renal phenotype: all of the coumarins (prenyletin, pimpinellin and sphondin) and triptolide, with the latter being unexpected. Triptolide decreases *pkd2* curvature (see above) but in this cystic kidney model it exacerbated the phenotype.

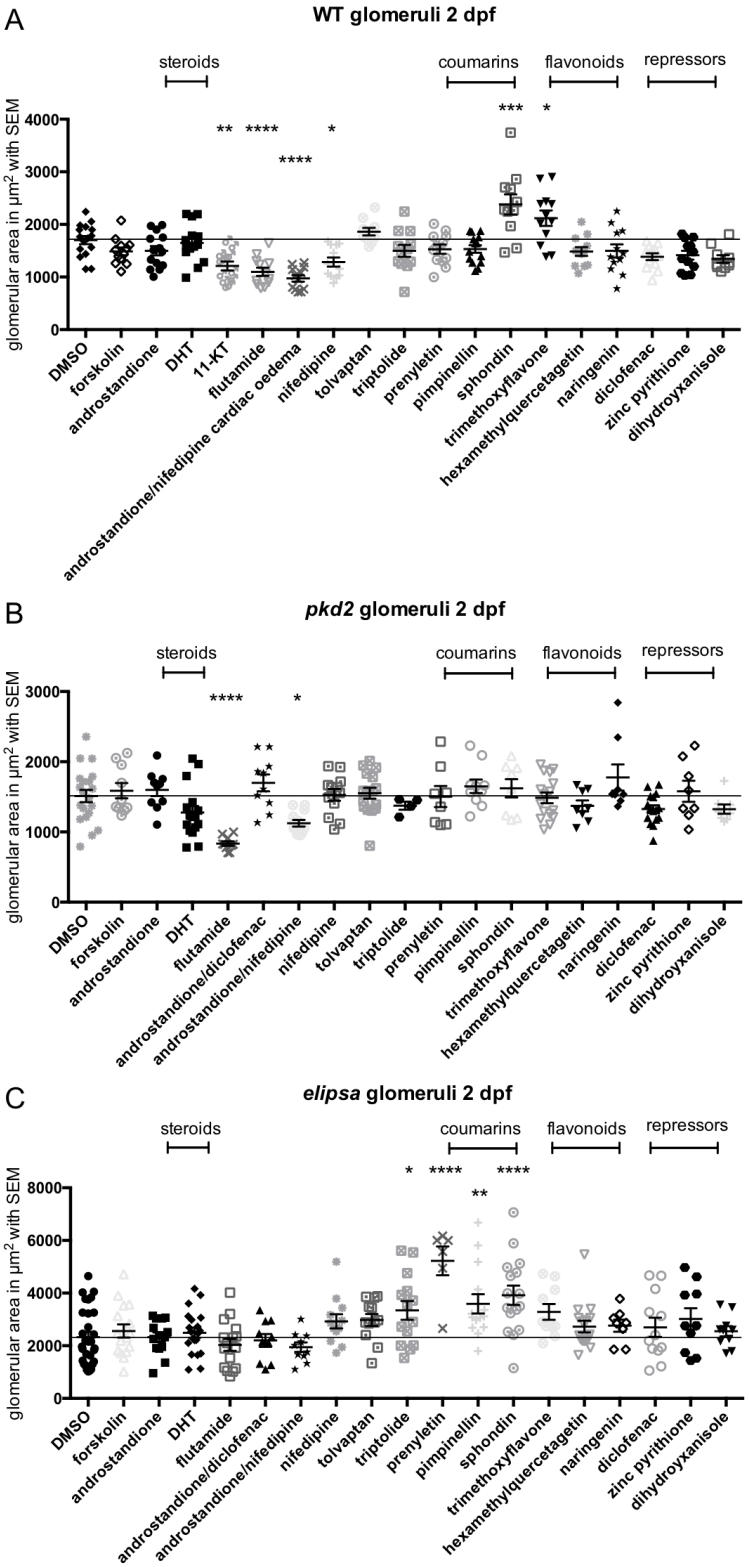

Figure 41 Glomerular area of WT (A), *pkd2* (B) and *elipsa* (C) after exposure to various compounds. Chemical classes as indicated. Mean of DMSO baseline indicated with black line. Significances via one-way anova with Dunnett's multiple comparison test; ****: $p \leq 0.0001$, **: $p \leq 0.01$, *: $p \leq 0.05$. Error bars indicate SEM.

In addition to renal size, the effects of compounds on the body axis were also quantified in WT and *elipsa* mutants (Figure 42 A and B respectively). For WT embryos tail curvature measurements were conducted as previously described, meaning a straight tail corresponded to 170-180°. As some of the exposed *elipsa* embryos switched from a ventral curvature to a

curly up phenotype, distinction between positive and negative angles became necessary and a straight tail was defined as 0° (analysis more thoroughly explained in Results Chapter 1).

WT embryos were largely unaffected by most of the compounds with the exception of androstandione, which caused a significant dorsal axis bend. The phenotype did not so much resemble a *pkd2* curly tail but rather the dorsal axis bending of gamma-secretase inhibitors such as DAPT (Arslanova *et al.*, 2010). Interestingly, similar to the results in glomerular area, androstandione/nifedipine co-exposure seemed to exaggerate this effect, although nifedipine itself did not affect the curvature on its own.

In *elipsa* mutants, androstandione and androstandione/nifedipine co-exposure both caused the curvature phenotype to switch from ventral to dorsal, indicating a very potent *curly up* effect of androstandione. Pimpinellin, sphondin and trimethoxyflavone reduced the ventral curl of *elipsa* significantly, suggesting they have a dorsal curling effect on body axis mutants (*elipsa* and *pkd2*) but not on WT embryos. Of note, triptolide alleviated both *elipsa* and *pkd2* curvatures, suggesting it might activate a pathway enabling embryos to develop a straight body axis.

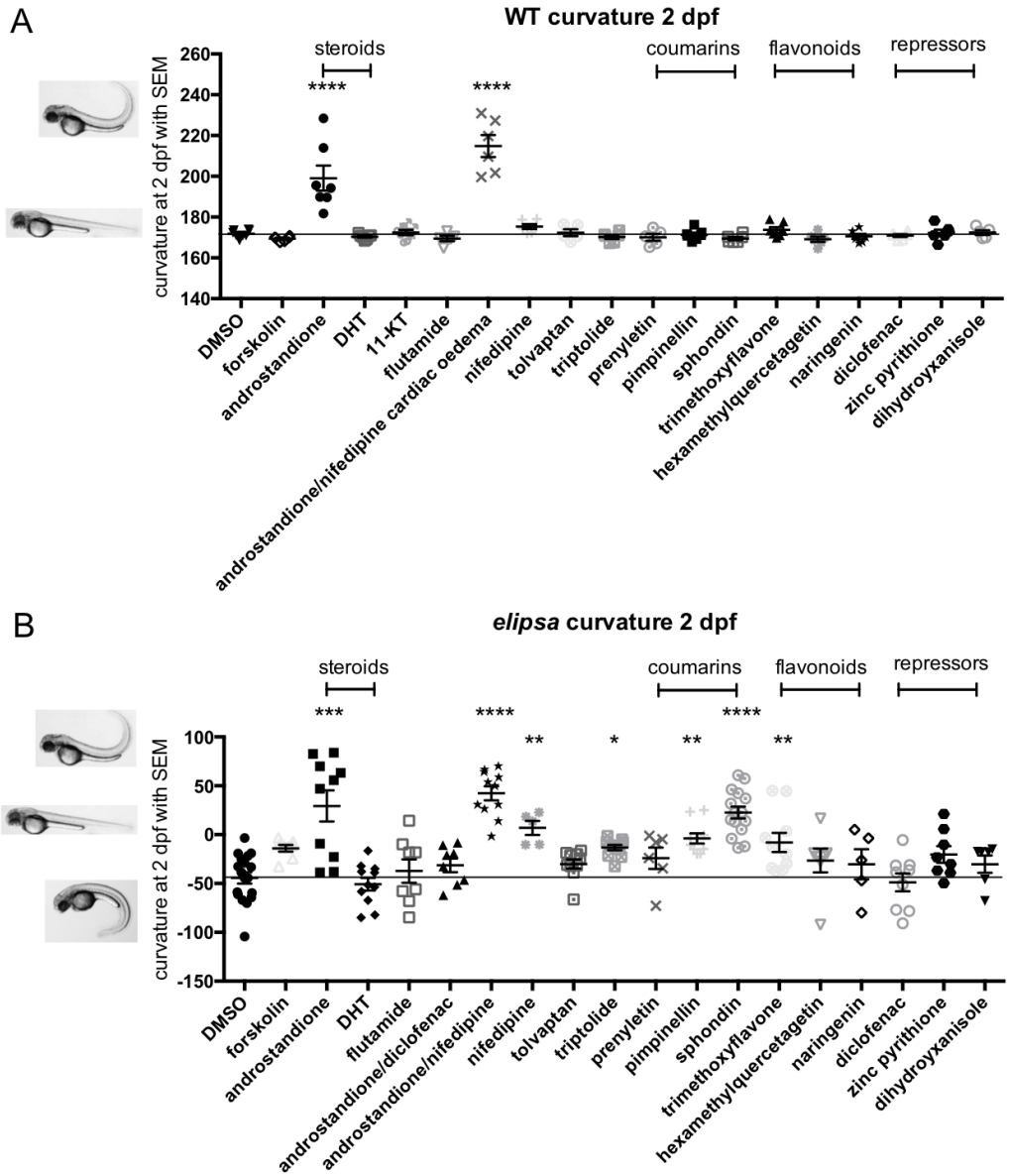

Figure 42 Curvature of WT (A) and *elipsa* (B) after exposure to various compounds. Chemical classes as indicated. Mean of DMSO baseline indicated with black line. Significances via one-way anova with Dunnett's multiple comparison test; ****: $p \leq 0.0001$, ***: $p \leq 0.001$, **: $p \leq 0.01$, *: $p \leq 0.05$. Error bars indicate SEM.

3. Spectrum compound validation in a 3D-cyst culture assay

In order to extend the findings of the zebrafish compound screen to a mammalian system, two cell lines were exposed to the Spectrum compounds in three-dimensional cyst assays. In these assays, cells are seeded into a matrix and form cysts over the time course of the experiment, which can subsequently be analysed by measuring cyst area. The lines used during this project comprised canine, renal MDCKII cells and ADPKD-patient-derived Ox161c1 cells with a *Pkd1*-null mutation.

3.1. Cystic MDCKII cells: determination of effective dosages

As there was no literature on any of the Spectrum compounds regarding performance in cyst assays at the time of the experiments, a dose-range experiment with single replicates was conducted to test the chemicals with regards to cell toxicity and ability to affect cyst size. The results are shown in Figure 43. All of the compounds showed the behaviour predicted from zebrafish data and the most efficient concentrations were subsequently chosen for two triplicate exposure experiments. The optimal concentrations were determined as follows: 0.01 µM for zinc pyrithione and 0.1 µM for hexamethylquercetagetin (both, as in zebrafish, were rather toxic); 1 µM for androstandione, prenyletin, sphondin and trimethoxyflavone; 10 µM for pimpinellin, naringenin, diclofenac and dihydroxyanisole.

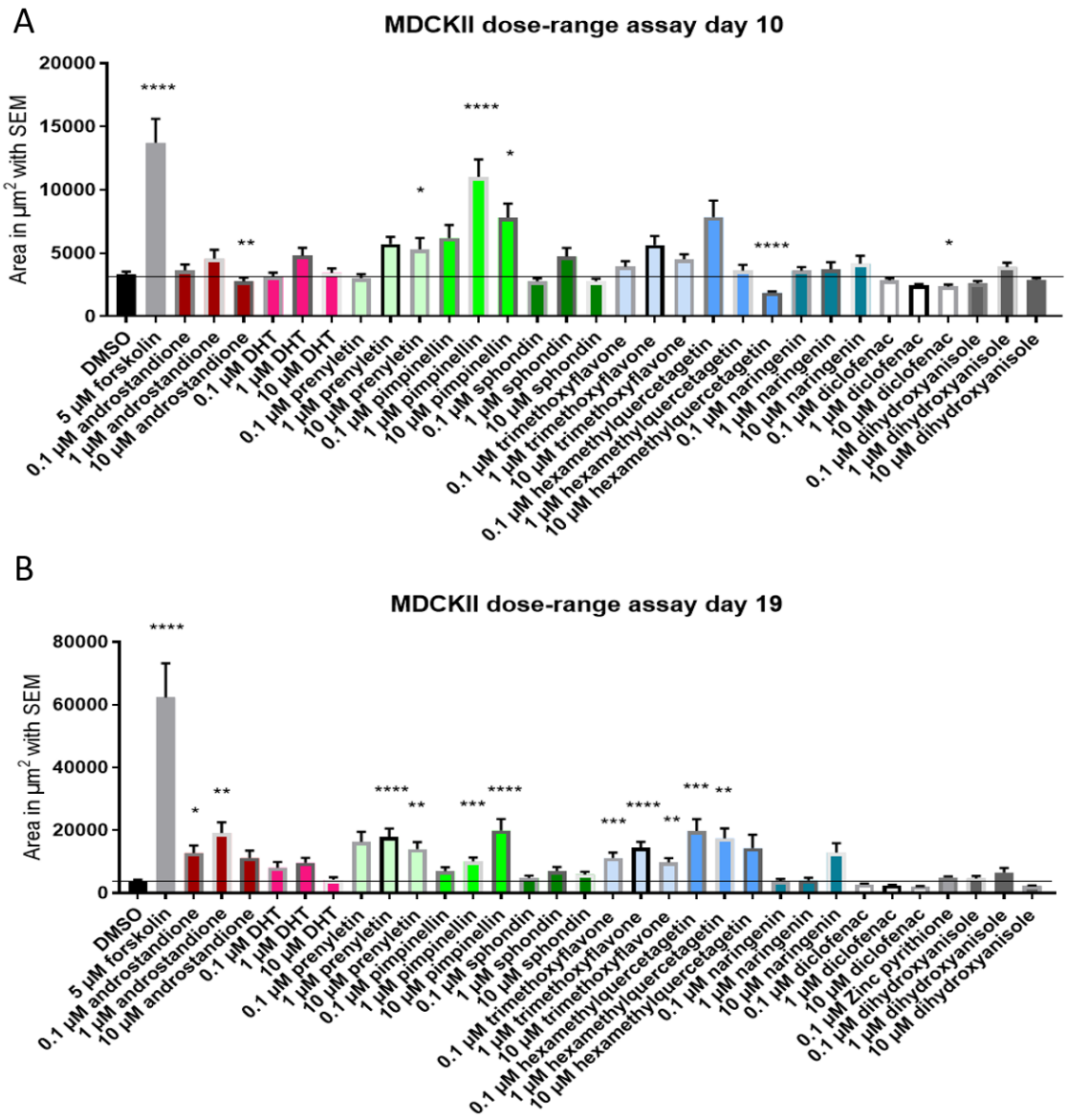

Figure 43 MDCKII dose-range assay on day 10 of exposure (A) and day 19 of exposure (B). Chemical classes as indicated. Mean of DMSO baseline indicated with black line. Significances via Kruskal-Wallis test with Dunn's multiple comparison test; ****: $p \leq 0.0001$, ***: $p \leq 0.001$, **: $p \leq 0.01$, *: $p \leq 0.05$. Error bars indicate SEM.

3.2. Cystic MDCKII cells: Spectrum compound validation

Figure 44 depicts the combined results of two experiments with biological triplicates of MDCKII cells exposed to the Spectrum hit compounds after 10, 14 and 17 days of exposure. At day 10 of the experiment, naringenin remained at control levels whereas zinc pyrithione, previously a repressor, exhibited aggravated cyst growth. The latter remained true until day 14 but by day 17, the endpoint of the assay, the expanding phenotype was reverted to cyst repression. Sphondin did not have an effect in one of the two experiments and subsequently the combined data suggested it did not cause a cyst expansion in MDCKII cells. Of note, sphondin was also the weakest of the coumarins in the zebrafish screen.

Generally, all of the compounds with the exception of sphondin behaved as expected at the endpoint of the MDCKII cyst assay. None of the enhancers reached the potency of the positive control (forskolin) in terms of cyst-expanding capabilities. Forskolin expanded cysts to about 2.5-times the area in comparison to the strongest compounds of the Spectrum library. Nevertheless, the expansion compared to the DMSO control was highly significant in most cases (sphondin and androstandione treated MDCKII cells showed highly significant expansion at days 10 and 14 which were lost by day 17, perhaps suggesting earlier mechanisms).

Amongst the repressors, diclofenac exhibited a second interesting ability besides cyst size reduction: It caused a shift in the ratio of cystic to tubular structures in the MDCKII cells (Figure 45).

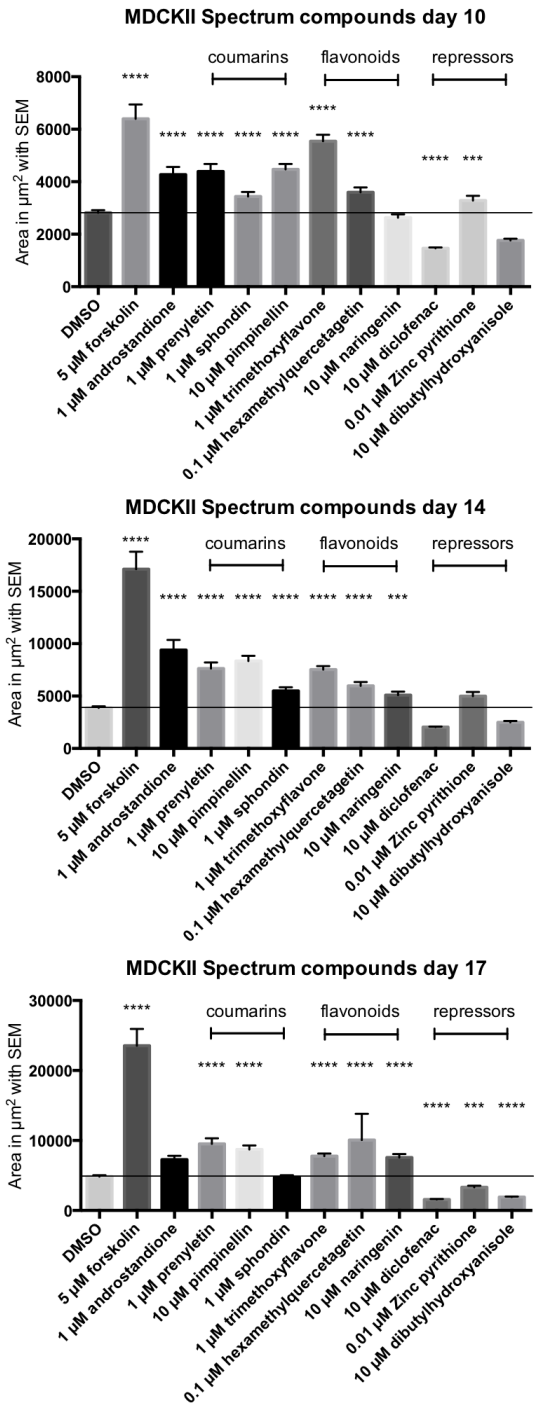

Figure 44 Cyst area of MDCKII cells after compound exposures of 10, 14 and 17 days. Chemical classes as indicated. Mean of DMSO baseline indicated with black line. Significances via Kruskal-Wallis test with Dunn's multiple comparison test; ****: $p \leq 0.0001$, ***: $p \leq 0.001$. Error bars indicate SEM.

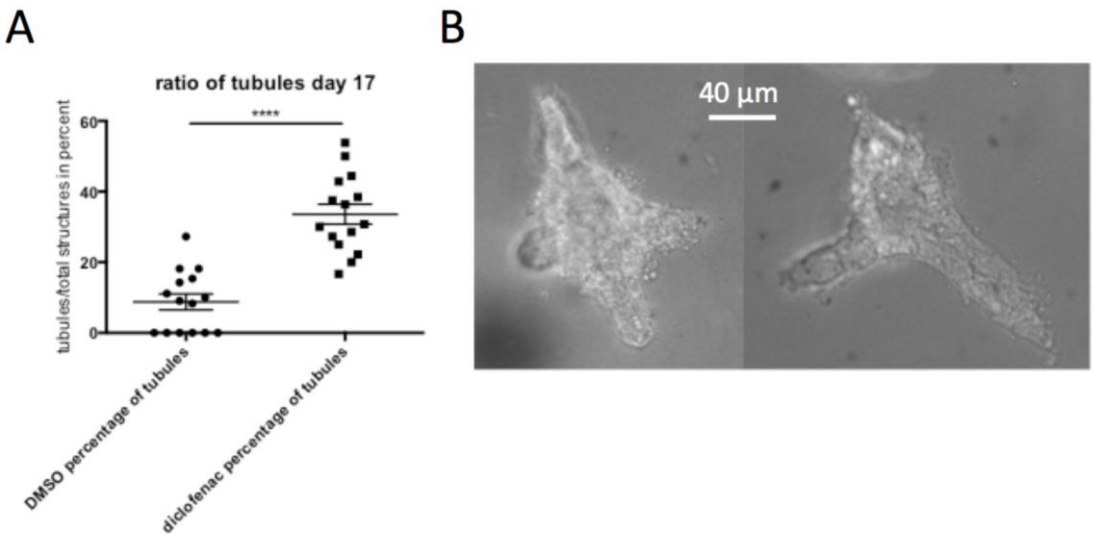

Figure 45 (A) Ratio of tubular structures over total number of structures in MDCKII 3D cyst assays in DMSO control and diclofenac exposures of 17 days. Significance via t-test; ****: $p \leq 0.0001$. Error bars indicate SD. (B) Example images of tubular structures after 10 day of diclofenac exposure in MDCKII cells.

3.3. Cystic MDCKII cells: Further testing of Spectrum compounds – co-exposures

Further to individual treatments, co-exposures of various compounds were conducted in MDCKII cyst assays (Figure 46, Figure 47 and Figure 48).

Figure 46 depicts the effects of enhancer combinations on MDCKII 3D cultures, where the strongest enhancing compounds from the steroid, coumarin and flavonoid class were tested in co-exposures. Overall, there was a high variability in cyst size over the time course of the experiments (co-exposures were analysed in comparison to the more potent single compound). Conversely, at day 10, pimpinellin/androstandione exposure led to an additive effect whereas trimethoxyflavone/androstandione caused a decreased cyst size in comparison to respective controls. At day 14, MDCKII cysts were generally smaller in all of the tested combinations than in individual chemical treatments, which did not chance on day 17. No clear additive effects in terms of cyst expansion were observed.

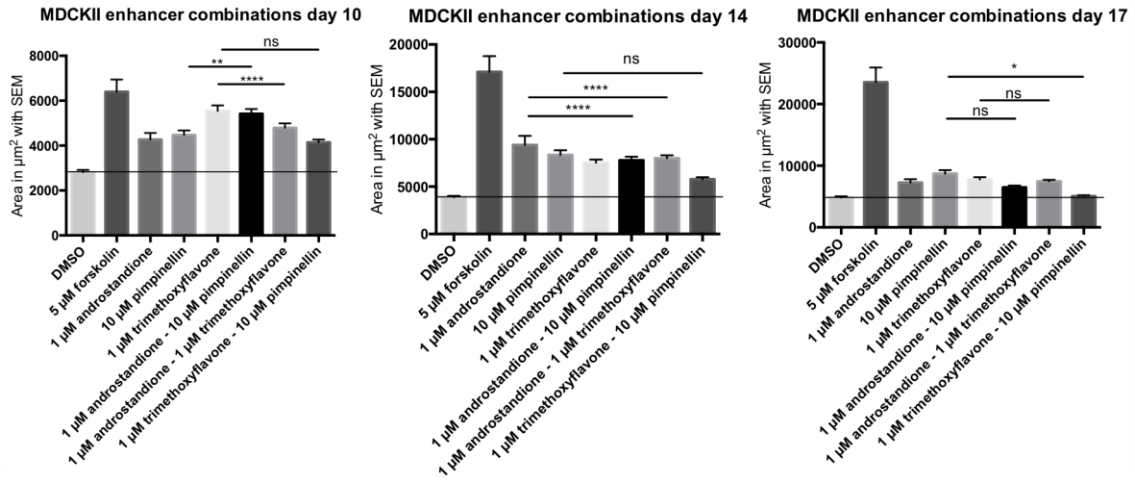

Figure 46 MDCKII enhancer co-exposures. Mean of DMSO baseline indicated with black line. Significances via Kruskal-Wallis test with Dunn's multiple comparison test; ****: $p \leq 0.0001$, **: $p \leq 0.01$, *: $p \leq 0.05$ and non-significant (ns): $p > 0.05$. Error bars indicate SEM.

Further exposures with the steroid pathway modulators (Figure 47) flutamide and DHT revealed that flutamide, which had no effect on *pkd2* zebrafish curvature but caused a decreased renal size, caused a large increase in cyst size in MDCKII assays. This was unexpected as steroids, such as androstandione and DHT increased cyst area; therefore, the assumption was made that the steroid antagonist flutamide should decrease cyst size. Flutamide was included to block the influence of DHT but proved a more potent enhancer on its own. Co-exposures of DHT and flutamide led to expansions similar to those observed in flutamide treatments; no additive or negating effects were observed.

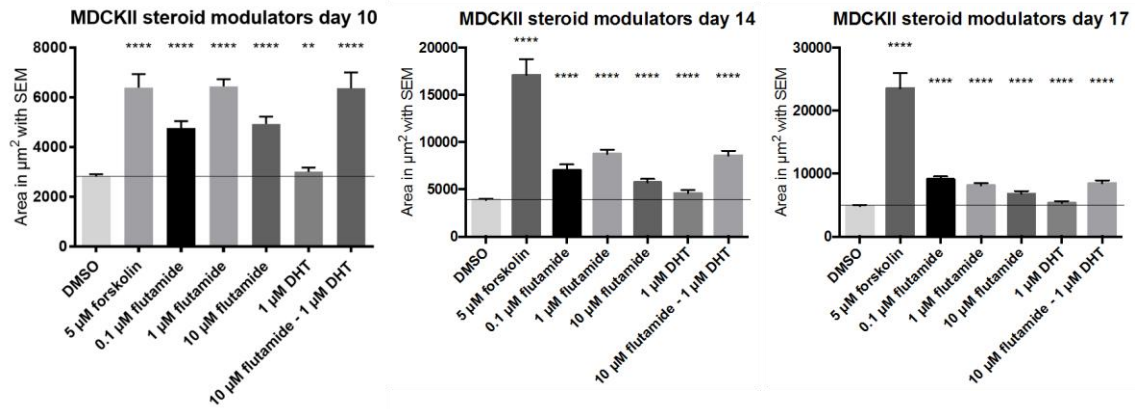

Figure 47 MDCKII steroid modulator exposures. Mean of DMSO baseline indicated with black line. Significances via Kruskal-Wallis test with Dunn's multiple comparison test; ****: $p \leq 0.0001$, **: $p \leq 0.01$. Error bars indicate SEM.

Finally, the cyst-repressing compounds were tested in co-exposures with low levels of forskolin to test their potency in overcoming cystogenesis (Figure 48). All repressors were able to reduce the expansion process significantly, but only diclofenac was potent enough to overcome the effects of forskolin completely and reduce cyst size to below DMSO control levels.

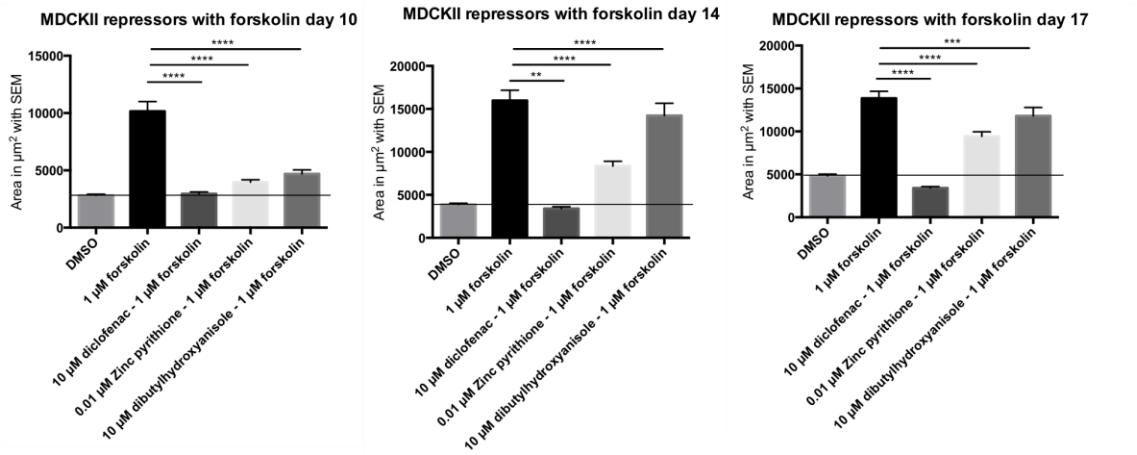

Figure 48 MDCKII repressor and forskolin co-exposures. Mean of DMSO baseline indicated with black line. Significances via Kruskal-Wallis test with Dunn's multiple comparison test; ****: $p \leq 0.0001$, ***: $p \leq 0.001$, **: $p \leq 0.01$. Error bars indicate SEM.

3.4. Spectrum compounds in a cell culture model of ADPKD: Ox161c1 cells

To test all compounds and compound combinations in a secondary model, ADPKD-patient-derived Ox161c1 cells, which carry a *PKD1* mutation predicted to cause a protein truncation, were also exposed to the various drugs (more detailed information on Ox161c1 cells can be found in the Materials and Methods section 1.12.2.). This cell line served as second validation of the Spectrum compounds in a human cell culture model of ADPKD.

Previous experiments in our laboratory had shown that Ox161c1 cells tolerated similar compound concentrations as MDCKII cells (Morgane Lannoy, personal communication); hence the assays were conducted as described above in two experiments with biological triplicates each.

3.5. Cystic Ox161c1 PKD-cells: Spectrum compound validation

Similar to MDCKII assays, Ox161c1 3D cell culture experiments largely validated the zebrafish screen results (Figure 49). Differences in cyst area were, however, less pronounced and statistically significant results were more difficult to confirm in Ox161c1 cells. Although there were trends for the repressors to decrease cyst size, these findings were not significant and, on the same note, all enhancers exhibited trends towards expanding processes but not all reached significance thresholds. All compounds, without exception, behaved as predicted at all time points measured, including sphondin and zinc pyrithione. Of note, although significant expansions were less frequent than in the MDCKII cells, the most potent expanding compounds performed at the same level or above that of the positive control in Ox161c1 cells - suggesting that forskolin was less effective in its cyst-inducing potency in this cell line (similar observations communicated by a colleague; Morgane Lannoy).

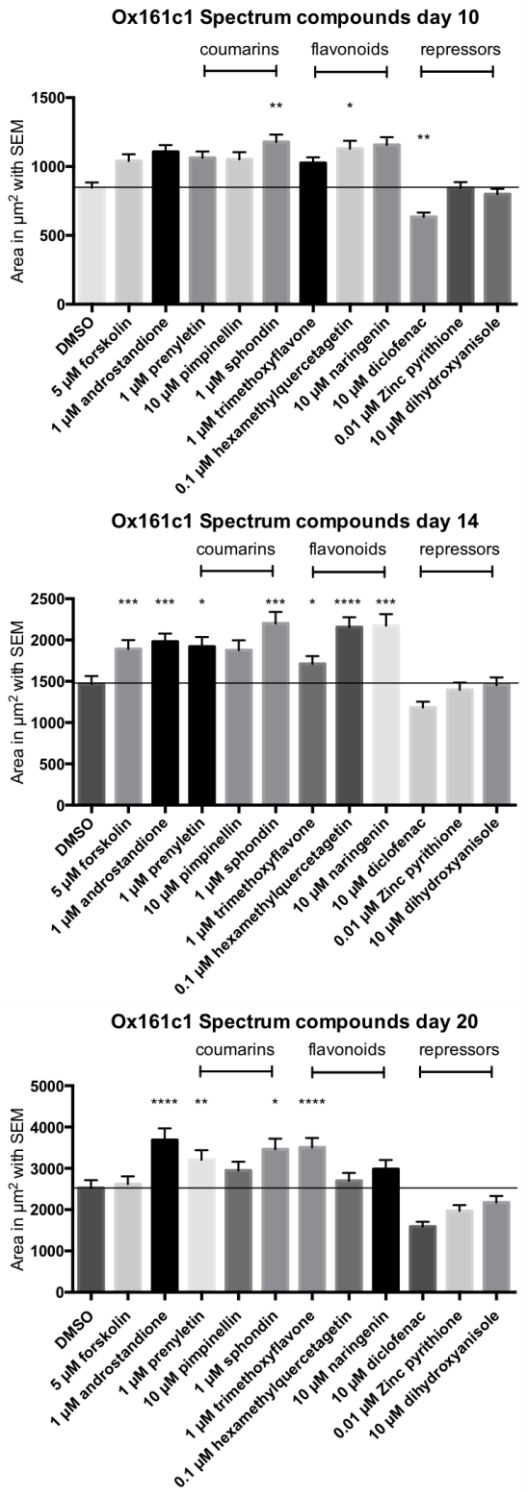

Figure 49 Cyst area of Ox161c1 cells after compound exposures of 10, 14 and 20 days exposure in (A), (B) and (C) respectively. Chemical classes as indicated. Mean of DMSO baseline indicated with black line. Significances via Kruskal-Wallis test with Dunn's multiple comparison test; ****: $p \leq 0.0001$, ***: $p \leq 0.001$, **: $p \leq 0.01$, *: $p \leq 0.05$. Error bars indicate SEM.

3.6. Cystic Ox161c1 PKD-cells: Further testing of Spectrum compounds – co-exposures

Co-exposures of the most potent enhancers from each compound class showed no additive effects in Ox161c1 cells, quite the contrary: All compound combinations bar androstandione/trimethoxyflavone at day 20 caused a decrease in cyst size in comparison to individual compounds (Figure 50).

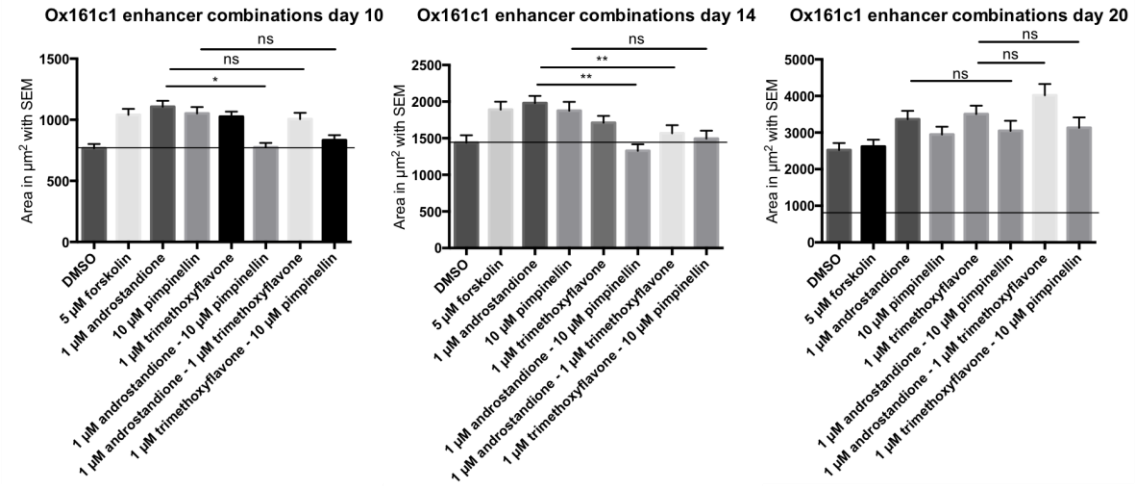

Figure 50 Ox161c1 enhancer co-exposures. Mean of DMSO baseline indicated with black line. Significances via Kruskal-Wallis test with Dunn's multiple comparison test; **: $p \leq 0.01$, *: $p \leq 0.05$ and non-significant (ns): $p > 0.05$. Error bars indicate SEM.

Flutamide exposure of Ox161c1 cells did not result in a decrease of cyst size, as expected of a steroid antagonist, but rather increased cyst area (Figure 51). DHT performed as expected but co-exposures of DHT and flutamide did not show an additive effect.

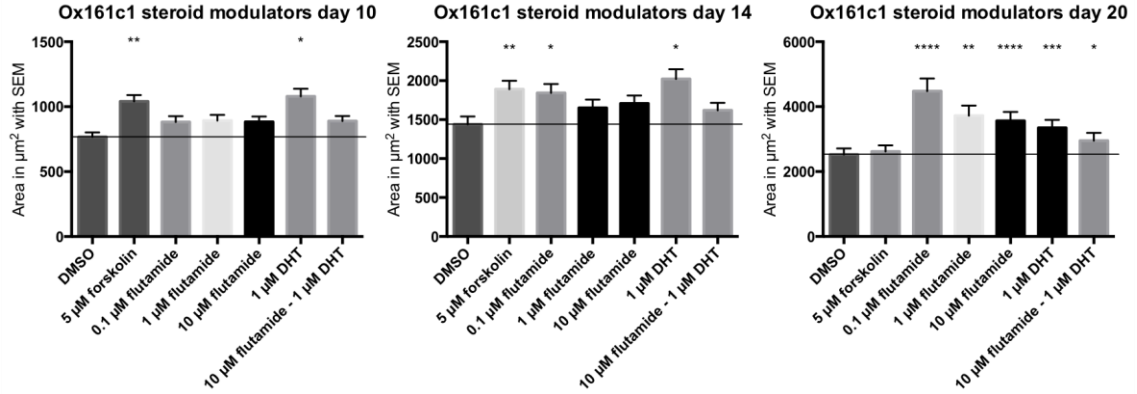

Figure 51 Ox161c1 steroid modulator exposures. Mean of DMSO baseline indicated with black line. Significances via Kruskal-Wallis test with Dunn's multiple comparison test; ****: $p \leq 0.0001$, ***: $p \leq 0.001$, **: $p \leq 0.01$, *: $p \leq 0.05$. Error bars indicate SEM.

Co-exposures of the repressors with forskolin in Ox161c1 cells revealed the same pattern as in MDCKII experiments. Diclofenac was strong enough in its inhibition properties to not only overcome forskolin stimulation, but was able to repress cyst size to below base levels whereas zinc pyrithione and dihydroxyanisole merely reduced cyst area (Figure 52). Further to combination exposures with forskolin, Ox161c1 cells were also co-exposed to the strongest enhancer (androstandione) and the most potent repressor (diclofenac). Here,

diclofenac was again able to overcome cystogenic effects and cyst size remained below control levels at all times (significant at days 10 and 14).

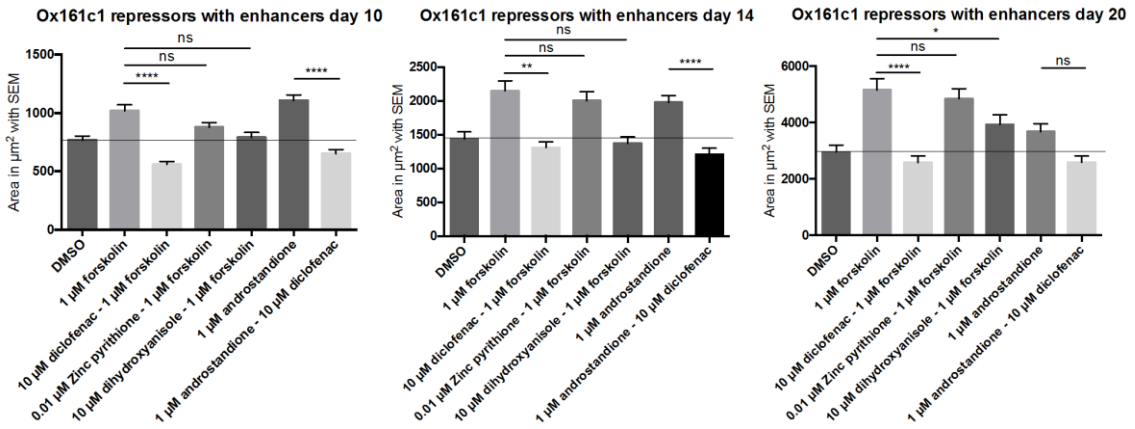

Figure 52 Ox161c1 repressor and forskolin co-exposures. Mean of DMSO baseline indicated with black line. Significances via Kruskal-Wallis test with Dunnett's multiple comparison test; ****: $p \leq 0.0001$, **: $p \leq 0.01$, *: $p \leq 0.05$. Error bars indicate SEM.

4. Screen of the PKIS collection (kinase inhibitor library)

4.1. Zebrafish PKIS screen results

As there were very limited amounts of compound provided with the PKIS collection, only the first screen round and one validation set could be conducted initially. After the first exposure round, 123 compounds of interest were determined and after a secondary validation step 18 compounds of interest remained (Figure 53). Similar to the Spectrum collection, the majority of these hit compounds were enhancers, with only a rough quarter being repressors. As the Spectrum library had already yielded an interesting set of enhancers - and suppressors are of greater interest with regard to their potential therapeutic values - only the four repressing compounds were pursued from this set. The four repressors of interest were GW785804X, GW780159X, SB-698596-AC and GW682841X.

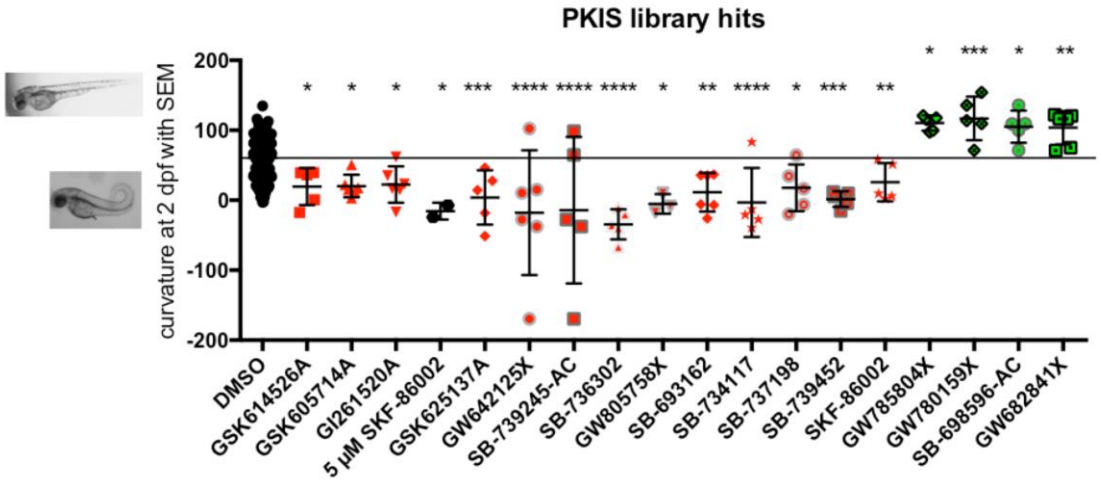

Figure 53 Hit compounds of PKIS library after initial compound screen with validation round. Enhancers of *pkd2* curvature in red, repressors in green. Mean of DMSO baseline indicated with black line. Significances via one-way anova with Dunn's multiple comparison test; ****: $p \leq 0.0001$, ***: $p \leq 0.001$, **: $p \leq 0.01$, *: $p \leq 0.05$. Error bars indicate SEM.

Table 15 contains information regarding the PKIS repressor compounds, including the name they will be referred to from here on. Interestingly, PKIS_04 and PKIS_59 were very similar in chemical structure (Figure 54).

Name	Referred to as	Chemical name	Most inhibited target known	Additional information
GW785804X	PKIS_04	4-(4-fluorophenyl)-5-(1,5-naphthyridin-2-yl)-1,3-thiazol-2-amine	KDR	originally designed against ALK5 ALK5 Binding – 0.042 µM TGFβ Cellular Assay – 0.032 µM[1] TGFBR1 inihitor[2], ALK5 inhibitor[3]
GW780159X	PKIS_59	4-(3-chlorophenyl)-5-(1,5-naphthyridin-2-yl)-1,3-thiazol-2-amine	KDR	originally designed against ALK5 ALK5 Binding – 0.023 µM TGFβ Cellular Assay – 0.016 µM[1] ALK5 inhibitor[3]
SB-698596-AC	PKIS_96	N-[5-(2,3-difluorophenyl)-1H-pyrazolo[3,4-c]pyridazin-3-yl]-2-(1-ethylpiperidin-4-yl)acetamide; 2,3-dihydroxybutanedioic acid	GSK3B	originally designed against GSK3A GSK3 inhibitor[4]
GW682841X	PKIS_41	2-(4-propan-2-ylphenyl)-4-(5-pyridin-2-yl-1H-pyrazol-4-yl) pyridine	MAP4K4	originally designed against ALK5 ALK5 Binding – 0.032 µM[1] ALK5 inhibitor[5]

Table 15 List of PKIS repressor compounds with significant effect on *pkd2* curvature including name, referred name, kinase the compound was designed against, most potent known target and further information. [1] (Elkins *et al.*, 2016), [2] (Singh *et al.*, 2003), [3] (Gellibert *et al.*, 2004), [4] (Witherington *et al.*, 2003), [5] (Gellibert *et al.*, 2006).

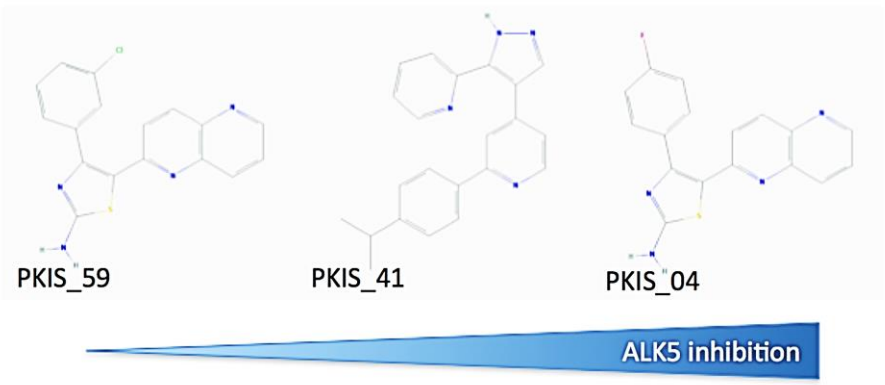

Figure 54 Chemical structure of PKIS hits in relation to ALK5 inhibition potency. Chemical structures obtained from PubChem (https://pubchem.ncbi.nlm.nih.gov/).

After a new batch of the chemicals was obtained following the materials transfer from GSK to UNC, testing continued. Exposures revealed that PKIS_96 did not replicate previous results with regard to the *pkd2* mutant curvature, whereas the three remaining compounds did (Figure 55 A). Interestingly, in all compounds there also was a trend towards slightly enlarged glomeruli, which was, however, not significant (Figure 55 B). Although PKIS_96 was unable to reproducibly repress the curvature, time constraints at the end of the project made it necessary to conduct experiments in parallel; hence this compound was taken through all assays and is depicted in the results below.

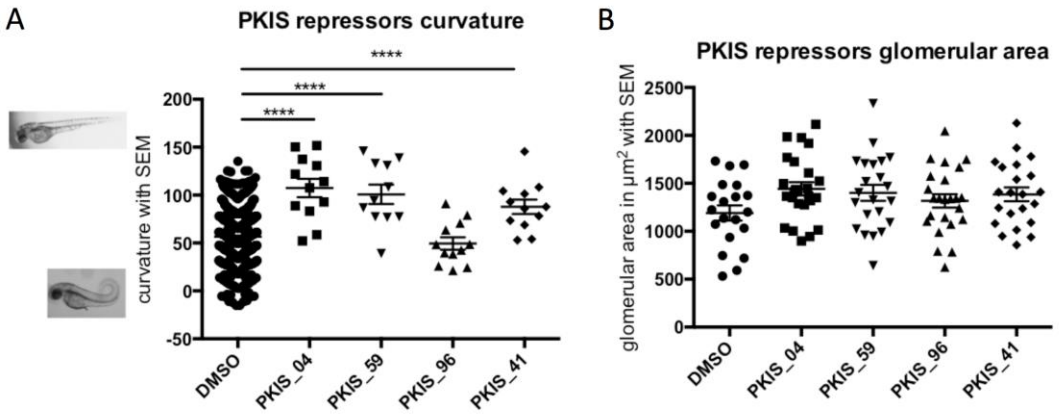

Figure 55 Effect of re-ordered PKIS repressor compounds on *pkd2* curvature (A) and glomerular area (B). Significances via one-way anova with Dunnett's multiple comparison test; ****: p ≤ 0.0001. Error bars indicate SEM.

As with the Spectrum compounds, PKIS repressors were also tested on WT and *elipsa* evaluating their effects on glomerular size and tail curvature (Figure 56). None of the compounds had any significant effects on either WT feature. Similarly, glomerular size in *elipsa*/*elipsa* was unaffected, although there were trends towards enlargement in PKIS_04 and PKIS_96. One compound, PKIS_41 significantly reduced the *elipsa* down curl phenotype and PKIS_04 exhibited a similar tendency.

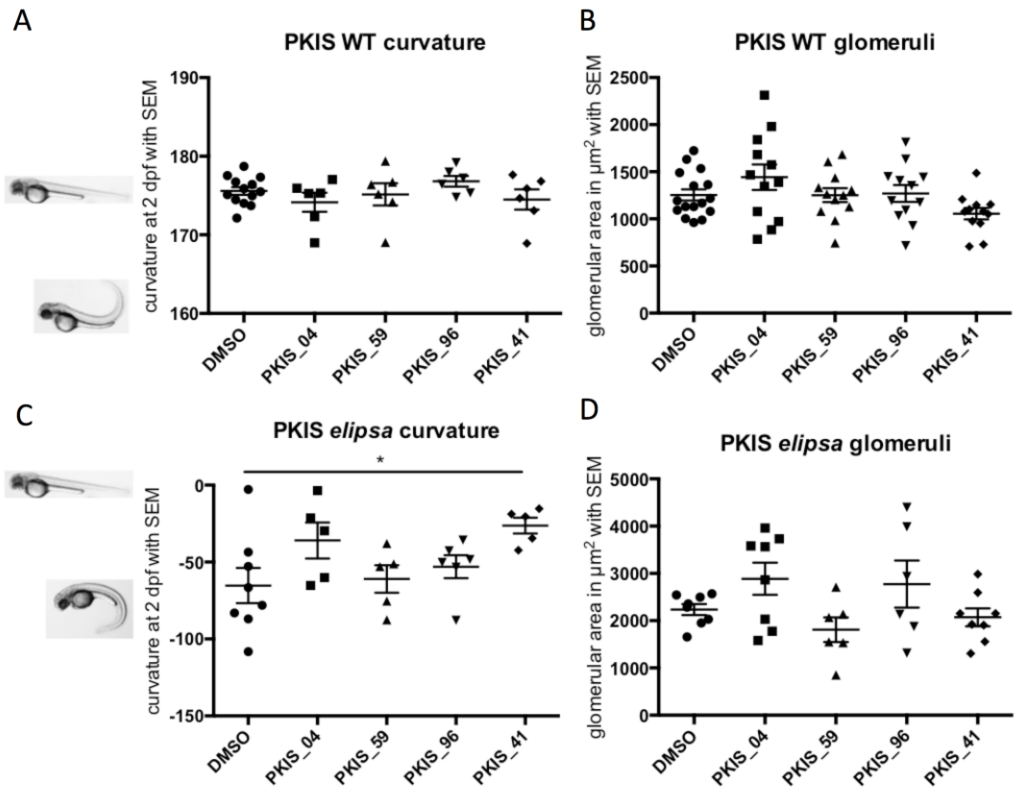

Figure 56 Curvature of WT (A) and *elipsa* (C) as well as glomerular area in WT (B) and *elipsa* (D) after exposure to various compounds. Significances via one-way anova with Dunnett's multiple comparison test; *: $p \leq 0.05$. Error bars indicate SEM.

Subsequent to initial characterisation of the PKIS repressors in zebrafish, cell culture assays with MDCKII and Ox161c1 cells were carried out for validation purposes. The results of these three-dimensional cyst assays are described in the following two paragraphs.

4.2. Validation of PKIS compounds in cyst culture: MDCKII cells

MDCKII assays with PKIS repressor compounds were carried out in the same manner as tests with the Spectrum compounds (biological triplicates in two independent experiments each). Exposures to different concentrations of the PKIS repressors in MCKII 3D cyst assays revealed the following (Figure 57): PKIS_04 and PKIS_59 exhibited dose-dependent capabilities to decrease cyst size at all time points measured. PKIS_41 conversely caused an expansion of cyst area at 0.1 µM, no effect in comparison to base line levels at 1 µM and a reduced cyst size at 10 µM at all time points. PKIS_96 was toxic at concentrations at 1 and 10 µM whereas 0.1 µM did not have a significant effect on MDCKII cystogenesis.

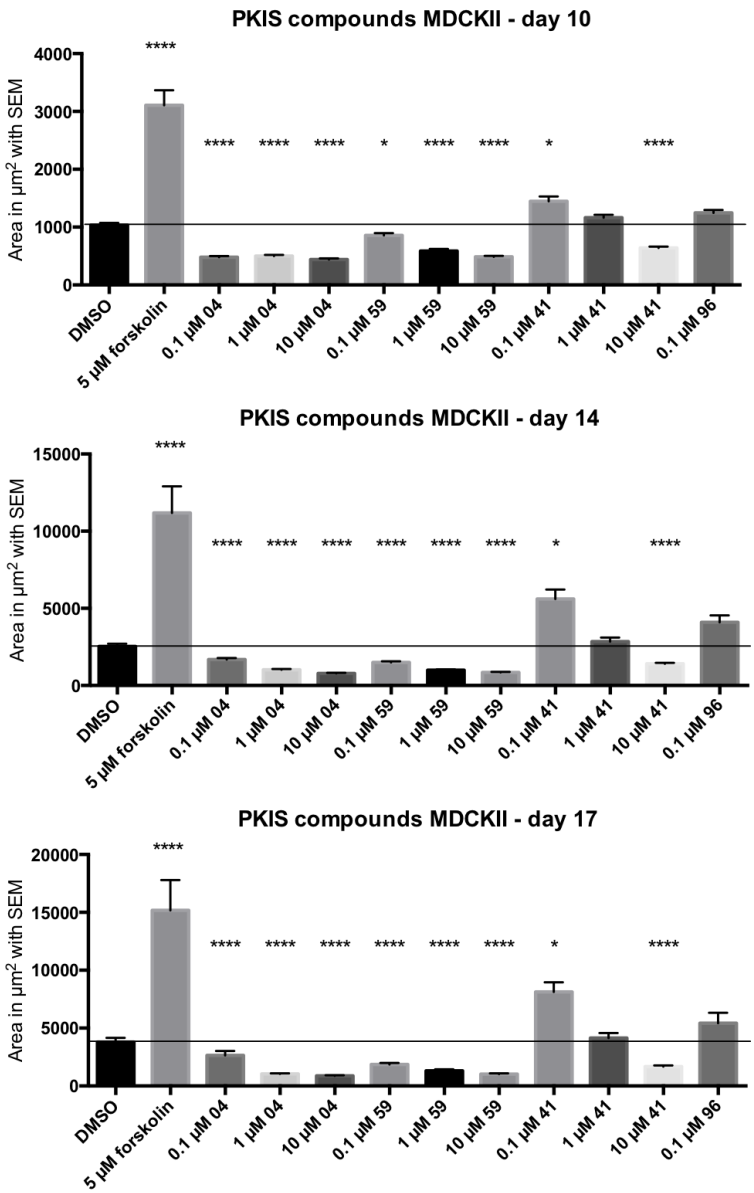

Figure 57 Cyst area of MDCKII cells after PKIS compound exposures of 10, 14 and 17 days exposure. Mean of DMSO baseline indicated with black line. Significances via Kruskal-Wallis test with Dunn's multiple comparison test; ****: $p \leq 0.0001$, *: $p \leq 0.05$. Error bars indicate SEM.

4.3. Validation of PKIS compounds in a cell culture model of ADPKD: Ox161c1 cells

The exposure results of *PKD1*$^{-/-}$ Ox161c1 cells to PKIS were less conclusive than the MDCKII experiments in the sense that none of the PKIS compounds exhibited dose-dependent effects (Figure 58). 0.1 µM PKIS_04 and 1 µM PKIS_59 showed an insignificant increase in cyst sizes at days 10 and 14 respectively. The remainder of the compounds behaved according to expectations. 10 µM of PKIS_04, PKIS_59 and PKIS_41 showed a significant decrease in cyst area at day 20 and lower concentrations showed similar trends. PKIS_96 exposures resulted in less cytotoxicity than in MDCKII cells but at 10 µM cells showed signs of stress.

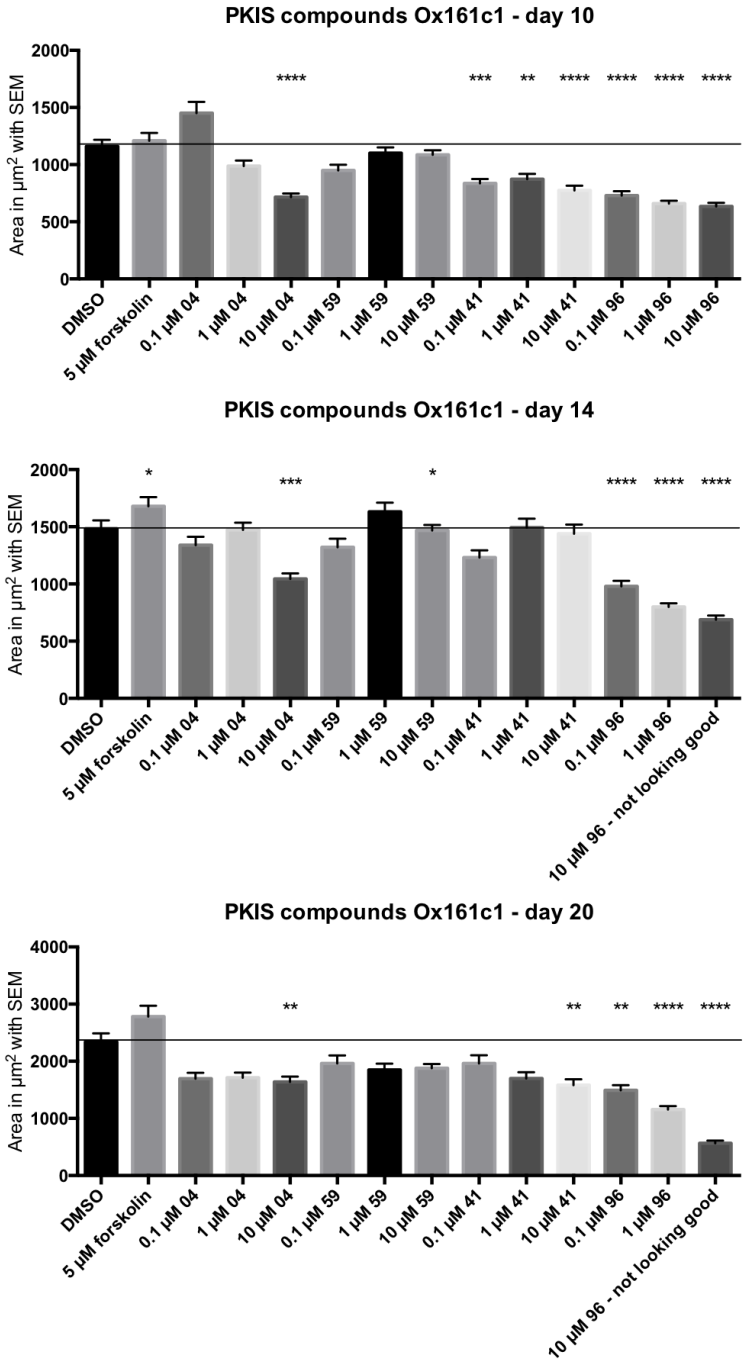

Figure 58 Cyst area of Ox161c1 cells after PKIS compound exposures of 10, 14 and 20 days exposure. Mean of DMSO baseline indicated with black line. Significances via Kruskal-Wallis test with Dunn's multiple comparison test; ****: $p \leq 0.0001$, ***: $p \leq 0.001$, **: $p \leq 0.01$, *: $p \leq 0.05$. Error bars indicate SEM.

4.4. Target of phenotype reduction: Alk5

Since PKIS_96 had failed to repress the curvature reproducibly in zebrafish and proved rather toxic in cell culture, this compound was excluded during target analysis. Similarly, PKIS_41 exhibited an inconsistent behaviour in MDCKII cells, although it did not in the Ox161c1 line. Two heat maps of potential targets were therefore generated one including and one excluding PKIS_41 (Figure 59 B and A respectively). PKIS_04 and PKIS_59 were structurally highly related and alongside with PKIS_41 designed to inhibit ALK5 (also known

as TGFBR1 - transforming growth factor, beta receptor I). Interestingly, ALK5 was not amongst the kinases tested in the first characterisation of the PKIS compound collection used for heat map generation (Elkins *et al.*, 2016). However, ALK5 inhibiting properties of these compounds have been described in independent papers (Gellibert *et al.*, 2006; Gellibert *et al.*, 2004). Amongst the kinases tested and available for heat map generation KDR was the most relevant target for PKIS_04 and _59 and MAP4K4 was most prominent candidate when combining all three repressors.

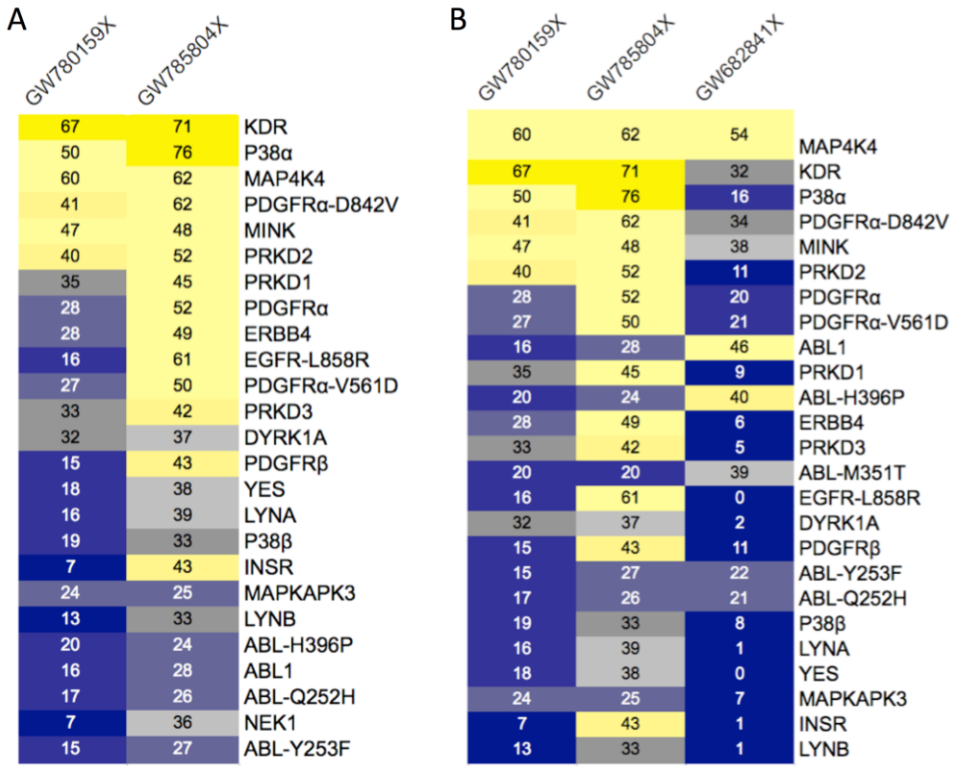

Figure 59 Heat maps of known kinases inhibited by PKIS repressor compounds with the top 25 inhibited kinase targets in decreasing order. Numbers represent percentage of inhibition; dark yellow 65 % and above, yellow 40 % and above, light grey 35-40 %, dark grey 30-35 %, grey/blue 20-30 %, light blue 15-20 % and dark blue > 15 %. (A) Structurally similar compounds PKIS_04 and PKIS_59. (B) Combined data of all three curvature repressors.

Interestingly, although KDR and MAP4K4 were the most likely targets based on the information contained in the heat maps, there were more potent inhibitors of both kinases in the original library. These more specific inhibitors, however, had no effect on the curly tail phenotype (Figure 60, KDR and MAP4K4 in A and B respectively). This suggested neither KDR nor MAP4K4 were the targets driving the curvature reduction.

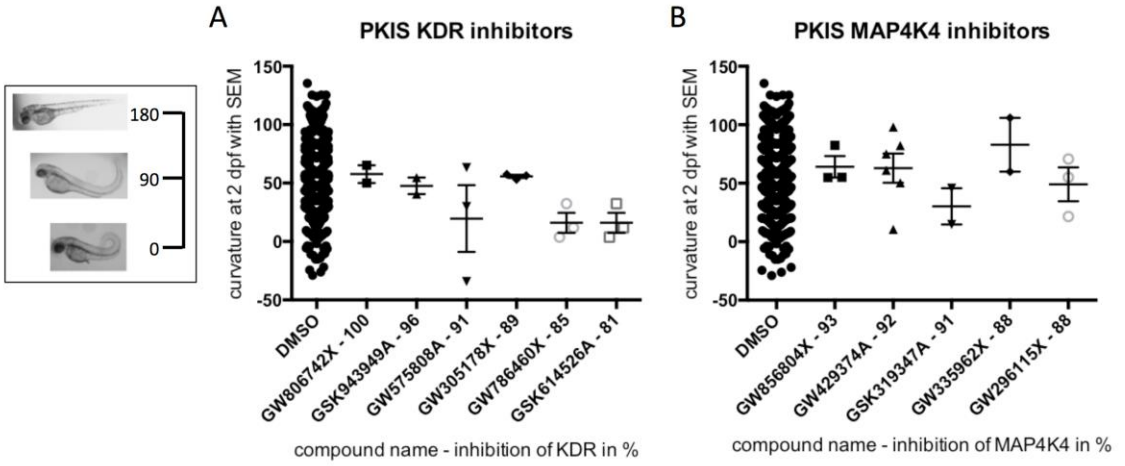

Figure 60 Potent KDR (A) and MAP4K4 (B) inhibitors in PKIS1 compound collection. Data from original compound screen on *pkd2* curly tails. Box on left: Examples of curvature severity with corresponding scale in degrees. No significances via one-way anova with Dunnett's multiple comparison test; $p > 0.05$. Error bars indicate SEM.

Since neither of the most promising, known targets seemed to cause the phenotype reduction and the chemicals had a tendency to inhibit a plethora of kinases, two, structurally-unrelated, ALK5 inhibitors with higher specificity were obtained: SD-208 ((Uhl *et al.*, 2004); IC_{50}: 49 nM, according to UCN) and SB431542 ((Inman *et al.*, 2002); IC_{50}: 94 nM, according to UCN), structures in Figure 62. Both chemicals have been described previously in biological systems as Alk5 inhibitors: SD208 had anti-cancer properties in malignant glioma in mice via TGFβ inhibition (Uhl *et al.*, 2004) and SB431542 suppressed TGF-beta-induced proliferation in human osteosarcoma cells (Laping *et al.*, 2002).

In exposures of *pkd2* mutant zebrafish both compounds, SD208 and SB431542, were able to repress the curvature according to expectations. SD208 potently alleviated the phenotype at 10 μM whereas much higher concentrations were necessary for SB431542, where only 100 μM caused a significant change (100 μM SB431542 had been described as TGFβ inhibitor at these developmental stages in zebrafish by (Park *et al.*, 2008)). TGFβ inhibition therefore is the likely effector in reducing the curly tail phenotype in *pkd2*-null zebrafish embryos.

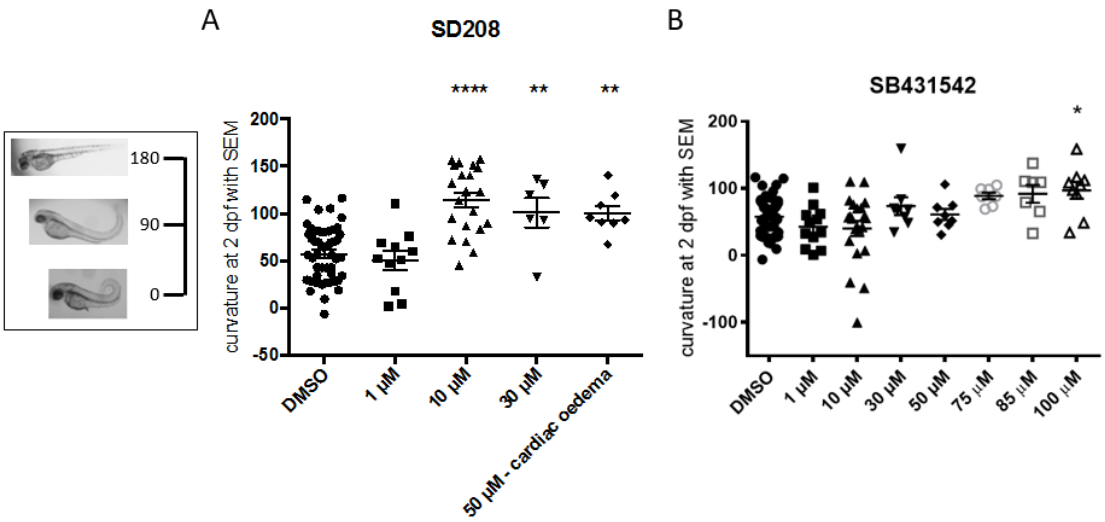

Figure 61 Effects of various concentrations of known Alk5 inhbitors on *pkd2*$^{-/-}$ curvature. Box on left: Examples of curvature severity with corresponding scale in degrees. (A) SD208. (B) SB431542. Significances via one-way anova with Dunnett's multiple comparison test; ****: p ≤ 0.0001, **: p ≤ 0.01, *: p ≤ 0.05. Error bars indicate SEM.

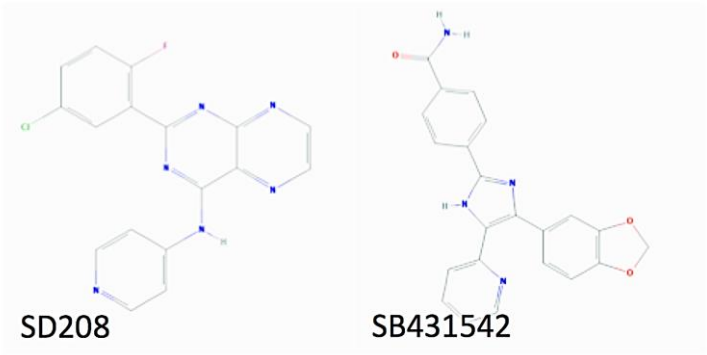

Figure 62 Structure of alternative Alk5 inhibitors tested during this project. Chemical structures obtained from PubChem (https://pubchem.ncbi.nlm.nih.gov/).

Discussion

1. Zebrafish *pkd2* mutants as ADPKD screening tool

Overall, the results of two drug library screens with the zebrafish *pkd2*$^{-/-}$ curly tail as ADPKD-related readout and subsequent validation of compound efficacy in 3D cyst assays with two different cell lines, demonstrates that the tail curvature phenotype in *pkd2*-deficient fish is a valid predictor for cystic behaviour. How the mechanism of generating this curly tail, possibly caused by overproduction or –deposition of ECM, relates to the mechanism underlying cystogenesis remains unclear. Nevertheless, *pkd2* mutant fish embryos proved to be a robust and valid model for screening potential ADPKD-candidate drugs. Interestingly, compound exposure of the *elipsa* mutant "cystic kidney" phenotype did not consistently lead to predicted outcomes. As this phenotype in ciliary mutants is very severe, it may have been

irreversibly altered by the time of exposure or involve a different mechanism. Furthermore, a dilated glomeruli phenotype in zebrafish, typically declared a "cystic kidney" in the literature, has very little in common with actual cystic behaviour. It should be noted that cilia in the zebrafish pronephros are motile and their beating motion thought to contribute to fluid movement along the tubule (Kramer-Zucker *et al.*, 2005). Loss of cilia therefore might lead to an inability to expel filtrate at normal rates, creating a backlog of fluid into the glomeruli, hence causing dilation. Thus, the underlying mechanism for cystic dilatation may be very different from that in mammalian kidney cyst formation. These differences are potential disadvantages in using zebrafish embryos as a model to study ADPKD – cilia are motile rather than non-motile in the kidney and the pronephros consists of just two nephrons compared to up the to two million nephrons in a human adult (Bertram *et al.*, 2011). *pkd2*-deficient zebrafish are not viable past 5 dpf and to date, no adult models of ADPKD exist in zebrafish.

Neither cAMP nor forskolin had an effect on the *pkd2* curly tail, although they are well-established controls in three-dimensional cyst assays (Hanaoka & Guggino, 2000; Yamaguchi *et al.*, 1995; Yamaguchi *et al.*, 2000). This suggested that the *cup* phenotype is independent of the classical forskolin, cAMP, Ca^{2+} axis and, in that regard, *pkd2* mutants are perhaps not an ideal ADPKD model.

An important point to consider when screening drugs on a freshwater species is that zebrafish need highly sophisticated excretion mechanisms to maintain homeostasis. To counter osmotic pressures, water molecules need to be constantly expelled while other chemicals are retained inside the body. Freshwater species therefore have a very effective transport machinery and compounds might become expelled much more efficiently than in mammals, resulting in reduced drug efficacy.

2. Screen hit compounds in the wider context

The Spectrum and PKIS screens yielded a number of positive hits, which were validated in both cyst assay cell lines. Amongst the compounds identified were previously reported chemicals affecting ADPKD prognosis, such as androgens (Gabow, 1990; Gabow *et al.*, 1992; Grantham, 1997; Stewart, 1994; Torres *et al.*, 1996) and PGE2 modulators (Y. Liu *et al.*, 2012b; Nasrallah *et al.*, 2014) but also a range of new molecules.

2.1. Steroids and L-type calcium channel inhibitors

Men suffering from ADPKD tend to have a worse prognosis than females with a faster progression towards renal failure and earlier mortality (Gabow *et al.*, 1992; Stewart, 1994). This sex dimorphism is also recapitulated in many renal disease rodent models (Aziz *et al.*,

2001; Cowley *et al.*, 1997; Fry *et al.*, 1985; Katsuyama *et al.*, 2000; Lager *et al.*, 2001; Nagao *et al.*, 2005; Nagao *et al.*, 2003; Ogborn *et al.*, 1987; Smith *et al.*, 2006), but is not well described in ADPKD model strains. Publications of various rodent models also showed that oestrogen exhibits reno-protective abilities and castration of males improved disease endpoints, suggesting that testosterone is renotrophic (Cowley *et al.*, 1997; Nagao *et al.*, 2005; Smith *et al.*, 2006). Interestingly, a study of sex hormones in MDCKII cells revealed that testosterone increased fluid and solute transport as well as cAMP levels by activating adenylate cyclase, whereas no effects on ATPase activity, cell proliferation or cellular protein content were found (oestrogens had no effect, (Sandhu *et al.*, 1997)).

The steroids identified as hit compounds from the Spectrum library were mostly androgens, although a progestogen, norethynodrel was also identified. After evaluating the chemical structures of the steroids tested during the project, a pattern emerged (depicted in Figure 63): The more complex the side-groups at C3 and C17, the less potent the effect on the curvature phenotype. Androstandione with its two keto-groups in these places showed the highest potency and even adding a hydrogen to these particular side-chains reduced potency (see DHT or epiandrosterone). Interestingly, epiandrosterone, another steroid hit compound, as well as DHT can be converted into androstandione (Ferraldeschi *et al.*, 2015; Sharifi, 2012).

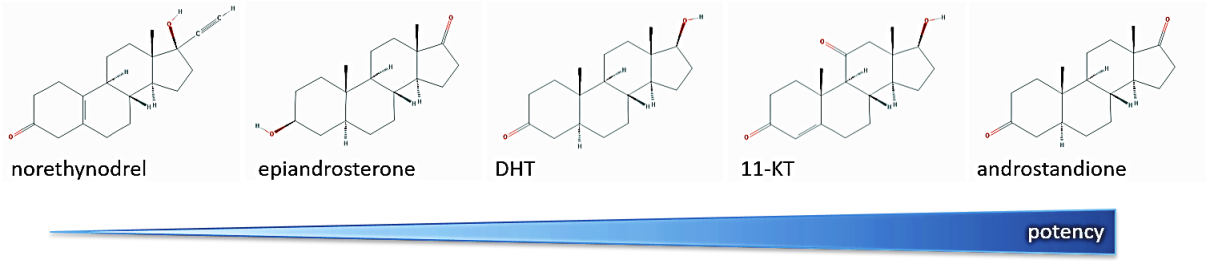

Figure 63 Steroids tested on *pkd2*$^{-/-}$ zebrafish in this project with structure and potency correlation. Chemical structures obtained from PubChem (https://pubchem.ncbi.nlm.nih.gov/).

Androstandione proved to be more effective in zebrafish assays and tested cell lines than the most potent human androgen, DHT (Vollmer, 1963), and the most potent zebrafish androgen 11-KT (Hossain *et al.*, 2008). The added potency of this compound led to the speculation that androstandione might not act solely via the androgen receptor (AR), which is expressed at very low levels at these stages (Gorelick *et al.*, 2008), but might also influence a secondary signalling pathway. Current experiments in the lab aim to generate a zebrafish *ar*-knockout line to test this hypothesis. If *ar*/*pkd2* double knockouts prove resistant to curvature-enhancing effects of androstandione exposure, then signal transduction occurs solely via the AR. However, should androstandione affect the curly tail in *ar*$^{-/-}$/*pkd2*$^{-/-}$ fish,

then a second pathway would be involved. Once the appropriate zebrafish mutant line has been established, these experiments will be carried out.

Potential candidates for this hypothesised secondary androstandione pathway are L-type calcium channels (LCCs). Testosterone has been described as potent LCC inhibitor (Scragg *et al.*, 2004) and nifedipine, a specific inhibitor of L-type channels, showed intermediate curvature-enhancing properties upon closer evaluation of the Spectrum screen data (it was originally dismissed due to stringent scoring criteria).

There is some evidence that LCC inhibitors like nifedipine worsen ADPKD in patients (Astor *et al.*, 2008; Saruta *et al.*, 2009) and several publications have linked treatment with L-type channel blockers in rats and dogs to higher glomerular filtration rates, therefore increasing filtration fractions and renal blood pressures (the filtration fraction is the fraction of fluid reaching the kidney passing through renal tubules) (Abe *et al.*, 1983; Dietz *et al.*, 1983; Heller *et al.*, 1990; Roy *et al.*, 1983). Increased blood pressure in the kidney (renal hypertension) has been associated with faster renal disease progression in various canine and rat models (Bidani *et al.*, 1987; S. A. Brown *et al.*, 1993; Griffin *et al.*, 1999).

L-type calcium channels are the predominant voltage-gated channels expressed in the kidney (Hayashi *et al.*, 2007; Homma *et al.*, 2013) and the most abundant renal L-type channel, $Ca_v1.2$, is localised predominantly to afferent renal arterioles (Hayashi *et al.*, 2007). LCC inhibitors have been shown to cause afferent arteriolar dilation while the efferent vasculature remained unaffected (Hayashi *et al.*, 2007; Homma *et al.*, 2013). Consequently, drugs of this type increase blood inflow into renal glomeruli while the outflow remains the same - raising renal blood pressure (for schematic depiction see Figure 64). Treatments with LCC activators, such as BayK8644, result in preferential afferent arteriolar constriction (Steinhausen *et al.*, 1989), underlining the validity of above findings. Interestingly, *$Ca_v1.2$* expression is increased 2-fold in *Pkd1*$^{-/-}$ and *Pkd2*$^{-/-}$ murine renal epithelial cells and the protein seems to be randomly distributed in *Pkd*-knockout lines while it is localised predominantly in cilia in healthy tissues (Jin *et al.*, 2014). *$Ca_v1.2$* knockdown also caused shortened cilia in PC-null cells whereas WT cilia were unaffected (X. Jin *et al.*, 2014). Furthermore, zebrafish *$ca_v1.2$* morphants exhibit "cystic kidneys" and *$Ca_v1.2$* knockdown in *Pkd1*$^{+/-}$ (lentiviral with *$Ca_v1.2$* shRNA) mice resulted in severe renal cysts while kidneys in WT animals were unaltered (Jin *et al.*, 2014).

Nifedipine also enhanced the curvature and enlarged renal size in *pkd2* mutant zebrafish, further supporting the notion that L-type calcium channel inhibition could have adverse effects in ADPKD models. In addition, data from a PKD rat model (Han:SPRD) further emphasises the deleterious effects of L-type channel blockers on renal outcomes (Nagao *et*

al., 2010; Nagao *et al.*, 2008). Interestingly, LCC inhibitor treatments in WT rats seemed to protect against renal injury (Harris *et al.*, 1987; Yoshioka *et al.*, 1988), suggesting the drugs might have differential effects in healthy and renal disease systems. Lastly, several publications suggest treating hypertension in patients with T- or N-type calcium channel blockers might be more beneficial for renal disease outcomes (Abe *et al.*, 2013; Fujita *et al.*, 2007; Fujiwara *et al.*, 1998; Homma *et al.*, 2013; Omae *et al.*, 2009).

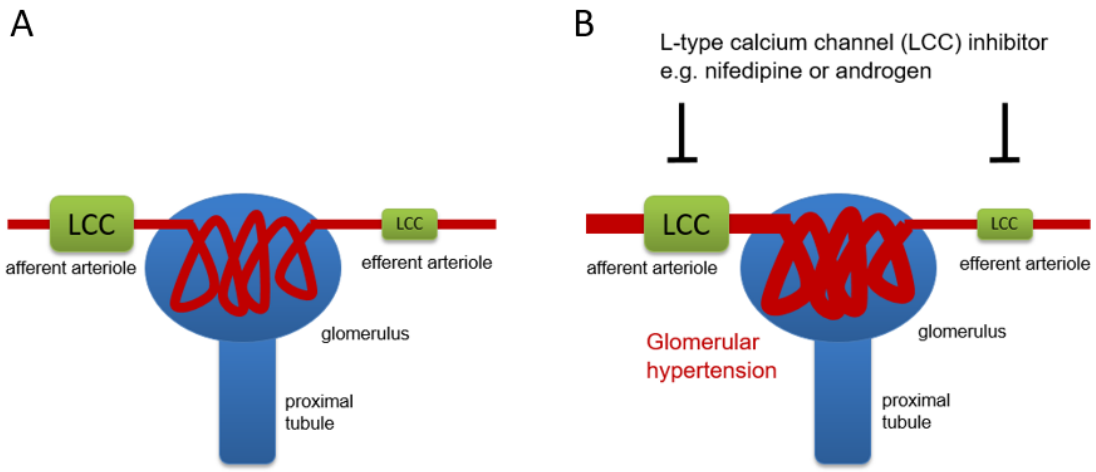

Figure 64 Schematic depiction of L-type calcium channel (LCC) function in a single nephron (nephron in blue, vasculature in red). (A) In normal conditions and (B) with LCC inhibition treatment for hypertension or in the presence of androgens.

In summary, there is a plethora of publications suggesting L-type calcium channel inhibition in PKD models and ADPKD patients may have adverse effects, specifically in PKD systems. Furthermore, there is some evidence suggesting androstandione, the most potent enhancer identified in this project, might act not only via the AR pathway but could also inhibit L-type calcium channels.

2.2. Coumarins

A second class of compounds enhancing the *cup* phenotype identified in the Spectrum library screen were coumarins. Coumarins are natural compounds found in various plants as secondary plant metabolites. Unfortunately, coumarins have not been well-characterised in the literature to date: All three coumarin hits in this project have been described to have antifungal or antimycobacterial properties (O'Neill *et al.*, 2013; Stein *et al.*, 2006) and (oxy-)prenylated coumarin derivatives, such as pimpinellin, may modulate $GABA_A$ receptors (Singhuber *et al.*, 2011). Of note, sphondin was reported to attenuate COX-2 protein expression and PGE2 release in A549 cells (human pulmonary epithelial cells). More precisely, sphondin did not alter COX-2 enzyme activity but rather suppressed expression of the gene (Yang *et al.*, 2002). COX enzymes and PGE2 release have previously been linked to ADPKD, as alluded to below in the discussion. Structurally, within the coumarin class,

the three-ring structure with more hydroxyl groups seems more potent, although no clear picture emerged (Figure 65).

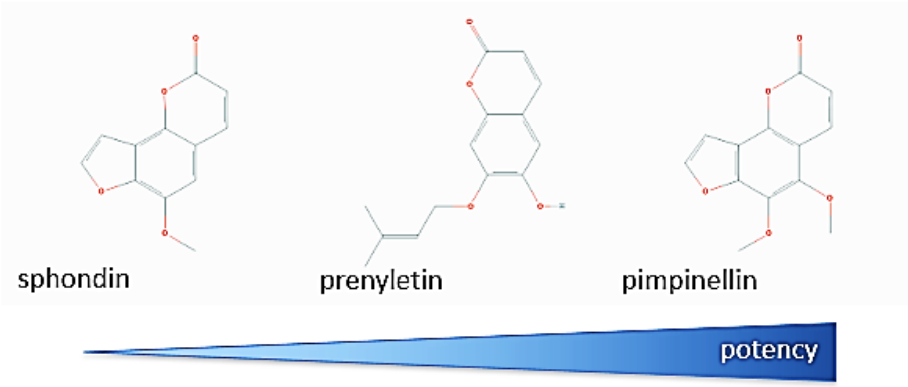

Figure 65 Coumarin hits with structure and relative potency. Chemical structures obtained from PubChem (https://pubchem.ncbi.nlm.nih.gov/).

2.3. Flavonoids

The third class of enhancers identified during the Spectrum library screen comprised flavonoids. Hexamethylquercetagetin and trimethoxyflavone were detected during the screening process whereas naringenin had been observed to induce dorsal curvature in WT embryos (Robert Wilkinson, unpublished). Hexamethylquercetagetin has, to date, not been described in the literature. However, a very similar compound, quercetin, has been linked to prevention of prostate cancer by inhibiting the EGFR pathway in a male rat model (Firdous *et al.*, 2014). Additionally, quercetin has been implicated in the regulation of Ca^{2+} levels in rat musculature (Sgaragli *et al.*, 1993). Trimethoxyflavone is deemed to have antioxidative properties (Bala *et al.*, 2014) and enhanced lipolysis in mature adipocytes, improving insulin resistance in cell culture (Okabe *et al.*, 2014).

The third flavonoid, naringenin, is mainly found in citrus fruit, especially in grapefruit. It has been associated with benefits in various diseases such as obesity, diabetes, hypertension, metabolic syndrome (reviewed in (Alam *et al.*, 2014)) and deemed cardioprotective in the cardiorenal syndrome (Y. Liu *et al.*, 2016). Interestingly, naringenin has been directly linked to *pkd2* in a *Dictyostelium discoideum* screen. Naringenin slows *Dictyostelium* growth by inhibiting proliferation (Russ *et al.*, 2006) and in a gene knockout screen, a *pkd2* mutant proved to be resistant to these effects (Waheed *et al.*, 2014). Additionally, cyst growth in 3D-culture MDCKII experiments was described as inhibited and TRPP2 knockdown in MDCKII cells alleviated those effects, suggesting naringenin acts in a *pkd2*-dependent manner (Waheed *et al.*, 2014). This stands in stark contrast to my findings: Not only were *pkd2*$^{-/-}$ fish affected by naringenin, suggesting the compounds acts not via PC2 but via an alternative pathway but

naringenin in MDCKII assays increased cyst size. Considering that three very similar flavonoids showed potent ADPKD-enhancing effects in all three models tested, this project provides powerful evidence that naringenin indeed worsens ADPKD model readouts.

Regarding the chemical structures of the flavonoids identified as hits during this project, unbound electrons in the middle ring and fewer side chains seemed to correlate with potency (Figure 66).

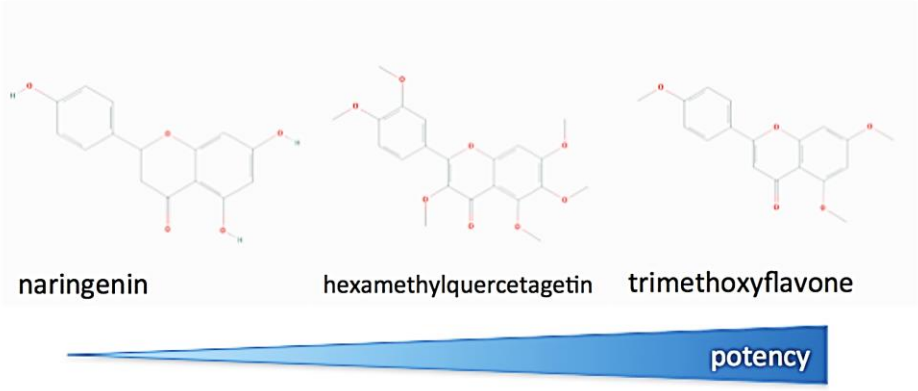

Figure 66 Flavonoid hits with structure and relative potency. Chemical structures obtained from PubChem (https://pubchem.ncbi.nlm.nih.gov/).

2.4. Xanthoxylin and dihydroxychalcone

Two further, structurally independent enhancers significantly altered the *cup* phenotype in the Spectrum screen: xanthoxylin and dihydroxychalcone. Xanthoxylin has been portrayed to possess antifungal/fungiostatic properties (Cechinel Filho *et al.*, 1996) and dihydroxychalcone seems to affect various pathways. It has been described to inhibit cell division in cell culture experiments (Xie *et al.*, 2014), induced apoptosis in human prostate cancer cells (Sheng *et al.*, 2015), functioned as an antileishmanial drug by inhibiting the enzyme glycerol-3-phosphatase dehydrogenase (G3PDH) (Passalacqua *et al.*, 2015) and, as component of propolis-extract derived from Argentinian honeybees (*Apis mellifera*), dihydroxychalcone reduced COX-2 activity (Salas *et al.*, 2016).

2.5. Repressors

Three compounds from the Spectrum collection and another three drugs from the PKIS library were identified to reduce APDKD-related readouts during this project. With the exception of two PKIS compounds, the repressors were structurally unrelated, so no inference to the active structure of the molecules could be made (Figure 67).

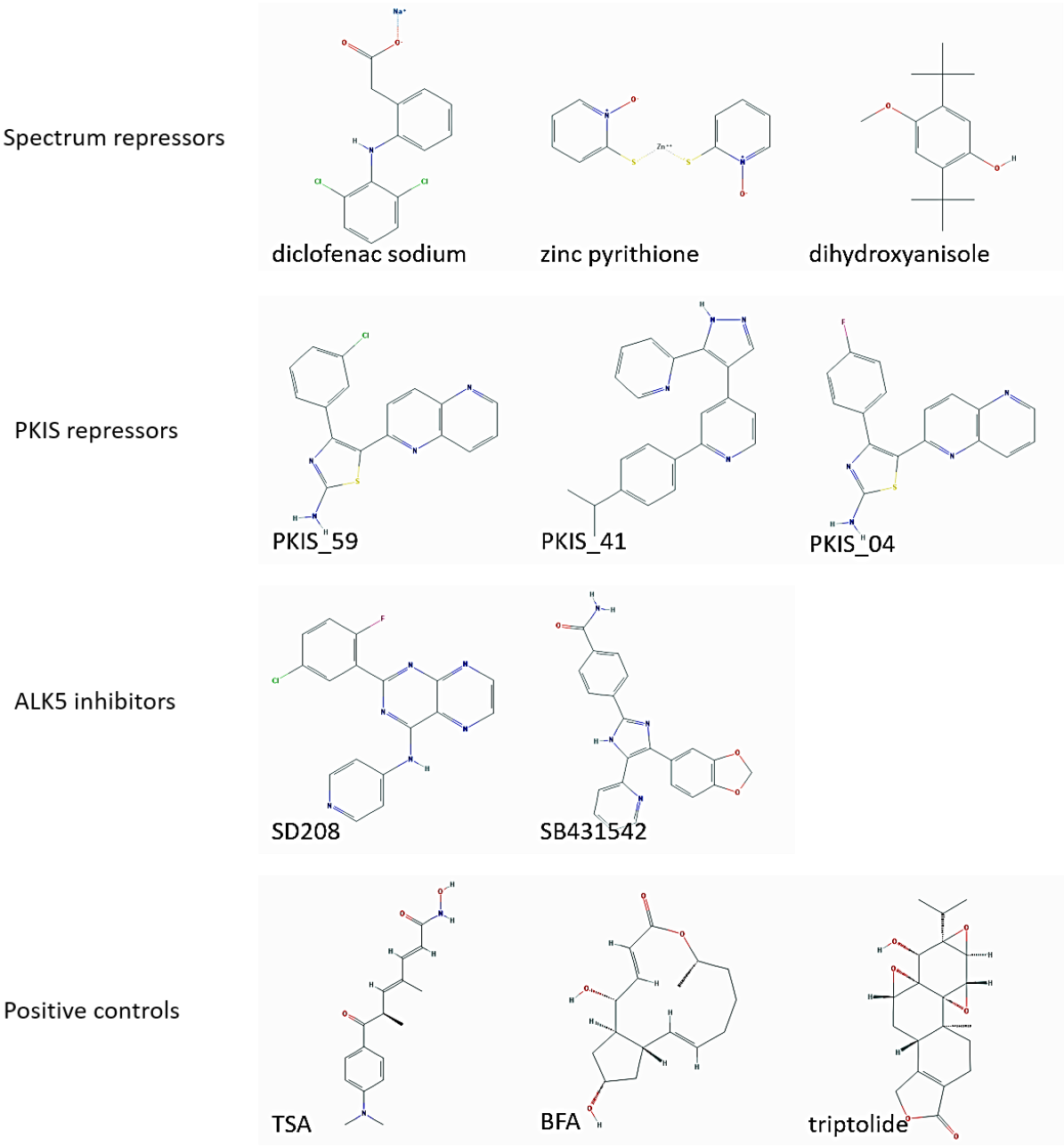

Figure 67 Chemical structures of all *pkd2* mutant curvature repressors used during this project. Chemical structures obtained from PubChem (https://pubchem.ncbi.nlm.nih.gov/).

2.5.1. TSA, BFA, triptolide and tolvaptan – known ADPKD model modulators

Three independent positive controls for *curly up* reduction were utilised during this project: TSA, BFA and triptolide (Figure 67). TSA was first identified in a small scale compound screen on *pkd2*$^{-/-}$ zebrafish (Cao *et al.*, 2009), BFA reduced *pkd2* curvature (Le Corre *et al.*, 2014) and triptolide had not previously been tested in zebrafish. In this project, all three compounds reduced the *cup* phenotype of *pkd2* mutants in narrow therapeutic windows.

Interestingly, tolvaptan, the only currently approved drug for slowing the progression of ADPKD, did not affect the *pkd2*$^{-/-}$ curvature and is presumed to have no effect on MDCKII

cyst size, as this cell line lacks VP2R (vasopressin 2 receptor, personal communication Albert Ong). In patients, tolvaptan treatment becomes ineffective in late disease stages (Hattanda *et al.*, 2016), presumably because renal tissues at these stages lose VP2R expression.

2.5.2. The Spectrum repressor compounds zinc pyrithione, dihydroxyanisole and diclofenac

Of the newly identified ADPKD modulators zinc pyrithione, an active ingredient in anti-dandruff shampoo, has clinical implications in the treatments of the skin conditions hidradenitis suppurativa and seborrhoeic dermatitis (Danesh *et al.*, 2015; Naldi *et al.*, 2015). To date (August 2016) there are no publications regarding the biological function of the dihydroxyanisole identified during this project (2,5-di-t-butyl-4-hydroxyanisole). A slightly different chemical, 3,5-di-t-butyl-4-hydroxyanisole, however, has been linked in a variety of papers to calcium regulation in rat musculature via activation of the sarcoplasmic reticulum Ca^{2+}-ATPase and guinea-pig gastric smooth muscle cells (Fusi *et al.*, 2001).

The only repressor of the Spectrum collection with a known mechanism implicated in ADPKD pathogenesis was diclofenac. Diclofenac is a non-steroidal anti-inflammatory drug (NSAID) inhibiting cyclooxygenase enzymes 1 and 2 (COX-1 and COX-2) with a higher affinity for COX-2. COX enzymes metabolise arachidonic acid to PGH2, a precursor of PGE2. Inhibition of COX therefore leads to a decrease in PGE2 synthesis and lower PGE2 levels have been linked to improvements in ADPKD (Elberg *et al.*, 2007; Liu *et al.*, 2012a). Figure 68 contains a more in-depth explanation of the relationships of PGE2 and ADPKD. Prostaglandin E2 seems to play direct and indirect roles in a variety of pathways associated with renal diseases (reviewed in (Nasrallah *et al.*, 2014)) and in a murine ADPKD model (renal epithelial *Pkd1*$^{-/-}$ cells) elevated PGE2 levels were directly correlated to increases in proliferation and chloride secretion (Liu *et al.*, 2012a). Interestingly, there is also evidence that PGE2 is required for ciliogenesis in zebrafish by promoting intraflagellar transport (Jin *et al.*, 2014).

Apart from reducing cyst size, MDCKII cell morphology was also affected by diclofenac treatment, resulting in a shift from cystic cells to tubular structures. Healthy renal cells in culture often form structures reminiscent of renal tubules (Mao *et al.*, 2011; Zeng *et al.*, 2007) rather than cysts. MDCKII cells still have the ability to form tubules but will predominantly form cysts in a collagen matrix. Diclofenac altered this phenotype significantly and it could be debated that this shift corresponds to a "healthier" cell status. Similar observations with regard to cell structure were made by a colleague in MDCKII 3D culture exposure to PGE2 antagonists (Morgane Lannoy, personal communication).

The reported reduction of COX-2 function by sphondin and dihydroxychalcone described above (both compounds enhanced the *curly up* phenotype), stand in contrast to current hypotheses. Furthermore, diclofenac has also been described to inhibit L-type calcium channels in rat cardiomyocytes (Yarishkin *et al.*, 2009), however, a more specific L-type calcium channel inhibitor (nifedipine) exaggerated PKD phenotypes in this project.

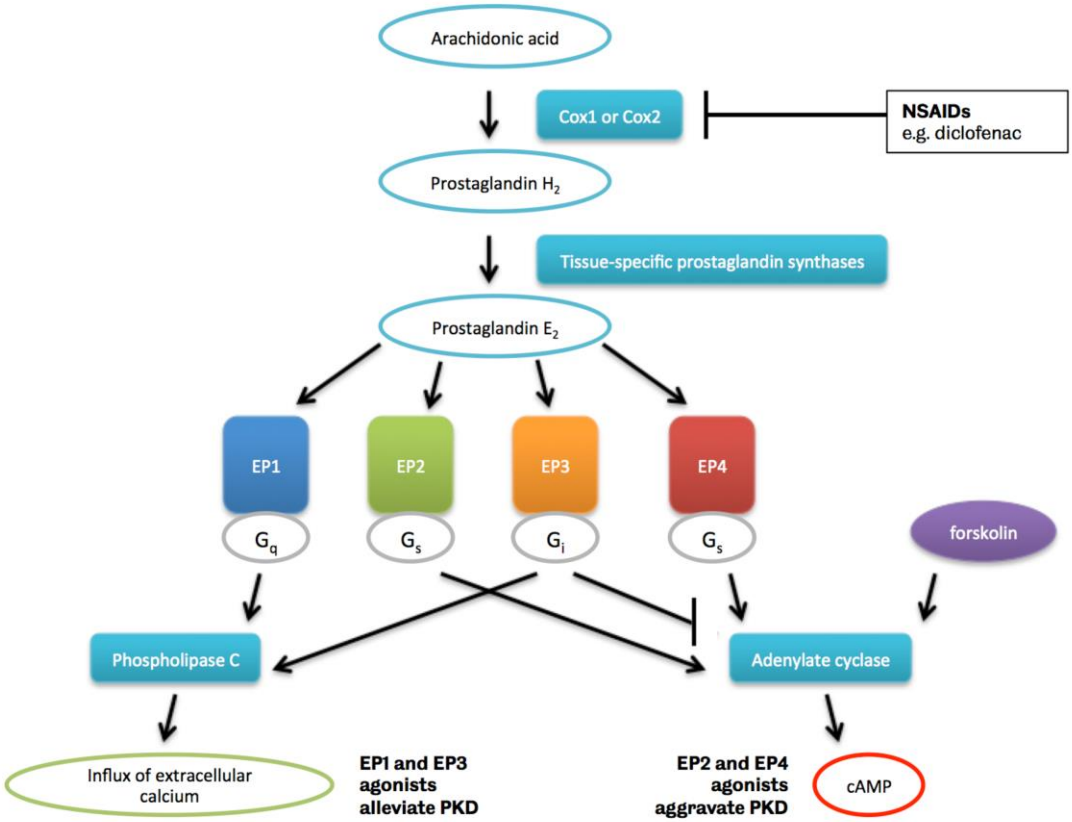

Figure 68 Schematic depiction of the prostaglandin pathway and its association with chronic renal diseases derived from information in current literature (reviewed in (Nasrallah *et al.*, 2014)).

2.5.3. PKIS repressor compounds affect the TGFβ pathway

The PKIS repressors identified during this project were, according to GSK, originally designed for ALK5 (activin receptor like kinase 5) inhibition. ALK5 is also referred to as TGFβ receptor 1 and is one of many proteins associated with the TGFβ superfamily. ALK5 was not represented in the kinase inhibition tests used for heat map generation but the two best target candidates suggested by those heat maps were quickly excluded to be the cause of the phenotype reduction. As separate publications suggested the PKIS hits were indeed ALK5 inhibitors (Gellibert *et al.*, 2006; Gellibert *et al.*, 2004; Singh *et al.*, 2003), structurally unrelated, known ALK5 inhibitors were obtained for further studies. Exposure experiment with SD208, a compound with high specificity for ALK5 and very low affinity for any other TGFβ components, recapitulated the *pkd2* zebrafish curvature reduction observed in the

PKIS compounds. SB431542, which blocks not only ALK5 but also ALK4 and ALK7 function (Inman *et al.*, 2002), was also able to repress the curly tail.

The main effectors of the TGFβ pathway, SMAD2 and 3, are upregulated in a variety of mouse models and in human tissues even at early ADPKD disease stages (Hassane *et al.*, 2010). A recent study in a *Pkd1*$^{-/-}$/*Alk5*$^{-/-}$ double knockout mouse model, however, did not show any alterations in downstream target expression (SMAD2/3) or progression of PKD compared to *Pkd1*$^{-/-}$ animals (Leonhard *et al.*, 2016). That study further suggested Alk5 is not the TGFβ component affecting SMAD2/3 expression but rather identified activins (alternative TGFβ superfamily ligands) and the activin receptor II b/Alk4 complex as driver of the phenotype. Figure 69 depicts both branches of the TGFβ family: On the right the Alk5 (TGFβR1)/TGFβR2 receptor complex and on the left the Alk4/activin receptor II b complex - both of which ultimately lead to SMAD2/3 activation. SMAD2 and 3 are transcription factors which translocate to the nucleus upon phosphorylation via the receptor complexes and regulate a plethora of downstream effects such as cell proliferation, differentiation, apoptosis and survival (reviewed in (Villapol *et al.*, 2013)). Since SD208 is described as a potent Alk5 inhibitor but has not been described to inhibit other members of the TGFβ-receptor family, it seems likely that Alk5 rather than Alk4 is the driver behind the reduced ADPKD-related zebrafish phenotype. There are plans to test a third ALK5 inhibitor with regard to the curly tail phenotype, but the supplier is currently unable to deliver.

To elucidate whether one or both of the two *alk5* copies in zebrafish, *tgfbr1a* and *tgfbr1b*, are truly responsible for the *pkd2* curvature reduction, knockdown experiments with morpholinos, or preferably, with the newly developed CRISPRi technology (a colleague, Aaron Savage, is currently gathering data for a methodology paper) could be performed in *pkd2* mutant animals. Of note, interesting cross-links between PGE2 and the TGFβ pathway have been described (Haidar *et al.*, 2015; Kumai *et al.*, 2014; Ramirez-Yanez *et al.*, 2006; Tian *et al.*, 2010) and TGFβ has been shown to regulate calcium homeostasis in the hearts of mice (Hsu *et al.*, 2015). Conversely, naringenin and triptolide have been linked to a suppression of SMAD3 and SMAD2/3 phosphorylation (activation) respectively (Chen *et al.*, 2014; Liu *et al.*, 2006), although they enhanced zebrafish and cell culture phenotypes.

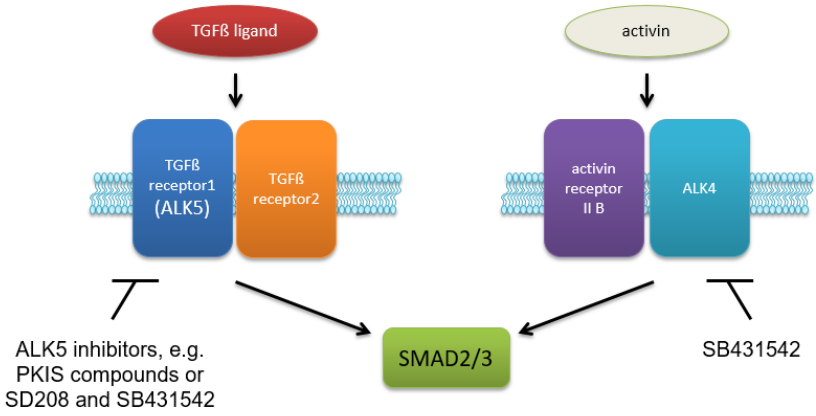

Figure 69 TGFβ superfamily ligands and receptors affecting SMAD2/3 activity with modulators of this system identified during this project.

2.6. Compound co-exposures in zebrafish and cell culture ADPKD models

Originally, zebrafish data suggested that co-exposures of coumarins or flavonoids in combination with steroids caused an additive effect - increasing *pkd2* mutant tail curvature in comparison to individual compounds. In cell culture, however, this was not recapitulated. Overall, co-exposures decreased cyst size rather than increasing it (in comparison to the more potent single compound). No clear explanation can be given for this discrepancy between models at this point.

Flutamide, an anti-androgen intended to negate steroid effects, did not behave as expected in any of the models tested. It had no effect on the curly tail phenotype in zebrafish, although previous publications had shown that flutamide causes biological alterations in exposure experiments (Schiller *et al.*, 2013; Schiller *et al.*, 2014), and in 3D cyst assays flutamide increased cyst size rather than decreasing it. The latter effect was more pronounced in MDCKII cells, where flutamide exceeded DHT expansion potency. In Ox161c1 assays, DHT was the stronger enhancer, but flutamide still caused an increase in cyst area above baseline levels. Perhaps neither of these models were particularly suited to test androgen effects: Zebrafish have very low levels of androgen receptor expression at the evaluated stages (Gorelick *et al.*, 2008; Thisse *et al.*, 2008) and there is some evidence to suggest that, in particular androstandione, acts via alternative pathways (details above) – this hypothesis will be tested in the near future. Both cell lines utilised during this project were derived from females of their respective species and there is the distinct possibility that this causes flutamide to act contrary to expectations. Furthermore, immortalised cell lines often lose certain proteins and become unsuitable for testing certain hypotheses (e.g. MDCKII cells lost VP2R and tolvaptan is thought to have no effect).

Interestingly, the repressor compounds in the Spectrum library (diclofenac, zinc pyrithione and dihydroxyanisole) were all able to counter low levels of forskolin stimulation in cyst assays. Zinc pyrithione and dihydroxyanisole reduced expanding processes in comparison to the stimulant and diclofenac was able to completely overcome it, presumably by antagonising the effects of forskolin on cAMP.

3. Summary of library screen findings

Overall, the *pkd2* mutant curly tail phenotype has proven to be a robust read-out for screening compounds that are active in mammalian cyst assays. Compounds that enhanced the *cup* phenotype also increased cyst size in cell culture and chemicals repressing the ADPKD-related readout in zebrafish decreased cyst size. Since cell culture experiments can take up to 20 days whereas the zebrafish exposures last only 3 days, zebrafish offer a rapid method for screening chemical libraries using an *in vivo* model.

A summary of screen hit compounds with described mechanisms of action can be found in Figure 70. The two most promising new avenues of therapy for ADPKD emerging from this project are diclofenac and the PKIS repressors, inhibiting COX and TGFβ pathways respectively. Both of these pathways have been linked to repression of ADPKD severity (Leonhard *et al.*, 2016; Seamon *et al.*, 1981).

Interestingly, the majority of compounds identified in this study worsened ADPKD-related outcomes. Future work will address potential mechanisms by which these may alter the cystic phenotype.

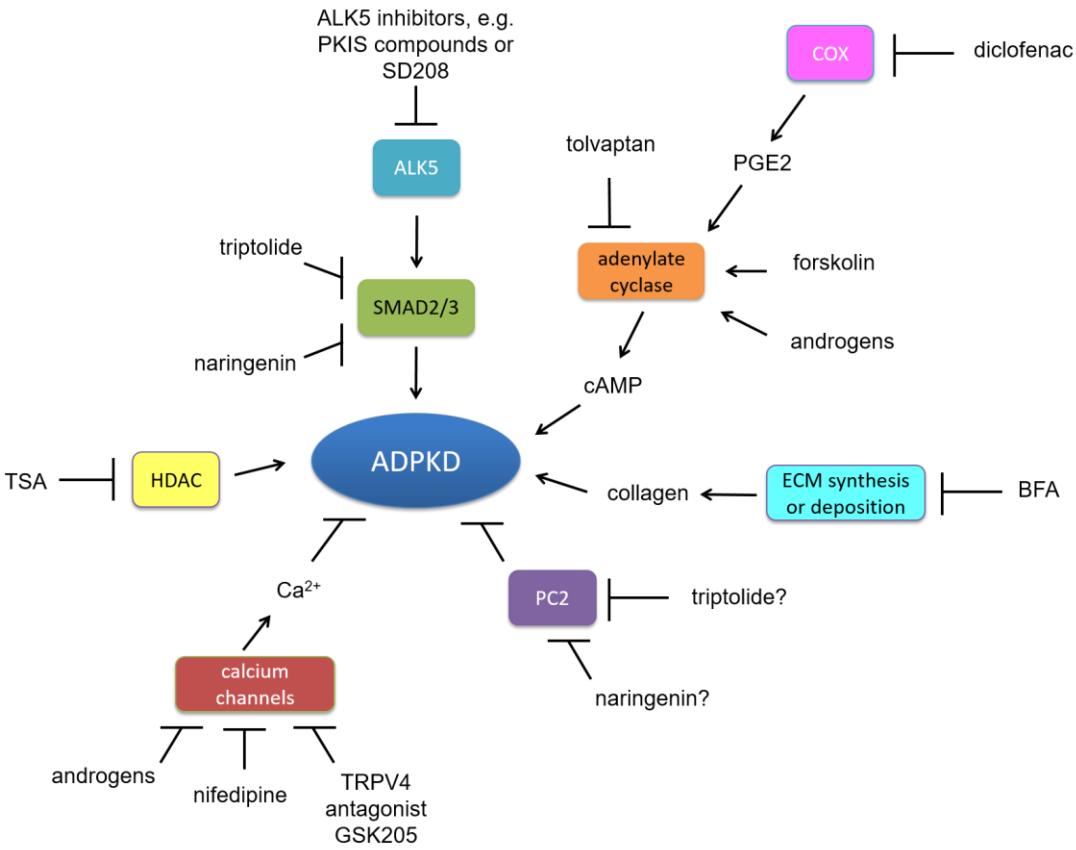

Figure 70 Compounds with proposed/speculative mechanisms of action utilised in this project. Questionmarks suggest interactions were previously described but new evidence suggests they are inaccurate. ALK5: activin A type II-like kinase 5, BFA: brefeldin A, cAMP: cyclic adenosine monophosphate, COX: cyclooxygenase, ECM: extracellular matrix, HDAC: histone deacetylases, PGE2: prostaglandin E2, TRPV4: Transient Receptor Potential Cation Channel Subfamily V Member 4, TSA: trichostatin A.

Results and Discussion Chapter 3: *in vivo* real-time renal tubular calcium signalling

Introduction

PC2 is a member of the transient receptor potential (TRP) superfamily and thought to function as a non-selective Ca^{2+} channel (also known as TRPP2) (Gonzalez-Perrett *et al.*, 2001; Hanaoka *et al.*, 2000; Luo *et al.*, 2003a). Several studies have shown a decrease in intracellular Ca^{2+} levels in PKD-deficient cells (Ahrabi *et al.*, 2007; Nauli *et al.*, 2003; Q. Qian *et al.*, 2003) but changes in intracellular Ca^{2+} concentrations *in vivo*, in particular in the kidney, had not been previously reported. Zebrafish with their rapid development, easy genetic manipulation and translucent bodies provided an ideal tool for this purpose. Although *pkd2* mutant zebrafish did not exhibit an obvious renal phenotype in terms of glomerular dilation or proliferation (see Results and Discussion Chapter 1, chapters 1.1. and 1.3. respectively), I hypothesised that there might be a detectable change in intracellular Ca^{2+} in the developing kidney. To study this, a new renal calcium-reporter line was created.

Several zebrafish calcium-reporter lines have been developed in recent years, allowing real-time Ca^{2+} visualisation by utilising a fluorescent marker as readout, *GCaMP7a* (Kyung *et al.*, 2015; Muto & Kawakami, 2013; Muto *et al.*, 2013; Yokota *et al.*, 2015). A GCaMP protein is basically a modified GFP (green fluorescent protein) with an attached calmodulin unit and its use in zebrafish was originally described by (Muto *et al.*, 2013). The calmodulin unit of the GCaMP fusion protein has a high affinity for Ca^{2+} (Akerboom *et al.*, 2012) and the binding of Ca^{2+} causes a conformational change (closing the beta-barrel structure of the fluorophore), allowing for excitation with appropriate wavelengths (Figure 71). In short, in the presence of Ca^{2+}, the GCaMP protein is able to fluoresce and the more calcium, the brighter the fluorescence.

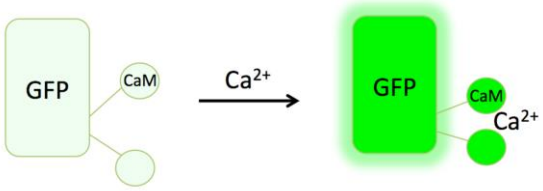

Figure 71 Schematic depiction of GCaMP function.

Several different GCaMP versions exist and the GCaMP7a utilised in study is slightly modified and more sensitive than the original GCaMP protein described in cell culture experiments (Nakai *et al.*, 2001). A colleague had previously generated a *UAS:GCaMP7a* line

(Robert Wilkinson - an initial attempt to create an endothelial:*GCaMP7a* line failed as fluorescence levels were undetectable). The cloning of direct promoter:*GCaMP7a* constructs during this project was unsuccessful and since amplification through the *UAS/Gal4* system was deemed beneficial, the strategy of generating renal *Gal4* lines, which would then be crossed to the *UAS:GCaMP7a* line, was pursued.

Once a renal *GCaMP7a* zebrafish line was established, fluorescence levels were monitored to quantify renal Ca^{2+} levels in wild-type animals and ADPKD models at different developmental stages.

Results

1. Generation of renal *GCaMP7a* lines

Two different renal promoters were utilised initially: *enpep*, which has been described as driving exclusively renal tubular expression (Seiler *et al.*, 2011) and *podocin*, described to drive expression in the glomerular podocytes (He *et al.*, 2011). After successful cloning of the final constructs (with a *cmcl2* marker, see Materials and Methods for more details), microinjections into an incross of *pkd2* carriers commenced and the marker-positive animals were raised. Subsequently two founders were identified for each construct and their offspring was evaluated. The lines established during the project comprised *podocin:Gal4*^{sh490}, *podocin:Gal4*^{sh491} and *enpep:Gal4*^{sh489}. As the *podocin* lines did not differ, work was only continued on *podocin:Gal4*^{sh490} (henceforth referred to as *podocin:Gal4*) and *enpep:Gal4*^{sh489} (referred to as *enpep:Gal4*).

1.1. The glomerular *podocin*-driven calcium-reporter line

Fluorescence of *podocin:Gal4;UAS:GCaMP7a* fish was not discernible via conventional fluorescent microscopy at any time point during development, suggesting that Ca^{2+} levels in the podocytes or expression of *podocin:Gal4* were low. In order to visualise the expression pattern *podocin:Gal4* animals were crossed to a *UAS:kaede* line (*kaede* is a photoconvertible fluorescent protein). This revealed the same expression pattern described in the original publication (He *et al.*, 2011) with restriction of expression exclusively to renal glomeruli (Figure 72). *podocin* drives expression from 48 hpf to at least 5 dpf in the pronephric glomeruli. Later expression patterns were not monitored. However, as *pkd2* mutant embryos did not display a glomerular phenotype and *podocin* promotes expression only in the glomeruli

(which were also covered by the *enpep* promoter, see below), this construct was not pursued any further.

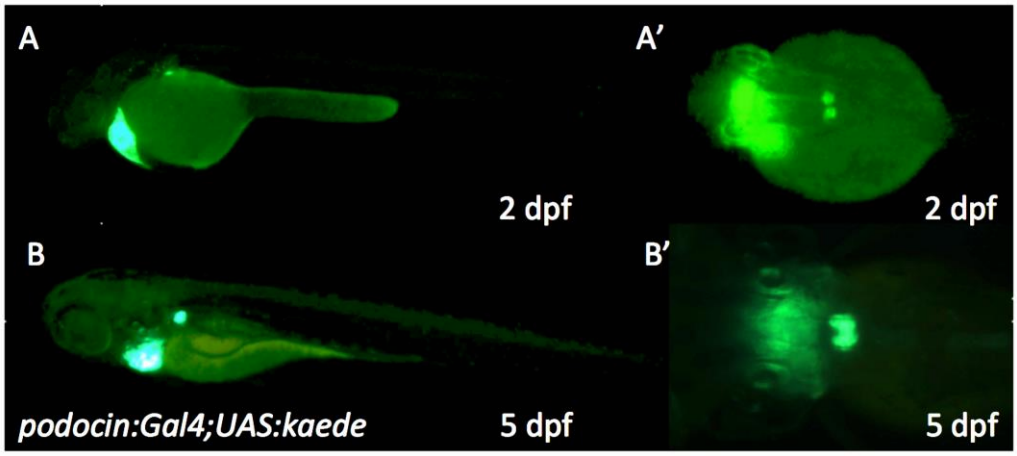

Figure 72 Expression pattern as driven by the *podocin* promoter in a *podocin:Gal4;UAS:kaede* cross. (A and A') at 2 dpf. (B and B') at 5 dpf. (A and B) Lateral view of whole animal. (A' and B') Dorsal view of head and trunk. Fluorescence in the heart due to *cmlc2.EGFP* transgenesis marker indicating transmission of *podocin:Gal4*.

1.2. A pronephric Ca^{2+} reporter: *enpep:Gal4;UAS:GCaMP7a*

Similar to the *podocin* driver line, expression patterns in *enpep:Gal4;UAS:GCaMP7a* were too faint to observe by conventional fluorescence microscopy. Renal tubular expression could be seen faintly at 1 dpf, but to get a more detailed picture *enpep:Gal4* fish were crossed to *UAS:kaede* as with the *podocin* line and the following expression patterns were observed (Figure 73): Similar to what was originally reported (Seiler *et al.*, 2011), expression was observed in the pronephric tubules from 24 hpf to 5 dpf (earlier and later expression was not monitored). It was, however, not as restricted exclusively to the tubules, but was also observed in the glomeruli at all time points monitored (Figure 73 A', B' and C'). Additionally, a rather strong expression was present in the hindbrain and spinal cord, looking distinctively like neurons (Figure 73 A, B and C). Further fluorescence was seen in the ocular region and the pectoral fins from 48 hpf (Figure 73 B, B', C and C').

The two original founders were evaluated and both showed the same expression in other tissues, suggesting the location of transgene insertion was not responsible for ectopic expression. Since expression in offspring of two founders was identical, only one line was established permanently: *enpep:Gal4*^{sh489}. Closer examination of the original paper revealed that pronephric restriction only occurred with a 2.3 kb promoter fragment. Shorter fragments produced extra-renal expression as described above. The promoter given to us, however, was only 2 kb long, suggesting the missing 300 bp probably contains a sequence restricting expression to the tubules.

Although there was some expression in tissues other than the kidney, this did not influence renal calcium analysis and subsequent experiments were conducted on *enpep:Gal4;UAS:GCaMP7a*. *enpep:Gal4;UAS:GCaMP7a* fish exhibited a faint renal tubular fluorescence observable under a powerful fluorescence microscope at 1 dpf, which grew too faint for conventional microscopes from 48 hpf. Sorting for renal *GCaMP7a* expression hence always occurred between 24 – 32 hpf.

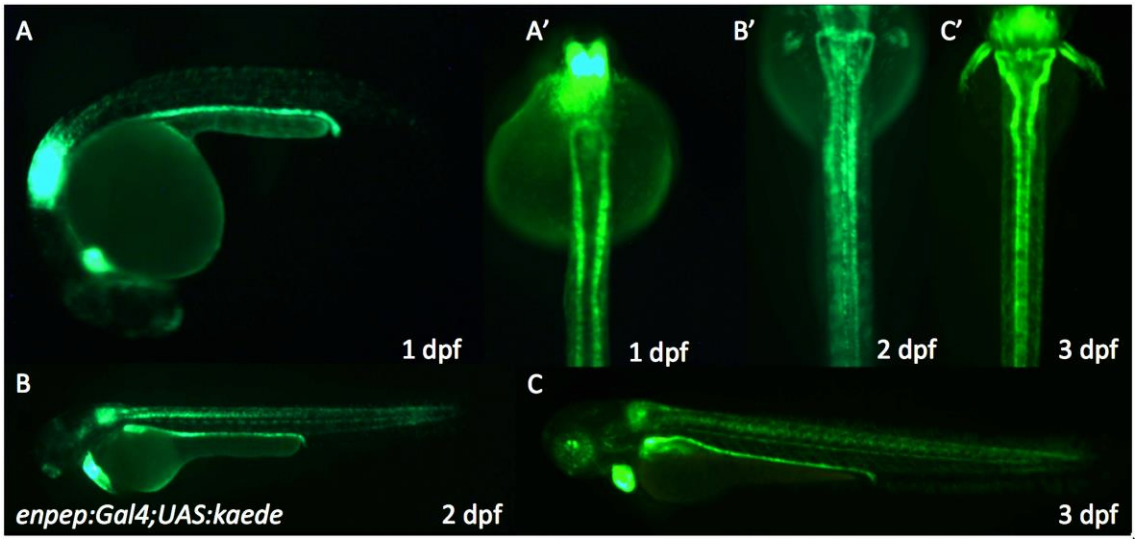

Figure 73 Expression pattern as driven by the *enpep* promoter in a *enpep:Gal4;UAS:kaede* cross. (A and A') at 1 dpf. (B and B') at 2 dpf. (C and C') at 3 dpf. (A,B and C) Lateral view of whole animal. (A', B' and C') Dorsal view of head and trunk. Fluorescence in the heart due to *cmlc2:eGFP* transgenesis marker indicating transmission of *podocin:Gal4*.

1.2.1. Proof-of-principle: Chemical alteration of calcium with known modulators

To test whether *GCaMP7a* fluorescence levels could be modulated in the *enpep:Gal4;UAS:GCaMP7a* line using Ca^{2+} modifying drugs, fish were exposed to thapsigargin (5 µM, 25 min) or 2-APB (2-aminoethoxydiphenyl borate - 50 µM, 2-3 h). Thapsigargin inhibits reuptake of cytoplasmic Ca^{2+} into the ER (via non-competitive inhibition of SERCA) and simultaneously causes Ca^{2+} release from the ER via ER stress pathways (Foufelle *et al.*, 2016; Rogers *et al.*, 1995) – hence, increasing cytoplasmic Ca^{2+} levels and, in theory, *GCaMP7a* fluorescence. 2-APB, in contrast, blocks release of Ca^{2+} ions from the ER via IP3R (Missiaen *et al.*, 2001) and lowers intracellular Ca^{2+} levels - it should therefore decrease fluorescence. A schematic depiction of the effects of thapsigargin and 2-APB can be found in Figure 74 B.

Treatments with thapsigargin or 2-APB yielded the expected results respectively (Figure 74 A) and treated fish were imaged for 30 min to observe whether fluorescence levels changed

after drug withdrawal (not the case, data not shown). Generally, these experiments confirmed that *GCaMP7a* fluorescence levels respond to changes in Ca^{2+} concentrations.

To my knowledge, this is the first description of renal real-time *in vivo* calcium imaging in an intact organism described in the literature to date.

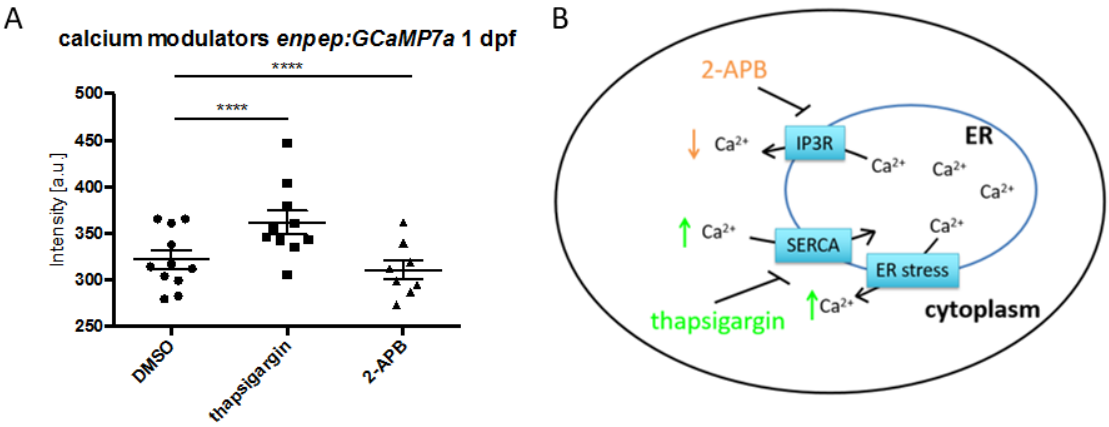

Figure 74 (A) Calcium levels in *enpep:Gal4;UAS:GCaMP7a* after exposure of calcium modulators thapsigargin (25 min) and 2-APB (2 - 3 h) imaged for 30 min at 20 sec intervals, means with SEM depicted. Significances via one-way anova with Dunnet's multiple comparison test; ****: $p \leq 0.0001$. (B) Schematic depiction of calcium modulator fuction in a cell. ER: endoplasmic reticulum, IP3R: inositol triphosphate receptor, SERCA: sarco/endoplasmic reticulum Ca^{2+}-ATPase.

2. Renal calcium at 24 - 34 hpf (pronephros formed, no filtration)

After proof-of-principle experiments confirmed GCaMP7a responsiveness to calcium fluctuations (described above), further experiments on the *enpep:Gal4;UAS:GCaMP7a* line were conducted during day one of embryonic development, when pronephric kidney formation is completed (maturation possibly ongoing) but filtration has yet commenced. This ensured Ca^{2+} baseline level observations were conducted in the absence of potential disruption by filtration or cilia-generated tubular flow in the pronephros. Imaging commenced on the lightsheet microscope in an area from the cloaca to the beginning of the yolk extension, covering the majority of the pronephros and providing an easily identifiable area for measurement (Figure 75).

Figure 75 Reference frame (blue) for imaging calcium levels during 1 dpf. Kindey schematically indicated in red.

2.1. Calcium oscillations in tubules at 1 dpf

Tubular Ca^{2+} was observed on the lightsheet microscope in 2 h-long time lapses, imaging at 15 - 20 sec intervals. Oscillations of entire tubules were measured (Figure 76 A) and some individuals, although not all, showed a slight decrease of fluorescence over time (example in Figure 76 B). This could be attributed to bleaching or a slow decrease of *GCaMP* expression or calcium over time. Bleaching describes a process in which prolonged excitation of fluorescent molecules results in denaturation and depletion over time. Cells are constantly replacing proteins but if destructive processes outweigh fluorescent protein synthesis, bleaching becomes apparent and fluorescence levels reduce. Bleaching was deemed to be the most likely cause for decreases in fluorescence in this case.

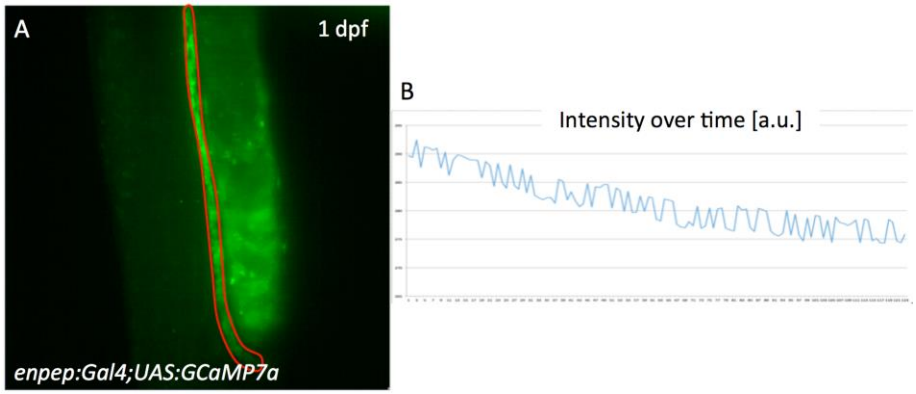

Figure 76 *enpep:Gal4;UAS:GCaMP7a* tubular oscillations at 1 dpf. (A) Illustration of measurement technique. Shape of the pronephric tubule was traced with a tool in the Zen software (example in red) and average fluorescence of the entire tubule was measured over time. (B) Example of tubular intensity over 2 h.

No differences were observed with regard to mean tubular intensity, frequency of oscillations, or peaks of less than 20 seconds between siblings and *pkd2* mutants (Figure 77 A, B and C respectively). The oscillations of entire tubules were measured and include individual flashing cells, which were characterised separately (see below).

The only significant change observed by monitoring overall tubular fluorescence was the distribution of oscillation durations. *pkd2* mutants exhibited a lower percentage of shorter durations (less than 60 seconds, Figure 77 D and more detailed in Figure 77 E) than siblings. Of note, the average oscillation duration was not significantly different between genotypes and the significance with regard to the distribution of durations was low. Although embryos from different parents were imaged at different dates, this could be an artefact of multiple testing.

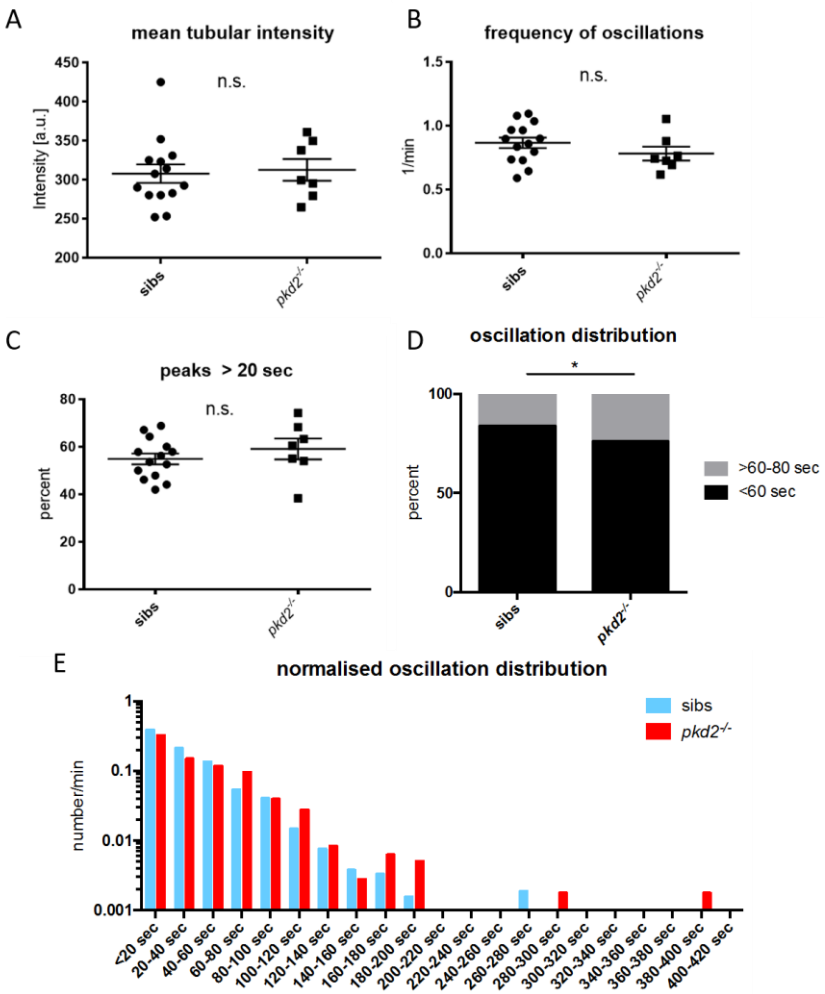

Figure 77 Tubular calcium oscillations in *enpep:Gal4;UAS:GCaMP7a*. Siblings: n = 14, *pkd2*$^{-/-}$: n = 7. Error bars indicate SEM. (A) Mean tubular intensity, (B) frequency of oscillations, (C) peaks longer than 20 seconds, (D) oscillation distribution and (E) oscillation distribution normalised over time in 7 *pkd2* mutants and 14 siblings. Significances in (A, B and C) via unpaired t-test, in (D) via paired t-test; *: $p \leq 0.05$ and non-significant (ns): $p > 0.05$.

2.2. Cellular calcium flashes in the pronephros

2.2.1. Populations of flashing cells in *enpep:Gal4;UAS:GCaMP7a* show *pkd2*-dependent decrease in flash frequency

While analysing the fluctuations in tubular Ca^{2+} it became apparent that individual cells within the pronephros exhibited distinctive behaviours in the time lapses: They showed rapid increases and decreases in fluorescence intensity. These cellular flashes contributed to the tubular oscillations described above, but were probably not their singular driver. The flashes were subsequently analysed by localising flashing cells within the imaged reference frame from the cloaca to the beginning of the yolk extension, fitting a circle around the location and deriving the intensity changes of as many cells per fish as possible (example in Figure 78 A). For each cell, many of which showed multiple flashes in the time course of 2 h, intensity changes (peak height) and duration of the event (peak duration) were derived for each flash. Examples are illustrated in Figure 78 B.

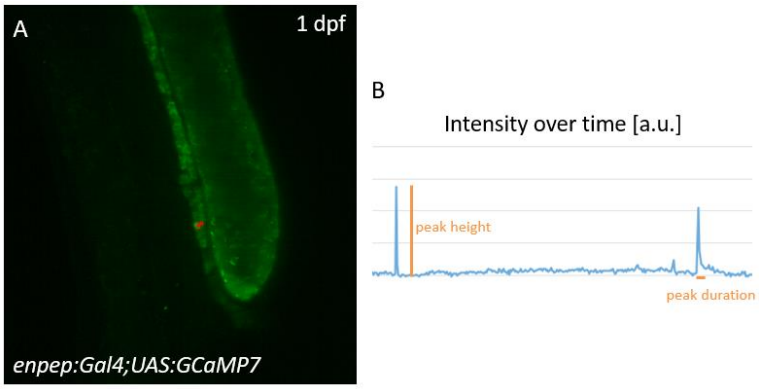

Figure 78 *enpep:Gal4;UAS:GCaMP7a* cellular flashes at 1 dpf. (A) Illustration of measurement technique. Individaul flashing cells were identified through frame-by-frame analysis and a measurement area established (example in red). (B) Example of cellular intensity over 2 h.

Cellular flashing events exhibited no disparities between genotypes in peak duration or height (Figure 79 A and B respectively). Similar to tubular oscillations however, there was a significant shift in the distribution of peak durations; this time with *pkd2* showing an increase of shorter flashes (up to 70 sec) compared to siblings (Figure 79 D). This was not accompanied by a shift of average peak duration.

Interestingly, the number of flashes over time was reduced significantly in a *pkd2* dose-dependent manner with WT having the highest amount of flashes during the time course of the experiment, followed by *pkd2* heterozygous animals and *pkd2* mutants, which exhibited the lowest number (Figure 79 C).

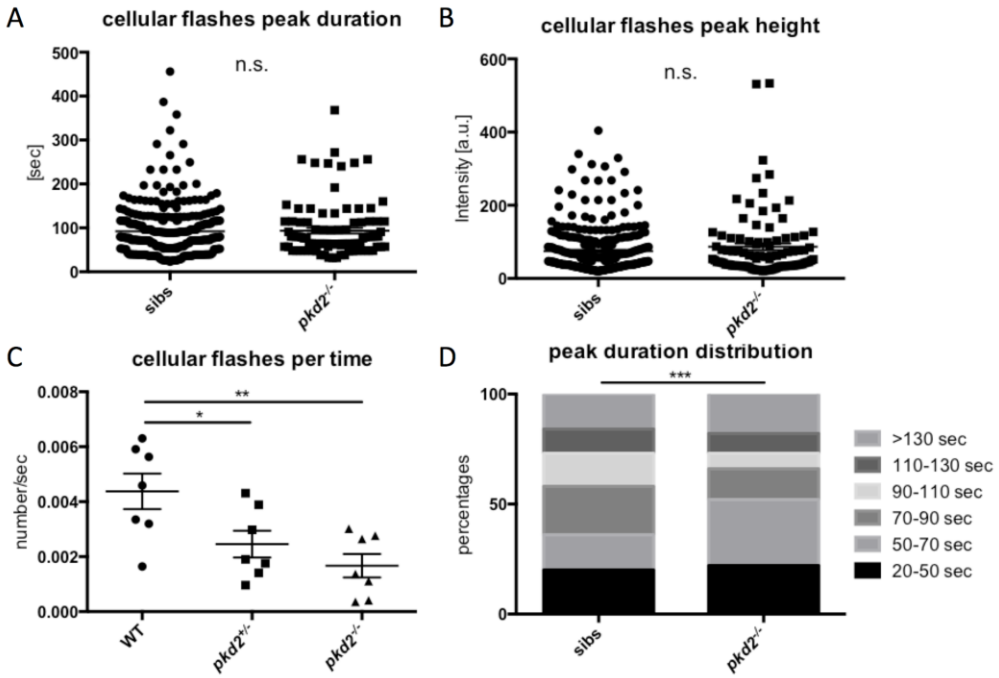

Figure 79 Cellular calcium flashes in *enpep:Gal4;UAS:GCaMP7a*. Siblings: n = 14, *pkd2*$^{-/-}$: n = 7. Error bars indicate SEM. (A) Cellular flash duration, (B) cellular flash intensity, (C) cellular flashes over time and (D) duration distribution in 7 *pkd2* mutants and 14 siblings. Significances in (A and B) via unpaired t-test, in (C) via one-way anova with Dunnet's multiple comparison test and in (D) via paired t-test; ***: $p \leq 0.001$, **: $p \leq 0.01$, *: $p \leq 0.05$ and non-significant (n.s.): $p > 0.05$.

2.2.2. Different cell populations in the embryonic zebrafish kidney

Upon closer observation of the flashing cells, different populations could be discerned. The flashing cell type present in all fish regardless of genotype (3 or fewer flashes in the 2 hours monitored) was dubbed "low-frequency flashing cells" (LFFCs). Cells flashing 4-12 times in the 2 h time lapses were named RCFs (recurrently flashing cells) and cells blinking more often FFCs (frequently flashing cells; >12 times in 2h). FFCs were not analysed in detail, as it was often difficult to determine baseline fluorescence levels (see Figure 80 A), they were, however, included in the count of flashing cells over time (Figure 82 C). Notably RCFs and FFCs did not occur in all animals. In the following subchapters, LFFCs and flashing cells (FCs) were analysed separately for further characterisation. Interestingly, *pkd2* mutants exhibited a larger percentage of LFFCs and numbers decreased in a *pkd2* dose-dependent manner towards WT (not significant). RFC numbers remained constant across all genotypes whereas FFC percentages declined from WT to *pkd2*$^{-/-}$.

Of note, FFCs were tightly clustered and restricted to a narrow region close to the cloaca (Figure 80 C). A literature search revealed the Corpuscles of Stannius, Ca^{2+} homeostasis organs exclusive to teleosts, reside in the same area (Cheng *et al.*, 2015). The Corpuscles of Stannius are spherical in shape and embedded in renal tissue. Although renal filtration has not begun at this stage, the close proximity of flashing cells to these structures suggests they are active, perhaps undergoing developmental processes.

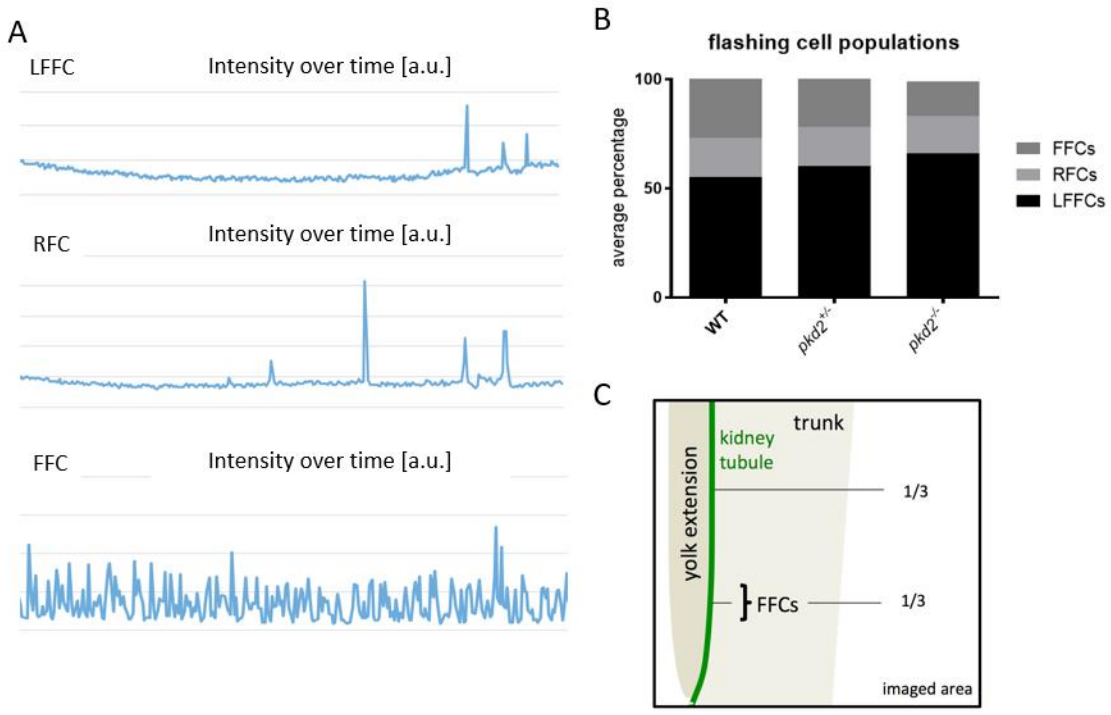

Figure 80 Diffferent populations of cellular flashes: LFFC (1-3 flashes in 2 h), RFC (recurrently flashing cell – 4-12 flashes in 2 h) and FFC (frequently flashing cell - >12 flashes in 2 h). (A) Examples of each cell category depicting calcium levels over time. (B) Distribution of flashing cell populations per genotype. Not significant via paired t-test ($p > 0.05$). WT: n = 7, *pkd2*$^{+/-}$: n = 7, *pkd2*$^{-/-}$: n = 7. (C) Schematic depiction of FFC location.

2.2.2.1. LFFCs (low-frequency flashing cells - 3 or fewer flashes in 2 h)

The LFFC population was by far the largest across all genotypes (more than 50 % of all flashing cells), therefore unsurprisingly the patterns observed in this category were similar to the overall population analysis: Flash duration and intensity were not significantly different between genotypes, but the duration distribution was shifted slightly, with more of short flashes (up to 70 seconds) in *pkd2* mutants (Figure 81 A, B and D respectively). As before, average flash duration was not affected. Furthermore, the number of flashes per time was reduced in a *pkd2* dose-dependent manner as seen in the overall population which was, however, not significant here (Figure 81 C).

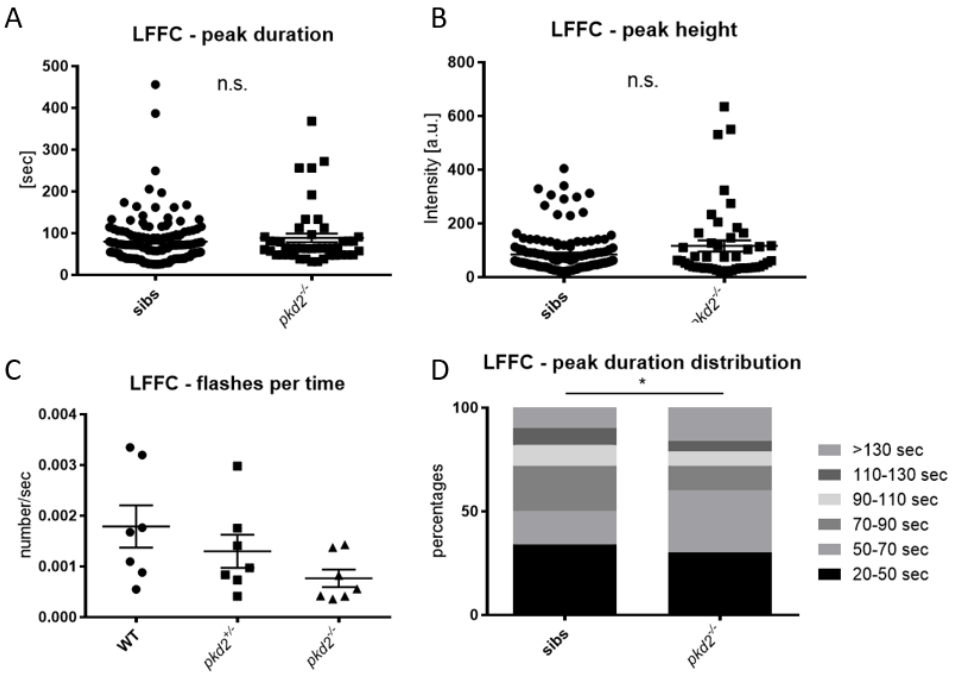

Figure 81 LFFCcellular flashes in *enpep:Gal4;UAS:GCaMP7a*. WT: n = 7, *pkd2*$^{+/-}$: n = 7, *pkd2*$^{-/-}$: n = 7. Error bars indicate SEM. (A) LFFC flash duration, (B) LFFC flash intensity, (C) LFFC flashes over time and (D) LFFC flash duration distribution in 7 *pkd2* mutants and 14 siblings. Significances in (A and B) via unpaired t-test, in (C) via one-way anova with Dunnet's multiple comparison test and in (D) via paired t-test; *: $p \leq 0.05$ and non-significant (n.s.): $p > 0.05$.

2.2.2.2. RFCs (recurrently flashing cells - 3 to 12 flashes in 2 h) and FFCs (frequently flashing cells - more than 12 flashes per 2 h)

As seen in the overall population and the LFFC subpopulation, flash duration or intensity of RFCs was not altered between genotypes (Figure 82 A and B respectively). Although there was no change in average peak duration, there was again a shift in the distribution of those durations. Peaks of less than 70 seconds were more prevalent in *pkd2* mutants than in siblings (Figure 82 D). As stated above, FFCs were not analysed in this manner as establishing a baseline was difficult.

The number of flashes over time (including FFCs) was reduced in a *pkd2* dose-dependent manner with WT being having the highest amount of flashes and *pkd2* mutants the lowest

(Figure 82 C) although this did not reach statistical significance. Of note, the percentage of FFC's decreased in a *pkd2* dose-dependent manner from WT to homozygous animals, corresponding with the reduced number of flashes over time in *pkd2*$^{-/-}$.

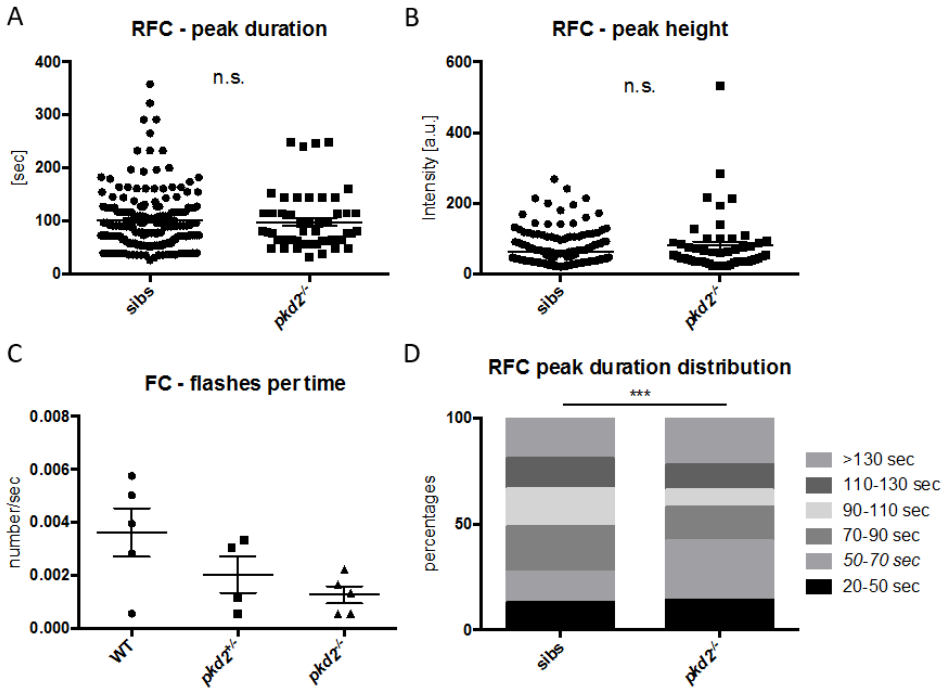

Figure 82 RFC cellular flashes in *enpep:Gal4;UAS:GCaMP7a*. WT: n = 7, *pkd2*$^{+/-}$: n = 7, *pkd2*$^{-/-}$: n = 7. Error bars indicate SEM. (A) RFC flash duration, (B) RFC flash intensity, (C) FC flashes over time – including FFCs and (D) RFC duration distribution in 7 *pkd2* mutants and 14 siblings. Significances in (A and B) via unpaired t-test, in (C) via one-way anova with Dunnet's multiple comparison test and in (D) via paired t-test; ***: p ≤ 0.001 and non-significant (ns): p > 0.05.

In summary, at day 1 of development two elements in renal Ca^{2+} signalling differed between *pkd2* mutants and their siblings: There was a slight shift in the distribution of both overall tubular Ca^{2+} and in the flashing cells - *pkd2*$^{-/-}$ show less short-term (< 1 min) fluctuations along the tubule but more short cellular flashes (< 70 sec). Additionally, cells in *pkd2* mutants flash less across all cell populations decreasing in a dose-dependent manner from WT.

3. Renal calcium at 48 - 58 hpf (actively filtering kidney) – *pkd2*$^{-/-}$ exhibit lower renal calcium levels

After failing to observe an overall change of renal Ca^{2+} levels on day 1 of zebrafish development between *pkd2* mutants and siblings, which would have been expected based on descriptions of cell culture models (more details see Introduction of Chapter 2.), embryos on the second day of development were studied next. At this stage, renal filtration has started and the kidney is functioning while filtration-specificity matures until 4 dpf.

Fluorescence levels in the previously imaged reference frame, from the cloaca to the beginning of the yolk extension, were markedly reduced in 2 dpf embryos. In particular, the area around the cloaca was devoid of detectable GCaMP7a fluorescence (explained in 5.2).

Subsequently the observation area was shifted more anteriorly and imaging now commenced in an anterior section of the tubules from just behind the glomeruli (new imaging area, see Figure 83).

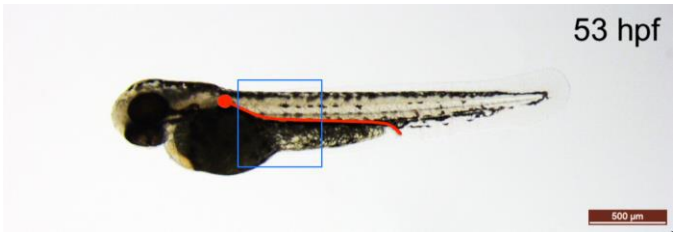

Figure 83 Reference frame (blue) for imaging calcium levels during 2 dpf. Kindey schematically indicated in red.

Time lapse experiments over 6 h at 2 dpf revealed that there was much less activity at this stage of development compared to day 1 – more precisely: no cellular flashes were observed for long periods of time (up to 5 h), followed by a brief burst of flashes, which was again trailed by inactivity. Cellular flashes were therefore not analysed at 2 days of age. Furthermore, tubular oscillations did not show a marked difference at day 1 and did not seem to be altered at this stage either, although this was not measured. For time purposes, experiments at 2 dpf were restricted to imaging seven time points in 2 min and subsequently mean tubular fluorescence intensity was analysed (examples in Figure 84 A and B).

Remarkably, there was a significant difference in Ca^{2+} levels at 2 dpf with lower concentrations in *pkd2* mutants compared to siblings. Of note, this decrease did not seem to occur in a *pkd2* dose-dependent manner as WT and heterozygous animals were no different.

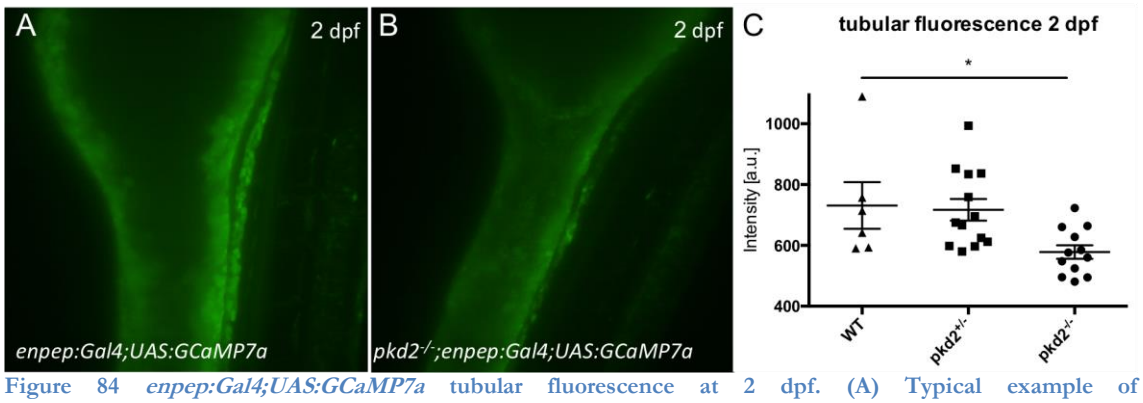

Figure 84 *enpep:Gal4;UAS:GCaMP7a* tubular fluorescence at 2 dpf. (A) Typical example of *enpep:Gal4;UAS:GCaMP7a*. (B) Representative example of *pkd2*$^{-/-}$*;enpep:Gal4;UAS:GCaMP7a*. (C) Tubular florescence in WT, *pkd2*$^{+/-}$ and *pkd2*$^{-/-}$ at 2 dpf. Significances via one-way anova with Dunnet's multiple comparison test; *: $p \leq 0.05$. Error bars indicate SEM.

4. GCaMP levels in cystic mutant *elipsa* and *elipsa/pkd2* double mutants – loss of cilia causes pronephric calcium level decrease

Since *pkd2* knockout did not cause a renal dilation phenotype, observing Ca^{2+} levels in an actual "cystic kidney" mutant was of interest. As before, *elipsa* mutants were employed for this purpose (for more details see Introduction and Results and Discussion Chapter 1).

Analysis of tubular fluorescence at 1 dpf revealed that siblings did not differ in anterior and posterior tubular fluorescence; similarly, *pkd2* mutants were not different from siblings. *elipsa* mutants, however, showed significantly weaker renal GCaMP7a fluorescence at around the time when cilia abolition is confirmed, suggesting much lower intracellular Ca^{2+} levels (Figure 85 A). Figure 85 B shows that this trend in *elipsa* mutants persisted on day 2 of embryonic development and *pkd2/elipsa* double mutants did not differ in comparison to the *elipsa* single mutant. *pkd2*, *elipsa* and *elipsa/pkd2* double mutants exhibited similar fluorescence levels at this stage. Obtaining double mutants carrying all relevant transgenes and mutations was very difficult, hence the number of observed animals was low - but no marked change was seen.

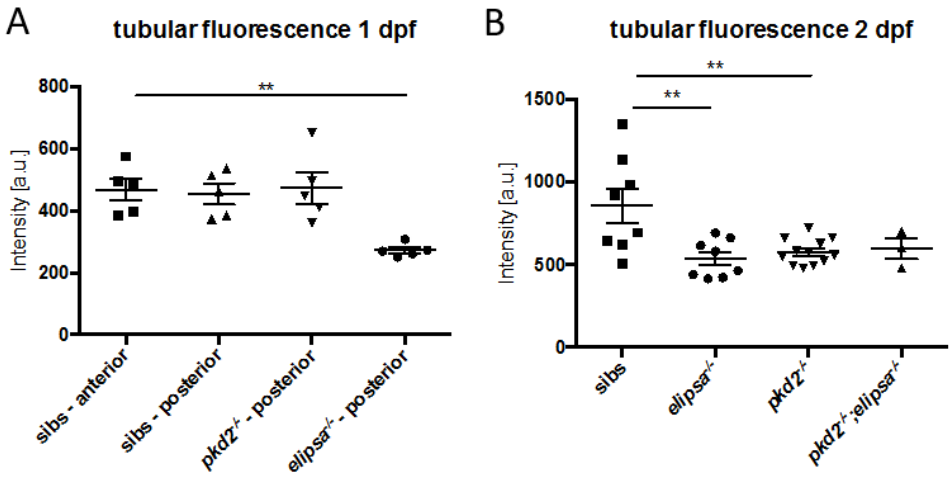

Figure 85 *enpep:Gal4;UAS:GCaMP7a* tubular intensity. Error bars indicate SEM. (A) In siblings, anterior and posterior tubule sections, *pkd2* mutants and *elipsa* mutants at 1 dpf. (B) In siblings, *elipsa* mutants and *pkd2/elipsa* double mutants at 2 dpf. Significances via one-way anova with Dunnet's multiple comparison test; **: $p \leq 0.01$.

5. Chemical modulation of kidney calcium levels after exposure to chemical screen hit compounds

In Results and Discussion Chapter 2, chapters 2.1. and 4.1. several classes of compounds were identified that altered *pkd2* curvature. Since *pkd2* is thought to function as a Ca^{2+} channel, the effect of these drugs on renal Ca^{2+} levels were tested by exposing *enpep:Gal4;UAS:GCaMP7a* fish. Compounds modulating intracellular Ca^{2+} levels would be of particular therapeutic interest since Ca^{2+} deregulation is one of the hallmarks of ADPKD.

5.1. Early exposures without distinction of genotypes

First, 24 h exposures were conducted from late epiboly stages to about 30 hpf by treating unsorted embryos overnight in 6-well plates. Sorting at these stages was impossible as the *enpep:Gal4;UAS:GCaMP7a* transgenes were not active yet and the *pkd2* genotype only arises from ca. 28 hpf. Embryos were not separated into *pkd2* genotypes in the analysis - it was deemed unnecessary since tubular fluorescence levels were indistinguishable at 1 dpf

between alleles. Genotyping was initially conducted to monitor variability but no large differences were found. Only thapsigargin and androstandione treatments had a significant effect on renal Ca^{2+} levels in these experiments with both compounds increasing Ca^{2+} concentrations. Interestingly, androstandione seemed just as potent in increasing GCaMP7a fluorescence as thapsigargin (Figure 86 A). Although not significant, flutamide, nifedipine, tolvaptan and dihydroxyanisole showed a trend towards decreasing tubular Ca^{2+} at this stage.

5.1.1. Genotype-dependent calcium modulation after compound exposure

In a separate experiment embryos were treated with a TRPV4 antagonist, GSK205. TRPV4 is proposed to form a putative channel complex with PC2 distinct from a PC1/PC2 complex in primary cilia (Kottgen *et al.*, 2008). TRPV4 expression has been described in the notochord, brain, endocardium, lateral line organs and, from 32 – 48 hpf, in the pronephros (Mangos *et al.*, 2007). Treatments from 28 hpf with 1 μM GSK205 significantly increased the *pkd2* curvature phenotype (Figure 86 B). Of note, treating embryos from 24 hpf for 4 h resulted in a difference in renal Ca^{2+} levels between alleles, although this was not significant – perhaps due to low numbers. GSK205 showed a trend towards increasing Ca^{2+} levels in siblings and decreasing GCaMP7a fluorescence in *pkd2* mutants after treatments from 24 hpf (Figure 86 B). The same compound exposed from late epiboly (Figure 86 A) did not show a trend, possibly because the genotypes were not separated.

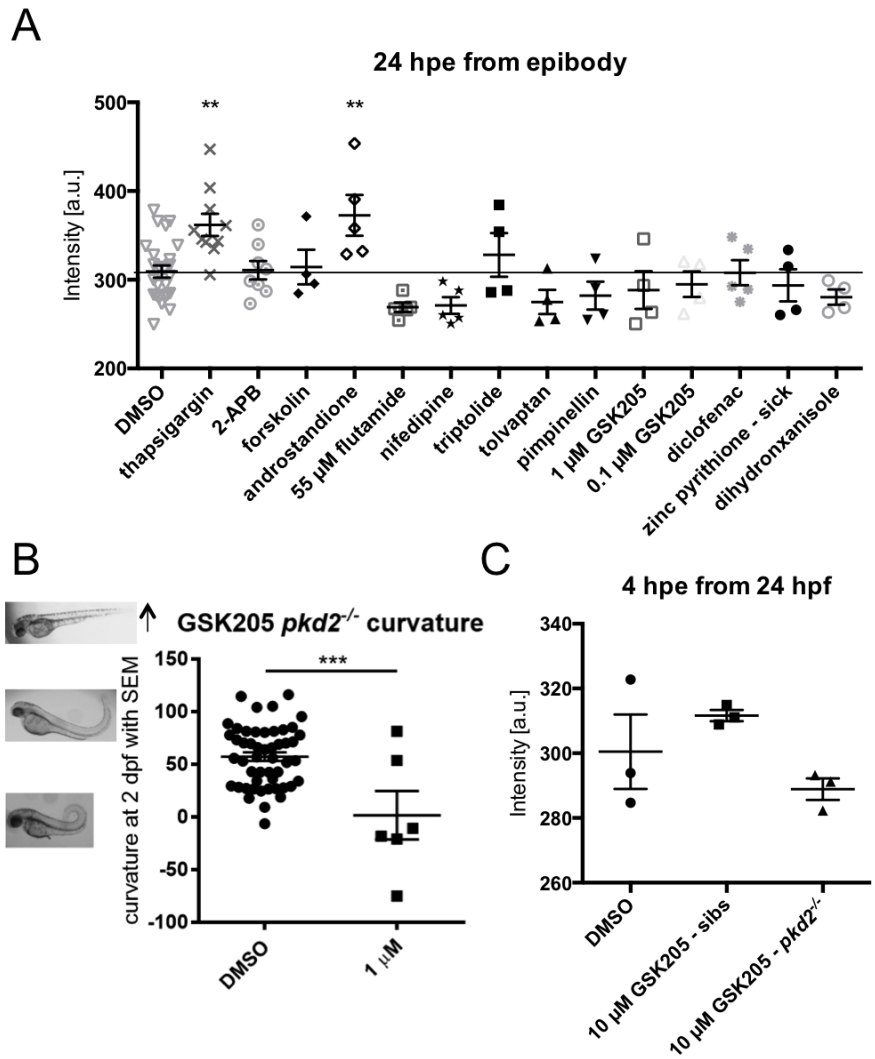

Figure 86 (A) *enpep:Gal4;UAS:GCaMP7a* tubular intensity after compound exposure. Exposures from late epiboly for 24 h, imaged at ca. 36 hpf. B) Curvature enhancing effects of GSK205 on *pkd2* curvature phenotype. (C) *enpep:Gal4;UAS:GCaMP7a* tubular intensity after compound exposure. Exposures of DMSO and GSK205 from 24 hpf for 4 h. Significances in (A and C) via one-way anova with Dunnet's multiple comparison test and in (B) via unpaired t-test; ***: $p \leq 0.001$, **: $p \leq 0.01$. Error bars indicate SEM.

5.2. Exposures of *enpep:Gal4;UAS:GCaMP7a* from ca. 28 hpf – characterisation of compounds in *pkd2* mutants and siblings

Early exposure experiments had revealed that compounds might have genotype-specific effects on Ca^{2+} levels, hence subsequent exposures were carried out at stages when genotypes could be distinguished. Embryos were sorted for GCaMP7a fluorescence at 24 hpf and exposed after *pkd2* curvature onset, ensuring sufficient numbers of both siblings and *pkd2* mutants were treated. In the absence of a noticeable disparity between heterozygous and WT animals, siblings were not classified into individual genotypes.

As there was a detectable difference in *pkd2* mutants and sibling GCaMP7a intensities at 2 dpf (described above), treatments with thapsigargin were conducted initially to establish the overall Ca^{2+} content in the kidney. These experiments served to show that *pkd2* mutant Ca^{2+}

concentrations could be increased to sibling levels by Ca^{2+} release from the ER and that calcium was not simply depleted from the system in general. Figure 87 suggests Ca^{2+} total deposits are indeed similar in the different alleles and Ca^{2+} can be increased to similar concentrations in *pkd2* mutant fish compared to siblings. Interestingly, the anterior and posterior halves of the imaged area responded differently to thapsigargin treatments, although this was not statistically significant.

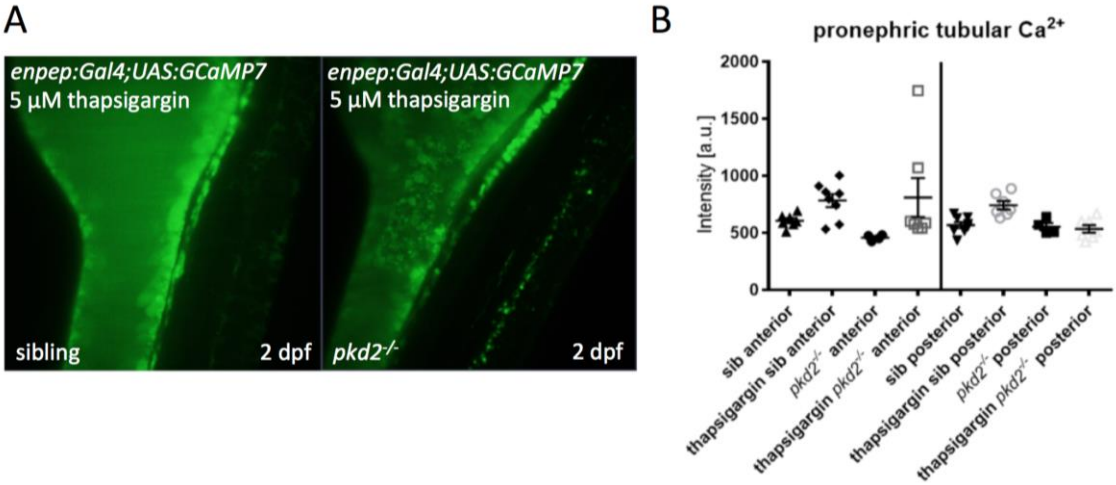

Figure 87 (A) Thapsigargin treatment (5 µM for 25 min) of *enpep:Gal4;UAS:GCaMP7a* siblings and *pkd2* mutants. (B) Graph with renal fluorescence intensities in untreated controls and thapsigargin-exposed embryos. Not significant via one-way anova with Tukey's multiple comparison test; $p > 0.05$. Error bars indicate SEM.

Visually, there was a disparity in thapsigargin treated animals with siblings appearing to show an increase of fluorescence along the majority of the length of the pronephric tubule, whereas *pkd2* mutants only seemed to display an increase in the anterior part (roughly to the beginning of the yolk extension, Figure 87 A). This was also reflected in the measurements of intensity, although it did not reach significance (Figure 87 B). Subsequently, *in situ* hybridisations were carried out with a *GCaMP7a* probe to determine expression along the tubule. There was no discernible change in *GCaMP7a* expression patterns between *pkd2* mutants and siblings at the time points observed (Figure 88), suggesting that *pkd2* mutant animals did not respond differently to thapsigargin treatments due to altered gene expression. A marked difference became apparent in expression patterns comparing developmental day 1, when expression was strong along the entire tubule to the cloaca (Figure 88 A and A'), and day 2, when posterior expression was not perceivable (Figure 88 B and B'). This suggests the inability to detect posterior GCaMP7a fluorescence at 2 dpf was due to the reduction of expression in this region (contrarily to what was observed during the initial characterisation of the *enpep:Gal4* line, see above).

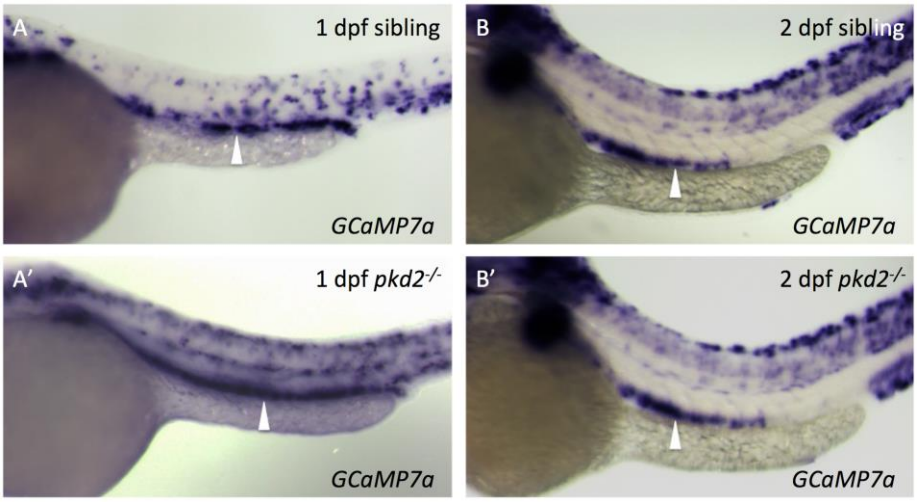

Figure 88 *In situ* hybridisation with *GCaMP7a* probe of *enpep:Gal4;UAS:GCaMP7a*. (A and A') 1 dpf sibling and *pkd2* mutant respectively. (B and B') 2 dpf sibling and *pkd2* mutant respectively. Renal tubules indicated with white arrowheads.

The results of *enpep:Gal4;UAS:GCaMP7a* treatments with Spectrum hit compounds and associated drugs from 28 hpf to ca. 52 hpf are depicted in Figure 90. Establishing a baseline fluorescence was difficult, possibly owing to the fact that Ca^{2+} is such a ubiquitous second messenger. The preparation of embryos for analysis on a lightsheet microscope involves many steps and temperature, oxygen levels, forces exerted on the embryos while loading them into imaging capillaries and exposure to anaesthetic are all liable to stress zebrafish embryos. Experiments were conducted with the utmost care to keep conditions as stable as possible but in spite of these efforts, a high variability in Ca^{2+} levels was observed. The controls had a variation of up to ±100 % compared to the mean over all experiments (see Figure 89). It was therefore difficult to obtain statistically significant results. In particular, the set of experiments including diclofenac treatment (experiment 1) resulted in much lower control fluorescence levels than previously observed and was therefore analysed separately (Figure 90 B and D).

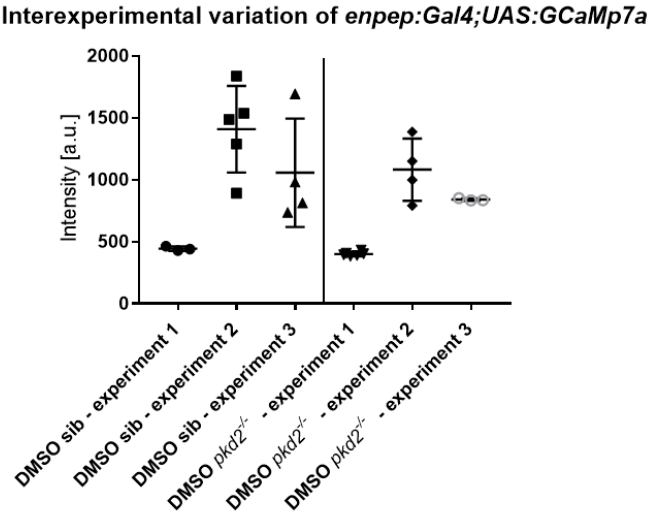

Figure 89 Interexperimental variation in fluorescence intensity with *enpep:Gal4;UAS:GCaMP7a*. Error bars indicate SEM.

Amongst compound-exposed siblings, only zinc pyrithione had a significant effect and decreased intracellular Ca^{2+} levels, although dihydroxyanisole, flutamide, forskolin and diclofenac showed similar trends (Figure 90 A and B). None of the compounds showed a strong calcium-increasing effect.

pkd2$^{-/-}$ embryos exposed to various compounds did not show GCaMP7a fluorescence alterations (Figure 90 C and D). Nifedipine, pimpinellin, GSK205 and diclofenac showed tendencies towards increasing Ca^{2+} levels whereas dihydroxyanisole, zinc pyrithione and forskolin exhibited Ca^{2+} -decreasing trends. Of note, dihydroxyanisole, zinc pyrithione and forskolin display similar inclinations in both genotypes while triptolide (weakly) and diclofenac behaved the opposite in *pkd2*$^{-/-}$ and siblings. Interestingly, dihydroxyanisole, zinc pyrithione and diclofenac all repressed the curvature phenotype of *pkd2* mutants but showed no consistent pattern in their effects on calcium.

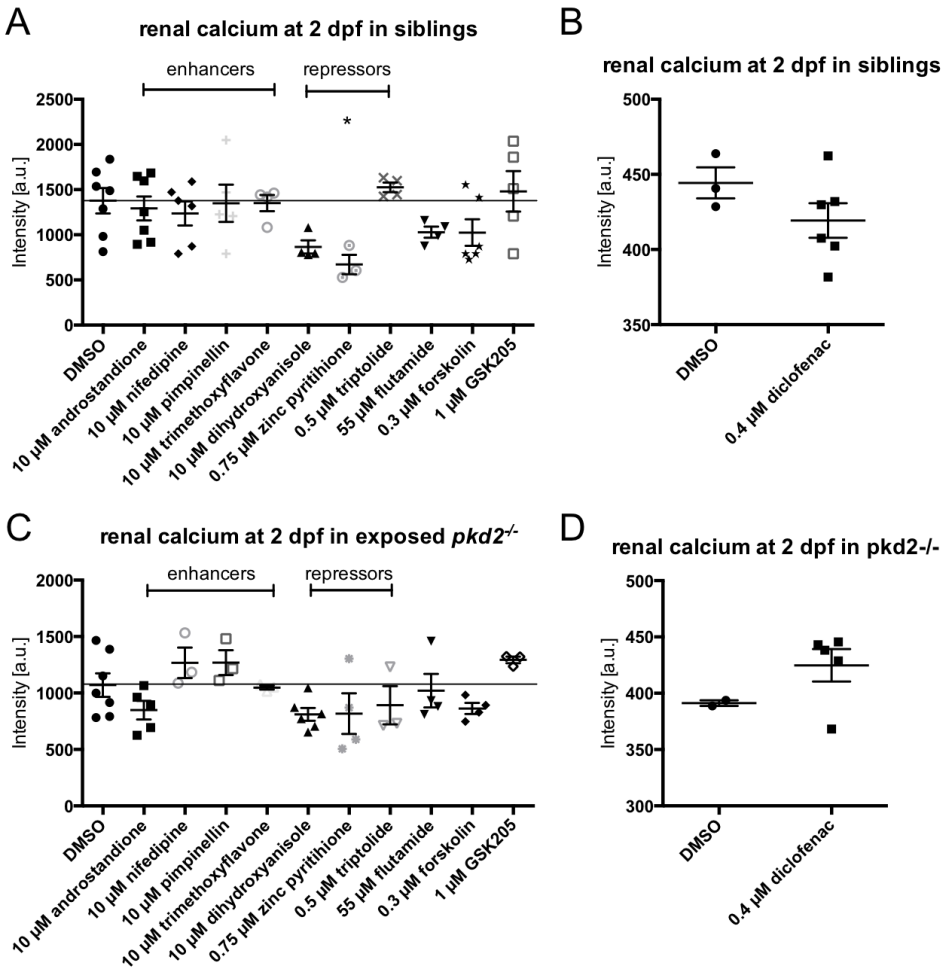

Figure 90 *enpep:Gal4;UAS:GCaMP7a* treated with various compounds from 28 hpf to ca. 52 hpf. (A and B) *pkd2* siblings and (C and D) *pkd2* mutants. Black lines mark means of DMSO controls. Significances in (A and C) via one-way anova with Dunnet's multiple comparison test and in (B and D) via unpaired t-test; *: $p \leq 0.05$. Error bars indicate SEM.

Due to the aforementioned baseline variability and low statistical significance (although clear differences were observable by eye), a second analysis method was employed. Intensities

measured within one experiment were divided by the mean of respective DMSO controls to adjust for interexperimental baseline variability: values greater than 1 suggest an increase of tubular fluorescence whereas values lower than 1 indicate a decrease. The results with corrected for baseline values are depicted in Figure 91. Thapsigargin measurements were included in these analyses to serve as a positive control of the new analysis method.

Thapsigargin significantly increased Ca^{2+} levels in both siblings and *pkd2* mutants as expected. In the sibling population, only one other compound altered GCaMP7a fluorescence levels significantly: flutamide, which increased Ca^{2+} concentrations (Figure 91 A).

In treated *pkd2*$^{-/-}$ animals, four compounds other than thapsigargin also increased renal Ca^{2+} levels contrary to expectations: nifedipine, pimpinellin, trimethoxyflavone and GSK205. Nifedipine, an L-type calcium channel inhibitor, and GSK205, a TRPV4 channel antagonist, were predicted to decrease *pkd2* Ca^{2+} levels even further in *pkd2*$^{-/-}$ by blocking other Ca^{2+} channels. Pimpinellin and trimethoxyflavone on the other hand, enhanced the curvature phenotype of *pkd2* mutants but increased the renal Ca^{2+} phenotype. Androstandione, which increased Ca^{2+} levels in exposures from epiboly, failed to do so in treatments from curvature onset.

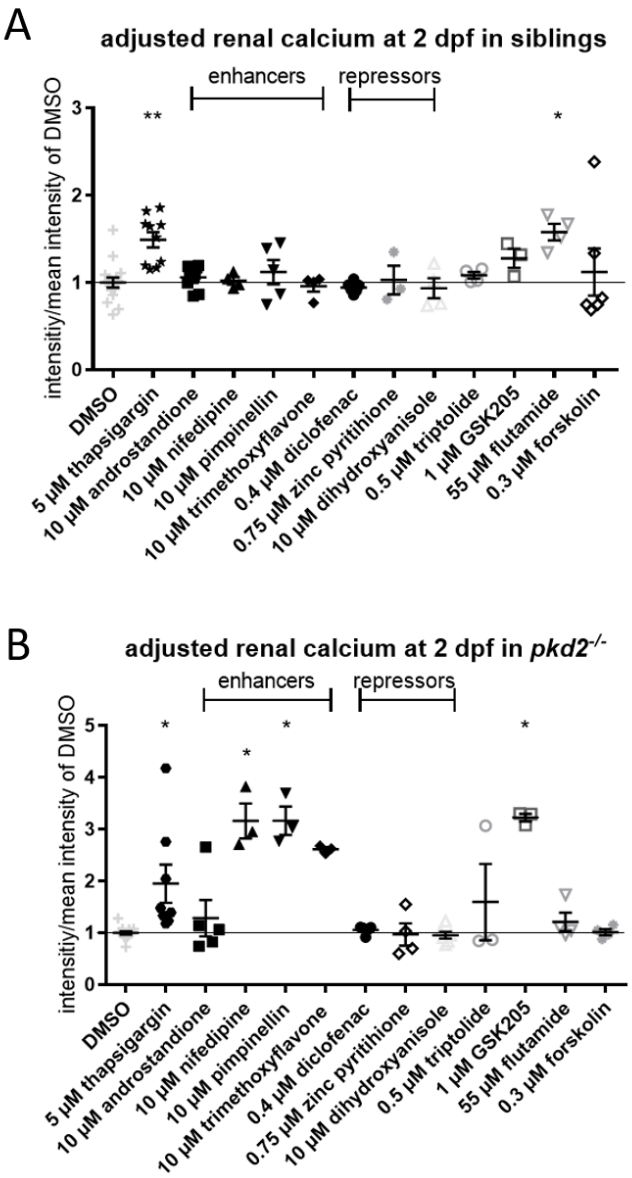

Figure 91 *enpep:Gal4;UAS:GCaMP7a* treated with various compounds from 28 hpf to ca. 52 hpf after adjustment for baseline variability. (A) *pkd2* siblings and (B) *pkd2* mutants. Black lines mark means of DMSO controls. Significances via Kruskal-Wallis test with Dunn's multiple comparison test; **: $p \leq 0.01$, *: $p \leq 0.05$. Error bars indicate SEM.

In addition to the Spectrum compounds and chemicals added to study functionalities, *enpep:Gal4;UAS:GCaMP7a* were also exposed to PKIS repressor hits. As all PKIS compounds were measured in one session, no adjustment for variation of baseline was necessary.

None of the treated sibling groups showed a significant difference with regard to tubular fluorescence. There was however a significant difference amongst the *pkd2* mutants, with PKIS_59 decreasing tubular Ca^{2+} levels just significantly (PKIS_59 was one of the two structurally similar compounds). Although these compounds repress the *pkd2* curly tail, there was no consistent effect on renal calcium.

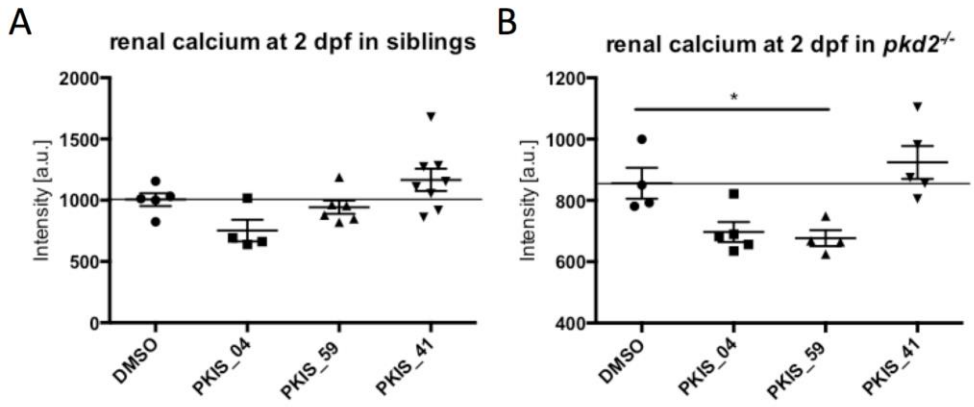

Figure 92 *enpep:Gal4;UAS:GCaMP7a* treated with PKIS compounds from 28 hpf to ca. 52 hpf. (A) *pkd2* siblings and (B) *pkd2* mutants. Black lines mark means of DMSO controls. Significances via one-way anova with Dunnet's multiple comparison test; *: $p \leq 0.05$. Error bars indicate SEM.

The exposure of *enpep:Gal4;UAS:GCaMP7a* to a variety of different compounds revealed, that some chemicals exhibited genotype-specific behaviour with regards to Ca^{2+} signalling. How these modulations fit in with current knowledge will be discussed below. The interexperimental variability in control Ca^{2+} levels required data transformation to control for this. Nevertheless, *pkd2* mutant pronephric Ca^{2+} always remained below sibling Ca^{2+} levels in controls although similar amounts of Ca^{2+} were present in the system.

Discussion

In order to determine the potential effects of *pkd2* loss on *in vivo* renal Ca^{2+}, a new zebrafish reporter line, *enpep:Gal4;UAS:GCaMP7a,* was established. Initial chemical modulations with drugs described to alter global calcium were successful and proved the functionality of this line. Although renal Ca^{2+} had previously been measured *in vivo* in a mouse GCaMP line, the opacity of mammalian skin necessitated anaesthesia of the animal and surgical removal of the kidney from the body cavity for imaging purposes (Burford *et al.*, 2014; Szebenyi *et al.*, 2015). The large variation of pronephric Ca^{2+} baseline levels that I observed in an intact organism underlines the sensitivity of calcium to any disruptions and inferring natural Ca^{2+} behaviour from measurements in an organ outside the body, might prove problematic. This is the first *in vivo* renal calcium reporter line in an intact organism described to date.

1. Calcium in the pronephric kidney – *pkd2*$^{-/-}$ display lowered levels

During day 1 of embryonic zebrafish development, the pronephros has already formed but is not yet filtering blood, as angiogenesis in the glomeruli is only completed at 40 – 48 hpf (Drummond *et al.*, 2010). Renal Ca^{2+} changes were observed along the entire length of the pronephros and, as well as general Ca^{2+} fluctuations in the tubules, individual renal cells also

exhibited interesting behaviours. Oscillations over the entire tubule and flashes of individual cells did not differ in average duration or intensity at 1 dpf. There was however, a shift to longer tubular flashes (> 60 sec) and shorter cellular flashes (< 70 sec) in *pkd2* mutant animals compared to sibling controls. Interestingly, neither of these shifts affected average respective durations and their physiological significance remains unclear. Previously published observations in a renal GCaMP mouse model describing regular oscillatory patterns lasting about 60 seconds in proximal tubules of adult animals (Szebenyi *et al.*, 2015), were not observed in the zebrafish line. The most interesting phenotypic disparity in 1 dpf zebrafish was a *pkd2*-dose-dependent decrease of cellular flash frequency from WT to homozygous animals, which persisted across the analysed cell types. An additional finding was that the most active cell population, the FFCs, seemed to correspond in location to the Corpuscles of Stannius. These spherical organs embedded in renal tissues regulate Ca^{2+} homeostasis in teleost fish and although the kidney is not actively filtering at this stage, the quantity of cellular flashes in the area suggests activity.

After renal filtration had commenced at 2 dpf, *pkd2* mutants exhibited significantly lower renal Ca^{2+} levels than their sibling controls. This confirmed previous *in vitro* observations that *Pkd1*-null cells displayed lowered intracellular Ca^{2+} levels and a lack of responsiveness to external flow (Nauli *et al.*, 2003). This is the first report of *in vivo* evidence showing that *pkd2* alters renal Ca^{2+} levels in an ADPKD model.

To find out whether Ca^{2+} release was lower in *pkd2*$^{-/-}$ or there were reduced total renal Ca^{2+} stores, exposures to thapsigargin were conducted since this leads to a rapid efflux of Ca^{2+} from ER stores. These experiments confirmed that Ca^{2+} stores in the tubules were similar between *pkd2* homozygous animals and siblings in the anterior tubule section. Whether *pkd2* mutants exhibit a decrease of intracellular Ca^{2+} in the posterior region because of impeded ER store release remains to be determined. At 2 dpf, filtrate is moving through the renal tubules aided by motile cilia. It is possible that *pkd2*$^{-/-}$ animals lack the ability to sense fluid flow and thus display lower pronephric Ca^{2+} levels.

2. Renal calcium in a classical "cystic kidney" and PKD/ciliary mutant zebrafish is diminished in comparison to siblings

elipsa mutants also displayed lower intracellular Ca^{2+} levels in the pronephric tubules at 2 dpf, similar to *pkd2* mutants. Unlike *pkd2* mutants, this decrease was already present at 1 dpf. Loss of cilia therefore caused an earlier effect on Ca^{2+}. Since *pkd2* and *elipsa* single mutants had comparably low pronephric GCaMP7a fluorescence levels at day 2, this could indicate that renal epithelial cells in both lines are unable to respond to pronephric filtrate flow stimuli. This might be the reason why combined knockout in the double mutants did not differ significantly from single knockouts. If this were the case, ciliary *pkd2* might function as a responding factor to fluid flow or other ciliary signals, as previously proposed (Nauli *et al.*, 2003). Alternatively, PC2 could act independently from PC1 as Ca^{2+} release channel in the ER (Giamarchi *et al.*, 2010; Koulen *et al.*, 2002; Mekahli *et al.*, 2012) by receiving a ciliary signal.

Figure 93 Relationship of cilia, *pkd2* and renal calcium based on observations in *pkd2*, *elipsa* and double mutants in the renal calcium reporter line *enpep:Gal4;UAS:GCaMP7a*.

3. Renal calcium response to compound library screen chemicals

Exposures of *enpep:Gal4;UAS:GCaMP7a* to a number of hit compounds from the chemical library screens did not yield a consistent picture and comparisons were complicated by interexperimental variation.

First and foremost, known Ca^{2+} modulators such as the L-type calcium channel inhibitor nifedipine and the TRPV4 antagonist GSK205 (TRPV4 is another TRP Ca^{2+} channel like *pkd2*) did not show expected reductions of pronephric Ca^{2+} but rather increased Ca^{2+} levels in the *pkd2* mutants. This increase was, however, not observed in exposed siblings and it is possible that the loss of *pkd2* in the mutants and additional chemical inhibition of a second channel led to compensatory changes in other calcium channels.

Interestingly, flutamide, which did not affect *pkd2* mutant curvature, also caused an increase in renal Ca^{2+} but only in the siblings. This might suggest that *pkd2*-loss made zebrafish embryos insensitive to flutamide, although this is merely speculation. The coumarin pimpinellin and the flavonoid trimethoxyflavone triggered increases in GCaMP fluorescence exclusively in *pkd2* mutants. These compounds had previously enhanced the curvature phenotype but now surprisingly alleviated the renal Ca^{2+} phenotype. PKIS_59, on the other hand, repressed the *cup* phenotype but lowered *pkd2* Ca^{2+} levels even further.

In summary, none of the compounds, enhancers or repressors, acted in an expected fashion. The compounds had behaved as expected in mammalian cyst culture models and it was hypothesised that at least some compounds would show calcium-altering behaviour accordingly. Some of the chemicals exhibited calcium-altering properties but there was no clear correlation with regard to enhancers or repressors of Ca^{2+} and the *curly up* phenotype. Overall, these results suggest that the compounds identified during the compound screens did not alter the tail curvature in a way that allows for predictions of their calcium-modifying properties.

Synopsis and outlook

During this project, several zebrafish models of ADPKD were characterised, a compound screen on *pkd2*$^{-/-}$ fish identified new modulators of the disease and, after the creation of an *in vivo* renal calcium reporter line, lower intracellular calcium levels were detected in *pkd2* mutant animals.

The initial characterisation of *Danio rerio* ADPKD models served two purposes: reassessing findings in the literature with particular regard to differences between models and identifying the ideal model/trait to conduct a chemical library screen. *pkd2* mutants and morphants (animals with chemical knockdown) displayed the same set of traits initially described (Sun *et al.*, 2004). Mutants and morphants exhibited a curly tail up and left/right polarity defects (assessed by heart looping) but only morphants developed "cystic kidneys". "Cystic kidneys", in the context of zebrafish embryos, describe dilated glomeruli rather than actual renal cysts but this is the closest model of mammalian cysts available in the zebrafish pronephros. Besides the renal disparities, morphants also exhibited some knockdown off-target effects (hydrocephalus and necrosis in brain and eye areas) and did not develop oedema at the same rate as *pkd2* mutants. Of note, previous studies had shown only partial rescue of the *pkd2* morphant phenotypes in co-injections with zebrafish *pkd2* or human *PKD2* RNA (Bisgrove *et al.*, 2005; Obara *et al.*, 2006), further implying off-target effects of the morpholino. These findings suggested that the renal readout of *pkd2* morphant animals was not ideal for a screen by lacking robustness and reliability. Therefore, the compound screen was conducted on the curly tail phenotype of *pkd2* mutants.

Due to the lack of a pronephric phenotype in *pkd2* mutants, a more distant model of mammalian renal cysts was analysed, the ciliary mutant *elipsa* (Omori *et al.*, 2008). Ciliary mutants in zebrafish are typically characterised by dilated glomeruli and renal tubules, as well as a downward tail curvature (Kramer-Zucker *et al.*, 2005; Sullivan-Brown *et al.*, 2008). Although the renal "cysts" in ciliary mutants might develop due to different causes, it was hypothesised that the processes underlying cyst expansion were similar in all models. Reports of a murine experiment suggested that the renal phenotype in *Pkd*-null mice could be reduced by genetically abolishing cilia, and a similar cross of mutant stains was performed in zebrafish to evaluate the double mutants (Ma *et al.*, 2013). Ciliary mutants have an opposite curl in their tail relative to *pkd2* mutants (Kramer-Zucker *et al.*, 2005; Sullivan-Brown *et al.*, 2008; Sun *et al.*, 2004), suggesting *pkd2* plays a downstream role in this phenotype. Furthermore, the *pkd2* tail phenotype appeared to be epistatic and cilia contributed an additional function, similar in effect to *pkd2* itself (the *curly up* tail in the double mutants was aggravated compared to

pkd2 mutants). The "cystic kidney" phenotype, on the other hand, was more severe in the double knockout animals than in the ciliary mutant. This latter trait suggested that *pkd2* and cilia act in parallel and there may be tissue-specific interactions. As *pkd2* mutants in zebrafish do not exhibit renal dilations, the fish and mouse experiments cannot be directly compared, but the murine study also found an increase in cystic behaviour compared to the ciliary single mutants (Ma *et al.*, 2013), as was described here in the zebrafish cross. Overall, a complex network of interactions between cilia or ciliary signals and *pkd2* emerged, suggesting partial redundancy of certain functions. Unexpectedly, the current model suggests a repressive signal of cilia on PC2 function. Of note, the mechanisms leading to *curly up* and curly down tail curvatures remain unclear; here, similar pathways were assumed between both phenotypes, however, this might not prove correct upon closer study. To tease apart the exact contributions of each gene would be complex and should probably involve knocking out genes that are most likely candidates in providing the function of factor X (similar in effect to *pkd2*) in the cilia – interesting candidates might be the *pkd2*-like genes or other ciliary calcium channels. In addition, tissue-specific knockdown of cilia or *pkd2* with the novel CRISPRi technology would allow a closer examination of interactions in individual tissues. The tissue-specificity of knockdowns via CRISPRi is merely restricted to the promoters used, therefore knockdown in all ciliated cells, irrespective of tissues (e.g. with the ciliary *ccdc114* promoter (Choksi *et al.*, 2014)) would allow a very detailed study of genetic interactions.

A second aim of this project was to conduct zebrafish high-throughput compound screens on an ADPKD-related phenotype. For this purpose, the 2000 compound-strong Spectrum library with a mix of FDA-approved and natural chemicals, as well as the PKIS set, a kinase inhibitor library with 367 molecules, were tested. Screening the chemicals for their ability to modify the *pkd2* mutant curvature revealed a total of 22 compounds that aggravated the phenotype and 7 chemicals alleviating it. The compounds carried forward into two cell lines in three-dimensional cyst assays confirmed the fish data, suggesting that the curly tail readout is a reliable predictor for the cystic phenotype. The most promising potential therapeutic targets identified during the compound screens were the COX inhibitor diclofenac and inhibitors of the TGFβ pathway, especially ALK5 blockers. Prostaglandins and the TGFβ signalling cascade have been previously linked to ADPKD (Hassane *et al.*, 2010; Liu *et al.*, 2012a). Diclofenac, as an already FDA-approved drug, which is sold without prescription in most countries, would be a very interesting and inexpensive therapeutic approach. The curly up phenotype in *pkd2*-deficient zebrafish has been linked to increased collagen production (Mangos *et al.*, 2010) and/or deposition (Le Corre *et al.*, 2014) and interestingly, one study

suggested an intricate crosslink between cAMP and collagen expression which is regulated via the TGFβ pathway (Perez-Aso *et al.*, 2014): low levels of cAMP stimulation increased collagen 1 and 3 synthesis whereas high concentrations of cAMP inhibited collagen 1 but increased collagen 3 production. Prostaglandin receptors, in particular EP4, have also been shown to inhibit TGFβ signalling, further suggesting that TGFβ might be one of the main contributors to the *cup* phenotype (reviewed in (Nasrallah *et al.*, 2014)). To further understand the role of TGFβ and prostaglandins, downstream targets of these pathways (e.g. SMAD2 or SMAD3 and prostaglandin receptors respectively) could be knocked down in *pkd*-deficient models (zebrafish or cell culture).

The variety of natural compounds, namely coumarins and flavonoids, found to aggravate model outcomes, could potentially explain some of the large intrafamilial variability within ADPKD progression (Milutinovic *et al.*, 1992). Even within individual families carrying the same mutation, there is a large disparity in the onset of renal failure. Some of this variability might be due to epigenetics (Li, 2011; Woo *et al.*, 2015) but dietary factors could also play a role, especially since flavonoids and coumarins occur at different concentrations in various plants; naringenin, for example, is very prevalent in citrus fruit (Alam *et al.*, 2014). Further research, perhaps with different dosage levels in rodent models, would be necessary to determine whether there is truly is a dietary effect.

Androgens, in particular testosterone, have been described in a number of studies on rodents and patients to be a risk factor for ADPKD disease progression (Aziz *et al.*, 2001; Cowley *et al.*, 1997; Fry *et al.*, 1985; Gabow *et al.*, 1992; Katsuyama *et al.*, 2000; Lager *et al.*, 2001; Nagao *et al.*, 2005; Nagao *et al.*, 2003; Ogborn *et al.*, 1987; Smith *et al.*, 2006; Stewart, 1994). This project identified several androgens (testosterone, 11-ketotestosterone, androstandione and epiandrosterone) as enhancers of zebrafish and/or cyst culture outcomes. Surprisingly, the strongest enhancer of the tail curvature phenotype, androstandione, was more potent than classical male hormones in respective species' models (testosterone in mammalian models and 11-KT in zebrafish, (Hossain *et al.*, 2008; Vollmer, 1963)). In zebrafish, this could have been attributed to differing abilities of the steroids to diffuse into the embryos, but cell culture experiments confirmed this trend. This led to the hypothesis that a non-canonical signalling route might be involved in producing the aggravated effects. To test this hypothesis, a zebrafish androgen receptor knockout line is currently being established to clarify whether androstandione acts solely via the androgen receptor or whether a secondary pathway is involved. A potential mechanism of action for this non-canonical pathway has also been identified – L-type calcium channels. These proteins have been linked to worse renal outcomes in a number of studies on both animal models and human patients (Abe *et*

al., 1983; Astor *et al.*, 2008; Dietz *et al.*, 1983; Heller *et al.*, 1990; Roy *et al.*, 1983; Saruta *et al.*, 2009). Early exposures (late epiboly to 24 hpf) with androstandione in *enpep:Gal4;UAS:GCaMP7a* fish showed an increase in renal calcium, supporting this hypothesis. Later exposures (27 hpf – 2 dpf), however did not cause a significant change. Should experiments confirm the activation of an alternative signalling pathway by androstandione, knockdown experiments of L-type calcium channels via morpholinos or, preferably via CRISPRi, could determine whether the contributing factors are indeed L-type calcium channels.

Current studies are trying to elucidate the exact mechanisms of action for some of the hit compounds. Tests are being carried out to evaluate the effects on proliferation- and apoptosis-rates in 3D cyst assays to determine whether cyst growth or shrinkage is linked to increased or decreased cell numbers.

In order to test the validity of the identified chemical targets for therapeutic purposes, more in-depth studies into the mechanisms of action are necessary and ultimately experiments on rodent models of ADPKD should be carried out.

Finally, calcium deregulation, one of the main hallmarks of ADPKD in a variety of models (reviewed in (Mangolini *et al.*, 2016)), was studied in zebrafish *pkd2* mutants by utilising a new transgenic reporter line (*enpep:Gal4;UAS:GCaMP7a*) to measure renal Ca^{2+} levels via a fluorescent readout. Before the onset of renal filtration, overall Ca^{2+} levels were indistinguishable between siblings and *pkd2*$^{-/-}$ animals although there was a *pkd2*-dose dependent reduction in cellular flashes. After the onset of filtration at 2 dpf, *pkd2*-null zebrafish embryos showed a significant decrease of renal Ca^{2+} which cannot be explained by diminished calcium stores. At 2 dpf, the tubules in *pkd2* mutants had similar ER calcium store release abilities as their siblings. These descriptions are the first, to date, of an *in vivo* calcium reporter in an ADPKD model.

Conversely, none of the chemicals identified during the compound screens seemed to have a predictable effect on renal calcium levels, but it is possible that the curvature readout used during the screen is not particularly sensitive to Ca^{2+} modulation. However, during this project only whole-tubular and whole-cellular calcium were measured. The differentiated (but not significant) response to thapsigargin treatment in the anterior and posterior tubular sections in *pkd2* mutants suggests that renal tubular segments may respond differently to chemicals, and should perhaps be analysed separately. Furthermore, Ca^{2+} is a widespread second messenger and subcellular compartmentalisation of calcium signalling is likely to play a more important role in the generation of a phenotype. Detailed insights into subcellular

Ca^{2+} could be gained by creating GCaMP lines with ciliary or endoplasmic reticulum targeted reporters (the two main compartments PC2 is localised to). The experimental procedures could also be improved to reduce inter-assay variation.

A summary of the most important phenotypes described above in the various zebrafish ADPKD models employed during this project, *elipsa*, *pkd2* and *elipsa/pkd2* mutants, with their respective onset can be found in Figure 94.

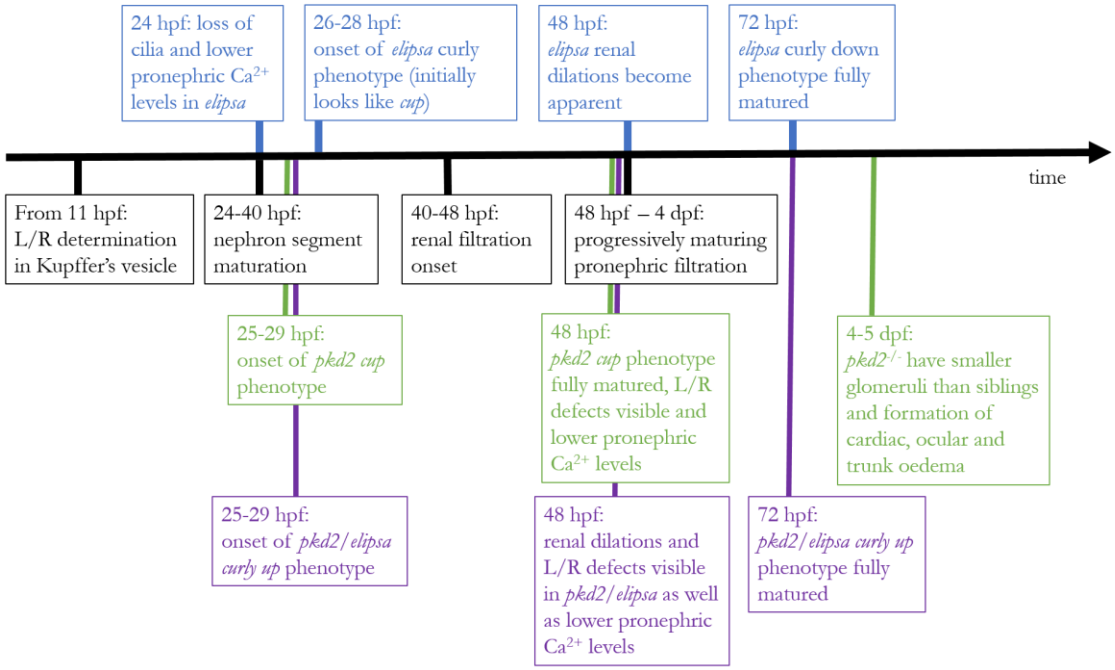

Figure 94 Overview of the most important developmental steps in zebrafish development with their respective timings post fertilisation. General developmental steps are depicted in black, *elipsa*, *pkd2* and *pkd2/elipsa* mutant characteristics are shown in blue, green and violet respectively.

Table 16 provides a summary of the compounds identified as modulators of the *pkd2* curvature phenotype during library screens and their respective effects on all the ADPKD models they were subsequently tested on.

Compound	*pkd2*-/- curvature	*pkd2*-/- glomerular size	*elipsa* curvature	*elipsa* glomerular size	WT curvature	WT glomerular size	Renal calcium siblings	Renal calcium *pkd2*-/-	MDCKII cyst size (assay endpoint)	Ox161c1 cyst size (assay endpoint)
Androstandione	↑	↔	Dorsal curl	↔	Dorsal curl	↔	↔	↔	increased	increased
Diclofenac	↓	↔	↔	↔	↔	↔	↔	↔	decreased	decreased*
Dihydroxyanisole	↓	↔	↔	↔	↔	↔	↔	↔	decreased	decreased*
Flutamide	↔	decreased	↔	↔	↔	decreased	↔	↔	increased	increased
Forskolin	↔	↔	↔	↔	↔	↔	↔	↔	increased	increased*
GSK205	↑	↔	↔	↔	↔	↔	increased	increased	n.a.	n.a.
Naringenin	↑	↔	↔	↔	↔	↔	n.a.	n.a.	increased	increased*
Nifedipine	↑	↔	↓	↔	↔	decreased	↔	increased	n.a.	n.a.
Pimpinellin	↑	↔	↓	increased	↔	↔	↔	increased	increased	increased*
PKIS_04	↓	↔	↔	↔	↔	↔	↔	↔	decreased	decreased
PKIS_59	↓	↔	↔	↔	↔	↔	↔	decreased	decreased	decreased*
PKIS_41	↓	↔	↓	↔	↔	↔	↔	↔	decreased	decreased
Prenyletin	↑	↔	↔	increased	↔	↔	n.a.	n.a.	increased	increased
Pyrithione zinc	↓	↔	↔	↔	↔	↔	↔	↔	decreased	decreased*
Sphondin	↑	↔	↓	increased	↔	increased	n.a.	n.a.	↔	increased
Tolvaptan	↔	↔	↔	↔	↔	↔	n.a.	n.a.	n.a.	n.a.
Trimethoxyflavone	↑	↔	↓	↔	↔	increased	↔	increased	increased	increased
Triptolide	↓	↔	↓	increased	↔	↔	↔	↔	n.a.	n.a.

Table 16 Summary of compounds tested in this project and their effects on various phenotypes. Upward arrow: aggravation of phenotype, downward arrow: alleviation of phenotype, sideways arrows: no change, asterisk: not significant but clear trend, n.a. (not available): compound not tested in this model.

This project has provided the first evidence of *pkd2* affecting *in vivo* renal Ca^{2+} levels in an ADPKD model and the first indications that *pkd2* indeed has a non-redundant function in the zebrafish pronephros. Morpholino data had suggested a function of *pkd2* in the pronephros (Sun *et al.*, 2004), but until now, no genetic evidence had been reported. Here, interaction of *pkd2* and cilia (enhanced dilation phenotype in the double knockout animals) and lower Ca^{2+} levels in *pkd2* mutants suggest that there is a renal function for *pkd2* in zebrafish. Unfortunately, *pkd2* mutant animals are not viable past 5 dpf at which point the kidney still consists of the 2-nephron pronephros; therefore true renal cysts could not be observed in this model. Whether the teleost mesonephros could actually develop renal cysts in response to *pkd2* loss-of-function has so far remained undetermined. An improvement of zebrafish models, such as the creation of an inducible renal *pkd2* knockout line (attempted during this project but the *lox* construct failed to rescue *pkd2*$^{-/-}$ phenotypes) or the creation of mosaic *pkd2*$^{-/-}$ animals via CRISPR knockout (animals were created but could not be analysed due to time constraints) might be able to elucidate whether zebrafish could develop renal cysts and serve as more accurate ADPKD models. The mosaic loss of *pkd2* would mimic the presumed loss-of-heterozygosity in patients more closely than a pan-renal *pkd2* knockout.

In conclusion, new insights into the interplay between ADPKD and its modifying factors were gained during this project and a number of potential new therapeutic compounds for this devastating disease have been identified.

List of Materials

Chemical/equipment	Supplier/company	Cat no/name
1.5 ml Eppendorf tubes	Starlab	S1615-5500
10-beta cells	New England Biolabs	C3019H
10x MEM	Thermofisher scientific	11430030
11-ketotestosterone	Sigma-Aldrich	K8250
15 ml falcon tubes	Sarstedt	62.553.542
2,5-Di-tert-butyl-4-hydroxyanisole	Sigma-Aldrich	447323
2-APB	Kindly provided by Deepa Bliss	
5,7,4'-trimethoxyflavone	Microsource Discovery Systems, Inc.	00300384
50 ml falcon tubes	SLS	352070
5alpha-androstan-3,17-dione	Microsource Discovery Systems, Inc.	00107108
Acetone	Sigma-Aldrich	179124
Agarose	Bioline	BIO-41025
antibodies	pH3 Alexa Flour 488	ab5176 Z25302
Arabinose	Sigma-Aldrich	A3256
Bay K8644	Sigma-Aldrich	B112
BCIP	Roche	10760994001
Blocking reagent	Roche	11096176001
BrdU	Sigma-Aldrich	N5002
cAMP	Tocris	1140
Carbenicillin	Sigma-Aldrich	C1389
Centrifuges	Progen Thermo	GenFuge 24D Heraeus Fresco17
Chloramphenicol	Merck	1.02366.0050
Chloroform	VWR International	22711.260
Citric acid	VWR International	100813M
Confocal microscope	Olympus Perkin Elmer	IX81 Ultraview Vox
diclofenac	Sigma-Aldrich	93484
DIG RNA labelling mix	Roche	11277073910
Disposable serological pipettes	Corning Incorporated	Costar, various sizes
DMSO	AppliChem	A3006
DNA ladder	New England Biolabs (100 bp) Thermofischer scientific (1 kb)	N3231S SM0311
DNAseI	Roche	04716728001
dNTPs	Roche	11969064001
EDTA	Sigma-Aldrich	E5134
EDTA-Trypsin	Gibco	11590626
Ethanol	Fisher scientific	E/0650/17
Ethidium bromide	Sigma-Aldrich	E7637
Exonuclease I	New England Biolabs	M0293L
FBS	Labtech International	s1810-500
Firepol	Solis Biodyne	04-12-00115
Flutamide	Sigma-Aldrich	F9397
Formamide	Sigma-Aldrich	P9037
Formamide	Sigma-Aldrich	F9037
Forskolin	Tocris	1099
Gel extraction kit	QiAgen	28706
Gel tanks	BioRad	PowerPack 300

Gibco DMEM/F-12 medium	Thermofisher scientific	21221-046
Glycerol	VWR International	24388.295
Heatblock	Techne	DriBlock DB-2A
hEGF	Sigma-Aldrich	E9644
Heparin	Sigma-Aldrich	H3393
hexamethoxyquercetagetin	Microsource Discovery Systems, Inc.	01505383
hydrocortisone	Sigma-Aldrich	H0135
Injection needles	World precision instruments	TW120-4
Isopropanol	Fisher scientific	BP2618-500
ITS liquid media supplement	Sigma-Aldrich	I3146
Kanamycin	Sigma-Aldrich	B5264
KCl	Sigma-Aldrich	P4504
LB	MP Biochemicals	3001-031
LBA	MP Biochemicals	3001-231
L-glutamine	Lonza	17-605C
Lightsheet microscope	Zeiss	Lightsheet Z.1
Loading dye	New England Biolabs	B7021S or B7025S
Low-melt agarose	Fisher scientific	BP165-25
Low-melt agarose	Fisher Scientific	BP165-25
Maleic acid	Sigma-Aldrich	M0375
Matrigel matrix	Corning B.V.	354230
Mega ShortScript T7 kit	Ambion	AM1354
MetaPhor agarose	Lonza	50180
Methanol	Fisher scientific	M/4000/17
Methyl cellulose	Sigma-Aldrich	M0387
MgCl2	VWR International	25108.260
microscopes	Leica Leica Zeiss Olympus	MZ16 M165FC Axio Zoom.V16 IX71
Midi prep kit	Macherey-Nagel	740410.100
Mini prep kit	QiAgen	27106
mMessage mMachine SP6 kit	Ambion	AM1340
Morpholino	Gene Tools, LLC	
Multi-well plates	Corning Incorporated	Costar, various sizes
NaCl	VWR International	10241AP
NaCl	Sigma-Aldrich	S7653
NaHCO3	Sigma-Aldrich	S5761
NaOH	VWR International	28244.262
Naringenin	Sigma-Aldrich	W530098
NBT	Roche	11383213001
NH4Ac	Sigma-Aldrich	A1542
Nifedipine	Sigma-Aldrich	N7634
NP40	BDH Laboratory Suppliers	56009
NU serum	Becton Dickinson	734-1318
Pasteur pipettes	SLS	PIP4206
PBS	Sigma-Aldrich	P4417
PCR plate lids	Starlab	E2796-0793
PCR plates	Starlab	I1402-9700
PCR purification kit	QiAgen	28106
PCR tubes	Starlab	I1402-8100
Penicillin/Streptomycin	Lonza	LZDE17-603E
Petri dishes	Thermofisher scientific	100315

PFA	VWR International	28794.295
PGE2	Tocris	2296
Phenol:Chloroform:Isoamyl Alcohol 25:24:1	Sigma-Aldrich	P2069
Phenosight system	Ash Biotech	Custom-made
Phusion polymerase	New England Biolabs	M0530S
pimpinellin	Microsource Discovery Systems, Inc.	00300013
prenyletin	Microsource Discovery Systems, Inc.	00100101
Primers	IDT	
pronase	Fluka	81748
proteinaseK	Sigma-Aldrich	P6556
PTU	Sigma-Aldrich	CDS004712
PTU (phenolthiourea)	Sigma-Aldrich	P7629
QuickLigase	New England Biolabs	M2200
Reddymix	Thermofisher scientific	AB0575DCLDA
Restriction enzymes	New England Biolabs	various
RNAse inhibitor	Promega	N251B
SAP (shrimp alkaline phosphatase)	Affimetrix	78390
SDS	BioRad	161-0416
Shaking rotators	Janke&Kunkel	VX1
Sodium citrate	VWR International	H3261
Sodium pyrithione	Sigma-Aldrich	H3261
Spectrum library	Microsource Discovery Systems, Inc.	27833.260
sphondin	Microsource Discovery Systems, Inc.	00300005
Sucrose	VWR International	102744B
SYBR Safe	Invitrogen	S33102
T7 RNA polymerase	Promega	P2078
T75 flasks	Greiner	658175
T7EI	New England Biolabs	M0302S
Testosterone	Sigma-Aldrich	R1881
Thapsigargin	Sigma-Aldrich	T9033
Thermocycler	BioRad	T100 thermocycler
Tolvaptan	Sigma-Aldrich	T7455
Tricaine	Sigma-Aldrich	E10521
TRIreagent	Ambion	AM9738
Tris	VWR International	0497
TritonX	Sigma-Aldrich	T8787
Tween20	Sigma-Aldrich	P7949
Vortex	Hook & Tucker	HATI Rotamixer
Zinc chloride	BDH	103794P
Zinc pyrithione	Sigma-Aldrich	H6377

Table of Figures

Table of Tables

References

Abe, M., Okada, K., & Soma, M. (2013). T-type Ca channel blockers in patients with chronic kidney disease in clinical practice. *Curr Hypertens Rev, 9*(3), 202-209.

Abe, Y., Komori, T., Miura, K., Takada, T., Imanishi, M., Okahara, T., & Yamamoto, K. (1983). Effects of the calcium antagonist nicardipine on renal function and renin release in dogs. *J Cardiovasc Pharmacol, 5*(2), 254-259.

Aguiari, G., Campanella, M., Manzati, E., Pinton, P., Banzi, M., Moretti, S., Piva, R., Rizzuto, R., & del Senno, L. (2003). Expression of polycystin-1 C-terminal fragment enhances the ATP-induced Ca2+ release in human kidney cells. *Biochem Biophys Res Commun, 301*(3), 657-664.

Ahrabi, A. K., Terryn, S., Valenti, G., Caron, N., Serradeil-Le Gal, C., Raufaste, D., Nielsen, S., Horie, S., Verbavatz, J. M., & Devuyst, O. (2007). PKD1 haploinsufficiency causes a syndrome of inappropriate antidiuresis in mice. [Research Support, Non-U.S. Gov't]. *J Am Soc Nephrol, 18*(6), 1740-1753. doi: 10.1681/ASN.2006010052

Akerboom, J., Chen, T. W., Wardill, T. J., Tian, L., Marvin, J. S., Mutlu, S., Calderon, N. C., Esposti, F., Borghuis, B. G., Sun, X. R., Gordus, A., Orger, M. B., Portugues, R., Engert, F., Macklin, J. J., Filosa, A., Aggarwal, A., Kerr, R. A., Takagi, R., Kracun, S., Shigetomi, E., Khakh, B. S., Baier, H., Lagnado, L., Wang, S. S., Bargmann, C. I., Kimmel, B. E., Jayaraman, V., Svoboda, K., Kim, D. S., Schreiter, E. R., & Looger, L. L. (2012). Optimization of a GCaMP calcium indicator for neural activity imaging. *J Neurosci, 32*(40), 13819-13840. doi: 10.1523/JNEUROSCI.2601-12.2012

Alam, M. A., Kauter, K., & Brown, L. (2013). Naringin improves diet-induced cardiovascular dysfunction and obesity in high carbohydrate, high fat diet-fed rats. *Nutrients, 5*(3), 637-650. doi: 10.3390/nu5030637

Alam, M. A., Subhan, N., Rahman, M. M., Uddin, S. J., Reza, H. M., & Sarker, S. D. (2014). Effect of citrus flavonoids, naringin and naringenin, on metabolic syndrome and their mechanisms of action. *Adv Nutr, 5*(4), 404-417. doi: 10.3945/an.113.005603

Amsterdam, A., Nissen, R. M., Sun, Z., Swindell, E. C., Farrington, S., & Hopkins, N. (2004). Identification of 315 genes essential for early zebrafish development. *Proc Natl Acad Sci U S A, 101*(35), 12792-12797. doi: 10.1073/pnas.0403929101

Andrade, Y. N., Fernandes, J., Vazquez, E., Fernandez-Fernandez, J. M., Arniges, M., Sanchez, T. M., Villalon, M., & Valverde, M. A. (2005). TRPV4 channel is involved in the coupling of fluid viscosity changes to epithelial ciliary activity. [Research Support, Non-U.S. Gov't]. *The Journal of cell biology, 168*(6), 869-874. doi: 10.1083/jcb.200409070

Anyatonwu, G. I., Estrada, M., Tian, X., Somlo, S., & Ehrlich, B. E. (2007). Regulation of ryanodine receptor-dependent calcium signaling by polycystin-2. *Proc Natl Acad Sci U S A, 104*(15), 6454-6459. doi: 10.1073/pnas.0610324104

Arslanova, D., Yang, T., Xu, X., Wong, S. T., Augelli-Szafran, C. E., & Xia, W. (2010). Phenotypic analysis of images of zebrafish treated with Alzheimer's gamma-secretase inhibitors. *BMC Biotechnol, 10*, 24. doi: 10.1186/1472-6750-10-24

Astor, B. C., Yi, S., Hiremath, L., Corbin, T., Pogue, V., Wilkening, B., Peterson, G., Lewis, J., Lash, J. P., Van Lente, F., Gassman, J., Wang, X., Bakris, G., Appel, L. J., & Contreras, G. (2008). N-terminal prohormone brain natriuretic peptide as a predictor of cardiovascular disease and mortality in blacks with hypertensive kidney disease: the African American Study of Kidney Disease and Hypertension (AASK). *Circulation, 117*(13), 1685-1692. doi: 10.1161/CIRCULATIONAHA.107.724187

Aziz, N., Anderson, E., Lee, G. Y., & Woo, D. D. (2001). Arrested testis development in the cpk mouse may be the result of abnormal steroid metabolism. *Mol Cell Endocrinol, 171*(1-2), 83-88.

Bae, K. T., & Grantham, J. J. (2010). Imaging for the prognosis of autosomal dominant polycystic kidney disease. [Review]. *Nature reviews. Nephrology, 6*(2), 96-106. doi: 10.1038/nrneph.2009.214

Bai, C. X., Giamarchi, A., Rodat-Despoix, L., Padilla, F., Downs, T., Tsiokas, L., & Delmas, P. (2008). Formation of a new receptor-operated channel by heteromeric assembly of TRPP2 and TRPC1 subunits. *EMBO Rep, 9*(5), 472-479. doi: 10.1038/embor.2008.29

Bala, A., Chetia, P., Dolai, N., Khandelwal, B., & Haldar, P. K. (2014). Cat's whiskers flavonoid attenuated oxidative DNA damage and acute inflammation: its importance in lymphocytes of patients with rheumatoid arthritis. *Inflammopharmacology, 22*(1), 55-61. doi: 10.1007/s10787-013-0193-5

Bao, L., Liu, F., Guo, H. B., Li, Y., Tan, B. B., Zhang, W. X., & Peng, Y. H. (2016). Naringenin inhibits proliferation, migration, and invasion as well as induces apoptosis of gastric cancer SGC7901 cell line by downregulation of AKT pathway. *Tumour Biol.* doi: 10.1007/s13277-016-5013-2

Barker, G., & Simmons, N. L. (1981). Identification of two strains of cultured canine renal epithelial cells (MDCK cells) which display entirely different physiological properties. *Q J Exp Physiol, 66*(1), 61-72.

Baxendale, S., Holdsworth, C. J., Meza Santoscoy, P. L., Harrison, M. R., Fox, J., Parkin, C. A., Ingham, P. W., & Cunliffe, V. T. (2012). Identification of compounds with anti-convulsant properties in a zebrafish model of epileptic seizures. *Dis Model Mech, 5*(6), 773-784. doi: 10.1242/dmm.010090

Bello-Reuss, E. (2007). Inhibition of tubule-cell proliferation to prevent cyst formation: a new avenue to treat ADPKD? *Kidney Int, 72*(2), 135-137. doi: 10.1038/sj.ki.5002377

Bertram, J. F., Douglas-Denton, R. N., Diouf, B., Hughson, M. D., & Hoy, W. E. (2011). Human nephron number: implications for health and disease. *Pediatr Nephrol, 26*(9), 1529-1533. doi: 10.1007/s00467-011-1843-8

Bertrand, S., Thisse, B., Tavares, R., Sachs, L., Chaumot, A., Bardet, P. L., Escriva, H., Duffraisse, M., Marchand, O., Safi, R., Thisse, C., & Laudet, V. (2007). Unexpected novel relational links uncovered by extensive developmental profiling of nuclear receptor expression. *PLoS Genet, 3*(11), e188. doi: 10.1371/journal.pgen.0030188

Bhunia, A. K., Piontek, K., Boletta, A., Liu, L., Qian, F., Xu, P. N., Germino, F. J., & Germino, G. G. (2002). PKD1 induces p21(waf1) and regulation of the cell cycle via direct activation of the JAK-STAT signaling pathway in a process requiring PKD2. *Cell, 109*(2), 157-168.

Bidani, A. K., Schwartz, M. M., & Lewis, E. J. (1987). Renal autoregulation and vulnerability to hypertensive injury in remnant kidney. *Am J Physiol, 252*(6 Pt 2), F1003-1010.

Bisgrove, B. W., Snarr, B. S., Emrazian, A., & Yost, H. J. (2005). Polaris and Polycystin-2 in dorsal forerunner cells and Kupffer's vesicle are required for specification of the zebrafish left-right axis. *Dev Biol, 287*(2), 274-288. doi: S0012-1606(05)00571-3 [pii]

Bloodgood, R. A. (2010). Sensory reception is an attribute of both primary cilia and motile cilia. [Review]. *J Cell Sci, 123*(Pt 4), 505-509. doi: 10.1242/jcs.066308

Boletta, A., Qian, F., Onuchic, L. F., Bragonzi, A., Cortese, M., Deen, P. M., Courtoy, P. J., Soria, M. R., Devuyst, O., Monaco, L., & Germino, G. G. (2001). Biochemical characterization of bona fide polycystin-1 in vitro and in vivo. [In Vitro Research Support, U.S. Gov't, P.H.S. Validation Studies]. *Am J Kidney Dis, 38*(6), 1421-1429. doi: 10.1053/ajkd.2001.29282

Boulter, C., Mulroy, S., Webb, S., Fleming, S., Brindle, K., & Sandford, R. (2001). Cardiovascular, skeletal, and renal defects in mice with a targeted disruption of the Pkd1 gene. *Proc Natl Acad Sci U S A, 98*(21), 12174-12179. doi: 10.1073/pnas.211191098

Brand, M., Granato, M., Nu sslein-Volhard, C. (2002). Keeping and raising zebrafish. *Oxford University Press, Oxford, UK, Zebrafish - A Practical Approach*.

Brand, M., Heisenberg, C. P., Warga, R. M., Pelegri, F., Karlstrom, R. O., Beuchle, D., Picker, A., Jiang, Y. J., Furutani-Seiki, M., van Eeden, F. J., Granato, M., Haffter, P., Hammerschmidt, M., Kane, D. A., Kelsh, R. N., Mullins, M. C., Odenthal, J., & Nusslein-Volhard, C. (1996). Mutations affecting development of the midline and general body shape during zebrafish embryogenesis. *Development, 123*, 129-142.

Braun, W. E., Schold, J. D., Stephany, B. R., Spirko, R. A., & Herts, B. R. (2014). Low-dose rapamycin (sirolimus) effects in autosomal dominant polycystic kidney disease: an open-label randomized controlled pilot study. *Clin J Am Soc Nephrol, 9*(5), 881-888. doi: 10.2215/CJN.02650313

Brown, N. E., & Murcia, N. S. (2003). Delayed cystogenesis and increased ciliogenesis associated with the re-expression of polaris in Tg737 mutant mice. [Research Support, Non-U.S. Gov't

Research Support, U.S. Gov't, P.H.S.]. *Kidney Int, 63*(4), 1220-1229. doi: 10.1046/j.1523-1755.2003.00863.x

Brown, S. A., Walton, C. L., Crawford, P., & Bakris, G. L. (1993). Long-term effects of antihypertensive regimens on renal hemodynamics and proteinuria. *Kidney Int, 43*(6), 1210-1218.

Burford, J. L., Villanueva, K., Lam, L., Riquier-Brison, A., Hackl, M. J., Pippin, J., Shankland, S. J., & Peti-Peterdi, J. (2014). Intravital imaging of podocyte calcium in glomerular injury and disease. *J Clin Invest, 124*(5), 2050-2058. doi: 10.1172/JCI71702

Busch-Nentwich, E., Kettleborough, R., Dooley, C. M., Scahill, C., Sealy, I., White, R., Herd, C., Mehroke, S., Wali, N., Carruthers, S., Hall, A., Collins, J., Gibbons, R., Pusztai, Z., Clark, R., and Stemple, D.L. . (2013). Sanger Institute Zebrafish Mutation Project mutant data submission. *ZFIN Direct Data Submission*

Cai, Y., Maeda, Y., Cedzich, A., Torres, V. E., Wu, G., Hayashi, T., Mochizuki, T., Park, J. H., Witzgall, R., & Somlo, S. (1999). Identification and characterization of polycystin-2, the PKD2 gene product. *J Biol Chem, 274*(40), 28557-28565.

Calvet, J. P. (1998). Molecular genetics of polycystic kidney disease. *J Nephrol, 11*(1), 24-34.

Candiano, G., Gusmano, R., Altieri, P., Bertelli, R., Ginevri, F., Coviello, D. A., Sessa, A., Caridi, G., & Ghiggeri, G. M. (1992). Extracellular matrix formation by epithelial cells from human polycystic kidney cysts in culture. *Virchows Arch B Cell Pathol Incl Mol Pathol, 63*(1), 1-9.

Cao, Y., Semanchik, N., Lee, S. H., Somlo, S., Barbano, P. E., Coifman, R., & Sun, Z. (2009). Chemical modifier screen identifies HDAC inhibitors as suppressors of PKD models. *Proc Natl Acad Sci U S A, 106*(51), 21819-21824. doi: 10.1073/pnas.0911987106

Cechinel Filho, V., Lima, E. O., Morais, V. M., Gomes, S. T., Miguel, O. G., & Yunes, R. A. (1996). Fungicide and fungiostatic effects of xanthoxyline. *J Ethnopharmacol, 53*(3), 171-173.

Chan, K. W. (1993). Adult polycystic kidney disease in Hong Kong Chinese: an autopsy study. *Pathology, 25*(3), 229-232.

Chang, K. H., Li, R., Papari-Zareei, M., Watumull, L., Zhao, Y. D., Auchus, R. J., & Sharifi, N. (2011). Dihydrotestosterone synthesis bypasses testosterone to drive castration-resistant prostate cancer. *Proc Natl Acad Sci U S A, 108*(33), 13728-13733. doi: 10.1073/pnas.1107898108

Chang, M. Y., & Ong, A. C. (2008). Autosomal dominant polycystic kidney disease: recent advances in pathogenesis and treatment. *Nephron Physiol, 108*(1), p1-7. doi: 000112495 [pii]

Chang, M. Y., Parker, E., Ibrahim, S., Shortland, J. R., Nahas, M. E., Haylor, J. L., & Ong, A. C. (2006). Haploinsufficiency of Pkd2 is associated with increased tubular cell proliferation and interstitial fibrosis in two murine Pkd2 models. *Nephrol Dial Transplant, 21*(8), 2078-2084. doi: gfl150 [pii]

Chang, N., Sun, C., Gao, L., Zhu, D., Xu, X., Zhu, X., Xiong, J. W., & Xi, J. J. (2013). Genome editing with RNA-guided Cas9 nuclease in zebrafish embryos. *Cell Res, 23*(4), 465-472. doi: 10.1038/cr.2013.45

Chen, D., Ma, Y., Wang, X., Yu, S., Li, L., Dai, B., Mao, Z., Liu, H., Liu, S., & Mei, C. (2014). Triptolide-containing formulation in patients with autosomal dominant polycystic kidney disease and proteinuria: an uncontrolled trial. *Am J Kidney Dis, 63*(6), 1070-1072. doi: 10.1053/j.ajkd.2014.01.418

Chen, J. N., van Eeden, F. J., Warren, K. S., Chin, A., Nusslein-Volhard, C., Haffter, P., & Fishman, M. C. (1997). Left-right pattern of cardiac BMP4 may drive asymmetry of the heart in zebrafish. *Development, 124*(21), 4373-4382.

Cheng, C. N., & Wingert, R. A. (2015). Nephron proximal tubule patterning and corpuscles of Stannius formation are regulated by the sim1a transcription factor and retinoic acid in zebrafish. *Dev Biol, 399*(1), 100-116. doi: 10.1016/j.ydbio.2014.12.020

Choi, Y. H., Suzuki, A., Hajarnis, S., Ma, Z., Chapin, H. C., Caplan, M. J., Pontoglio, M., Somlo, S., & Igarashi, P. (2011). Polycystin-2 and phosphodiesterase 4C are components of a ciliary A-kinase anchoring protein complex that is disrupted in cystic kidney diseases. *Proc Natl Acad Sci U S A, 108*(26), 10679-10684. doi: 10.1073/pnas.1016214108

Choksi, S. P., Lauter, G., Swoboda, P., & Roy, S. (2014). Switching on cilia: transcriptional networks regulating ciliogenesis. *Development, 141*(7), 1427-1441. doi: 10.1242/dev.074666

Cornec-Le Gall, E., Audrezet, M. P., Chen, J. M., Hourmant, M., Morin, M. P., Perrichot, R., Charasse, C., Whebe, B., Renaudineau, E., Jousset, P., Guillodo, M. P., Grall-Jezequel, A., Saliou, P., Ferec, C., & Le Meur, Y. (2013). Type of PKD1 Mutation Influences Renal Outcome in ADPKD. *J Am Soc Nephrol, 24*(6), 1006-1013. doi: 10.1681/ASN.2012070650

Cowley, B. D., Jr., Rupp, J. C., Muessel, M. J., & Gattone, V. H., 2nd. (1997). Gender and the effect of gonadal hormones on the progression of inherited polycystic kidney disease in rats. *Am J Kidney Dis, 29*(2), 265-272.

Coxam, B., Sabine, A., Bower, N. I., Smith, K. A., Pichol-Thievend, C., Skoczylas, R., Astin, J. W., Frampton, E., Jaquet, M., Crosier, P. S., Parton, R. G., Harvey, N. L., Petrova, T. V., Schulte-Merker, S., Francois, M., & Hogan, B. M. (2014). Pkd1 regulates lymphatic vascular morphogenesis during development. *Cell Rep, 7*(3), 623-633. doi: 10.1016/j.celrep.2014.03.063

Dalgaard, O. Z. (1957). Bilateral polycystic disease of the kidneys; a follow-up of two hundred and eighty-four patients and their families. *Acta Med Scand Suppl, 328*, 1-255.

Danesh, M. J., & Kimball, A. B. (2015). Pyrithione zinc as a general management strategy for hidradenitis suppurativa. *J Am Acad Dermatol, 73*(5), e175. doi: 10.1016/j.jaad.2015.07.026

DeCaen, P. G., Delling, M., Vien, T. N., & Clapham, D. E. (2013). Direct recording and molecular identification of the calcium channel of primary cilia. [Research Support, N.I.H., Extramural Research Support, Non-U.S. Gov't]. *Nature, 504*(7479), 315-318. doi: 10.1038/nature12832

Delling, M., DeCaen, P. G., Doerner, J. F., Febvay, S., & Clapham, D. E. (2013). Primary cilia are specialized calcium signalling organelles. [Research Support, N.I.H., Extramural Research Support, Non-U.S. Gov't]. *Nature, 504*(7479), 311-314. doi: 10.1038/nature12833

Desai, P. J., Castle, E. P., Daley, S. M., Swanson, S. K., Ferrigni, R. G., Humphreys, M. R., & Andrews, P. E. (2008). Bilateral laparoscopic nephrectomy for significantly enlarged polycystic kidneys: a technique to optimize outcome in the largest of specimens. *BJU Int, 101*(8), 1019-1023. doi: 10.1111/j.1464-410X.2007.07423.x

Dietz, J. R., Davis, J. O., Freeman, R. H., Villarreal, D., & Echtenkamp, S. F. (1983). Effects of intrarenal infusion of calcium entry blockers in anesthetized dogs. *Hypertension, 5*(4), 482-488.

Donaldson, J. G., Finazzi, D., & Klausner, R. D. (1992). Brefeldin A inhibits Golgi membrane-catalysed exchange of guanine nucleotide onto ARF protein. *Nature, 360*(6402), 350-352. doi: 10.1038/360350a0

Dressler, G. R. (2006). The cellular basis of kidney development. *Annu Rev Cell Dev Biol, 22*, 509-529. doi: 10.1146/annurev.cellbio.22.010305.104340

Drummond, I. A. (2000). The zebrafish pronephros: a genetic system for studies of kidney development. *Pediatr Nephrol, 14*(5), 428-435.

Drummond, I. A., & Davidson, A. J. (2010). Zebrafish kidney development. *Methods Cell Biol, 100*, 233-260. doi: 10.1016/B978-0-12-384892-5.00009-8

Drummond, I. A., Majumdar, A., Hentschel, H., Elger, M., Solnica-Krezel, L., Schier, A. F., Neuhauss, S. C., Stemple, D. L., Zwartkruis, F., Rangini, Z., Driever, W., & Fishman, M. C. (1998). Early development of the zebrafish pronephros and analysis of mutations affecting pronephric function. *Development, 125*(23), 4655-4667.

Elberg, G., Elberg, D., Lewis, T. V., Guruswamy, S., Chen, L., Logan, C. J., Chan, M. D., & Turman, M. A. (2007). EP2 receptor mediates PGE2-induced cystogenesis of human renal epithelial cells. *Am J Physiol Renal Physiol, 293*(5), F1622-1632. doi: 10.1152/ajprenal.00036.2007

Elkins, J. M., Fedele, V., Szklarz, M., Abdul Azeez, K. R., Salah, E., Mikolajczyk, J., Romanov, S., Sepetov, N., Huang, X. P., Roth, B. L., Al Haj Zen, A., Fourches, D., Muratov, E., Tropsha, A., Morris, J., Teicher, B. A., Kunkel, M., Polley, E., Lackey, K. E., Atkinson, F. L., Overington, J. P., Bamborough, P., Muller, S., Price, D. J., Willson, T. M., Drewry, D. H., Knapp, S., & Zuercher, W. J. (2016). Comprehensive characterization of the Published Kinase Inhibitor Set. *Nat Biotechnol, 34*(1), 95-103. doi: 10.1038/nbt.3374

Erickson, K. F., Chertow, G. M., & Goldhaber-Fiebert, J. D. (2013). Cost-effectiveness of tolvaptan in autosomal dominant polycystic kidney disease. [Research Support, N.I.H., Extramural]. *Annals of internal medicine, 159*(6), 382-389. doi: 10.7326/0003-4819-159-6-201309170-00004

Erlund, I., Meririnne, E., Alfthan, G., & Aro, A. (2001). Plasma kinetics and urinary excretion of the flavanones naringenin and hesperetin in humans after ingestion of orange juice and grapefruit juice. *J Nutr, 131*(2), 235-241.

Essner, J. J., Vogan, K. J., Wagner, M. K., Tabin, C. J., Yost, H. J., & Brueckner, M. (2002). Conserved function for embryonic nodal cilia. *Nature, 418*(6893), 37-38. doi: 10.1038/418037a

Fan, L. X., Li, X., Magenheimer, B., Calvet, J. P., & Li, X. (2012). Inhibition of histone deacetylases targets the transcription regulator Id2 to attenuate cystic epithelial cell proliferation. *Kidney Int, 81*(1), 76-85. doi: 10.1038/ki.2011.296

Fedeles, S. V., Tian, X., Gallagher, A. R., Mitobe, M., Nishio, S., Lee, S. H., Cai, Y., Geng, L., Crews, C. M., & Somlo, S. (2011). A genetic interaction network of five genes for human polycystic kidney and liver diseases defines polycystin-1 as the central determinant of cyst formation. *Nat Genet, 43*(7), 639-647. doi: 10.1038/ng.860

Ferraldeschi, R., Welti, J., Luo, J., Attard, G., & de Bono, J. S. (2015). Targeting the androgen receptor pathway in castration-resistant prostate cancer: progresses and prospects. *Oncogene, 34*(14), 1745-1757. doi: 10.1038/onc.2014.115

Fick, G. M., Johnson, A. M., Hammond, W. S., & Gabow, P. A. (1995). Causes of death in autosomal dominant polycystic kidney disease. *J Am Soc Nephrol, 5*(12), 2048-2056.

Field, S., Riley, K. L., Grimes, D. T., Hilton, H., Simon, M., Powles-Glover, N., Siggers, P., Bogani, D., Greenfield, A., & Norris, D. P. (2011). Pkd1l1 establishes left-right asymmetry and physically interacts with Pkd2. *Development, 138*(6), 1131-1142. doi: 10.1242/dev.058149

Firdous, A. B., Sharmila, G., Balakrishnan, S., RajaSingh, P., Suganya, S., Srinivasan, N., & Arunakaran, J. (2014). Quercetin, a natural dietary flavonoid, acts as a chemopreventive agent against prostate cancer in an in vivo model by inhibiting the EGFR signaling pathway. *Food Funct, 5*(10), 2632-2645. doi: 10.1039/c4fo00255e

Fogelgren, B., Lin, S. Y., Zuo, X., Jaffe, K. M., Park, K. M., Reichert, R. J., Bell, P. D., Burdine, R. D., & Lipschutz, J. H. (2011). The exocyst protein Sec10 interacts with Polycystin-2 and knockdown causes PKD-phenotypes. *PLoS Genet, 7*(4), e1001361. doi: 10.1371/journal.pgen.1001361

Foggensteiner, L., Bevan, A. P., Thomas, R., Coleman, N., Boulter, C., Bradley, J., Ibraghimov-Beskrovnaya, O., Klinger, K., & Sandford, R. (2000). Cellular and subcellular distribution of polycystin-2, the protein product of the PKD2 gene. *J Am Soc Nephrol, 11*(5), 814-827.

Foufelle, F., & Fromenty, B. (2016). Role of endoplasmic reticulum stress in drug-induced toxicity. *Pharmacol Res Perspect, 4*(1), e00211. doi: 10.1002/prp2.211

Francescatto, L., Rothschild, S. C., Myers, A. L., & Tombes, R. M. (2010). The activation of membrane targeted CaMK-II in the zebrafish Kupffer's vesicle is required for left-right asymmetry. *Development, 137*(16), 2753-2762. doi: 10.1242/dev.049627

Fry, J. L., Jr., Koch, W. E., Jennette, J. C., McFarland, E., Fried, F. A., & Mandell, J. (1985). A genetically determined murine model of infantile polycystic kidney disease. *J Urol, 134*(4), 828-833.

Fu, X., Wang, Y., Schetle, N., Gao, H., Putz, M., von Gersdorff, G., Walz, G., & Kramer-Zucker, A. G. (2008). The subcellular localization of TRPP2 modulates its function. *J Am Soc Nephrol, 19*(7), 1342-1351. doi: 10.1681/ASN.2007070730

Fujita, T., Ando, K., Nishimura, H., Ideura, T., Yasuda, G., Isshiki, M., Takahashi, K., & Cilnidipine versus Amlodipine Randomised Trial for Evaluation in Renal Desease Study, I. (2007). Antiproteinuric effect of the calcium channel blocker cilnidipine added to renin-angiotensin inhibition in hypertensive patients with chronic renal disease. *Kidney Int, 72*(12), 1543-1549. doi: 10.1038/sj.ki.5002623

Fujiwara, K., Kanno, Y., Hayashi, K., Takenaka, T., & Saruta, T. (1998). Renal protective effects of efonidipine in partially nephrectomized spontaneously hypertensive rats. *Clin Exp Hypertens, 20*(3), 295-312.

Fusi, F., Saponara, S., Gagov, H., & Sgaragli, G. (2001). Effects of some sterically hindered phenols on whole-cell Ca(2+) current of guinea-pig gastric fundus smooth muscle cells. *Br J Pharmacol, 132*(6), 1326-1332. doi: 10.1038/sj.bjp.0703935

Fusi, F., Tzankova, V., Valoti, M., Pessina, F., & Sgaragli, G. (2001). 3,5-di-t-butyl-4-hydroxyanisole (DTBHA) activation of rat skeletal muscle sarcoplasmic reticulum Ca(2+)-ATPase. *Biochem Pharmacol, 62*(12), 1613-1619.

Gabow, P. A. (1990). Autosomal dominant polycystic kidney disease--more than a renal disease. [Research Support, U.S. Gov't, P.H.S. Review]. *Am J Kidney Dis, 16*(5), 403-413.

Gabow, P. A., Johnson, A. M., Kaehny, W. D., Kimberling, W. J., Lezotte, D. C., Duley, I. T., & Jones, R. H. (1992). Factors affecting the progression of renal disease in autosomal-dominant polycystic kidney disease. [Research Support, U.S. Gov't, P.H.S.]. *Kidney Int, 41*(5), 1311-1319.

Gallagher, A. R., Cedzich, A., Gretz, N., Somlo, S., & Witzgall, R. (2000). The polycystic kidney disease protein PKD2 interacts with Hax-1, a protein associated with the actin cytoskeleton. *Proc Natl Acad Sci U S A, 97*(8), 4017-4022. doi: 97/8/4017 [pii]

Gao, H., Wang, Y., Wegierski, T., Skouloudaki, K., Putz, M., Fu, X., Engel, C., Boehlke, C., Peng, H., Kuehn, E. W., Kim, E., Kramer-Zucker, A., & Walz, G. (2010). PRKCSH/80K-H, the protein mutated in polycystic liver disease, protects polycystin-2/TRPP2 against HERP-mediated degradation. *Hum Mol Genet, 19*(1), 16-24. doi: 10.1093/hmg/ddp463

Gattone, V. H., 2nd, Wang, X., Harris, P. C., & Torres, V. E. (2003). Inhibition of renal cystic disease development and progression by a vasopressin V2 receptor antagonist. [Research Support, Non-U.S. Gov't Research Support, U.S. Gov't, P.H.S.]. *Nat Med, 9*(10), 1323-1326. doi: 10.1038/nm935

Gellibert, F., de Gouville, A. C., Woolven, J., Mathews, N., Nguyen, V. L., Bertho-Ruault, C., Patikis, A., Grygielko, E. T., Laping, N. J., & Huet, S. (2006). Discovery of 4-{4-[3-(pyridin-2-yl)-1H-pyrazol-4-yl]pyridin-2-yl}-N-(tetrahydro-2H- pyran-4-yl)benzamide (GW788388): a potent, selective, and orally active transforming growth factor-beta type I receptor inhibitor. *J Med Chem, 49*(7), 2210-2221. doi: 10.1021/jm0509905

Gellibert, F., Woolven, J., Fouchet, M. H., Mathews, N., Goodland, H., Lovegrove, V., Laroze, A., Nguyen, V. L., Sautet, S., Wang, R., Janson, C., Smith, W., Krysa, G., Boullay, V., De Gouville, A. C., Huet, S., & Hartley, D. (2004). Identification of 1,5-naphthyridine derivatives as a novel series of potent and selective TGF-beta type I receptor inhibitors. *J Med Chem, 47*(18), 4494-4506. doi: 10.1021/jm0400247

Geng, L., Okuhara, D., Yu, Z., Tian, X., Cai, Y., Shibazaki, S., & Somlo, S. (2006). Polycystin-2 traffics to cilia independently of polycystin-1 by using an N-terminal RVxP motif. [Comparative Study Research Support, N.I.H., Extramural Research Support, Non-U.S. Gov't]. *Journal of cell science, 119*(Pt 7), 1383-1395. doi: 10.1242/jcs.02818

Germino, G. G. (1997). Autosomal dominant polycystic kidney disease: a two-hit model. *Hospital practice, 32*(3), 81-82, 85-88, 91-82 passim.

Giamarchi, A., Feng, S., Rodat-Despoix, L., Xu, Y., Bubenshchikova, E., Newby, L. J., Hao, J., Gaudioso, C., Crest, M., Lupas, A. N., Honore, E., Williamson, M. P., Obara, T., Ong, A. C., & Delmas, P. (2010). A polycystin-2 (TRPP2) dimerization domain essential for the function of heteromeric polycystin complexes. *EMBO J, 29*(7), 1176-1191. doi: 10.1038/emboj.2010.18

Giamarchi, A., Padilla, F., Coste, B., Raoux, M., Crest, M., Honore, E., & Delmas, P. (2006). The versatile nature of the calcium-permeable cation channel TRPP2. [Research Support, Non-U.S. Gov't Review]. *EMBO reports, 7*(8), 787-793. doi: 10.1038/sj.embor.7400745

Goetz, J. G., Steed, E., Ferreira, R. R., Roth, S., Ramspacher, C., Boselli, F., Charvin, G., Liebling, M., Wyart, C., Schwab, Y., & Vermot, J. (2014). Endothelial cilia mediate low flow sensing during zebrafish vascular development. *Cell Rep, 6*(5), 799-808. doi: 10.1016/j.celrep.2014.01.032

Goldberg, S., Adair-Kirk, T. L., Senior, R. M., & Miner, J. H. (2010). Maintenance of glomerular filtration barrier integrity requires laminin alpha5. [Research Support, N.I.H., Extramural Research Support, Non-U.S. Gov't]. *J Am Soc Nephrol, 21*(4), 579-586. doi: 10.1681/ASN.2009091004

Gonzalez-Perrett, S., Kim, K., Ibarra, C., Damiano, A. E., Zotta, E., Batelli, M., Harris, P. C., Reisin, I. L., Arnaout, M. A., & Cantiello, H. F. (2001). Polycystin-2, the protein mutated in autosomal dominant polycystic kidney disease (ADPKD), is a Ca2+-permeable nonselective cation channel. *Proc Natl Acad Sci U S A, 98*(3), 1182-1187.

Gorelick, D. A., Watson, W., & Halpern, M. E. (2008). Androgen receptor gene expression in the developing and adult zebrafish brain. *Dev Dyn, 237*(10), 2987-2995. doi: 10.1002/dvdy.21700

Grantham, J. J. (1997). Mechanisms of progression in autosomal dominant polycystic kidney disease. [Research Support, U.S. Gov't, P.H.S. Review]. *Kidney international. Supplement, 63*, S93-97.

Grantham, J. J., Bennett, W. M., & Perrone, R. D. (2011). mTOR inhibitors and autosomal dominant polycystic kidney disease. *N Engl J Med, 364*(3), 286-287; author reply 287-289. doi: 10.1056/NEJMc1010845#SA1

Grantham, J. J., Cook, L. T., Torres, V. E., Bost, J. E., Chapman, A. B., Harris, P. C., Guay-Woodford, L. M., & Bae, K. T. (2008). Determinants of renal volume in autosomal-dominant polycystic kidney disease. *Kidney Int, 73*(1), 108-116. doi: 10.1038/sj.ki.5002624

Grantham, J. J., Geiser, J. L., & Evan, A. P. (1987). Cyst formation and growth in autosomal dominant polycystic kidney disease. [Research Support, Non-U.S. Gov't Research Support, U.S. Gov't, P.H.S.]. *Kidney Int, 31*(5), 1145-1152.

Grantham, J. J., Ye, M., Gattone, V. H., 2nd, & Sullivan, L. P. (1995). In vitro fluid secretion by epithelium from polycystic kidneys. [In Vitro Research Support, Non-U.S. Gov't Research Support, U.S. Gov't, P.H.S.]. *The Journal of clinical investigation, 95*(1), 195-202. doi: 10.1172/JCI117638

Griffin, K. A., Picken, M. M., Bakris, G. L., & Bidani, A. K. (1999). Class differences in the effects of calcium channel blockers in the rat remnant kidney model. *Kidney Int, 55*(5), 1849-1860. doi: 10.1046/j.1523-1755.1999.00434.x

Griffin, M. D., Torres, V. E., Grande, J. P., & Kumar, R. (1996). Immunolocalization of polycystin in human tissues and cultured cells. [Research Support, U.S. Gov't, P.H.S.]. *Proceedings of the Association of American Physicians, 108*(3), 185-197.

Haffter, P., Granato, M., Brand, M., Mullins, M. C., Hammerschmidt, M., Kane, D. A., Odenthal, J., van Eeden, F. J., Jiang, Y. J., Heisenberg, C. P., Kelsh, R. N., Furutani-Seiki, M., Vogelsang, E., Beuchle, D., Schach, U., Fabian, C., & Nusslein-Volhard, C. (1996). The identification of genes with unique and essential functions in the development of the zebrafish, Danio rerio. *Development, 123*, 1-36.

Haidar, M., Echebli, N., Ding, Y., Kamau, E., & Langsley, G. (2015). Transforming growth factor beta2 promotes transcription of COX2 and EP4, leading to a prostaglandin E2-driven autostimulatory loop that enhances virulence of Theileria annulata-transformed macrophages. *Infect Immun, 83*(5), 1869-1880. doi: 10.1128/IAI.02975-14

Hanaoka, K., & Guggino, W. B. (2000). cAMP regulates cell proliferation and cyst formation in autosomal polycystic kidney disease cells. *J Am Soc Nephrol, 11*(7), 1179-1187.

Hanaoka, K., Qian, F., Boletta, A., Bhunia, A. K., Piontek, K., Tsiokas, L., Sukhatme, V. P., Guggino, W. B., & Germino, G. G. (2000). Co-assembly of polycystin-1 and -2 produces unique cation-permeable currents. *Nature, 408*(6815), 990-994. doi: 10.1038/35050128

Happe, H., & Peters, D. J. (2014). Translational research in ADPKD: lessons from animal models. *Nat Rev Nephrol, 10*(10), 587-601. doi: 10.1038/nrneph.2014.137

Harris, D. C., Hammond, W. S., Burke, T. J., & Schrier, R. W. (1987). Verapamil protects against progression of experimental chronic renal failure. *Kidney Int, 31*(1), 41-46.

Harris, P. C., Bae, K. T., Rossetti, S., Torres, V. E., Grantham, J. J., Chapman, A. B., Guay-Woodford, L. M., King, B. F., Wetzel, L. H., Baumgarten, D. A., Kenney, P. J., Consugar, M., Klahr, S., Bennett, W. M., Meyers, C. M., Zhang, Q. J., Thompson, P. A., Zhu, F., & Miller, J. P. (2006). Cyst number but not the rate of cystic growth is associated with the mutated gene in autosomal dominant polycystic kidney disease. *J Am Soc Nephrol, 17*(11), 3013-3019. doi: ASN.2006080835 [pii]

Hassane, S., Leonhard, W. N., van der Wal, A., Hawinkels, L. J., Lantinga-van Leeuwen, I. S., ten Dijke, P., Breuning, M. H., de Heer, E., & Peters, D. J. (2010). Elevated TGFbeta-Smad signalling in experimental Pkd1 models and human patients with polycystic kidney disease. *J Pathol, 222*(1), 21-31. doi: 10.1002/path.2734

Hateboer, N., v Dijk, M. A., Bogdanova, N., Coto, E., Saggar-Malik, A. K., San Millan, J. L., Torra, R., Breuning, M., & Ravine, D. (1999). Comparison of phenotypes of polycystic kidney disease types 1 and 2. European PKD1-PKD2 Study Group. *Lancet, 353*(9147), 103-107. doi: S0140673698034953 [pii]

Hattanda, F., Makita, M., Kawashima, K., Kondo, K., Kusunoki, Y., Matsuoka, N., Yamamoto, J., Nakagaki, T., Nishio, S., & Atsumi, T. (2016). Efficacy and Safety of Tolvaptan on Adpkd Patients in Late-Stage Ckd. *Nephrology Dialysis Transplantation, 31*, 92-92.

Hayashi, K., Wakino, S., Sugano, N., Ozawa, Y., Homma, K., & Saruta, T. (2007). Ca2+ channel subtypes and pharmacology in the kidney. *Circ Res, 100*(3), 342-353. doi: 10.1161/01.RES.0000256155.31133.49

He, B., Ebarasi, L., Hultenby, K., Tryggvason, K., & Betsholtz, C. (2011). Podocin-green fluorescence protein allows visualization and functional analysis of podocytes. [Research Support, Non-U.S. Gov't]. *Journal of the American Society of Nephrology : JASN, 22*(6), 1019-1023. doi: 10.1681/ASN.2010121291

Heckel, E., Boselli, F., Roth, S., Krudewig, A., Belting, H. G., Charvin, G., & Vermot, J. (2015). Oscillatory Flow Modulates Mechanosensitive klf2a Expression through trpv4 and trpp2 during Heart Valve Development. *Curr Biol, 25*(10), 1354-1361. doi: 10.1016/j.cub.2015.03.038

Heller, J., & Horacek, V. (1990). The effect of two different calcium antagonists on the glomerular haemodynamics in the dog. *Pflugers Arch, 415*(6), 751-755.

Higashihara, E., Torres, V. E., Chapman, A. B., Grantham, J. J., Bae, K., Watnick, T. J., Horie, S., Nutahara, K., Ouyang, J., Krasa, H. B., Czerwiec, F. S., Tempoformula, & Study, I. (2011). Tolvaptan in autosomal dominant polycystic kidney disease: three years' experience. *Clin J Am Soc Nephrol, 6*(10), 2499-2507. doi: 10.2215/CJN.03530411

Homma, K., Hayashi, K., Yamaguchi, S., Fujishima, S., Hori, S., & Itoh, H. (2013). Renal microcirculation and calcium channel subtypes. *Curr Hypertens Rev, 9*(3), 182-186.

Hong, C. C., Peterson, Q. P., Hong, J. Y., & Peterson, R. T. (2006). Artery/vein specification is governed by opposing phosphatidylinositol-3 kinase and MAP kinase/ERK signaling. [Research Support, N.I.H., Extramural Research Support, Non-U.S. Gov't]. *Curr Biol, 16*(13), 1366-1372. doi: 10.1016/j.cub.2006.05.046

Hopp, K., Ward, C. J., Hommerding, C. J., Nasr, S. H., Tuan, H. F., Gainullin, V. G., Rossetti, S., Torres, V. E., & Harris, P. C. (2012). Functional polycystin-1 dosage governs autosomal dominant polycystic kidney disease severity. *J Clin Invest, 122*(11), 4257-4273. doi: 10.1172/JCI64313

Horvath, P., & Barrangou, R. (2010). CRISPR/Cas, the immune system of bacteria and archaea. [Research Support, Non-U.S. Gov't Review]. *Science, 327*(5962), 167-170. doi: 10.1126/science.1179555

Hossain, M. S., Larsson, A., Scherbak, N., Olsson, P. E., & Orban, L. (2008). Zebrafish androgen receptor: isolation, molecular, and biochemical characterization. *Biol Reprod, 78*(2), 361-369. doi: 10.1095/biolreprod.107.062018

Hostetter, C. L., Sullivan-Brown, J. L., & Burdine, R. D. (2003). Zebrafish pronephros: a model for understanding cystic kidney disease. *Dev Dyn, 228*(3), 514-522. doi: 10.1002/dvdy.10371

Hsu, J. C., Cheng, C. C., Kao, Y. H., Chen, Y. C., Chung, C. C., & Chen, Y. J. (2015). Testosterone regulates cardiac calcium homeostasis with enhanced ryanodine receptor 2 expression through activation of TGF-beta. *Int J Cardiol, 190*, 11-14. doi: 10.1016/j.ijcard.2015.04.116

Huan, Y., & van Adelsberg, J. (1999). Polycystin-1, the PKD1 gene product, is in a complex containing E-cadherin and the catenins. [Research Support, Non-U.S. Gov't

Research Support, U.S. Gov't, P.H.S.]. *The Journal of clinical investigation, 104*(10), 1459-1468. doi: 10.1172/JCI5111

Huang, C. J., Tu, C. T., Hsiao, C. D., Hsieh, F. J., & Tsai, H. J. (2003). Germ-line transmission of a myocardium-specific GFP transgene reveals critical regulatory elements in the cardiac myosin light chain 2 promoter of zebrafish. *Dev Dyn, 228*(1), 30-40. doi: 10.1002/dvdy.10356

Hughes, J., Ward, C. J., Peral, B., Aspinwall, R., Clark, K., San Millan, J. L., Gamble, V., & Harris, P. C. (1995). The polycystic kidney disease 1 (PKD1) gene encodes a novel protein with multiple cell recognition domains. [Comparative Study Research Support, Non-U.S. Gov't]. *Nature genetics, 10*(2), 151-160. doi: 10.1038/ng0695-151

Hwang, W. Y., Fu, Y., Reyon, D., Maeder, M. L., Tsai, S. Q., Sander, J. D., Peterson, R. T., Yeh, J. R., & Joung, J. K. (2013). Efficient genome editing in zebrafish using a CRISPR-Cas system. *Nat Biotechnol, 31*(3), 227-229. doi: 10.1038/nbt.2501

Ibraghimov-Beskrovnaya, O., Bukanov, N. O., Donohue, L. C., Dackowski, W. R., Klinger, K. W., & Landes, G. M. (2000). Strong homophilic interactions of the Ig-like domains of polycystin-1, the protein product of an autosomal dominant polycystic kidney disease gene, PKD1. *Hum Mol Genet, 9*(11), 1641-1649.

Igarashi, P., & Somlo, S. (2002). Genetics and pathogenesis of polycystic kidney disease. [Research Support, U.S. Gov't, P.H.S. Review]. *J Am Soc Nephrol, 13*(9), 2384-2398.

Ikemura, M., Sasaki, Y., Giddings, J. C., & Yamamoto, J. (2012). Preventive effects of hesperidin, glucosyl hesperidin and naringin on hypertension and cerebral thrombosis in stroke-prone spontaneously hypertensive rats. *Phytother Res, 26*(9), 1272-1277. doi: 10.1002/ptr.3724

Imamura, M., & Prasad, C. (1998). Modulation of GABA-gated chloride ion influx in the brain by dehydroepiandrosterone and its metabolites. *Biochem Biophys Res Commun, 243*(3), 771-775. doi: 10.1006/bbrc.1998.8177

Inman, G. J., Nicolas, F. J., Callahan, J. F., Harling, J. D., Gaster, L. M., Reith, A. D., Laping, N. J., & Hill, C. S. (2002). SB-431542 is a potent and specific inhibitor of transforming growth factor-beta superfamily type I activin receptor-like kinase (ALK) receptors ALK4, ALK5, and ALK7. *Mol Pharmacol, 62*(1), 65-74.

Iwasaki, K., Taguchi, M., Bonkowsky, J. L., & Kuwada, J. Y. (2013). Expression of arginine vasotocin receptors in the developing zebrafish CNS. *Gene Expr Patterns, 13*(8), 335-342. doi: 10.1016/j.gep.2013.06.005

Jacobson, H. R. (1981). Functional segmentation of the mammalian nephron. *Am J Physiol, 241*(3), F203-218.

Jiang, S. T., Chiou, Y. Y., Wang, E., Lin, H. K., Lin, Y. T., Chi, Y. C., Wang, C. K., Tang, M. J., & Li, H. (2006). Defining a link with autosomal-dominant polycystic kidney disease in mice with congenitally low expression of Pkd1. *Am J Pathol, 168*(1), 205-220. doi: 10.2353/ajpath.2006.050342

Jin, D., Ni, T. T., Sun, J., Wan, H., Amack, J. D., Yu, G., Fleming, J., Chiang, C., Li, W., Papierniak, A., Cheepala, S., Conseil, G., Cole, S. P., Zhou, B., Drummond, I. A., Schuetz, J. D., Malicki, J., & Zhong, T. P. (2014). Prostaglandin signalling regulates ciliogenesis by modulating intraflagellar transport. *Nat Cell Biol, 16*(9), 841-851. doi: 10.1038/ncb3029

Jin, X., Muntean, B. S., Aal-Aaboda, M. S., Duan, Q., Zhou, J., & Nauli, S. M. (2014). L-type calcium channel modulates cystic kidney phenotype. *Biochim Biophys Acta, 1842*(9), 1518-1526. doi: 10.1016/j.bbadis.2014.06.001

Kamura, K., Kobayashi, D., Uehara, Y., Koshida, S., Iijima, N., Kudo, A., Yokoyama, T., & Takeda, H. (2011). Pkd1l1 complexes with Pkd2 on motile cilia and functions to establish the left-right axis. *Development, 138*(6), 1121-1129. doi: 10.1242/dev.058271

Kaneko, T., Hasegawa, S., & Hirano, T. (1992). Embryonic origin and development of the corpuscles of Stannius in chum salmon (Oncorhynchus keta). *Cell Tissue Res, 268*(1), 65-70.

Karlsson, J., von Hofsten, J., & Olsson, P. E. (2001). Generating transparent zebrafish: a refined method to improve detection of gene expression during embryonic development. *Marine biotechnology, 3*(6), 522-527. doi: 10.1007/s1012601-0053-4

Katsuyama, M., Masuyama, T., Komura, I., Hibino, T., & Takahashi, H. (2000). Characterization of a novel polycystic kidney rat model with accompanying polycystic liver. *Exp Anim, 49*(1), 51-55.

Kim, K., Drummond, I., Ibraghimov-Beskrovnaya, O., Klinger, K., & Arnaout, M. A. (2000). Polycystin 1 is required for the structural integrity of blood vessels. [Research Support, Non-U.S. Gov't Research Support, U.S. Gov't, P.H.S.]. *Proc Natl Acad Sci U S A, 97*(4), 1731-1736.

Kim, U. K., Jin, D. K., Ahn, C., Shin, J. H., Lee, K. B., Kim, S. H., Chae, J. J., Hwang, D. Y., Lee, J. G., Namkoong, Y., & Lee, C. C. (2000). Novel mutations of the PKD1 gene in Korean patients with autosomal dominant polycystic kidney disease. [Research Support, Non-U.S. Gov't]. *Mutation research, 432*(1-2), 39-45.

Kimmel, C. B., Ballard, W. W., Kimmel, S. R., Ullmann, B., & Schilling, T. F. (1995). Stages of embryonic development of the zebrafish. [Research Support, U.S. Gov't, P.H.S.]. *Developmental dynamics : an official publication of the American Association of Anatomists, 203*(3), 253-310. doi: 10.1002/aja.1002030302

Kimmel, C. B., Warga, R. M., & Schilling, T. F. (1990). Origin and organization of the zebrafish fate map. *Development, 108*(4), 581-594.

Kitambi, S. S., Nilsson, E. S., Sekyrova, P., Ibarra, C., Tekeoh, G. N., Andang, M., Ernfors, P., & Uhlen, P. (2012). Small molecule screening platform for assessment of cardiovascular toxicity on adult zebrafish heart. *BMC Physiol, 12*, 3. doi: 10.1186/1472-6793-12-3

Klausner, R. D., Donaldson, J. G., & Lippincott-Schwartz, J. (1992). Brefeldin A: insights into the control of membrane traffic and organelle structure. *J Cell Biol, 116*(5), 1071-1080.

Kolpakova-Hart, E., Nicolae, C., Zhou, J., & Olsen, B. R. (2008). Col2-Cre recombinase is co-expressed with endogenous type II collagen in embryonic renal epithelium and drives development of polycystic kidney disease following inactivation of ciliary genes. *Matrix Biol, 27*(6), 505-512. doi: 10.1016/j.matbio.2008.05.002

Kottgen, M., Benzing, T., Simmen, T., Tauber, R., Buchholz, B., Feliciangeli, S., Huber, T. B., Schermer, B., Kramer-Zucker, A., Hopker, K., Simmen, K. C., Tschucke, C. C., Sandford, R., Kim, E., Thomas, G., & Walz, G. (2005). Trafficking of TRPP2 by PACS proteins represents a novel mechanism of ion channel regulation. [Research Support, Non-U.S. Gov't Research Support, U.S. Gov't, P.H.S.]. *The EMBO journal, 24*(4), 705-716. doi: 10.1038/sj.emboj.7600566

Kottgen, M., Buchholz, B., Garcia-Gonzalez, M. A., Kotsis, F., Fu, X., Doerken, M., Boehlke, C., Steffl, D., Tauber, R., Wegierski, T., Nitschke, R., Suzuki, M., Kramer-Zucker, A., Germino, G. G., Watnick, T., Prenen, J., Nilius, B., Kuehn, E. W., & Walz, G. (2008). TRPP2 and TRPV4 form a polymodal sensory channel complex. *J Cell Biol, 182*(3), 437-447. doi: 10.1083/jcb.200805124

Koulen, P., Cai, Y., Geng, L., Maeda, Y., Nishimura, S., Witzgall, R., Ehrlich, B. E., & Somlo, S. (2002). Polycystin-2 is an intracellular calcium release channel. *Nat Cell Biol, 4*(3), 191-197. doi: 10.1038/ncb754

Kramer, A., Sausville, J., Haririan, A., Bartlett, S., Cooper, M., & Phelan, M. (2009). Simultaneous bilateral native nephrectomy and living donor renal transplantation are successful for polycystic kidney disease: the University of Maryland experience. *J Urol, 181*(2), 724-728. doi: 10.1016/j.juro.2008.10.008

Kramer-Zucker, A. G., Olale, F., Haycraft, C. J., Yoder, B. K., Schier, A. F., & Drummond, I. A. (2005). Cilia-driven fluid flow in the zebrafish pronephros, brain and Kupffer's vesicle is required for normal organogenesis. *Development, 132*(8), 1907-1921. doi: 132/8/1907 [pii]

Kramer-Zucker, A. G., Wiessner, S., Jensen, A. M., & Drummond, I. A. (2005). Organization of the pronephric filtration apparatus in zebrafish requires Nephrin, Podocin and the FERM domain protein Mosaic eyes. *Dev Biol, 285*(2), 316-329. doi: S0012-1606(05)00442-2 [pii]

Kumai, Y., Kwong, R. W., & Perry, S. F. (2014). The role of cAMP-mediated intracellular signaling in regulating Na+ uptake in zebrafish larvae. *Am J Physiol Regul Integr Comp Physiol, 306*(1), R51-60. doi: 10.1152/ajpregu.00317.2013

Kyung, T., Lee, S., Kim, J. E., Cho, T., Park, H., Jeong, Y. M., Kim, D., Shin, A., Kim, S., Baek, J., Kim, J., Kim, N. Y., Woo, D., Chae, S., Kim, C. H., Shin, H. S., Han, Y. M., Kim, D., & Heo, W. D. (2015). Optogenetic control of endogenous Ca(2+) channels in vivo. *Nat Biotechnol, 33*(10), 1092-1096. doi: 10.1038/nbt.3350

Lager, D. J., Qian, Q., Bengal, R. J., Ishibashi, M., & Torres, V. E. (2001). The pck rat: a new model that resembles human autosomal dominant polycystic kidney and liver disease. [Research Support, U.S. Gov't, P.H.S.]. *Kidney Int, 59*(1), 126-136. doi: 10.1046/j.1523-1755.2001.00473.x

Lantinga-van Leeuwen, I. S., Dauwerse, J. G., Baelde, H. J., Leonhard, W. N., van de Wal, A., Ward, C. J., Verbeek, S., Deruiter, M. C., Breuning, M. H., de Heer, E., & Peters, D. J. (2004). Lowering of Pkd1 expression is sufficient to cause polycystic kidney disease. *Hum Mol Genet, 13*(24), 3069-3077. doi: ddh336 [pii]

Lantinga-van Leeuwen, I. S., Leonhard, W. N., van der Wal, A., Breuning, M. H., de Heer, E., & Peters, D. J. (2007). Kidney-specific inactivation of the Pkd1 gene induces rapid cyst formation in developing

kidneys and a slow onset of disease in adult mice. [Research Support, Non-U.S. Gov't]. *Hum Mol Genet, 16*(24), 3188-3196. doi: 10.1093/hmg/ddm299

Laping, N. J., Grygielko, E., Mathur, A., Butter, S., Bomberger, J., Tweed, C., Martin, W., Fornwald, J., Lehr, R., Harling, J., Gaster, L., Callahan, J. F., & Olson, B. A. (2002). Inhibition of transforming growth factor (TGF)-beta1-induced extracellular matrix with a novel inhibitor of the TGF-beta type I receptor kinase activity: SB-431542. *Mol Pharmacol, 62*(1), 58-64.

Le Corre, S., Eyre, D., & Drummond, I. A. (2014). Modulation of the Secretory Pathway Rescues Zebrafish Polycystic Kidney Disease Pathology. *Journal of the American Society of Nephrology, 25*(8), 1749-1759. doi: 10.1681/Asn.2013101060

Leonhard, W. N., Kunnen, S. J., Plugge, A. J., Pasternack, A., Jianu, S. B., Veraar, K., El Bouazzaoui, F., Hoogaars, W. M., Ten Dijke, P., Breuning, M. H., De Heer, E., Ritvos, O., & Peters, D. J. (2016). Inhibition of Activin Signaling Slows Progression of Polycystic Kidney Disease. *J Am Soc Nephrol.* doi: 10.1681/ASN.2015030287

Leuenroth, S. J., Bencivenga, N., Chahboune, H., Hyder, F., & Crews, C. M. (2010). Triptolide reduces cyst formation in a neonatal to adult transition Pkd1 model of ADPKD. *Nephrol Dial Transplant, 25*(7), 2187-2194. doi: 10.1093/ndt/gfp777

Leuenroth, S. J., Bencivenga, N., Igarashi, P., Somlo, S., & Crews, C. M. (2008). Triptolide reduces cystogenesis in a model of ADPKD. [Research Support, N.I.H., Extramural Research Support, Non-U.S. Gov't]. *J Am Soc Nephrol, 19*(9), 1659-1662. doi: 10.1681/ASN.2008030259

Leuenroth, S. J., Okuhara, D., Shotwell, J. D., Markowitz, G. S., Yu, Z., Somlo, S., & Crews, C. M. (2007). Triptolide is a traditional Chinese medicine-derived inhibitor of polycystic kidney disease. *Proc Natl Acad Sci U S A, 104*(11), 4389-4394. doi: 10.1073/pnas.0700499104

Levey, A. S., & Stevens, L. A. (2011). mTOR inhibitors and autosomal dominant polycystic kidney disease. *N Engl J Med, 364*(3), 287; author reply 287-289. doi: 10.1056/NEJMc1010845#SA2

Li, X. (2011). Epigenetics and autosomal dominant polycystic kidney disease. *Biochim Biophys Acta, 1812*(10), 1213-1218. doi: 10.1016/j.bbadis.2010.10.008

Li, X., Luo, Y., Starremans, P. G., McNamara, C. A., Pei, Y., & Zhou, J. (2005). Polycystin-1 and polycystin-2 regulate the cell cycle through the helix-loop-helix inhibitor Id2. *Nat Cell Biol, 7*(12), 1202-1212. doi: 10.1038/ncb1326

Li, Y., Wright, J. M., Qian, F., Germino, G. G., & Guggino, W. B. (2005). Polycystin 2 interacts with type I inositol 1,4,5-trisphosphate receptor to modulate intracellular Ca2+ signaling. *J Biol Chem, 280*(50), 41298-41306. doi: M510082200 [pii]

Li, Z., Bishop, A. C., Alyamani, M., Garcia, J. A., Dreicer, R., Bunch, D., Liu, J., Upadhyay, S. K., Auchus, R. J., & Sharifi, N. (2015). Conversion of abiraterone to D4A drives anti-tumour activity in prostate cancer. *Nature, 523*(7560), 347-351. doi: 10.1038/nature14406

Lin, F., Hiesberger, T., Cordes, K., Sinclair, A. M., Goldstein, L. S., Somlo, S., & Igarashi, P. (2003). Kidney-specific inactivation of the KIF3A subunit of kinesin-II inhibits renal ciliogenesis and produces polycystic kidney disease. *Proc Natl Acad Sci U S A, 100*(9), 5286-5291. doi: 10.1073/pnas.0836980100

Liu, S., Lu, W., Obara, T., Kuida, S., Lehoczky, J., Dewar, K., Drummond, I. A., & Beier, D. R. (2002). A defect in a novel Nek-family kinase causes cystic kidney disease in the mouse and in zebrafish. *Development, 129*(24), 5839-5846.

Liu, X., Wang, W., Hu, H., Tang, N., Zhang, C., Liang, W., & Wang, M. (2006). Smad3 specific inhibitor, naringenin, decreases the expression of extracellular matrix induced by TGF-beta1 in cultured rat hepatic stellate cells. *Pharm Res, 23*(1), 82-89. doi: 10.1007/s11095-005-9043-5

Liu, Y., An, W., & Gao, A. (2016). Protective effects of naringenin in cardiorenal syndrome. *J Surg Res, 203*(2), 416-423. doi: 10.1016/j.jss.2016.03.003

Liu, Y., Rajagopal, M., Lee, K., Battini, L., Flores, D., Gusella, G. L., Pao, A. C., & Rohatgi, R. (2012a). Prostaglandin E-2 mediates proliferation and chloride secretion in ADPKD cystic renal epithelia. *American Journal of Physiology-Renal Physiology, 303*(10), F1425-F1434. doi: 10.1152/ajprenal.00010.2012

Liu, Y., Rajagopal, M., Lee, K., Battini, L., Flores, D., Gusella, G. L., Pao, A. C., & Rohatgi, R. (2012b). Prostaglandin E(2) mediates proliferation and chloride secretion in ADPKD cystic renal epithelia. *Am J Physiol Renal Physiol, 303*(10), F1425-1434. doi: 10.1152/ajprenal.00010.2012

Loftus, H., & Ong, A. C. (2013). Cystic kidney diseases: many ways to form a cyst. [Review]. *Pediatric nephrology, 28*(1), 33-49. doi: 10.1007/s00467-012-2221-x

Low, S. H., Vasanth, S., Larson, C. H., Mukherjee, S., Sharma, N., Kinter, M. T., Kane, M. E., Obara, T., & Weimbs, T. (2006). Polycystin-1, STAT6, and P100 function in a pathway that transduces ciliary mechanosensation and is activated in polycystic kidney disease. *Dev Cell, 10*(1), 57-69. doi: 10.1016/j.devcel.2005.12.005

Lu, W., Peissel, B., Babakhanlou, H., Pavlova, A., Geng, L., Fan, X., Larson, C., Brent, G., & Zhou, J. (1997). Perinatal lethality with kidney and pancreas defects in mice with a targetted Pkd1 mutation. [Research Support, Non-U.S. Gov't Research Support, U.S. Gov't, P.H.S.]. *Nature genetics, 17*(2), 179-181. doi: 10.1038/ng1097-179

Lu, W., Shen, X., Pavlova, A., Lakkis, M., Ward, C. J., Pritchard, L., Harris, P. C., Genest, D. R., Perez-Atayde, A. R., & Zhou, J. (2001). Comparison of Pkd1-targeted mutants reveals that loss of polycystin-1 causes cystogenesis and bone defects. *Hum Mol Genet, 10*(21), 2385-2396.

Luo, Y., Vassilev, P. M., Li, X., Kawanabe, Y., & Zhou, J. (2003a). Native polycystin 2 functions as a plasma membrane Ca2+-permeable cation channel in renal epithelia. *Mol Cell Biol, 23*(7), 2600-2607.

Luo, Y., Vassilev, P. M., Li, X., Kawanabe, Y., & Zhou, J. (2003b). Native polycystin 2 functions as a plasma membrane Ca2+-permeable cation channel in renal epithelia. [Research Support, Non-U.S. Gov't Research Support, U.S. Gov't, P.H.S.]. *Molecular and cellular biology, 23*(7), 2600-2607.

Ma, M., Tian, X., Igarashi, P., Pazour, G. J., & Somlo, S. (2013). Loss of cilia suppresses cyst growth in genetic models of autosomal dominant polycystic kidney disease. [Research Support, N.I.H., Extramural]. *Nature genetics, 45*(9), 1004-1012. doi: 10.1038/ng.2715

Magistroni, R., He, N., Wang, K., Andrew, R., Johnson, A., Gabow, P., Dicks, E., Parfrey, P., Torra, R., San-Millan, J. L., Coto, E., Van Dijk, M., Breuning, M., Peters, D., Bogdanova, N., Ligabue, G., Albertazzi, A., Hateboer, N., Demetriou, K., Pierides, A., Deltas, C., St George-Hyslop, P., Ravine, D., & Pei, Y. (2003). Genotype-renal function correlation in type 2 autosomal dominant polycystic kidney disease. *J Am Soc Nephrol, 14*(5), 1164-1174.

Majumdar, A., & Drummond, I. A. (1999). Podocyte differentiation in the absence of endothelial cells as revealed in the zebrafish avascular mutant, cloche. *Dev Genet, 24*(3-4), 220-229. doi: 10.1002/(SICI)1520-6408(1999)24:3/4<220::AID-DVG5>3.0.CO;2-1 [pii]

Malhas, A. N., Abuknesha, R. A., & Price, R. G. (2002). Interaction of the leucine-rich repeats of polycystin-1 with extracellular matrix proteins: possible role in cell proliferation. [Research Support, Non-U.S. Gov't]. *J Am Soc Nephrol, 13*(1), 19-26.

Malicki, J., Schier, A. F., Solnica-Krezel, L., Stemple, D. L., Neuhauss, S. C., Stainier, D. Y., Abdelilah, S., Rangini, Z., Zwartkruis, F., & Driever, W. (1996). Mutations affecting development of the zebrafish ear. *Development, 123*, 275-283.

Mangolini, A., de Stephanis, L., & Aguiari, G. (2016). Role of calcium in polycystic kidney disease: From signaling to pathology. *World J Nephrol, 5*(1), 76-83. doi: 10.5527/wjn.v5.i1.76

Mangos, S., Lam, P. Y., Zhao, A., Liu, Y., Mudumana, S., Vasilyev, A., Liu, A., & Drummond, I. A. (2010). The ADPKD genes pkd1a/b and pkd2 regulate extracellular matrix formation. *Dis Model Mech, 3*(5-6), 354-365. doi: 10.1242/dmm.003194

Mangos, S., Liu, Y., & Drummond, I. A. (2007). Dynamic expression of the osmosensory channel trpv4 in multiple developing organs in zebrafish. *Gene Expr Patterns, 7*(4), 480-484. doi: 10.1016/j.modgep.2006.10.011

Maninger, N., Wolkowitz, O. M., Reus, V. I., Epel, E. S., & Mellon, S. H. (2009). Neurobiological and neuropsychiatric effects of dehydroepiandrosterone (DHEA) and DHEA sulfate (DHEAS). *Front Neuroendocrinol, 30*(1), 65-91. doi: 10.1016/j.yfrne.2008.11.002

Manning, G., Whyte, D. B., Martinez, R., Hunter, T., & Sudarsanam, S. (2002). The protein kinase complement of the human genome. *Science, 298*(5600), 1912-1934. doi: 10.1126/science.1075762

Mao, Z. G., Streets, A. J., & Ong, A. C. M. (2011). Thiazolidinediones inhibit MDCK cyst growth through disrupting oriented cell division and apicobasal polarity. *American Journal of Physiology-Renal Physiology, 300*(6), F1375-F1384. doi: 10.1152/ajprenal.00482.2010

Martin, J., Han, C., Gordon, L. A., Terry, A., Prabhakar, S., She, X., Xie, G., Hellsten, U., Chan, Y. M., Altherr, M., Couronne, O., Aerts, A., Bajorek, E., Black, S., Blumer, H., Branscomb, E., Brown, N. C., Bruno, W. J., Buckingham, J. M., Callen, D. F., Campbell, C. S., Campbell, M. L., Campbell, E. W., Caoile, C., Challacombe, J. F., Chasteen, L. A., Chertkov, O., Chi, H. C., Christensen, M., Clark, L. M., Cohn, J. D., Denys, M., Detter, J. C., Dickson, M., Dimitrijevic-Bussod, M., Escobar, J., Fawcett, J. J., Flowers, D., Fotopulos, D., Glavina, T., Gomez, M., Gonzales, E., Goodstein, D., Goodwin, L. A., Grady, D. L., Grigoriev, I., Groza, M., Hammon, N., Hawkins, T., Haydu, L., Hildebrand, C. E., Huang, W., Israni, S., Jett, J., Jewett, P. B., Kadner, K., Kimball, H., Kobayashi, A., Krawczyk, M. C., Leyba, T., Longmire, J. L., Lopez, F., Lou, Y., Lowry, S., Ludeman, T., Manohar, C. F., Mark, G. A., McMurray, K. L., Meincke, L. J., Morgan, J., Moyzis, R. K., Mundt, M. O., Munk, A. C., Nandkeshwar, R. D., Pitluck, S., Pollard, M., Predki, P., Parson-Quintana, B., Ramirez, L., Rash, S., Retterer, J., Ricke, D. O., Robinson, D. L., Rodriguez, A., Salamov, A., Saunders, E. H., Scott, D., Shough, T., Stallings, R. L., Stalvey, M., Sutherland, R. D., Tapia, R., Tesmer, J. G., Thayer, N., Thompson, L. S., Tice, H., Torney, D. C., Tran-Gyamfi, M., Tsai, M., Ulanovsky, L. E., Ustaszewska, A., Vo, N., White, P. S., Williams, A. L., Wills, P. L., Wu, J. R., Wu, K., Yang, J., Dejong, P., Bruce, D., Doggett, N. A., Deaven, L., Schmutz, J., Grimwood, J., Richardson, P., Rokhsar, D. S., Eichler, E. E., Gilna, P., Lucas, S. M., Myers, R. M., Rubin, E. M., & Pennacchio, L. A. (2004). The sequence and analysis of duplication-rich human chromosome 16. [Comparative Study Research Support, U.S. Gov't, Non-P.H.S.]. *Nature, 432*(7020), 988-994. doi: 10.1038/nature03187

McAteer, J. A., Dougherty, G. S., Gardner, K. D., Jr., & Evan, A. P. (1986). Scanning electron microscopy of kidney cells in culture: surface features of polarized epithelia. *Scan Electron Microsc*(Pt 3), 1135-1150.

McGrath, J., Somlo, S., Makova, S., Tian, X., & Brueckner, M. (2003). Two populations of node monocilia initiate left-right asymmetry in the mouse. *Cell, 114*(1), 61-73.

Mekahli, D., Parys, J. B., Bultynck, G., Missiaen, L., & De Smedt, H. (2013). Polycystins and cellular Ca2+ signaling. *Cell Mol Life Sci, 70*(15), 2697-2712. doi: 10.1007/s00018-012-1188-x

Mekahli, D., Sammels, E., Luyten, T., Welkenhuyzen, K., van den Heuvel, L. P., Levtchenko, E. N., Gijsbers, R., Bultynck, G., Parys, J. B., De Smedt, H., & Missiaen, L. (2012). Polycystin-1 and polycystin-2 are both required to amplify inositol-trisphosphate-induced Ca2+ release. *Cell Calcium, 51*(6), 452-458. doi: 10.1016/j.ceca.2012.03.002

Milutinovic, J., Rust, P. F., Fialkow, P. J., Agodoa, L. Y., Phillips, L. A., Rudd, T. G., & Sutherland, S. (1992). Intrafamilial phenotypic expression of autosomal dominant polycystic kidney disease. [Research Support, U.S. Gov't, P.H.S.]. *Am J Kidney Dis, 19*(5), 465-472.

Missiaen, L., Callewaert, G., De Smedt, H., & Parys, J. B. (2001). 2-Aminoethoxydiphenyl borate affects the inositol 1,4,5-trisphosphate receptor, the intracellular Ca2+ pump and the non-specific Ca2+ leak from the non-mitochondrial Ca2+ stores in permeabilized A7r5 cells. *Cell Calcium, 29*(2), 111-116. doi: 10.1054/ceca.2000.0163

Mochizuki, T., Wu, G., Hayashi, T., Xenophontos, S. L., Veldhuisen, B., Saris, J. J., Reynolds, D. M., Cai, Y., Gabow, P. A., Pierides, A., Kimberling, W. J., Breuning, M. H., Deltas, C. C., Peters, D. J., & Somlo, S. (1996). PKD2, a gene for polycystic kidney disease that encodes an integral membrane protein. *Science, 272*(5266), 1339-1342.

Muto, A., & Kawakami, K. (2013). Prey capture in zebrafish larvae serves as a model to study cognitive functions. *Frontiers in Neural Circuits, 7*. doi: ARTN 110

Muto, A., Ohkura, M., Abe, G., Nakai, J., & Kawakami, K. (2013). Real-time visualization of neuronal activity during perception. [Research Support, Non-U.S. Gov't]. *Curr Biol, 23*(4), 307-311. doi: 10.1016/j.cub.2012.12.040

Muto, S., Aiba, A., Saito, Y., Nakao, K., Nakamura, K., Tomita, K., Kitamura, T., Kurabayashi, M., Nagai, R., Higashihara, E., Harris, P. C., Katsuki, M., & Horie, S. (2002). Pioglitazone improves the phenotype and molecular defects of a targeted Pkd1 mutant. *Hum Mol Genet, 11*(15), 1731-1742.

Nagao, S., Kugita, M., Yoshihara, D., & Yamaguchi, T. (2012). Animal models for human polycystic kidney disease. [Research Support, Non-U.S. Gov't Review]. *Experimental animals / Japanese Association for Laboratory Animal Science, 61*(5), 477-488.

Nagao, S., Kusaka, M., Nishii, K., Marunouchi, T., Kurahashi, H., Takahashi, H., & Grantham, J. (2005). Androgen receptor pathway in rats with autosomal dominant polycystic kidney disease. [Research Support, N.I.H., Extramural Research Support, U.S. Gov't, P.H.S.]. *J Am Soc Nephrol, 16*(7), 2052-2062. doi: 10.1681/ASN.2004070595

Nagao, S., Morita, M., Kugita, M., Yoshihara, D., Yamaguchi, T., Kurahashi, H., Calvet, J. P., & Wallace, D. P. (2010). Polycystic kidney disease in Han:SPRD Cy rats is associated with elevated expression and mislocalization of SamCystin. *Am J Physiol Renal Physiol, 299*(5), F1078-1086. doi: 10.1152/ajprenal.00504.2009

Nagao, S., Nishii, K., Yoshihara, D., Kurahashi, H., Nagaoka, K., Yamashita, T., Takahashi, H., Yamaguchi, T., Calvet, J. P., & Wallace, D. P. (2008). Calcium channel inhibition accelerates polycystic kidney disease progression in the Cy/+ rat. *Kidney Int, 73*(3), 269-277. doi: 10.1038/sj.ki.5002629

Nagao, S., Yamaguchi, T., Kusaka, M., Maser, R. L., Takahashi, H., Cowley, B. D., & Grantham, J. J. (2003). Renal activation of extracellular signal-regulated kinase in rats with autosomal-dominant polycystic kidney disease. *Kidney Int, 63*(2), 427-437. doi: 10.1046/j.1523-1755.2003.00755.x

Nakai, J., Ohkura, M., & Imoto, K. (2001). A high signal-to-noise Ca(2+) probe composed of a single green fluorescent protein. *Nat Biotechnol, 19*(2), 137-141. doi: 10.1038/84397

Naldi, L., & Diphoorn, J. (2015). Seborrhoeic dermatitis of the scalp. *BMJ Clin Evid, 2015*.

Nasrallah, R., Hassouneh, R., & Hebert, R. L. (2014). Chronic kidney disease: targeting prostaglandin E2 receptors. *Am J Physiol Renal Physiol, 307*(3), F243-250. doi: 10.1152/ajprenal.00224.2014

Nauli, S. M., Alenghat, F. J., Luo, Y., Williams, E., Vassilev, P., Li, X., Elia, A. E., Lu, W., Brown, E. M., Quinn, S. J., Ingber, D. E., & Zhou, J. (2003). Polycystins 1 and 2 mediate mechanosensation in the primary cilium of kidney cells. *Nat Genet, 33*(2), 129-137. doi: 10.1038/ng1076

Nauli, S. M., Rossetti, S., Kolb, R. J., Alenghat, F. J., Consugar, M. B., Harris, P. C., Ingber, D. E., Loghman-Adham, M., & Zhou, J. (2006). Loss of polycystin-1 in human cyst-lining epithelia leads to ciliary dysfunction. [Research Support, N.I.H., Extramural Research Support, U.S. Gov't, Non-P.H.S.]. *Journal of the American Society of Nephrology : JASN, 17*(4), 1015-1025. doi: 10.1681/ASN.2005080830

Newby, L. J., Streets, A. J., Zhao, Y., Harris, P. C., Ward, C. J., & Ong, A. C. (2002). Identification, characterization, and localization of a novel kidney polycystin-1-polycystin-2 complex. [Research Support, Non-U.S. Gov't]. *The Journal of biological chemistry, 277*(23), 20763-20773. doi: 10.1074/jbc.M107788200

Nonaka, S., Tanaka, Y., Okada, Y., Takeda, S., Harada, A., Kanai, Y., Kido, M., & Hirokawa, N. (1998). Randomization of left-right asymmetry due to loss of nodal cilia generating leftward flow of extraembryonic fluid in mice lacking KIF3B motor protein. [Research Support, Non-U.S. Gov't]. *Cell, 95*(6), 829-837.

O'Brien, L. E., Zegers, M. M., & Mostov, K. E. (2002). Opinion: Building epithelial architecture: insights from three-dimensional culture models. *Nat Rev Mol Cell Biol, 3*(7), 531-537. doi: 10.1038/nrm859

O'Neill, T., Johnson, J. A., Webster, D., & Gray, C. A. (2013). The Canadian medicinal plant Heracleum maximum contains antimycobacterial diynes and furanocoumarins. *J Ethnopharmacol, 147*(1), 232-237. doi: 10.1016/j.jep.2013.03.009

Obara, T., Mangos, S., Liu, Y., Zhao, J., Wiessner, S., Kramer-Zucker, A. G., Olale, F., Schier, A. F., & Drummond, I. A. (2006). Polycystin-2 immunolocalization and function in zebrafish. *J Am Soc Nephrol, 17*(10), 2706-2718. doi: ASN.2006040412 [pii]

Ogborn, M. R., Crocker, J. F., & McCarthy, S. C. (1987). RU38486 prolongs survival in murine congenital polycystic kidney disease. *J Steroid Biochem, 28*(6), 783-784.

Okabe, Y., Shimada, T., Horikawa, T., Kinoshita, K., Koyama, K., Ichinose, K., Aburada, M., & Takahashi, K. (2014). Suppression of adipocyte hypertrophy by polymethoxyflavonoids isolated from Kaempferia parviflora. *Phytomedicine, 21*(6), 800-806. doi: 10.1016/j.phymed.2014.01.014

Omae, K., Ogawa, T., & Nitta, K. (2009). Influence of T-calcium channel blocker treatment on deterioration of renal function in chronic kidney disease. *Heart Vessels, 24*(4), 301-307. doi: 10.1007/s00380-008-1125-y

Omori, Y., Zhao, C., Saras, A., Mukhopadhyay, S., Kim, W., Furukawa, T., Sengupta, P., Veraksa, A., & Malicki, J. (2008). Elipsa is an early determinant of ciliogenesis that links the IFT particle to membrane-associated small GTPase Rab8. *Nat Cell Biol, 10*(4), 437-444. doi: 10.1038/ncb1706

Ong, A. C. (2000). Polycystin expression in the kidney and other tissues: complexity, consensus and controversy. *Exp Nephrol, 8*(4-5), 208-214. doi: 20670 [pii]

Ong, A. C., Devuyst, O., Knebelmann, B., Walz, G., & Diseases, E.-E. W. G. f. I. K. (2015). Autosomal dominant polycystic kidney disease: the changing face of clinical management. *Lancet, 385*(9981), 1993-2002. doi: 10.1016/S0140-6736(15)60907-2

Ong, A. C., & Harris, P. C. (2005a). Molecular pathogenesis of ADPKD: the polycystin complex gets complex. *Kidney Int, 67*(4), 1234-1247. doi: 10.1111/j.1523-1755.2005.00201.x

Ong, A. C., & Harris, P. C. (2005b). Molecular pathogenesis of ADPKD: the polycystin complex gets complex. [Research Support, Non-U.S. Gov't]. *Kidney international, 67*(4), 1234-1247. doi: 10.1111/j.1523-1755.2005.00201.x

Ong, A. C., & Wagner, B. (2005). Detection of proximal tubular motile cilia in a patient with renal sarcoidosis associated with hypercalcemia. [Case Reports]. *Am J Kidney Dis, 45*(6), 1096-1099.

Otto, E. A., Schermer, B., Obara, T., O'Toole, J. F., Hiller, K. S., Mueller, A. M., Ruf, R. G., Hoefele, J., Beekmann, F., Landau, D., Foreman, J. W., Goodship, J. A., Strachan, T., Kispert, A., Wolf, M. T., Gagnadoux, M. F., Nivet, H., Antignac, C., Walz, G., Drummond, I. A., Benzing, T., & Hildebrandt, F. (2003). Mutations in INVS encoding inversin cause nephronophthisis type 2, linking renal cystic disease to the function of primary cilia and left-right axis determination. *Nat Genet, 34*(4), 413-420. doi: 10.1038/ng1217

Owens, K. N., Santos, F., Roberts, B., Linbo, T., Coffin, A. B., Knisely, A. J., Simon, J. A., Rubel, E. W., & Raible, D. W. (2008). Identification of genetic and chemical modulators of zebrafish mechanosensory hair cell death. [Research Support, N.I.H., Extramural Research Support, Non-U.S. Gov't]. *PLoS Genet, 4*(2), e1000020. doi: 10.1371/journal.pgen.1000020

Paavola, J., Schliffke, S., Rossetti, S., Kuo, I. Y., Yuan, S., Sun, Z., Harris, P. C., Torres, V. E., & Ehrlich, B. E. (2013). Polycystin-2 mutations lead to impaired calcium cycling in the heart and predispose to dilated cardiomyopathy. *J Mol Cell Cardiol, 58*, 199-208. doi: 10.1016/j.yjmcc.2013.01.015

Park, S. O., Lee, Y. J., Seki, T., Hong, K. H., Fliess, N., Jiang, Z., Park, A., Wu, X., Kaartinen, V., Roman, B. L., & Oh, S. P. (2008). ALK5- and TGFBR2-independent role of ALK1 in the pathogenesis of hereditary hemorrhagic telangiectasia type 2. *Blood, 111*(2), 633-642. doi: 10.1182/blood-2007-08-107359

Parker, E., Newby, L. J., Sharpe, C. C., Rossetti, S., Streets, A. J., Harris, P. C., O'Hare, M. J., & Ong, A. C. M. (2007). Hyperproliferation of PKD1 cystic cells is induced by insulin-like growth factor-1 activation of the Ras/Raf signalling system. *Kidney International, 72*(2), 157-165. doi: 10.1038/sj.ki.5002229

Passalacqua, T. G., Torres, F. A., Nogueira, C. T., de Almeida, L., Del Cistia, M. L., dos Santos, M. B., Regasini, L. O., Graminha, M. A., Marchetto, R., & Zottis, A. (2015). The 2',4'-dihydroxychalcone could be explored to develop new inhibitors against the glycerol-3-phosphate dehydrogenase from Leishmania species. *Bioorg Med Chem Lett, 25*(17), 3564-3568. doi: 10.1016/j.bmcl.2015.06.085

Paul, B. M., Consugar, M. B., Ryan Lee, M., Sundsbak, J. L., Heyer, C. M., Rossetti, S., Kubly, V. J., Hopp, K., Torres, V. E., Coto, E., Clementi, M., Bogdanova, N., de Almeida, E., Bichet, D. G., & Harris, P. C. (2014). Evidence of a third ADPKD locus is not supported by re-analysis of designated PKD3 families. *Kidney Int, 85*(2), 383-392. doi: 10.1038/ki.2013.227

Pavel, M. A., Lv, C. X., Ng, C., Yang, L., Kashyap, P., Lam, C., Valentino, V., Fung, H. Y., Campbell, T., Moller, S. G., Zenisek, D., Holtzman, N. G., & Yu, Y. (2016). Function and regulation of TRPP2 ion channel revealed by a gain-of-function mutant. *Proceedings of the National Academy of Sciences of the United States of America, 113*(17), E2363-E2372. doi: 10.1073/pnas.1517066113

Pazour, G. J. (2004). Intraflagellar transport and cilia-dependent renal disease: the ciliary hypothesis of polycystic kidney disease. *J Am Soc Nephrol, 15*(10), 2528-2536. doi: 10.1097/01.ASN.0000141055.57643.E0

Pazour, G. J., San Agustin, J. T., Follit, J. A., Rosenbaum, J. L., & Witman, G. B. (2002). Polycystin-2 localizes to kidney cilia and the ciliary level is elevated in orpk mice with polycystic kidney disease. [Letter Research Support, U.S. Gov't, P.H.S.]. *Curr Biol, 12*(11), R378-380.

Peal, D. S., Mills, R. W., Lynch, S. N., Mosley, J. M., Lim, E., Ellinor, P. T., January, C. T., Peterson, R. T., & Milan, D. J. (2011). Novel chemical suppressors of long QT syndrome identified by an in vivo functional screen. [Comparative Study

Research Support, N.I.H., Extramural]. *Circulation, 123*(1), 23-30. doi: 10.1161/CIRCULATIONAHA.110.003731

Pei, Y., Lan, Z., Wang, K., Garcia-Gonzalez, M., He, N., Dicks, E., Parfrey, P., Germino, G., & Watnick, T. (2012). A missense mutation in PKD1 attenuates the severity of renal disease. *Kidney Int, 81*(4), 412-417. doi: 10.1038/ki.2011.370

Pei, Y., Paterson, A. D., Wang, K. R., He, N., Hefferton, D., Watnick, T., Germino, G. G., Parfrey, P., Somlo, S., & St George-Hyslop, P. (2001). Bilineal disease and trans-heterozygotes in autosomal dominant polycystic kidney disease. [Research Support, Non-U.S. Gov't]. *American journal of human genetics, 68*(2), 355-363.

Pei, Y., Watnick, T., He, N., Wang, K., Liang, Y., Parfrey, P., Germino, G., & St George-Hyslop, P. (1999). Somatic PKD2 mutations in individual kidney and liver cysts support a "two-hit" model of cystogenesis in type 2 autosomal dominant polycystic kidney disease. *J Am Soc Nephrol, 10*(7), 1524-1529.

Pennekamp, P., Karcher, C., Fischer, A., Schweickert, A., Skryabin, B., Horst, J., Blum, M., & Dworniczak, B. (2002). The ion channel polycystin-2 is required for left-right axis determination in mice. *Curr Biol, 12*(11), 938-943. doi: S0960982202008692 [pii]

Perez-Aso, M., Fernandez, P., Mediero, A., Chan, E. S., & Cronstein, B. N. (2014). Adenosine 2A receptor promotes collagen production by human fibroblasts via pathways involving cyclic AMP and AKT but independent of Smad2/3. *FASEB J, 28*(2), 802-812. doi: 10.1096/fj.13-241646

Perner, B., Englert, C., & Bollig, F. (2007). The Wilms tumor genes wt1a and wt1b control different steps during formation of the zebrafish pronephros. [Research Support, Non-U.S. Gov't]. *Dev Biol, 309*(1), 87-96. doi: 10.1016/j.ydbio.2007.06.022

Perrone, R. D., Ruthazer, R., & Terrin, N. C. (2001). Survival after end-stage renal disease in autosomal dominant polycystic kidney disease: contribution of extrarenal complications to mortality. *Am J Kidney Dis, 38*(4), 777-784. doi: 10.1053/ajkd.2001.27720

Persu, A., Duyme, M., Pirson, Y., Lens, X. M., Messiaen, T., Breuning, M. H., Chauveau, D., Levy, M., Grunfeld, J. P., & Devuyst, O. (2004). Comparison between siblings and twins supports a role for modifier genes in ADPKD. [Comparative Study Research Support, Non-U.S. Gov't Twin Study]. *Kidney international, 66*(6), 2132-2136. doi: 10.1111/j.1523-1755.2004.66003.x

Peterson, R. T., & Fishman, M. C. (2011). Designing zebrafish chemical screens. *Methods in cell biology, 105*, 525-541. doi: 10.1016/B978-0-12-381320-6.00023-0

Piontek, K., Menezes, L. F., Garcia-Gonzalez, M. A., Huso, D. L., & Germino, G. G. (2007). A critical developmental switch defines the kinetics of kidney cyst formation after loss of Pkd1. *Nat Med, 13*(12), 1490-1495. doi: 10.1038/nm1675

Praetorius, H. A., Frokiaer, J., Nielsen, S., & Spring, K. R. (2003). Bending the primary cilium opens Ca2+-sensitive intermediate-conductance K+ channels in MDCK cells. *J Membr Biol, 191*(3), 193-200. doi: 10.1007/s00232-002-1055-z

Praetorius, H. A., & Spring, K. R. (2001). Bending the MDCK cell primary cilium increases intracellular calcium. *J Membr Biol, 184*(1), 71-79.

Praetorius, H. A., & Spring, K. R. (2003). Removal of the MDCK cell primary cilium abolishes flow sensing. *J Membr Biol, 191*(1), 69-76. doi: 10.1007/s00232-002-1042-4

Pritchard, L., Sloane-Stanley, J. A., Sharpe, J. A., Aspinwall, R., Lu, W., Buckle, V., Strmecki, L., Walker, D., Ward, C. J., Alpers, C. E., Zhou, J., Wood, W. G., & Harris, P. C. (2000). A human PKD1 transgene generates functional polycystin-1 in mice and is associated with a cystic phenotype. *Hum Mol Genet, 9*(18), 2617-2627.

Qian, F., Germino, F. J., Cai, Y., Zhang, X., Somlo, S., & Germino, G. G. (1997). PKD1 interacts with PKD2 through a probable coiled-coil domain. *Nat Genet, 16*(2), 179-183. doi: 10.1038/ng0697-179

Qian, F., Watnick, T. J., Onuchic, L. F., & Germino, G. G. (1996). The molecular basis of focal cyst formation in human autosomal dominant polycystic kidney disease type I. [Research Support, Non-U.S. Gov't

Qian, F., Wei, W., Germino, G., & Oberhauser, A. (2005). The nanomechanics of polycystin-1 extracellular region. *J Biol Chem, 280*(49), 40723-40730. doi: 10.1074/jbc.M509650200

Qian, Q., Hunter, L. W., Li, M., Marin-Padilla, M., Prakash, Y. S., Somlo, S., Harris, P. C., Torres, V. E., & Sieck, G. C. (2003). Pkd2 haploinsufficiency alters intracellular calcium regulation in vascular smooth muscle cells. *Hum Mol Genet, 12*(15), 1875-1880.

Ramasubbu, K., Gretz, N., & Bachmann, S. (1998). Increased epithelial cell proliferation and abnormal extracellular matrix in rat polycystic kidney disease. *J Am Soc Nephrol, 9*(6), 937-945.

Ramirez-Yanez, G. O., Hamlet, S., Jonarta, A., Seymour, G. J., & Symons, A. L. (2006). Prostaglandin E2 enhances transforming growth factor-beta 1 and TGF-beta receptors synthesis: an in vivo and in vitro study. *Prostaglandins Leukot Essent Fatty Acids, 74*(3), 183-192. doi: 10.1016/j.plefa.2006.01.003

Raphael, K. L., Strait, K. A., Stricklett, P. K., Miller, R. L., Nelson, R. D., Piontek, K. B., Germino, G. G., & Kohan, D. E. (2009). Inactivation of Pkd1 in principal cells causes a more severe cystic kidney disease than in intercalated cells. *Kidney Int, 75*(6), 626-633. doi: 10.1038/ki.2008.659

Rees, S., Kittikulsuth, W., Roos, K., Strait, K. A., Van Hoek, A., & Kohan, D. E. (2014). Adenylyl cyclase 6 deficiency ameliorates polycystic kidney disease. *J Am Soc Nephrol, 25*(2), 232-237. doi: 10.1681/ASN.2013010077

Rennekamp, A. J., & Peterson, R. T. (2015). 15 years of zebrafish chemical screening. *Curr Opin Chem Biol, 24*, 58-70. doi: 10.1016/j.cbpa.2014.10.025

Ridges, S., Heaton, W. L., Joshi, D., Choi, H., Eiring, A., Batchelor, L., Choudhry, P., Manos, E. J., Sofla, H., Sanati, A., Welborn, S., Agarwal, A., Spangrude, G. J., Miles, R. R., Cox, J. E., Frazer, J. K., Deininger, M., Balan, K., Sigman, M., Muschen, M., Perova, T., Johnson, R., Montpellier, B., Guidos, C. J., Jones, D. A., & Trede, N. S. (2012). Zebrafish screen identifies novel compound with selective toxicity against leukemia. *Blood, 119*(24), 5621-5631. doi: 10.1182/blood-2011-12-398818

Riera, M., Burtey, S., & Fontes, M. (2006). Transcriptome analysis of a rat PKD model: Importance of genes involved in extracellular matrix metabolism. *Kidney Int, 69*(9), 1558-1563. doi: 10.1038/sj.ki.5000309

Robu, M. E., Larson, J. D., Nasevicius, A., Beiraghi, S., Brenner, C., Farber, S. A., & Ekker, S. C. (2007). p53 activation by knockdown technologies. *PLoS Genet, 3*(5), e78. doi: 10.1371/journal.pgen.0030078

Rogers, T. B., Inesi, G., Wade, R., & Lederer, W. J. (1995). Use of thapsigargin to study Ca2+ homeostasis in cardiac cells. *Bioscience Reports, 15*(5), 341-349. doi: Doi 10.1007/Bf01788366

Roitbak, T., Ward, C. J., Harris, P. C., Bacallao, R., Ness, S. A., & Wandinger-Ness, A. (2004). A polycystin-1 multiprotein complex is disrupted in polycystic kidney disease cells. [Research Support, Non-U.S. Gov't]

Research Support, U.S. Gov't, P.H.S.]. *Molecular biology of the cell, 15*(3), 1334-1346. doi: 10.1091/mbc.E03-05-0296

Rossetti, S., Chauveau, D., Kubly, V., Slezak, J. M., Saggar-Malik, A. K., Pei, Y., Ong, A. C., Stewart, F., Watson, M. L., Bergstralh, E. J., Winearls, C. G., Torres, V. E., & Harris, P. C. (2003). Association of mutation position in polycystic kidney disease 1 (PKD1) gene and development of a vascular phenotype. *Lancet, 361*(9376), 2196-2201. doi: S0140-6736(03)13773-7 [pii]

Rossi, A., Kontarakis, Z., Gerri, C., Nolte, H., Holper, S., Kruger, M., & Stainier, D. Y. (2015). Genetic compensation induced by deleterious mutations but not gene knockdowns. *Nature, 524*(7564), 230-233. doi: 10.1038/nature14580

Rothschild, S. C., Francescatto, L., Drummond, I. A., & Tombes, R. M. (2011). CaMK-II is a PKD2 target that promotes pronephric kidney development and stabilizes cilia. *Development, 138*(16), 3387-3397. doi: 10.1242/dev.066340

Roxo-Rosa, M., Jacinto, R., Sampaio, P., & Lopes, S. S. (2015). The zebrafish Kupffer's vesicle as a model system for the molecular mechanisms by which the lack of Polycystin-2 leads to stimulation of CFTR. *Biol Open, 4*(11), 1356-1366. doi: 10.1242/bio.014076

Roy, M. W., Guthrie, G. P., Jr., Holladay, F. P., & Kotchen, T. A. (1983). Effects of verapamil on renin and aldosterone in the dog and rat. *Am J Physiol, 245*(4), E410-416.

Rundle, D. R., Gorbsky, G., & Tsiokas, L. (2004). PKD2 interacts and co-localizes with mDia1 to mitotic spindles of dividing cells: role of mDia1 IN PKD2 localization to mitotic spindles. *J Biol Chem, 279*(28), 29728-29739. doi: 10.1074/jbc.M400544200

Russ, M., Martinez, R., Ali, H., & Steimle, P. A. (2006). Naringenin is a novel inhibitor of Dictyostelium cell proliferation and cell migration. *Biochemical and Biophysical Research Communications, 345*(1), 516-522. doi: 10.1016/j.bbrc.2006.04.047

Saadi-Kheddouci, S., Berrebi, D., Romagnolo, B., Cluzeaud, F., Peuchmaur, M., Kahn, A., Vandewalle, A., & Perret, C. (2001). Early development of polycystic kidney disease in transgenic mice expressing an activated mutant of the beta-catenin gene. *Oncogene, 20*(42), 5972-5981. doi: 10.1038/sj.onc.1204825

Salas, A. L., Alberto, M. R., Zampini, I. C., Cuello, A. S., Maldonado, L., Rios, J. L., Schmeda-Hirschmann, G., & Isla, M. I. (2016). Biological activities of polyphenols-enriched propolis from Argentina arid regions. *Phytomedicine, 23*(1), 27-31. doi: 10.1016/j.phymed.2015.11.007

Sandhu, S., Silbiger, S. R., Lei, J., & Neugarten, J. (1997). Effects of sex hormones on fluid and solute transport in Madin-Darby canine kidney cells. *Kidney Int, 51*(5), 1535-1539.

Saruta, T., Hayashi, K., Ogihara, T., Nakao, K., Fukui, T., Fukiyama, K., & Group, C.-J. S. (2009). Effects of candesartan and amlodipine on cardiovascular events in hypertensive patients with chronic kidney disease: subanalysis of the CASE-J Study. *Hypertens Res, 32*(6), 505-512. doi: 10.1038/hr.2009.44

Saydmohammed, M., Vollmer, L. L., Onuoha, E. O., Vogt, A., & Tsang, M. (2011). A high-content screening assay in transgenic zebrafish identifies two novel activators of fgf signaling. *Birth Defects Res C Embryo Today, 93*(3), 281-287. doi: 10.1002/bdrc.20216

Schafer, K., Bader, M., Gretz, N., Oberbaumer, I., & Bachmann, S. (1994). Focal overexpression of collagen IV characterizes the initiation of epithelial changes in polycystic kidney disease. *Exp Nephrol, 2*(3), 190-195.

Scheffers, M. S., van der Bent, P., Prins, F., Spruit, L., Breuning, M. H., Litvinov, S. V., de Heer, E., & Peters, D. J. (2000). Polycystin-1, the product of the polycystic kidney disease 1 gene, co-localizes with desmosomes in MDCK cells. [Research Support, Non-U.S. Gov't]. *Hum Mol Genet, 9*(18), 2743-2750.

Schiller, V., Wichmann, A., Kriehuber, R., Schafers, C., Fischer, R., & Fenske, M. (2013). Transcriptome alterations in zebrafish embryos after exposure to environmental estrogens and anti-androgens can reveal endocrine disruption. *Reprod Toxicol, 42*, 210-223. doi: 10.1016/j.reprotox.2013.09.003

Schiller, V., Zhang, X., Hecker, M., Schafers, C., Fischer, R., & Fenske, M. (2014). Species-specific considerations in using the fish embryo test as an alternative to identify endocrine disruption. *Aquat Toxicol, 155*, 62-72. doi: 10.1016/j.aquatox.2014.06.005

Schottenfeld, J., Sullivan-Brown, J., & Burdine, R. D. (2007). Zebrafish curly up encodes a Pkd2 ortholog that restricts left-side-specific expression of southpaw. *Development, 134*(8), 1605-1615. doi: dev.02827 [pii]

Schulte-Merker, S., & Stainier, D. Y. (2014). Out with the old, in with the new: reassessing morpholino knockdowns in light of genome editing technology. *Development, 141*(16), 3103-3104. doi: 10.1242/dev.112003

Scragg, J. L., Jones, R. D., Channer, K. S., Jones, T. H., & Peers, C. (2004). Testosterone is a potent inhibitor of L-type Ca(2+) channels. *Biochem Biophys Res Commun, 318*(2), 503-506. doi: 10.1016/j.bbrc.2004.04.054

Seamon, K. B., & Daly, J. W. (1981). Forskolin: a unique diterpene activator of cyclic AMP-generating systems. *J Cyclic Nucleotide Res, 7*(4), 201-224.

Seiler, C., & Pack, M. (2011). Transgenic labeling of the zebrafish pronephric duct and tubules using a promoter from the enpep gene. *Gene Expr Patterns, 11*(1-2), 118-121. doi: 10.1016/j.gep.2010.10.002

Serra, A. L., Poster, D., Kistler, A. D., Krauer, F., Raina, S., Young, J., Rentsch, K. M., Spanaus, K. S., Senn, O., Kristanto, P., Scheffel, H., Weishaupt, D., & Wuthrich, R. P. (2010). Sirolimus and kidney growth in autosomal dominant polycystic kidney disease. [Randomized Controlled Trial Research Support, Non-U.S. Gov't]. *N Engl J Med, 363*(9), 820-829. doi: 10.1056/NEJMoa0907419

Sgaragli, G. P., Valoti, M., Gorelli, B., Fusi, F., Palmi, M., & Mantovani, P. (1993). Calcium antagonist and antiperoxidant properties of some hindered phenols. *Br J Pharmacol, 110*(1), 369-377.

Sharifi, N. (2012). The 5alpha-androstanedione pathway to dihydrotestosterone in castration-resistant prostate cancer. *J Investig Med, 60*(2), 504-507. doi: 10.231/JIM.0b013e31823874a4

Sheng, Y., Zou, M., Wang, Y., & Li, Q. (2015). 2',4'-dihydroxychalcone, a flavonoid isolated from Herba oxytropis, suppresses PC-3 human prostate cancer cell growth by induction of apoptosis. *Oncol Lett, 10*(6), 3737-3741. doi: 10.3892/ol.2015.3795

Shibazaki, S., Yu, Z., Nishio, S., Tian, X., Thomson, R. B., Mitobe, M., Louvi, A., Velazquez, H., Ishibe, S., Cantley, L. G., Igarashi, P., & Somlo, S. (2008). Cyst formation and activation of the extracellular regulated kinase pathway after kidney specific inactivation of Pkd1. *Hum Mol Genet, 17*(11), 1505-1516. doi: 10.1093/hmg/ddn039

Singh, J., Chuaqui, C. E., Boriack-Sjodin, P. A., Lee, W. C., Pontz, T., Corbley, M. J., Cheung, H. K., Arduini, R. M., Mead, J. N., Newman, M. N., Papadatos, J. L., Bowes, S., Josiah, S., & Ling, L. E. (2003). Successful shape-based virtual screening: The discovery of a potent inhibitor of the type I TGF beta receptor kinase (T beta RI). *Bioorganic & Medicinal Chemistry Letters, 13*(24), 4355-4359. doi: 10.1016/j.bmcl.2003.09.028

Singhuber, J., Baburin, I., Ecker, G. F., Kopp, B., & Hering, S. (2011). Insights into structure-activity relationship of GABAA receptor modulating coumarins and furanocoumarins. *Eur J Pharmacol, 668*(1-2), 57-64. doi: 10.1016/j.ejphar.2011.06.034

Smith, L. A., Bukanov, N. O., Husson, H., Russo, R. J., Barry, T. C., Taylor, A. L., Beier, D. R., & Ibraghimov-Beskrovnaya, O. (2006). Development of polycystic kidney disease in juvenile cystic kidney mice: insights into pathogenesis, ciliary abnormalities, and common features with human disease. *J Am Soc Nephrol, 17*(10), 2821-2831. doi: 10.1681/ASN.2006020136

Somlo, S., Rutecki, G., Giuffra, L. A., Reeders, S. T., Cugino, A., & Whittier, F. C. (1993). A kindred exhibiting cosegregation of an overlap connective tissue disorder and the chromosome 16 linked form of autosomal dominant polycystic kidney disease. *J Am Soc Nephrol, 4*(6), 1371-1378.

Spithoven, E. M., Kramer, A., Meijer, E., Orskov, B., Wanner, C., Abad, J. M., Areste, N., de la Torre, R. A., Caskey, F., Couchoud, C., Finne, P., Heaf, J., Hoitsma, A., de Meester, J., Pascual, J., Postorino, M., Ravani, P., Zurriaga, O., Jager, K. J., Gansevoort, R. T., Registry, E.-E., Euro, C. C., & Wgikd. (2014). Renal replacement therapy for autosomal dominant polycystic kidney disease (ADPKD) in Europe: prevalence and survival--an analysis of data from the ERA-EDTA Registry. *Nephrol Dial Transplant, 29 Suppl 4*, iv15-25. doi: 10.1093/ndt/gfu017

Stein, A. C., Alvarez, S., Avancini, C., Zacchino, S., & von Poser, G. (2006). Antifungal activity of some coumarins obtained from species of Pterocaulon (Asteraceae). *J Ethnopharmacol, 107*(1), 95-98. doi: 10.1016/j.jep.2006.02.009

Steinhausen, M., Blum, M., Fleming, J. T., Holz, F. G., Parekh, N., & Wiegman, D. L. (1989). Visualization of renal autoregulation in the split hydronephrotic kidney of rats. *Kidney Int, 35*(5), 1151-1160.

Stewart, J. H. (1994). End-stage renal failure appears earlier in men than in women with polycystic kidney disease. *Am J Kidney Dis, 24*(2), 181-183.

Stommel, E. W., Stephens, R. E., & Alkon, D. L. (1980). Motile statocyst cilia transmit rather than directly transduce mechanical stimuli. [Research Support, U.S. Gov't, P.H.S.]. *The Journal of cell biology, 87*(3 Pt 1), 652-662.

Streets, A. J., Moon, D. J., Kane, M. E., Obara, T., & Ong, A. C. (2006). Identification of an N-terminal glycogen synthase kinase 3 phosphorylation site which regulates the functional localization of polycystin-2 in vivo and in vitro. *Hum Mol Genet, 15*(9), 1465-1473. doi: ddl070 [pii]

Streets, A. J., Newby, L. J., O'Hare, M. J., Bukanov, N. O., Ibraghimov-Beskrovnaya, O., & Ong, A. C. (2003). Functional analysis of PKD1 transgenic lines reveals a direct role for polycystin-1 in mediating cell-cell adhesion. [Research Support, Non-U.S. Gov't]. *Journal of the American Society of Nephrology : JASN, 14*(7), 1804-1815.

Streets, A. J., Wagner, B. E., Harris, P. C., Ward, C. J., & Ong, A. C. (2009). Homophilic and heterophilic polycystin 1 interactions regulate E-cadherin recruitment and junction assembly in MDCK cells. *J Cell Sci, 122*(Pt 9), 1410-1417. doi: 10.1242/jcs.045021

Subramanian, B., Ko, W. C., Yadav, V., DesRochers, T. M., Perrone, R. D., Zhou, J., & Kaplan, D. L. (2012). The regulation of cystogenesis in a tissue engineered kidney disease system by abnormal matrix interactions. [Research Support, N.I.H., Extramural
Research Support, Non-U.S. Gov't]. *Biomaterials, 33*(33), 8383-8394. doi: 10.1016/j.biomaterials.2012.08.020

Sullivan-Brown, J., Schottenfeld, J., Okabe, N., Hostetter, C. L., Serluca, F. C., Thiberge, S. Y., & Burdine, R. D. (2008). Zebrafish mutations affecting cilia motility share similar cystic phenotypes and suggest a mechanism of cyst formation that differs from pkd2 morphants. *Dev Biol, 314*(2), 261-275. doi: 10.1016/j.ydbio.2007.11.025

Sun, Z., Amsterdam, A., Pazour, G. J., Cole, D. G., Miller, M. S., & Hopkins, N. (2004). A genetic screen in zebrafish identifies cilia genes as a principal cause of cystic kidney. *Development, 131*(16), 4085-4093. doi: 10.1242/dev.01240
dev.01240 [pii]

Sun, Z., & Hopkins, N. (2001). vhnf1, the MODY5 and familial GCKD-associated gene, regulates regional specification of the zebrafish gut, pronephros, and hindbrain. *Genes Dev, 15*(23), 3217-3229. doi: 10.1101/gad946701

Sussman, C. R., Ward, C. J., Leightner, A. C., Smith, J. L., Agarwal, R., Harris, P. C., & Torres, V. E. (2014). Phosphodiesterase 1A modulates cystogenesis in zebrafish. *J Am Soc Nephrol, 25*(10), 2222-2230. doi: 10.1681/ASN.2013040421

Sussman, C. R., Zhao, J., Plata, C., Lu, J., Daly, C., Angle, N., DiPiero, J., Drummond, I. A., Liang, J. O., Boron, W. F., Romero, M. F., & Chang, M. H. (2009). Cloning, localization, and functional expression of the electrogenic Na+ bicarbonate cotransporter (NBCe1) from zebrafish. *Am J Physiol Cell Physiol, 297*(4), C865-875. doi: 10.1152/ajpcell.00679.2008

Sutters, M., & Germino, G. G. (2003). Autosomal dominant polycystic kidney disease: molecular genetics and pathophysiology. *J Lab Clin Med, 141*(2), 91-101. doi: 10.1067/mlc.2003.13

Szebenyi, K., Furedi, A., Kolacsek, O., Csohany, R., Prokai, A., Kis-Petik, K., Szabo, A., Bosze, Z., Bender, B., Tovari, J., Enyedi, A., Orban, T. I., Apati, A., & Sarkadi, B. (2015). Visualization of Calcium Dynamics in Kidney Proximal Tubules. *J Am Soc Nephrol, 26*(11), 2731-2740. doi: 10.1681/ASN.2014070705

Takahashi, A., Tabuchi, M., Suzuki, W., Iizuka, S., Nagata, M., Ikeya, Y., Takeda, S., Shimada, T., & Aburada, M. (2006). Insulin resistance and low sympathetic nerve activity in the Tsumura Suzuki obese diabetic mouse: a new model of spontaneous type 2 diabetes mellitus and obesity. *Metabolism, 55*(12), 1664-1669. doi: 10.1016/j.metabol.2006.08.007

Takakura, A., Contrino, L., Beck, A. W., & Zhou, J. (2008). Pkd1 inactivation induced in adulthood produces focal cystic disease. *J Am Soc Nephrol, 19*(12), 2351-2363. doi: 10.1681/ASN.2007101139
ASN.2007101139 [pii]

Takakura, A., Contrino, L., Zhou, X., Bonventre, J. V., Sun, Y., Humphreys, B. D., & Zhou, J. (2009). Renal injury is a third hit promoting rapid development of adult polycystic kidney disease. [Research Support, N.I.H., Extramural
Research Support, Non-U.S. Gov't]. *Hum Mol Genet, 18*(14), 2523-2531. doi: 10.1093/hmg/ddp147

Tao, Y., Kim, J., Faubel, S., Wu, J. C., Falk, S. A., Schrier, R. W., & Edelstein, C. L. (2005). Caspase inhibition reduces tubular apoptosis and proliferation and slows disease progression in polycystic kidney disease. *Proc Natl Acad Sci U S A, 102*(19), 6954-6959. doi: 10.1073/pnas.0408518102

Tao, Y., Kim, J., Schrier, R. W., & Edelstein, C. L. (2005). Rapamycin markedly slows disease progression in a rat model of polycystic kidney disease. [Research Support, N.I.H., Extramural Research Support, U.S. Gov't, P.H.S.]. *J Am Soc Nephrol, 16*(1), 46-51. doi: 10.1681/ASN.2004080660

The International Polycystic Kidney Disease Consortium. (1995). Polycystic kidney disease: the complete structure of the PKD1 gene and its protein. The International Polycystic Kidney Disease Consortium. [Research Support, Non-U.S. Gov't Research Support, U.S. Gov't, P.H.S.]. *Cell, 81*(2), 289-298.

Thisse, C., & Thisse, B. (2008). High-resolution in situ hybridization to whole-mount zebrafish embryos. *Nat Protoc, 3*(1), 59-69. doi: 10.1038/nprot.2007.514

Tian, M., & Schiemann, W. P. (2010). PGE2 receptor EP2 mediates the antagonistic effect of COX-2 on TGF-beta signaling during mammary tumorigenesis. *FASEB J, 24*(4), 1105-1116. doi: 10.1096/fj.09-141341

Torres, R. A., Almarsson, O., & Bruice, T. C. (1996). Molecular mechanics calculations of the riboacetal internucleotide linkage in double and triple helices. *Proc Natl Acad Sci U S A, 93*(14), 6875-6880.

Torres, V. E., Bankir, L., & Grantham, J. J. (2009). A case for water in the treatment of polycystic kidney disease. *Clin J Am Soc Nephrol, 4*(6), 1140-1150. doi: 10.2215/CJN.00790209

Torres, V. E., Chapman, A. B., Devuyst, O., Gansevoort, R. T., Grantham, J. J., Higashihara, E., Perrone, R. D., Krasa, H. B., Ouyang, J., Czerwiec, F. S., & Investigators, T. T. (2012). Tolvaptan in patients with autosomal dominant polycystic kidney disease. *N Engl J Med, 367*(25), 2407-2418. doi: 10.1056/NEJMoa1205511

Torres, V. E., Chapman, A. B., Perrone, R. D., Bae, K. T., Abebe, K. Z., Bost, J. E., Miskulin, D. C., Steinman, T. I., Braun, W. E., Winklhofer, F. T., Hogan, M. C., Oskoui, F. R., Kelleher, C., Masoumi, A., Glockner, J., Halin, N. J., Martin, D. R., Remer, E., Patel, N., Pedrosa, I., Wetzel, L. H., Thompson, P. A., Miller, J. P., Meyers, C. M., Schrier, R. W., & Group, H. P. S. (2012). Analysis of baseline parameters in the HALT polycystic kidney disease trials. *Kidney Int, 81*(6), 577-585. doi: 10.1038/ki.2011.411

Torres, V. E., & Harris, P. C. (2006). Mechanisms of Disease: autosomal dominant and recessive polycystic kidney diseases. [Review]. *Nature clinical practice. Nephrology, 2*(1), 40-55; quiz 55. doi: 10.1038/ncpneph0070

Torres, V. E., & Harris, P. C. (2009). Autosomal dominant polycystic kidney disease: the last 3 years. [Review]. *Kidney international, 76*(2), 149-168. doi: 10.1038/ki.2009.128

Torres, V. E., & Harris, P. C. (2014). Strategies targeting cAMP signaling in the treatment of polycystic kidney disease. *J Am Soc Nephrol, 25*(1), 18-32. doi: 10.1681/ASN.2013040398

Torres, V. E., Harris, P. C., & Pirson, Y. (2007). Autosomal dominant polycystic kidney disease. *Lancet, 369*(9569), 1287-1301. doi: 10.1016/S0140-6736(07)60601-1

Torres, V. E., King, B. F., Chapman, A. B., Brummer, M. E., Bae, K. T., Glockner, J. F., Arya, K., Risk, D., Felmlee, J. P., Grantham, J. J., Guay-Woodford, L. M., Bennett, W. M., Klahr, S., Meyers, C. M., Zhang, X., Thompson, P. A., Miller, J. P., & Consortium for Radiologic Imaging Studies of Polycystic Kidney, D. (2007). Magnetic resonance measurements of renal blood flow and disease progression in autosomal dominant polycystic kidney disease. *Clin J Am Soc Nephrol, 2*(1), 112-120. doi: 10.2215/CJN.00910306

Torres, V. E., Wang, X., Qian, Q., Somlo, S., Harris, P. C., & Gattone, V. H., 2nd. (2004). Effective treatment of an orthologous model of autosomal dominant polycystic kidney disease. *Nat Med, 10*(4), 363-364. doi: 10.1038/nm1004

Uhl, M., Aulwurm, S., Wischhusen, J., Weiler, M., Ma, J. Y., Almirez, R., Mangadu, R., Liu, Y. W., Platten, M., Herrlinger, U., Murphy, A., Wong, D. H., Wick, W., Higgins, L. S., & Weller, M. (2004). SD-208, a novel transforming growth factor beta receptor I kinase inhibitor, inhibits growth and invasiveness and enhances immunogenicity of murine and human glioma cells in vitro and in vivo. *Cancer Res, 64*(21), 7954-7961. doi: 10.1158/0008-5472.CAN-04-1013

van Rooijen, E., Giles, R. H., Voest, E. E., van Rooijen, C., Schulte-Merker, S., & van Eeden, F. J. (2008). LRRC50, a conserved ciliary protein implicated in polycystic kidney disease. [Research Support, Non-U.S. Gov't]. *Journal of the American Society of Nephrology : JASN, 19*(6), 1128-1138. doi: 10.1681/ASN.2007080917

Vasilyev, A., Liu, Y., Mudumana, S., Mangos, S., Lam, P. Y., Majumdar, A., Zhao, J., Poon, K. L., Kondrychyn, I., Korzh, V., & Drummond, I. A. (2009). Collective cell migration drives morphogenesis of the kidney nephron. *PLoS Biol, 7*(1), e9. doi: 10.1371/journal.pbio.1000009

Vaz, Z. R., Filho, V. C., Yunes, R. A., & Calixto, J. B. (1996). Antinociceptive action of 2-(4-bromobenzoyl)-3-methyl-4,6-dimethoxy benzofuran, a novel xanthoxyline derivative on chemical and thermal models of nociception in mice. *J Pharmacol Exp Ther, 278*(1), 304-312.

Villapol, S., Logan, T. T., & Symes, A. J. (2013). Role of TGF-β Signaling in Neurogenic Regions After Brain Injury, Trends in Cell Signaling Pathways in Neuronal Fate Decision. *InTech*.

Vize, P. D., Seufert, D. W., Carroll, T. J., & Wallingford, J. B. (1997). Model systems for the study of kidney development: use of the pronephros in the analysis of organ induction and patterning. *Dev Biol, 188*(2), 189-204. doi: 10.1006/dbio.1997.8629

Vollmer, E. P. (1963). *Biology of the prostate and related tissues [proceedings*. Bethesda Md.,: U.S.Dept.of Health, Education, and Welfare, Public Health Service, National Cancer Institute; for sale by the Supt.of Docs., U.S.Govt.Print.Off.

Waheed, A., Ludtmann, M. H., Pakes, N., Robery, S., Kuspa, A., Dinh, C., Baines, D., Williams, R. S., & Carew, M. A. (2014). Naringenin inhibits the growth of Dictyostelium and MDCK-derived cysts in a TRPP2 (polycystin-2)-dependent manner. *Br J Pharmacol, 171*(10), 2659-2670. doi: 10.1111/bph.12443

Wallace, D. P. (2011). Cyclic AMP-mediated cyst expansion. [Research Support, N.I.H., Extramural Review]. *Biochimica et biophysica acta, 1812*(10), 1291-1300. doi: 10.1016/j.bbadis.2010.11.005

Watnick, T. J., Torres, V. E., Gandolph, M. A., Qian, F., Onuchic, L. F., Klinger, K. W., Landes, G., & Germino, G. G. (1998). Somatic mutation in individual liver cysts supports a two-hit model of cystogenesis in autosomal dominant polycystic kidney disease. [Research Support, Non-U.S. Gov't

Weimbs, T. (2011). Third-hit signaling in renal cyst formation. [Comment Editorial Research Support, U.S. Gov't, Non-P.H.S.]. *J Am Soc Nephrol, 22*(5), 793-795. doi: 10.1681/ASN.2011030284

Wildman, S. S., Hooper, K. M., Turner, C. M., Sham, J. S., Lakatta, E. G., King, B. F., Unwin, R. J., & Sutters, M. (2003). The isolated polycystin-1 cytoplasmic COOH terminus prolongs ATP-stimulated Cl- conductance through increased Ca2+ entry. [Research Support, Non-U.S. Gov't]. *American journal of physiology. Renal physiology, 285*(6), F1168-1178. doi: 10.1152/ajprenal.00171.2003

Wilson, P. D. (2004a). Polycystic kidney disease. [Review]. *N Engl J Med, 350*(2), 151-164. doi: 10.1056/NEJMra022161

Wilson, P. D. (2004b). Polycystic kidney disease: new understanding in the pathogenesis. *Int J Biochem Cell Biol, 36*(10), 1868-1873. doi: 10.1016/j.biocel.2004.03.012

Wilson, P. D. (2011). Apico-basal polarity in polycystic kidney disease epithelia. *Biochim Biophys Acta, 1812*(10), 1239-1248. doi: 10.1016/j.bbadis.2011.05.008

Wilson, P. D., Geng, L., Li, X., & Burrow, C. R. (1999). The PKD1 gene product, "polycystin-1," is a tyrosine-phosphorylated protein that colocalizes with alpha2beta1-integrin in focal clusters in adherent renal epithelia. [Research Support, U.S. Gov't, P.H.S.]. *Laboratory investigation; a journal of technical methods and pathology, 79*(10), 1311-1323.

Wingert, R. A., & Davidson, A. J. (2011). Zebrafish nephrogenesis involves dynamic spatiotemporal expression changes in renal progenitors and essential signals from retinoic acid and irx3b. [Research Support, N.I.H., Extramural

Research Support, Non-U.S. Gov't]. *Developmental dynamics : an official publication of the American Association of Anatomists, 240*(8), 2011-2027. doi: 10.1002/dvdy.22691

Wingert, R. A., Selleck, R., Yu, J., Song, H. D., Chen, Z., Song, A., Zhou, Y., Thisse, B., Thisse, C., McMahon, A. P., & Davidson, A. J. (2007). The cdx genes and retinoic acid control the positioning and segmentation of the zebrafish pronephros. *PLoS Genet, 3*(10), 1922-1938. doi: 10.1371/journal.pgen.0030189

Witherington, J., Bordas, V., Haigh, D., Hickey, D. M., Ife, R. J., Rawlings, A. D., Slingsby, B. P., Smith, D. G., & Ward, R. W. (2003). 5-aryl-pyrazolo[3,4-b]pyridazines: potent inhibitors of glycogen synthase kinase-3 (GSK-3). *Bioorg Med Chem Lett, 13*(9), 1581-1584.

Woo, Y. M., Shin, Y., Hwang, J. A., Hwang, Y. H., Lee, S., Park, E. Y., Kong, H. K., Park, H. C., Lee, Y. S., & Park, J. H. (2015). Epigenetic silencing of the MUPCDH gene as a possible prognostic biomarker for cyst growth in ADPKD. *Sci Rep, 5*, 15238. doi: 10.1038/srep15238

Woolf, A. S., Price, K. L., Scambler, P. J., & Winyard, P. J. (2004). Evolving concepts in human renal dysplasia. [Research Support, Non-U.S. Gov't

Wu, G., D'Agati, V., Cai, Y., Markowitz, G., Park, J. H., Reynolds, D. M., Maeda, Y., Le, T. C., Hou, H., Jr., Kucherlapati, R., Edelmann, W., & Somlo, S. (1998). Somatic inactivation of Pkd2 results in polycystic kidney disease. *Cell, 93*(2), 177-188. doi: S0092-8674(00)81570-6 [pii]

Wu, G., Markowitz, G. S., Li, L., D'Agati, V. D., Factor, S. M., Geng, L., Tibara, S., Tuchman, J., Cai, Y., Park, J. H., van Adelsberg, J., Hou, H., Jr., Kucherlapati, R., Edelmann, W., & Somlo, S. (2000). Cardiac defects and renal failure in mice with targeted mutations in Pkd2. *Nat Genet, 24*(1), 75-78. doi: 10.1038/71724

Wu, G., Tian, X., Nishimura, S., Markowitz, G. S., D'Agati, V., Park, J. H., Yao, L., Li, L., Geng, L., Zhao, H., Edelmann, W., & Somlo, S. (2002). Trans-heterozygous Pkd1 and Pkd2 mutations modify expression of polycystic kidney disease. *Hum Mol Genet, 11*(16), 1845-1854.

Wu, L. H., Lin, C., Lin, H. Y., Liu, Y. S., Wu, C. Y., Tsai, C. F., Chang, P. C., Yeh, W. L., & Lu, D. Y. (2016). Naringenin Suppresses Neuroinflammatory Responses Through Inducing Suppressor of Cytokine Signaling 3 Expression. *Mol Neurobiol, 53*(2), 1080-1091. doi: 10.1007/s12035-014-9042-9

Wu, M., Gu, J., Mei, S., Xu, D., Jing, Y., Yao, Q., Chen, M., Yang, M., Chen, S., Yang, B., Qi, N., Hu, H., Wuthrich, R. P., & Mei, C. (2016). Resveratrol delays polycystic kidney disease progression through

attenuation of nuclear factor kappaB-induced inflammation. *Nephrol Dial Transplant*. doi: 10.1093/ndt/gfw058

Xia, S., Li, X., Johnson, T., Seidel, C., Wallace, D. P., & Li, R. (2010). Polycystin-dependent fluid flow sensing targets histone deacetylase 5 to prevent the development of renal cysts. *Development, 137*(7), 1075-1084. doi: 10.1242/dev.049437

Xie, C., Sun, Y., Pan, C. Y., Tang, L. M., & Guan, L. P. (2014). 2,4-Dihydroxychalcone derivatives as novel potent cell division cycle 25B phosphatase inhibitors and protein tyrosine phosphatase 1B inhibitors. *Pharmazie, 69*(4), 257-262.

Xu, C., Rossetti, S., Jiang, L., Harris, P. C., Brown-Glaberman, U., Wandinger-Ness, A., Bacallao, R., & Alper, S. L. (2007). Human ADPKD primary cyst epithelial cells with a novel, single codon deletion in the PKD1 gene exhibit defective ciliary polycystin localization and loss of flow-induced Ca2+ signaling. [Research Support, N.I.H., Extramural

Research Support, Non-U.S. Gov't]. *American journal of physiology. Renal physiology, 292*(3), F930-945. doi: 10.1152/ajprenal.00285.2006

Yamaguchi, T., Hempson, S. J., Reif, G. A., Hedge, A. M., & Wallace, D. P. (2006). Calcium restores a normal proliferation phenotype in human polycystic kidney disease epithelial cells. *J Am Soc Nephrol, 17*(1), 178-187. doi: 10.1681/ASN.2005060645

Yamaguchi, T., Nagao, S., Takahashi, H., Ye, M., & Grantham, J. J. (1995). Cyst fluid from a murine model of polycystic kidney disease stimulates fluid secretion, cyclic adenosine monophosphate accumulation, and cell proliferation by Madin-Darby canine kidney cells in vitro. *Am J Kidney Dis, 25*(3), 471-477.

Yamaguchi, T., Pelling, J. C., Ramaswamy, N. T., Eppler, J. W., Wallace, D. P., Nagao, S., Rome, L. A., Sullivan, L. P., & Grantham, J. J. (2000). cAMP stimulates the in vitro proliferation of renal cyst epithelial cells by activating the extracellular signal-regulated kinase pathway. [Research Support, Non-U.S. Gov't

Yang, L. L., Liang, Y. C., Chang, C. W., Lee, W. S., Kuo, C. T., Wang, C. C., Lee, H. M., & Lin, C. H. (2002). Effects of sphondin, isolated from Heracleum laciniatum, on IL-1beta-induced cyclooxygenase-2 expression in human pulmonary epithelial cells. *Life Sci, 72*(2), 199-213.

Yarishkin, O. V., Hwang, E. M., Kim, D., Yoo, J. C., Kang, S. S., Kim, D. R., Shin, J. H., Chung, H. J., Jeong, H. S., Kang, D., Han, J., Park, J. Y., & Hong, S. G. (2009). Diclofenac, a Non-steroidal Anti-inflammatory Drug, Inhibits L-type Ca Channels in Neonatal Rat Ventricular Cardiomyocytes. *Korean J Physiol Pharmacol, 13*(6), 437-442. doi: 10.4196/kjpp.2009.13.6.437

Ye, H., Wang, X., Sussman, C. R., Hopp, K., Irazabal, M. V., Bakeberg, J. L., LaRiviere, W. B., Manganiello, V. C., Vorhees, C. V., Zhao, H., Harris, P. C., van Deursen, J., Ward, C. J., & Torres, V. E. (2016). Modulation of Polycystic Kidney Disease Severity by Phosphodiesterase 1 and 3 Subfamilies. *J Am Soc Nephrol, 27*(5), 1312-1320. doi: 10.1681/ASN.2015010057

Yoder, B. K., Hou, X., & Guay-Woodford, L. M. (2002). The polycystic kidney disease proteins, polycystin-1, polycystin-2, polaris, and cystin, are co-localized in renal cilia. *J Am Soc Nephrol, 13*(10), 2508-2516.

Yokota, Y., Nakajima, H., Wakayama, Y., Muto, A., Kawakami, K., Fukuhara, S., & Mochizuki, N. (2015). Endothelial Ca2+ oscillations reflect VEGFR signaling-regulated angiogenic capacity in vivo. *Elife, 4*. doi: ARTN e08817

Yoshioka, T., Shiraga, H., Yoshida, Y., Fogo, A., Glick, A. D., Deen, W. M., Hoyer, J. R., & Ichikawa, I. (1988). "Intact nephrons" as the primary origin of proteinuria in chronic renal disease. Study in the rat model of subtotal nephrectomy. *J Clin Invest, 82*(5), 1614-1623. doi: 10.1172/JCI113773

Yuan, S., Zhao, L., Brueckner, M., & Sun, Z. (2015). Intraciliary calcium oscillations initiate vertebrate left-right asymmetry. *Curr Biol, 25*(5), 556-567. doi: 10.1016/j.cub.2014.12.051

Zeng, F., Zhang, M. Z., Singh, A. B., Zent, R., & Harris, R. C. (2007). ErbB4 isoforms selectively regulate growth factor induced Madin-Darby canine kidney cell tubulogenesis. *Mol Biol Cell, 18*(11), 4446-4456. doi: 10.1091/mbc.E07-03-0223

Zhao, C., & Malicki, J. (2007). Genetic defects of pronephric cilia in zebrafish. *Mech Dev, 124*(7-8), 605-616. doi: 10.1016/j.mod.2007.04.004

Zhao, C., & Malicki, J. (2011). Nephrocystins and MKS proteins interact with IFT particle and facilitate transport of selected ciliary cargos. *EMBO J, 30*(13), 2532-2544. doi: 10.1038/emboj.2011.165